PERTURBING THE NEURONAL NETWORK DYNAMICS IN THE HIGHER-ORDER THALAMO-CORTICAL NETWORK

Wei Angel Huang

A dissertation submitted to the faculty of the University of North Carolina at Chapel Hill in partial fulfillment of the requirements for the degree of Doctor of Philosophy in the Curriculum of Neuroscience of the School of Medicine.

Chapel Hill
2022

Approved by:

Paul Manis

Eran Dayan

Flavio Frohlich

Hiroyuki Kato

Joe Hopfinger

ABSTRACT

Wei Angel Huang: Perturbing the Neuronal Network Dynamics in the Higher-Order Thalamo-Cortical Visual System
(Under the direction of Flavio Frohlich)

Understanding the brain's dynamics and its role in cognitive functions will open up new avenues for the treatment of psychiatric illnesses. Oscillations reveal rhythmic features in the dynamics that are associated with different mental states and cognitive processes. One cognitive function of transdiagnostic importance is sustained attention. Sustained attention is the ability to focus our cognitive resources to process unpredictable information for an extended period of time. Temporary loss of sustained attention could lead to accidents while driving, and long-term sustained attention deficit is linked to many psychiatric disorders. Sustained visual attention requires an active engagement of higher-order visual circuitry to maintain a mental state for processing unpredictable visual inputs. The coordinated activity of groups of neurons in such circuitry gives rise to cortico-thalamo-cortical oscillations, which are crucial for mediating top-down control signals and bottom-up information transduction. Through its widespread interconnection with the cortex, the higher-order visual thalamus is ideally positioned to serve such a role by coordinating cortico-cortical synchrony that supports attentional engagement. However, the causal mechanisms underlying the oscillatory synchronization in the posterior visual thalamo-cortical network as well as their function during sustained attention remains unknown. Thus, basic science and translational work with causal perturbation is needed to shine a light on the role of these oscillatory dynamics in neuronal processing and behavior.

The studies in this dissertation attempted to address this question by targeting the higher-order thalamo-cortical visual system and combining multiple causal perturbation tools (eg. optogenetics and transcranial brain stimulation), simultaneous multisite electrophysiological recordings, and a sustained

attention task. Through a logical process of target identification, engagement, and validation, our work contributes to understanding: 1. how does the higher-order visual thalamus causally coordinate thalamo-cortical communications to enhance attentional behavior, and 2. how does transcranial alternating current stimulation affect single-neuron activity as well as long-range circuit dynamics in this network? Taken together, this work provides causal evidence underlying the mechanism of brain stimulations and its effect on behavior, which ultimately could inform the broader scientific community on how to rationally refine targeted circuit-based therapeutics for treating cognitive deficits.

ACKNOWLEDGEMENTS

This work would not have become a reality without the kind support and help of many groups, from our funding agency to the vet who took care of our animals. I would like to first express my deepest gratitude to my mentor and advisor Flavio Fröhlich for his guidance and support throughout my Ph.D. study and research. His motivation, enthusiasm, caring, and immense knowledge have not only shaped my scientific thinking but also guided me along my personal journey.

Besides my advisor, I would like to thank my thesis committee members for their encouragement, vital feedback, and mentorship: Paul Manis, Hiroyuki Kato, Eran Dayan, and Joe Hopfinger. I thank my collaborators Angel Peterchev, my rotation mentors Ben Philpot and Yun Li, and my F31 co-mentors Charles Schroeder, Jonathan Pillow, Jennifer Bizley, and Garret Stuber, for their generous contribution and support to my work and development.

In addition, I am grateful to all of the previous and current Frohlich lab members for generously sharing their time, knowledge, and stories with me to make the lab such an exciting and enjoyable place to be in, particularly Charles Zhou, Ehsan Negahbani, Iain Stitt, Sankar Alagapan, Sangtae Ahn, Yuhui Li, Guoshi Li, Chris Walker, and Trevor Mcpherson; as well as current members: Susanne Radtke-Schuller, Justin Riddle, Mengsen Zhang, Qi Fang, and Grace Ross. I would also like to thank my talented undergraduate/post-bac research assistants who helped with data collection and made me a better mentor: Peyton Siekierski, Zhouxiao Lu, Sydney Rucker, Nivi Ramasamy, Rohan Patel, Chris Kramer, Nathan Pierron, Numair Attaar, Annabel Hinkle, Aasim Khan, Stefano Quaglioni, Justice Robinson, Preethi Irukulapati, and Harshini Matada.

I would also like to thank the Biological & Biomedical Sciences Program and my first-year mentor Donita Robinson, who has provided warm support and guided me through the transition into graduate school.

Last but not least, I would like to give my special thanks to my family for their unconditional love and support: my parents, who cheered for me every step of the way; my baby girl Lia, who joined our family a couple of months ago and whose heart-warming smiles and hugs have accompanied me to the finish line; and of course, my husband Chris, who has always been there for me and whom I hope to share the rest of my life's journey with.

TABLE OF CONTENTS

LIST OF TABLES

LIST OF FIGURES

LIST OF ABBREVIATIONS

ASD	Autism Spectrum Disorder
dPFC	Dorso prefrontal cortex
EEG	Electroencephalography
fMRI	Functional magnetic resonance imaging
LFP	Local field potential
LP/Pul	Lateral posterior nucleus / Pulvinar complex of the thalamus
MRI	Magnetic resonance imaging
NIH	National Institute of Health
NIMH	National Institute of Mental Health
PFC	Prefrontal cortex
PLV	Phase-locking value
PPC	Posterior parietal cortex
SU	Single unit
tACS	Transcranial alternating current stimulation
USDA	United States Department of Agriculture
V1	Primary visual cortex
VC	Visual cortex

CHAPTER 1: GENERAL INTRODUCTION

The brain is a sophisticated network that is composed of many specialized and tightly interconnected cortical and subcortical regions. These regions constantly communicate with each other to process and integrate information from both our internal states and the outside world, which enables cognitive functions and behavioral engagement (Sporns, Tononi, & Edelman, 2000).

Two important ways for the brain regions to communicate are through: 1) direct information flow via neurons firing action potentials, and 2) indirect information flow via rhythmic fluctuations in the cell membrane and synaptic currents (G. Buzsaki & Draguhn, 2004; Fröhlich, 2016). Since we are interested in the circuit-level mechanisms in this dissertation, we will focus on the latter. When a group of neurons acts together, the average electrical potentials in the nearby extracellular space (i.e. local field potentials, LFP) fluctuate, giving rise to oscillations. Oscillations are often calculated by converting LFPs in the time domain to the frequency domain through signal processing techniques (e.g. Fourier transform, wavelet convolution, etc.). The oscillatory features such as frequencies (measured in cycles per second, i.e. Hz) and phases have been shown to relate to sensory processing, cognitive integration, and behavioral performance (Boyce, Glasgow, Williams, & Adamantidis, 2016; Cardin et al., 2009; C. S. Herrmann, Struber, Helfrich, & Engel, 2016; Lustenberger et al., 2016). In humans, the frequency bands of interest are roughly grouped into delta (1-4 Hz), theta (4-8 Hz), alpha (8-12 Hz), beta (12-30 Hz), and gamma (30-200 Hz). The exact cut-off of each band in different animal species is ideally based on a consistent biophysical mechanism of generation or a specific function that is known to relate to the band of study (Uhlhaas, Haenschel, Nikolic, & Singer, 2008). For example, alpha-band oscillation is the first discovered oscillatory activity in the human visual cortex using electroencephalogram (EEG) recordings (Berger, 1929) which is distinctively enhanced when

eyes are closed versus open. Typically, the slower frequencies (delta, theta, alpha, and beta) are more likely to be found in long-range communications whereas the faster frequencies (gamma) are more likely to be involved in local communications (Kopell, Ermentrout, Whittington, & Traub, 2000; von Stein, Chiang, & Konig, 2000; von Stein & Sarnthein, 2000).

Just oscillating at the same frequency does not imply synchrony or efficient information transduction between the two regions. It is also important to look at the phase relationship between the oscillations of the two regions. Phase refers to the relative position of a periodic oscillator in a cycle and can be used to compare two oscillations occurring simultaneously (J. M. Palva, Palva, & Kaila, 2005). A frequently used matrix to assess the phase synchronization between neuronal oscillation in different brain regions is the phase-locking value (PLV) (J. P. Lachaux, E. Rodriguez, J. Martinerie, & F. J. Varela, 1999; Liebe, Hoerzer, Logothetis, & Rainer, 2012). It quantifies the correlation of relative phases by calculating the consistency of the phase differences between the two signals. Perfect phase-locking results from consistent phase differences and will yield a PLV of 1, and two random signals with inconsistent phase differences will yield a PLV of 0. A slightly modified version of PLV is coherence, which takes into account the amplitude of the signals in addition to the phase (Fries, 2015; Siegel, Donner, & Engel, 2012). Additionally, phase-amplitude cross-frequency coupling allows the organization of activity at a different temporal scale (Fries, 2005; Vanhatalo et al., 2004). The phase of lower frequency oscillations (such as theta) can modulate the amplitude of higher frequency oscillations (such as gamma) (Canolty & Knight, 2010). A well-known example of cross-frequency coupling is between theta and gamma frequency activities. It was found in many systems to encode and compress units of information in an ordered way (J. Lisman, 2005; J. E. Lisman & Jensen, 2013). For example, in the hippocampus, the ensembles of neuron firing representing different spatial information are encoded in the fast gamma subcycles, which are embedded into each slow theta cycle and stored in memory (J. Lisman, 2005; J. E. Lisman & Jensen, 2013).

More importantly, these oscillations and their communications are dynamic and can change over time. They can shift in power, phase, and frequency based on the internal state, physical environment,

behavioral demand, etc. To provide a fundamental understanding of how the neuronal activity in or between specific brain regions affects certain cognitive processes or behavior in a reproducible way, we need to establish causation. Recent work has emphasized the importance of developing causal perturbation tools and studying the causal relationship between oscillatory features and cognitive functions or behavior (Wolff & Ölveczky, 2018).

The two tools that I used in this work to stimulate the neurons are optogenetics and transcranial alternating current stimulation (tACS). In animal research, optogenetics allows temporally-precise targeting of optogenetically-labeled neurons by optical stimulation (Khoshkhoo, Vogt, & Sohal, 2017; Tye & Deisseroth, 2012). It works by first injecting viral vectors expressing light-activated ion channels in the neuron population of interest and then delivering light stimulation to the population (Jessica A. Cardin et al., 2010). To further enhance its power to dissect the circuitry and its function, optogenetics can also be combined with transgenetic models, different targeting strategies, and extracellular recordings to achieve cell-type specificity, projection specificity, and the understanding of the neuronal mechanism at work, respectively (Deisseroth, 2014; Steinberg, Christoffel, Deisseroth, & Malenka, 2015; Urban & Roth, 2015). Therefore, otogenetics, is a powerful tool for studying the causal role of neuronal dynamics and specific oscillatory features in cross-regional communication as well as the resulting behavior.

However, its invasive nature limited the use of optogenetics in human subjects. In humans, non-invasive brain stimulation is a crucial causal perturbation tool to study the brain-behavior linkage. Among the tools, transcranial electric stimulation (tES) has gained popularity due to 1) its long-standing safety track record with the use of low-amplitude electric current (A. Antal et al., 2017) and 2) its portability and potential to be applied at home (Sandran, Hillier, & Hordacre, 2019). Several different versions of tES include: transcranial direct current stimulation (tDCS), which applies direct current to modulating cortical excitability; transcranial alternating current stimulation (tACS), which applies a rhythmic weak electric field to modulate oscillations at targeted frequencies; and transcranial random noise stimulation (tRNS), which applies alternating current oscillating at random frequencies to modulate neural excitability (Fröhlich

et al., 2021; Moret, Donato, Nucci, Cona, & Campana, 2019). Among them, tACS is the most suitable tool to directly engage oscillatory features by applying alternating current at the same frequency that is under study. Although tACS is suggested to modulate frequency-specific oscillations by entrainment in both computational modeling and human studies, a direct investigation of the neuronal mechanism is still lacking. By using an animal model, we can leverage the benefit of combining invasive electrophysiology recording with tACS to reveal how different neuron types react to tACS and how they are entrained to enhance oscillations.

With the tools in hand, we are ready to study the causal mechanism underlying a cognitive ability that is essential for the survival of all animals, and especially for the cognitive development in humans – visual sustained attention. Sustained attention refers to the process of allocating cognitive resources to respond to infrequent, but behavior-relevant, stimuli over an extended period (Sarter, Givens, & Bruno, 2001). Dysfunction of this process is linked to attention deficit and impulsivity in many psychiatric disorders such as schizophrenia and attention deficit hyperactivity disorder (ADHD) (Barkley, 1997; Bora, Vahip, & Akdeniz, 2006; S. K. Liu et al., 2002; Nuechterlein et al., 2015; Pagliaccio et al., 2017; Tucha et al., 2017). Clinically, the continuous performance task (CPT) has been used to measure sustained attention performance which is highly sensitive to brain damage or dysfunction (Banaschewski et al., 2003; Lee & Park, 2006; Levinoff, Saumier, & Chertkow, 2005). It requires the participant to respond to an infrequent stimulus over a prolonged time (Turner, Peak, & Burne, 2015).

An adaptation of the CPT to animal models is the 5-choice serial reaction time task (5-CSRTT) (Bari, Dalley, & Robbins, 2008). Although there were differences in the task implementation such as adding a reward after the completion of each trial the 5-CSRTT still captures the key features to illicit sustained attention: temporally and spatially unpredictable stimulus, and the delay period without visual input before the presentation of the stimulus. The 5-CSRTT has been widely used in rodents to investigate the use of pharmacological agents in changing sustained attention performance (Featherstone, Rizos, Nobrega, Kapur, & Fletcher, 2007; Robbins, 2002). Despite a long history of behavioral and pharmacological investigation

of sustained attention in animal models, its neuronal circuit substrate, especially the interaction between the thalamic control signals and information from sensory cortices, has remained mostly unexplored (Fortenbaugh, DeGutis, & Esterman, 2017; Sarter et al., 2001). Recently, we showed that the 5-CSRTT recruits frontoparietal synchronization (Sellers et al., 2016) and thalamus-visual cortex synchronization (Yu et al., 2016) in the theta frequency band (peak ~5 Hz) in ferrets, which laid the foundation for my thesis work.

Human imaging studies have shown that both the fronto-parietal network and the subcortical structures (eg. basal ganglia, thalamus) are part of the sustained attention network (Lewin et al., 1996; Riccio, Reynolds, Lowe, & Moore, 2002). Unlike the relatively abundant literature on the top-down control function of the fronto-parietal network (Buschman & Miller, 2007; Scolari, Seidl-Rathkopf, & Kastner, 2015; Sellers et al., 2016), the higher-order thalamus has only gained interest recently. The higher-order visual thalamus serves an important role in coordinating cortical activity during visual processing (McAlonan, Cavanaugh, & Wurtz, 2008; Yuri B Saalmann, Mark A Pinsk, Liang Wang, Xin Li, & Sabine Kastner, 2012). In primates, higher-order visual thalamic activity is causally involved in visual responsiveness and high-frequency synchronous activity in V4 (Huihui Zhou, Robert John Schafer, & Robert Desimone, 2016) and synchronizes the activity of interconnected V4 and temporo-occipital cortex during the delay period in a visuospatial selective attention task (Yuri B Saalmann et al., 2012). The pulvinar theta oscillations are also implicated in sensory sampling and controlling cortical sensitivity (Fiebelkorn, Pinsk, & Kastner, 2019; Kastner, Fiebelkorn, & Eradath, 2020). In addition, a human fMRI study has shown that the structural abnormality in pulvinar is related to atypical pulvinar-cortical functional connectivity and attention deficits in the ADHD group (X. Li et al., 2012)**.** Together, these results support a fundamental role of the pulvinar in maintaining and perhaps guiding the cortical activity of the posterior visual network in attention-demanding tasks.

Another two important nodes in the posterior visual network are the posterior parietal cortex (PPC), and the (primary) visual cortex (VC). The PPC is a node of the dorsal attention network and is part of the

network substrate of sustained attention in humans. Attention is carried out in the process of sensory-motor transformations. PPC serves an important role in attending to behaviorally-relevant stimuli, integrating multisensory inputs, and coordinating goal-directed motor output accordingly (Motter & Mountcastle, 1981; Colby & Goldberg, 1999; Andersen & Buneo, 2002). Causal evidence of these functions was found in human patients with lesions as well as animal models with inactivation in PPC (Grea et al., 2002; Y. Zhou & Freedman, 2019). In addition, PPC is reciprocally connected with the LP/Pul and the (primary) visual cortex (Gharbawie, Stepniewska, Burish, & Kaas, 2010; Raczkowski & Rosenquist, 1983; Szczepanski, Pinsk, Douglas, Kastner, & Saalmann, 2013; Taktakishvili, Sivan-Loukianova, Kultas-Ilinsky, & Ilinsky, 2002; Yu et al., 2016), making it an ideal candidate to interact with the signals from both regions. With VC serving as a sensory input readout region, the posterior visual network provides us with a suitable target to study the circuit dynamics underlying causal perturbation and attentional behavior.

To bridge the animal and human research as well as provide mechanistic insights underlying the brain-behavior linkage, it is crucial to choose an animal model that is at the right level of complexity. In this dissertation, I presented studies that use the ferret as an animal model due to its following strengths:

1. Compared to rodents, ferrets have a relatively well-developed higher-order visual system, including the presence of a distinct higher-order visual nucleus in the thalamus (Z. C. Zhou et al., 2016), which is a crucial target in this dissertation. In ferrets, the lateral nucleus of the lateral posterior thalamic nucleus and the pulvinar complex (LP/Pul) resembles the primate inferior pulvinar nucleus as it is reciprocally connected with PPC and VC (C. Yu et al., 2016). This also provides the anatomical foundation for LP/Pul to coordinate the communication in the posterior visual network.
2. Ferrets have a gyrencephalic cerebral cortex (Gilardi & Kalebic, 2021). Like the primate brain, ferrets have an expanded neocortex with gyri and sulci (Fernández, Llinares-Benadero, & Borrell, 2016) which is considered an important characteristic underlying increased cognitive capabilities in humans (Fernández et al., 2016; Rakic & Lombroso, 1998; Sousa, Meyer, Santpere, Gulden, & Sestan, 2017). Cortical folding is especially important for the study of the effects of electrical stimulation due to the

differences in conductivity of the tissues in a lissencephalic brain without folding (as in rodents). Modeling studies have suggested that electric fields travel in a particular fashion in a folded brain and affect brain tissue and neurons differently (P. C. Miranda, Mekonnen, Salvador, & Ruffini, 2013; Thielscher, Opitz, & Windhoff, 2011). Thus, the ferret is a suitable model to study the neural mechanism underlying non-invasive brain stimulations and potentially their effects on behavior.

3. Ferrets display distinct theta and alpha oscillations in the awake state, which are analogous to those in humans (Stitt, Zhou, Radtke-Schuller, & Fröhlich, 2018). This is in contrast to rodents where there is only one wide range of theta bands (4-12 Hz) (Gyorgy Buzsaki, 2006; Corsi-Cabrera, Pérez-Garci, Río-Portilla, Ugalde, & Guevara, 2001). This division of theta and alpha bands is of particular importance to our study because it allows us to study their antagonistic roles that are modulated by the thalamo-cortical functional interaction during visual engagement (Rana & Vaina, 2014).
4. In comparison to non-human primates, ferrets are small, cost-effective, and have a rather sophisticated visual system that is ideal for optogenetic perturbations (Hasse & Briggs, 2017; Z. C. Zhou, Yu, Sellers, & Fröhlich, 2016) to manipulate oscillations due to their smaller brain size.
5. Ferrets are amenable to freely-moving behavioral training. Traditional head-fixed paradigms in primates preclude natural movement and impose an artificial state of restrained behavior (Juczewski, Koussa, Kesner, Lee, & Lovinger, 2020). The sustained attention study in this dissertation addressed a gap in the literature about the attention circuit dynamics during naturalistic freely moving behavior.

In summary, network and circuit-level interrogations within and between the nodes highlight that thalamo-cortical circuit play key roles in sensory-driven behavior. Despite this body of literature, it remains unclear how to perturb the higher-order visual thalamo-cortical network, and what is their causal role in modulating cognitive functions. This knowledge gap produces general questions: 1) how do frequency-specific oscillations in the higher-order cognitive brain areas enable visual sustained attention, and 2) how to causally entrain oscillatory features in this network in a non-invasive way and what is the neuronal

mechanism underlying the entrainment. The work in this dissertation aims to address this question in the following chapters:

In Chapter 2, I presented a study investigating how the oscillations in the higher-order visual thalamo-cortical network were modulated during a sustained attention task and causally affected attentional performance. We identified oscillatory features that are attention modulated, causally engaged those oscillations by applying optogenetic stimulation, and successfully enhanced task accuracy in a frequency-specific way.

In Chapter 3, I presented a study investigating the neuronal mechanisms of how tACS entrained endogenous alpha oscillations in head-fixed awake ferrets. In both the ferret experiments and the computational model, we found the fast-spiking inhibitory interneurons to be more entrained by tACS, likely due to their stronger endogenous coupling to the alpha oscillation.

In Chapter 4, I reviewed the studies of tACS using animal models to provide an overview of the current state of research and their translational value.

In Chapter 5, I provided a general discussion on how these works contribute to the neuroscientific body of literature and how to use these findings as a foundation for future studies.

REFERENCES

Banaschewski, T., Brandeis, D., Heinrich, H., Albrecht, B., Brunner, E., & Rothenberger, A. (2003). Association of ADHD and conduct disorder–brain electrical evidence for the existence of a distinct subtype. Journal of Child Psychology and Psychiatry, 44(3), 356-376.

Bari, A., Dalley, J. W., & Robbins, T. W. (2008). The application of the 5-choice serial reaction time task for the assessment of visual attentional processes and impulse control in rats. Nat Protoc, 3(5), 759-767. doi:10.1038/nprot.2008.41

Barkley, R. A. (1997). Behavioral inhibition, sustained attention, and executive functions: constructing a unifying theory of ADHD. Psychological bulletin, 121(1), 65.

Barnett, L., & Seth, A. K. (2014). The MVGC multivariate Granger causality toolbox: a new approach to Granger-causal inference. Journal of Neuroscience Methods, 223, 50-68.

Barthó, P., Hirase, H., Monconduit, L., Zugaro, M., Harris, K. D., & Buzsaki, G. (2004). Characterization of neocortical principal cells and interneurons by network interactions and extracellular features. Journal of Neurophysiology, 92(1), 600-608.

Barthó, P., Slézia, A., Mátyás, F., Faradzs-Zade, L., Ulbert, I., Harris, K. D., & Acsády, L. (2014). Ongoing network state controls the length of sleep spindles via inhibitory activity. Neuron, 82(6), 1367-1379.

Bassett, D. S., & Gazzaniga, M. S. (2011). Understanding complexity in the human brain. Trends Cogn Sci, 15(5), 200-209. doi:10.1016/j.tics.2011.03.006

Bassett, D. S., & Sporns, O. (2017). Network neuroscience. Nat Neurosci, 20(3), 353-364. doi:10.1038/nn.4502

Beltramo, R., D'Urso, G., Dal Maschio, M., Farisello, P., Bovetti, S., Clovis, Y., . . . Fellin, T. (2013). Layer-specific excitatory circuits differentially control recurrent network dynamics in the neocortex. Nature neuroscience, 16(2), 227-234. doi:10.1038/nn.3306

Berger, H. (1929). Über das Elektrenkephalogramm des Menschen. Archiv für Psychiatrie und Nervenkrankheiten, 87(1), 527-570.

Bikson, M., Inoue, M., Akiyama, H., Deans, J. K., Fox, J. E., Miyakawa, H., & Jefferys, J. G. (2004). Effects of uniform extracellular DC electric fields on excitability in rat hippocampal slices in vitro. The Journal of physiology, 557(Pt 1), 175-190. doi:10.1113/jphysiol.2003.055772

Bindman, L. J., Lippold, O. C., & Redfearn, J. W. (1964). The Action of Brief Polarizing Currents on the Cerebral Cortex of the Rat (1) during Current Flow and (2) in the Production of Long-Lasting after-Effects. J Physiol, 172, 369-382.

Bollimunta, A., Mo, J., Schroeder, C. E., & Ding, M. (2011). Neuronal Mechanisms and Attentional Modulation of Corticothalamic Alpha Oscillations. 31(13), 4935-4943. doi:10.1523/JNEUROSCI.5580-10.2011 %J The Journal of Neuroscience

Bora, E., Vahip, S., & Akdeniz, F. (2006). Sustained attention deficits in manic and euthymic patients with bipolar disorder. Progress in Neuro-Psychopharmacology and Biological Psychiatry, 30(6), 1097-1102.

Boyce, R., Glasgow, S. D., Williams, S., & Adamantidis, A. (2016). Causal evidence for the role of REM sleep theta rhythm in contextual memory consolidation. Science, 352(6287), 812-816. doi:10.1126/science.aad5252

Boyle, M. R., & Frohlich, F. (2013). EEG feedback-controlled transcranial alternating current stimulation. Paper presented at the Neural Engineering (NER), 2013 6th International IEEE/EMBS Conference on.

Braitenberg, V., & Schüz, A. (2013). Anatomy of the cortex: statistics and geometry (Vol. 18): Springer Science & Business Media.

Brignani, D., Ruzzoli, M., Mauri, P., & Miniussi, C. (2013). Is transcranial alternating current stimulation effective in modulating brain oscillations? PloS One, 8(2), e56589.

Bullmore, E., & Sporns, O. (2012). The economy of brain network organization. Nat Rev Neurosci, 13(5), 336-349. doi:10.1038/nrn3214

Buschman, T. J., & Miller, E. K. (2007). Top-down versus bottom-up control of attention in the prefrontal and posterior parietal cortices. Science, 315(5820), 1860-1862.

Buzsaki, G. (2006). Rhythms of the Brain: Oxford university press.

Buzsaki, G., & Draguhn, A. (2004). Neuronal oscillations in cortical networks. Science, 304(5679), 1926-1929. doi:10.1126/science.1099745

Canolty, R. T., Edwards, E., Dalal, S. S., Soltani, M., Nagarajan, S. S., Kirsch, H. E., . . . Knight, R. T. (2006). High gamma power is phase-locked to theta oscillations in human neocortex. Science, 313(5793), 1626-1628. doi:10.1126/science.1128115

Canolty, R. T., & Knight, R. T. (2010). The functional role of cross-frequency coupling. Trends Cogn Sci, 14(11), 506-515. doi:10.1016/j.tics.2010.09.001

Cardin, J. A., Carlen, M., Meletis, K., Knoblich, U., Zhang, F., Deisseroth, K., . . . Moore, C. I. (2009). Driving fast-spiking cells induces gamma rhythm and controls sensory responses. Nature, 459(7247), 663-667. doi:10.1038/nature08002

Chan, C. Y., Hounsgaard, J., & Nicholson, C. (1988). Effects of electric fields on transmembrane potential and excitability of turtle cerebellar Purkinje cells in vitro. J Physiol, 402, 751-771.

Corbetta, M., & Shulman, G. L. (2002). Control of goal-directed and stimulus-driven attention in the brain. Nat Rev Neurosci, 3(3), 201-215. doi:10.1038/nrn755

Corsi-Cabrera, M., Pérez-Garci, E., Río-Portilla, Y. D., Ugalde, E., & Guevara, M. A. (2001). EEG bands during wakefulness, slow-wave, and paradoxical sleep as a result of principal component analysis in the rat. Sleep, 24(4), 374-380.

Creutzfeldt, O. D., Fromm, G. H., & Kapp, H. (1962). Influence of transcortical d-c currents on cortical neuronal activity. Exp Neurol, 5, 436-452.

Datta, A., Bansal, V., Diaz, J., Patel, J., Reato, D., & Bikson, M. (2009). Gyri-precise head model of transcranial direct current stimulation: improved spatial focality using a ring electrode versus conventional rectangular pad. Brain stimulation, 2(4), 201-207. e201.

de Kloet, S. F., Bruinsma, B., Terra, H., Heistek, T. S., Passchier, E. M. J., van den Berg, A. R., . . . Mansvelder, H. D. (2021). Bi-directional regulation of cognitive control by distinct prefrontal cortical output neurons to thalamus and striatum. Nat Commun, 12(1), 1994. doi:10.1038/s41467-021-22260-7

Deans, J. K., Powell, A. D., & Jefferys, J. G. (2007). Sensitivity of coherent oscillations in rat hippocampus to AC electric fields. The Journal of physiology, 583(Pt 2), 555-565. doi:10.1113/jphysiol.2007.137711

Deans, J. K., Powell, A. D., & Jefferys, J. G. (2007). Sensitivity of coherent oscillations in rat hippocampus to AC electric fields. The Journal of Physiology, 583(2), 555-565.

Deans, J. K., Powell, A. D., & Jefferys, J. G. R. (2007). Sensitivity of coherent oscillations in rat hippocampus to AC electric fields. The Journal of Physiology, 583(Pt 2), 555-565. doi:10.1113/jphysiol.2007.137711

Deco, G., Jirsa, V. K., & McIntosh, A. R. (2011). Emerging concepts for the dynamical organization of resting-state activity in the brain. Nature Reviews: Neuroscience, 12(1), 43-56. doi:10.1038/nrn2961

Deisseroth, K. (2014). Circuit dynamics of adaptive and maladaptive behaviour. Nature, 505(7483), 309-317. doi:10.1038/nature12982

Engel, A. K., Fries, P., & Singer, W. (2001). Dynamic predictions: oscillations and synchrony in top-down processing. Nat Rev Neurosci, 2(10), 704-716. doi:10.1038/35094565

Featherstone, R. E., Rizos, Z., Nobrega, J. N., Kapur, S., & Fletcher, P. J. (2007). Gestational methylazoxymethanol acetate treatment impairs select cognitive functions: parallels to schizophrenia. Neuropsychopharmacology, 32(2), 483-492. doi:10.1038/sj.npp.1301223

Fedorov, A., Beichel, R., Kalpathy-Cramer, J., Finet, J., Fillion-Robin, J.-C., Pujol, S., . . . Sonka, M. (2012). 3D Slicer as an image computing platform for the Quantitative Imaging Network. Magnetic Resonance Imaging, 30(9), 1323-1341.

Fernández, V., Llinares-Benadero, C., & Borrell, V. (2016). Cerebral cortex expansion and folding: what have we learned? The EMBO journal, 35(10), 1021-1044.

Fiebelkorn, I. C., Pinsk, M. A., & Kastner, S. (2019). The mediodorsal pulvinar coordinates the macaque fronto-parietal network during rhythmic spatial attention. Nat Commun, 10(1), 215. doi:10.1038/s41467-018-08151-4

Figee, M., & Mayberg, H. (2021). The future of personalized brain stimulation. Nature Medicine, 27(2), 196-197. doi:10.1038/s41591-021-01243-7

Fortenbaugh, F. C., DeGutis, J., & Esterman, M. (2017). Recent theoretical, neural, and clinical advances in sustained attention research. Annals of the New York Academy of Sciences.

Foster, B. L., He, B. J., Honey, C. J., Jerbi, K., Maier, A., & Saalmann, Y. B. (2016). Spontaneous Neural Dynamics and Multi-scale Network Organization. Front Syst Neurosci, 10, 7. doi:10.3389/fnsys.2016.00007

Fries, P. (2005). A mechanism for cognitive dynamics: neuronal communication through neuronal coherence. Trends Cogn Sci, 9(10), 474-480. doi:10.1016/j.tics.2005.08.011

Fries, P. (2005). A mechanism for cognitive dynamics: neuronal communication through neuronal coherence. Trends in cognitive sciences, 9(10), 474-480.

Fries, P. (2015). Rhythms for Cognition: Communication through Coherence. Neuron, 88(1), 220-235. doi:10.1016/j.neuron.2015.09.034

Fritsch, B., Reis, J., Martinowich, K., Schambra, H. M., Ji, Y., Cohen, L. G., & Lu, B. (2010). Direct current stimulation promotes BDNF-dependent synaptic plasticity: potential implications for motor learning. Neuron, 66(2), 198-204. doi:10.1016/j.neuron.2010.03.035

Fröhlich, F. (2014a). Endogenous and exogenous electric fields as modifiers of brain activity: rational design of noninvasive brain stimulation with transcranial alternating current stimulation. Dialogues Clin. Neurosci., 16(1), 93-102.

Fröhlich, F. (2014b). Endogenous and exogenous electric fields as modifiers of brain activity: rational design of noninvasive brain stimulation with transcranial alternating current stimulation. Dialogues in Clinical Neuroscience, 16(1), 93-102.

Fröhlich, F. (2016). Network neuroscience: Academic Press.

Fröhlich, F. (2016). Network neuroscience. Amsterdam ; Boston: Academic Press.

Fröhlich, F., Force, R., Huang, W. A., Lustenberger, C., McPherson, T., Riddle, J., & Walker, C. (2021). Target Engagement with Transcranial Current Stimulation Transcranial Direct Current Stimulation in Neuropsychiatric Disorders (pp. 211-242): Springer.

Frohlich, F., & McCormick, D. A. (2010). Endogenous electric fields may guide neocortical network activity. Neuron, 67(1), 129-143. doi:10.1016/j.neuron.2010.06.005

Fröhlich, F., & McCormick, D. A. (2010). Endogenous electric fields may guide neocortical network activity. Neuron, 67(1), 129-143.

Geweke, J. (1982). Measurement of linear dependence and feedback between multiple time series. Journal of the American statistical association, 77(378), 304-313.

Geweke, J. F. (1984). Measures of conditional linear dependence and feedback between time series. Journal of the American Statistical Association, 79(388), 907-915.

Gharbawie, O. A., Stepniewska, I., Burish, M. J., & Kaas, J. H. (2010). Thalamocortical connections of functional zones in posterior parietal cortex and frontal cortex motor regions in New World monkeys. Cereb Cortex, 20(10), 2391-2410. doi:10.1093/cercor/bhp308

Gilardi, C., & Kalebic, N. (2021). The Ferret as a Model System for Neocortex Development and Evolution. Frontiers in Cell and Developmental Biology, 9. doi:10.3389/fcell.2021.661759

Gluckman, B. J., Neel, E. J., Netoff, T. I., Ditto, W. L., Spano, M. L., & Schiff, S. J. (1996). Electric field suppression of epileptiform activity in hippocampal slices. Journal of neurophysiology, 76(6), 4202-4205.

Gluckman, B. J., Nguyen, H., Weinstein, S. L., & Schiff, S. J. (2001). Adaptive electric field control of epileptic seizures. The Journal of neuroscience : the official journal of the Society for Neuroscience, 21(2), 590-600.

Granger, C. W. (1969). Investigating causal relations by econometric models and cross-spectral methods. Econometrica: Journal of the Econometric Society, 424-438.

Grea, H., Pisella, L., Rossetti, Y., Desmurget, M., Tilikete, C., Grafton, S., . . . Vighetto, A. (2002). A lesion of the posterior parietal cortex disrupts on-line adjustments during aiming movements. Neuropsychologia, 40(13), 2471-2480.

Grossman, N., Bono, D., Dedic, N., Kodandaramaiah, S. B., Rudenko, A., Suk, H.-J., . . . Tsai, L.-H. (2017). Noninvasive Deep Brain Stimulation via Temporally Interfering Electric Fields. Cell, 169(6), 1029-1041. e1016.

Grover, S., Nguyen, J. A., Viswanathan, V., & Reinhart, R. M. G. (2021). High-frequency neuromodulation improves obsessive–compulsive behavior. Nature Medicine, 27(2), 232-238. doi:10.1038/s41591-020-01173-w

Haberbosch, L., Datta, A., Thomas, C., Jooß, A., Köhn, A., Rönnefarth, M., . . . Schmidt, S. (2019). Safety Aspects, Tolerability and Modeling of Retinofugal Alternating Current Stimulation. Frontiers in Neuroscience, 13(783). doi:10.3389/fnins.2019.00783

Hasse, J. M., & Briggs, F. (2017). Corticogeniculate feedback sharpens the temporal precision and spatial resolution of visual signals in the ferret. Proceedings of the National Academy of Sciences, 114(30), E6222-E6230. doi:10.1073/pnas.1704524114

Heck, C. N., King-Stephens, D., Massey, A. D., Nair, D. R., Jobst, B. C., Barkley, G. L., . . . Gwinn, R. P. (2014). Two-year seizure reduction in adults with medically intractable partial onset epilepsy treated with responsive neurostimulation: Final results of the RNS System Pivotal trial. Epilepsia, 55(3), 432-441.

Helfrich, R. F., Fiebelkorn, I. C., Szczepanski, S. M., Lin, J. J., Parvizi, J., Knight, R. T., & Kastner, S. (2018). Neural Mechanisms of Sustained Attention Are Rhythmic. Neuron, 99(4), 854-865 e855. doi:10.1016/j.neuron.2018.07.032

Helfrich, Randolph F., Schneider, Till R., Rach, S., Trautmann-Lengsfeld, Sina A., Engel, Andreas K., & Herrmann, Christoph S. (2014). Entrainment of Brain Oscillations by Transcranial Alternating Current Stimulation. Current Biology, 24(3), 333-339. doi:10.1016/j.cub.2013.12.041

Herrmann, C. S., Murray, M. M., Ionta, S., Hutt, A., & Lefebvre, J. (2016a). Shaping intrinsic neural oscillations with periodic stimulation. The Journal of neuroscience, 36(19), 5328-5337.

Herrmann, C. S., Murray, M. M., Ionta, S., Hutt, A., & Lefebvre, J. (2016b). Shaping intrinsic neural oscillations with periodic stimulation. Journal of Neuroscience, 36(19), 5328-5337.

Herrmann, C. S., Struber, D., Helfrich, R. F., & Engel, A. K. (2016). EEG oscillations: From correlation to causality. Int J Psychophysiol, 103, 12-21. doi:10.1016/j.ijpsycho.2015.02.003

Hu, H., Vervaeke, K., & Storm, J. F. (2002). Two forms of electrical resonance at theta frequencies, generated by M-current, h-current and persistent Na+ current in rat hippocampal pyramidal cells. The Journal of physiology, 545(Pt 3), 783-805.

Huang, W. A., Stitt, I. M., Negahbani, E., Passey, D. J., Ahn, S., Davey, M., . . . Fröhlich, F. (2021). Transcranial alternating current stimulation entrains alpha oscillations by preferential phase

synchronization of fast-spiking cortical neurons to stimulation waveform. Nat Commun, 12(1), 3151. doi:10.1038/s41467-021-23021-2

Huang, Y., Liu, A. A., Lafon, B., Friedman, D., Dayan, M., Wang, X., . . . Parra, L. C. (2017). Measurements and models of electric fields in the in vivo human brain during transcranial electric stimulation. Elife, 6, e18834.

Hutcheon, B., & Yarom, Y. (2000). Resonance, oscillation and the intrinsic frequency preferences of neurons. Trends in neurosciences, 23(5), 216-222.

Izhikevich, E. M. (2007). Dynamical systems in neuroscience: MIT press.

Izhikevich, E. M., & Edelman, G. M. (2008). Large-scale model of mammalian thalamocortical systems. Proceedings of the national academy of sciences, 105(9), 3593-3598.

Juczewski, K., Koussa, J. A., Kesner, A. J., Lee, J. O., & Lovinger, D. M. (2020). Stress and behavioral correlates in the head-fixed method: stress measurements, habituation dynamics, locomotion, and motor-skill learning in mice. Scientific reports, 10(1), 12245. doi:10.1038/s41598-020-69132-6

Kasten, F. H., & Herrmann, C. S. (2017). Transcranial Alternating Current Stimulation (tACS) Enhances Mental Rotation Performance during and after Stimulation. Frontiers in human neuroscience, 11, 2-2. doi:10.3389/fnhum.2017.00002

Kasten, F. H., & Herrmann, C. S. (2017). Transcranial alternating current stimulation (tACS) enhances mental rotation performance during and after stimulation. Frontiers in Human Neuroscience, 11.

Khoshkhoo, S., Vogt, D., & Sohal, V. S. (2017). Dynamic, Cell-Type-Specific Roles for GABAergic Interneurons in a Mouse Model of Optogenetically Inducible Seizures. Neuron, 93(2), 291-298. doi:10.1016/j.neuron.2016.11.043

Kim, H., Ährlund-Richter, S., Wang, X., Deisseroth, K., & Carlén, M. (2016). Prefrontal Parvalbumin Neurons in Control of Attention. Cell, 164(1-2), 208-218. doi:10.1016/j.cell.2015.11.038

Kim, S.-Y., Adhikari, A., Lee, S. Y., Marshel, J. H., Kim, C. K., Mallory, C. S., . . . Lim, B. K. (2013). Diverging neural pathways assemble a behavioural state from separable features in anxiety. Nature, 496(7444), 219-223.

Koch, C., Massimini, M., Boly, M., & Tononi, G. (2016). Neural correlates of consciousness: progress and problems. Nature Reviews: Neuroscience, 17(5), 307-321. doi:10.1038/nrn.2016.22

Kopell, N., Ermentrout, G. B., Whittington, M. A., & Traub, R. D. (2000). Gamma rhythms and beta rhythms have different synchronization properties. Proc Natl Acad Sci U S A, 97(4), 1867-1872.

Krause, B., Márquez-Ruiz, J., & Cohen Kadosh, R. (2013). The effect of transcranial direct current stimulation: a role for cortical excitation/inhibition balance? Frontiers in Human Neuroscience, 7, 602.

Krause, M. R., Vieira, P. G., Csorba, B. A., Pilly, P. K., & Pack, C. C. (2019). Transcranial alternating current stimulation entrains single-neuron activity in the primate brain. Proceedings of the National Academy of Sciences, 116(12), 5747-5755. doi:10.1073/pnas.1815958116

Kumar, R. J., Rajasekhar, E., Subhan, C., Panduranga, P., & Gupta, N. (2014). Dielectric Studies of Acrylic Resin, Alginate, Dental Plaster, Dental Stone, Glass Ionomer and Silver Amalgam. Indian Journal of Advances in Chemical Science, 2(2), 98-103.

Laakso, I., & Hirata, A. (2013). Computational analysis shows why transcranial alternating current stimulation induces retinal phosphenes. J Neural Eng, 10(4), 046009. doi:10.1088/1741-2560/10/4/046009

Lachaux, J.-P., Rodriguez, E., Martinerie, J., & Varela, F. J. (1999). Measuring phase synchrony in brain signals. Human Brain Mapping, 8(4), 194-208.

Lachaux, J. P., Rodriguez, E., Martinerie, J., & Varela, F. J. (1999). Measuring phase synchrony in brain signals. Hum Brain Mapp, 8(4), 194-208.

Lafon, B., Henin, S., Huang, Y., Friedman, D., Melloni, L., Thesen, T., . . . Parra, L. C. (2017). Low frequency transcranial electrical stimulation does not entrain sleep rhythms measured by human intracranial recordings. Nature Communications, 8(1), 1199.

Langner, R., & Eickhoff, S. B. (2013). Sustaining attention to simple tasks: a meta-analytic review of the neural mechanisms of vigilant attention. Psychol Bull, 139(4), 870-900. doi:10.1037/a0030694

Lee, J., & Park, S. (2006). The role of stimulus salience in CPT-AX performance of schizophrenia patients. Schizophrenia Research, 81(2), 191-197.

Lefebvre, J., Hutt, A., & Frohlich, F. (2017). Stochastic resonance mediates the state-dependent effect of periodic stimulation on cortical alpha oscillations. eLife, 6, e32054.

Levinoff, E. J., Saumier, D., & Chertkow, H. (2005). Focused attention deficits in patients with Alzheimer's disease and mild cognitive impairment. Brain and cognition, 57(2), 127-130.

Lewin, J. S., Friedman, L., Wu, D., Miller, D. A., Thompson, L. A., Klein, S. K., . . . Duerk, J. L. (1996). Cortical Localization of Human Sustained Attention: Detection with Functional MR Using a Visual Vigilance Paradigm. Journal of Computer Assisted Tomography, 20(5), 695-701.

Li, G., Henriquez, C. S., & Fröhlich, F. (2017a). Unified thalamic model generates multiple distinct oscillations with state-dependent entrainment by stimulation. PLoS Computational Biology, 13(10), e1005797.

Li, G., Henriquez, C. S., & Fröhlich, F. (2017b). Unified thalamic model generates multiple distinct oscillations with state-dependent entrainment by stimulation. PLoS Comput. Biol., 13(10), e1005797. doi:10.1371/journal.pcbi.1005797

Li, G., Henriquez, C. S., & Fröhlich, F. (2018). Rhythmic Modulation of Thalamic Oscillations Depends on Intrinsic Cellular Dynamics. Journal of Neural Engineering.

Li, X., Sroubek, A., Kelly, M. S., Lesser, I., Sussman, E., He, Y., . . . Foxe, J. J. (2012). Atypical pulvinar–cortical pathways during sustained attention performance in children with attention-deficit/hyperactivity disorder. Journal of the American Academy of Child & Adolescent Psychiatry, 51(11), 1197-1207. e1194.

Liebe, S., Hoerzer, G. M., Logothetis, N. K., & Rainer, G. (2012). Theta coupling between V4 and prefrontal cortex predicts visual short-term memory performance. Nat Neurosci, 15(3), 456-462, S451-452. doi:10.1038/nn.3038

Lisman, J. (2005). The theta/gamma discrete phase code occuring during the hippocampal phase precession may be a more general brain coding scheme. Hippocampus, 15(7), 913-922. doi:10.1002/hipo.20121

Lisman, J. E., & Jensen, O. (2013). The theta-gamma neural code. Neuron, 77(6), 1002-1016. doi:10.1016/j.neuron.2013.03.007

Liu, A., Vöröslakos, M., Kronberg, G., Henin, S., Krause, M. R., Huang, Y., . . . Krekelberg, B. (2018). Immediate neurophysiological effects of transcranial electrical stimulation. Nature Communications, 9(1), 5092.

Liu, S. K., Chiu, C.-H., Chang, C.-J., Hwang, T.-J., Hwu, H.-G., & Chen, W. J. (2002). Deficits in sustained attention in schizophrenia and affective disorders: stable versus state-dependent markers. American Journal of Psychiatry, 159(6), 975-982.

Lustenberger, C., Boyle, M. R., Alagapan, S., Mellin, J. M., Vaughn, B. V., & Frohlich, F. (2016). Feedback-Controlled Transcranial Alternating Current Stimulation Reveals a Functional Role of Sleep Spindles in Motor Memory Consolidation. Curr Biol, 26(16), 2127-2136. doi:10.1016/j.cub.2016.06.044

Manger, P. R., Masiello, I., & Innocenti, G. M. (2002). Areal Organization of the Posterior Parietal Cortex of the Ferret (Mustela putorius). Cerebral Cortex, 12(12), 1280-1297. doi:10.1093/cercor/12.12.1280

Marquez-Ruiz, J., Leal-Campanario, R., Sanchez-Campusano, R., Molaee-Ardekani, B., Wendling, F., Miranda, P. C., . . . Delgado-Garcia, J. M. (2012). Transcranial direct-current stimulation modulates synaptic mechanisms involved in associative learning in behaving rabbits. Proc Natl Acad Sci U S A, 109(17), 6710-6715. doi:10.1073/pnas.1121147109

Mazzoni, A., Lindén, H., Cuntz, H., Lansner, A., Panzeri, S., & Einevoll, G. T. (2015). Computing the Local Field Potential (LFP) from Integrate-and-Fire Network Models. PLoS computational biology, 11(12), e1004584. doi:10.1371/journal.pcbi.1004584

McAlonan, K., Cavanaugh, J., & Wurtz, R. H. (2008). Guarding the gateway to cortex with attention in visual thalamus. Nature, 456(7220), 391-394.

Miranda, P. C., Lomarev, M., & Hallett, M. (2006). Modeling the current distribution during transcranial direct current stimulation. Clinical Neurophysiology, 117(7), 1623-1629.

Miranda, P. C., Mekonnen, A., Salvador, R., & Ruffini, G. (2013). The electric field in the cortex during transcranial current stimulation. Neuroimage, 70, 48-58. doi:10.1016/j.neuroimage.2012.12.034

Molaee-Ardekani, B., Márquez-Ruiz, J., Merlet, I., Leal-Campanario, R., Gruart, A., Sánchez-Campusano, R., . . . Wendling, F. (2013). Effects of transcranial Direct Current Stimulation (tDCS) on cortical activity: a computational modeling study. Brain stimulation, 6(1), 25-39.

Moliadze, V., Antal, A., & Paulus, W. (2010). Boosting brain excitability by transcranial high frequency stimulation in the ripple range. The Journal of Physiology, 588(24), 4891-4904.

Moret, B., Donato, R., Nucci, M., Cona, G., & Campana, G. (2019). Transcranial random noise stimulation (tRNS): a wide range of frequencies is needed for increasing cortical excitability. Scientific reports, 9(1), 15150. doi:10.1038/s41598-019-51553-7

Morrell, M. J. (2011). Responsive cortical stimulation for the treatment of medically intractable partial epilepsy. Neurology, 77(13), 1295-1304.

Negahbani, E., Kasten, F. H., Herrmann, C. S., & Fröhlich, F. (2018). Targeting alpha-band oscillations in a cortical model with amplitude-modulated high-frequency transcranial electric stimulation. Neuroimage, 173, 3-12.

Negahbani, E., Stitt, I. M., Davey, M., Doan, T. T., Dannhauer, M., Hoover, A. C., . . . Fröhlich, F. (2019). Transcranial Alternating Current Stimulation (tACS) Entrains Alpha Oscillations by Preferential Phase Synchronization of Fast-Spiking Cortical Neurons to Stimulation Waveform. BioRxiv, 563163. doi:10.1101/563163

Neuling, T., Rach, S., & Herrmann, C. S. (2013). Orchestrating neuronal networks: sustained after-effects of transcranial alternating current stimulation depend upon brain states. Frontiers in Human Neuroscience, 7, 161.

Nitsche, M. A., & Paulus, W. (2000). Excitability changes induced in the human motor cortex by weak transcranial direct current stimulation. The Journal of physiology, 527 Pt 3, 633-639.

Noury, N., Hipp, J. F., & Siegel, M. (2016). Physiological processes non-linearly affect electrophysiological recordings during transcranial electric stimulation. Neuroimage, 140(Supplement C), 99-109. doi:https://doi.org/10.1016/j.neuroimage.2016.03.065

Noury, N., Hipp, J. F., & Siegel, M. (2016). Physiological processes non-linearly affect electrophysiological recordings during transcranial electric stimulation. Neuroimage, 140, 99-109.

Noury, N., & Siegel, M. (2017). Phase properties of transcranial electrical stimulation artifacts in electrophysiological recordings. Neuroimage, 158, 406-416.

Noury, N., & Siegel, M. (2018). Analyzing EEG and MEG signals recorded during tES, a reply. Neuroimage, 167, 53-61.

Nuechterlein, K. H., Green, M. F., Calkins, M. E., Greenwood, T. A., Gur, R. E., Gur, R. C., . . . Seidman, L. J. (2015). Attention/vigilance in schizophrenia: performance results from a large multi-site study of the Consortium on the Genetics of Schizophrenia (COGS). Schizophrenia research, 163(1), 38-46.

Okun, M., Steinmetz, N. A., Cossell, L., Iacaruso, M. F., Ko, H., Barthó, P., . . . Carandini, M. (2015). Diverse coupling of neurons to populations in sensory cortex. Nature, 521(7553), 511.

Olson, C. R., & Musil, S. Y. (1992). Topographic organization of cortical and subcortical projections to posterior cingulate cortex in the cat: evidence for somatic, ocular, and complex subregions. J Comp Neurol, 324(2), 237-260. doi:10.1002/cne.903240207

Opitz, A., Falchier, A., Yan, C.-G., Yeagle, E. M., Linn, G. S., Megevand, P., . . . Schroeder, C. E. (2016). Spatiotemporal structure of intracranial electric fields induced by transcranial electric stimulation in humans and nonhuman primates. Scientific Reports, 6, 31236.

Ozen, S., Sirota, A., Belluscio, M. A., Anastassiou, C. A., Stark, E., Koch, C., & Buzsaki, G. (2010). Transcranial electric stimulation entrains cortical neuronal populations in rats. The Journal of neuroscience, 30(34), 11476-11485. doi:10.1523/JNEUROSCI.5252-09.2010

Pachitariu, M., Steinmetz, N. A., Kadir, S. N., Carandini, M., & Harris, K. D. (2016). Fast and accurate spike sorting of high-channel count probes with KiloSort. Paper presented at the Advances in neural information processing systems.

Pagliaccio, D., Wiggins, J. L., Adleman, N. E., Harkins, E., Curhan, A., Towbin, K. E., . . . Leibenluft, E. (2017). Behavioral and neural sustained attention deficits in bipolar disorder and familial risk of bipolar disorder. Biological psychiatry, 82(9), 669-678.

Palva, J. M., Palva, S., & Kaila, K. (2005). Phase Synchrony among Neuronal Oscillations in the Human Cortex. The Journal of Neuroscience, 25(15), 3962-3972. doi:10.1523/jneurosci.4250-04.2005

Palva, S., & Palva, J. M. (2011). Functional Roles of Alpha-Band Phase Synchronization in Local and Large-Scale Cortical Networks. Frontiers in Psychology, 2(204). doi:10.3389/fpsyg.2011.00204

Petersen, S. E., & Posner, M. I. (2012). The attention system of the human brain: 20 years after. Annual review of neuroscience, 35, 73-89.

Pikhovych, A., Stolberg, N. P., Jessica Flitsch, L., Walter, H. L., Graf, R., Fink, G. R., . . . Rueger, M. A. (2016). Transcranial Direct Current Stimulation Modulates Neurogenesis and Microglia Activation in the Mouse Brain. Stem Cells Int, 2016, 2715196. doi:10.1155/2016/2715196

Pikovsky, A., Kurths, J., Rosenblum, M., & Kurths, J. (2003). Synchronization: a universal concept in nonlinear sciences (Vol. 12): Cambridge university press.

Pikovsky, A., Rosenblum, M., & Kurths, J. (2003). Synchronization: a universal concept in nonlinear sciences (Vol. 12): Cambridge university press.

Polanía, R., Nitsche, M. A., Korman, C., Batsikadze, G., & Paulus, W. (2012). The importance of timing in segregated theta phase-coupling for cognitive performance. Current Biology, 22(14), 1314-1318.

Purpura, D. P., & McMurtry, J. G. (1965). Intracellular Activities and Evoked Potential Changes during Polarization of Motor Cortex. Journal of neurophysiology, 28, 166-185.

Purushothaman, G., Marion, R., Li, K., & Casagrande, V. A. (2012). Gating and control of primary visual cortex by pulvinar. Nat Neurosci, 15(6), 905-912. doi:10.1038/nn.3106

Raco, V., Bauer, R., Olenik, M., Brkic, D., & Gharabaghi, A. (2014). Neurosensory effects of transcranial alternating current stimulation. Brain Stimul, 7(6), 823-831. doi:10.1016/j.brs.2014.08.005

Raczkowski, D., & Rosenquist, A. C. (1983). Connections of the multiple visual cortical areas with the lateral posterior-pulvinar complex and adjacent thalamic nuclei in the cat. J Neurosci, 3(10), 1912-1942.

Radman, T., Ramos, R. L., Brumberg, J. C., & Bikson, M. (2009). Role of cortical cell type and morphology in subthreshold and suprathreshold uniform electric field stimulation in vitro. Brain stimulation, 2(4), 215-228. e213.

Radman, T., Ramos, R. L., Brumberg, J. C., & Bikson, M. (2009). Role of cortical cell type and morphology in subthreshold and suprathreshold uniform electric field stimulation in vitro. Brain Stimul, 2(4), 215-228, 228 e211-213. doi:10.1016/j.brs.2009.03.007

Radman, T., Su, Y., An, J. H., Parra, L. C., & Bikson, M. (2007). Spike timing amplifies the effect of electric fields on neurons: implications for endogenous field effects. The Journal of neuroscience, 27(11), 3030-3036.

Radtke-Schuller, S. (2018). Cyto- and Myeloarchitectural Brain Atlas of the Ferret (Mustela putorius) in MRI Aided Stereotaxic Coordinates (1 ed.): Springer International Publishing.

Rakic, P., & Lombroso, P. J. (1998). Development of the cerebral cortex: I. Forming the cortical structure. Journal of the American Academy of Child & Adolescent Psychiatry, 37(1), 116-117.

Rana, K. D., & Vaina, L. M. (2014). Functional roles of 10 Hz alpha-band power modulating engagement and disengagement of cortical networks in a complex visual motion task. PLoS One, 9(10), e107715-e107715. doi:10.1371/journal.pone.0107715

Reato, D., Bikson, M., & Parra, L. C. (2015). Lasting modulation of in vitro oscillatory activity with weak direct current stimulation. Journal of neurophysiology, 113(5), 1334-1341. doi:10.1152/jn.00208.2014

Reato, D., Rahman, A., Bikson, M., & Parra, L. C. (2010). Low-intensity electrical stimulation affects network dynamics by modulating population rate and spike timing. Journal of Neuroscience, 30(45), 15067-15079.

Reato, D., Rahman, A., Bikson, M., & Parra, L. C. (2010a). Low-intensity electrical stimulation affects network dynamics by modulating population rate and spike timing. The Journal of neuroscience : the official journal of the Society for Neuroscience, 30(45), 15067-15079. doi:10.1523/JNEUROSCI.2059-10.2010

Reato, D., Rahman, A., Bikson, M., & Parra, L. C. (2010b). Low-intensity electrical stimulation affects network dynamics by modulating population rate and spike timing. J Neurosci, 30(45), 15067-15079. doi:30/45/15067 [pii]10.1523/JNEUROSCI.2059-10.2010

Reato, D., Rahman, A., Bikson, M., & Parra, L. C. (2013). Effects of weak transcranial alternating current stimulation on brain activity—a review of known mechanisms from animal studies. Frontiers in Human Neuroscience, 7, 687.

Riccio, C. A., Reynolds, C. R., Lowe, P., & Moore, J. J. (2002). The continuous performance test: a window on the neural substrates for attention? Archives of Clinical Neuropsychology, 17(3), 235-272. doi:http://dx.doi.org/10.1016/S0887-6177(01)00111-1

Riddle, J., McPherson, T., Atkins, A. K., Walker, C., Ahn, S., & Frohlich, F. Brain-derived neurotrophic factor (BDNF) polymorphism may influence the efficacy of tACS to modulate neural oscillations. Brain Stimulation: Basic, Translational, and Clinical Research in Neuromodulation. doi:10.1016/j.brs.2020.04.012

Robbins, T. (2002). The 5-choice serial reaction time task: behavioural pharmacology and functional neurochemistry. Psychopharmacology, 163(3-4), 362-380.

Rohan, J. G., Carhuatanta, K. A., McInturf, S. M., Miklasevich, M. K., & Jankord, R. (2015). Modulating Hippocampal Plasticity with In Vivo Brain Stimulation. The Journal of neuroscience : the official

journal of the Society for Neuroscience, 35(37), 12824-12832. doi:10.1523/JNEUROSCI.2376-15.2015

Roth, M. M., Dahmen, J. C., Muir, D. R., Imhof, F., Martini, F. J., & Hofer, S. B. (2016). Thalamic nuclei convey diverse contextual information to layer 1 of visual cortex. Nat Neurosci, 19(2), 299-307. doi:10.1038/nn.4197

Roth, M. M., Dahmen, J. C., Muir, D. R., Imhof, F., Martini, F. J., & Hofer, S. B. (2016). Thalamic nuclei convey diverse contextual information to layer 1 of visual cortex. Nat Neurosci, 19(2), 299.

Saalmann, Y. B., Pinsk, M. A., Wang, L., Li, X., & Kastner, S. (2012). The pulvinar regulates information transmission between cortical areas based on attention demands. Science, 337(6095), 753-756. doi:10.1126/science.1223082

Saalmann, Y. B., Pinsk, M. A., Wang, L., Li, X., & Kastner, S. (2012). The pulvinar regulates information transmission between cortical areas based on attention demands. Science, 337(6095), 753-756.

Sadleir, R. J., Vannorsdall, T. D., Schretlen, D. J., & Gordon, B. (2010). Transcranial direct current stimulation (tDCS) in a realistic head model. Neuroimage, 51(4), 1310-1318.

Sahlem, G. L., Badran, B. W., Halford, J. J., Williams, N. R., Korte, J. E., Leslie, K., . . . Bachman, D. L. (2015). Oscillating square wave transcranial direct current stimulation (tDCS) delivered during slow wave sleep does not improve declarative memory more than sham: a randomized sham controlled crossover study. Brain stimulation, 8(3), 528-534.

Sanchez-Vives, M. V., & McCormick, D. A. (2000). Cellular and network mechanisms of rhythmic recurrent activity in neocortex. Nature neuroscience, 3(10), 1027-1034. doi:10.1038/79848

Sandran, N., Hillier, S., & Hordacre, B. (2019). Strategies to implement and monitor in-home transcranial electrical stimulation in neurological and psychiatric patient populations: a systematic review. Journal of NeuroEngineering and Rehabilitation, 16(1), 58. doi:10.1186/s12984-019-0529-5

Sarter, M., Givens, B., & Bruno, J. P. (2001). The cognitive neuroscience of sustained attention: where top-down meets bottom-up. Brain Research Reviews, 35(2), 146-160.

Saturnino, G. B., Puonti, O., Nielsen, J. D., Antonenko, D., Madsen, K. H., & Thielscher, A. (2019). SimNIBS 2.1: a comprehensive pipeline for individualized electric field modelling for transcranial brain stimulation. Brain and human body modeling, 3-25.

Scangos, K. W., Makhoul, G. S., Sugrue, L. P., Chang, E. F., & Krystal, A. D. (2021). State-dependent responses to intracranial brain stimulation in a patient with depression. Nature Medicine, 27(2), 229-231. doi:10.1038/s41591-020-01175-8

Schmidt, S. L., Iyengar, A. K., Foulser, A. A., Boyle, M. R., & Frohlich, F. (2014). Endogenous cortical oscillations constrain neuromodulation by weak electric fields. Brain Stimul, 7(6), 878-889. doi:10.1016/j.brs.2014.07.033

Schmidt, S. L., Iyengar, A. K., Foulser, A. A., Boyle, M. R., & Fröhlich, F. (2014). Endogenous cortical oscillations constrain neuromodulation by weak electric fields. Brain stimulation, 7(6), 878-889.

Scolari, M., Seidl-Rathkopf, K. N., & Kastner, S. (2015). Functions of the human frontoparietal attention network: Evidence from neuroimaging. Current Opinion in Behavioral Sciences, 1, 32-39. doi:https://doi.org/10.1016/j.cobeha.2014.08.003

Sellers, K. K., Yu, C., Zhou, Z. C., Stitt, I., Li, Y., Radtke-Schuller, S., . . . Fröhlich, F. (2016). Oscillatory dynamics in the frontoparietal attention network during sustained attention in the ferret. Cell reports, 16(11), 2864-2874. doi:10.1016/j.celrep.2016.08.055

Siegel, M., Donner, T. H., & Engel, A. K. (2012). Spectral fingerprints of large-scale neuronal interactions. Nature Reviews: Neuroscience, 13(2), 121-134. doi:10.1038/nrn3137

Singer, W. (1999). Neuronal synchrony: a versatile code for the definition of relations? Neuron, 24(1), 49-65, 111-125.

So, P. P. M., Stuchly, M. A., & Nyenhuis, J. A. (2004). Peripheral nerve stimulation by gradient switching fields in magnetic resonance imaging. IEEE Transactions on Biomedical Engineering, 51(11), 1907-1914. doi:10.1109/TBME.2004.834251

Sousa, A. M., Meyer, K. A., Santpere, G., Gulden, F. O., & Sestan, N. (2017). Evolution of the human nervous system function, structure, and development. Cell, 170(2), 226-247.

Spellman, T., Rigotti, M., Ahmari, S. E., Fusi, S., Gogos, J. A., & Gordon, J. A. (2015). Hippocampal-prefrontal input supports spatial encoding in working memory. Nature, 522(7556), 309-314.

Sporns, O., Tononi, G., & Edelman, G. M. (2000). Connectivity and complexity: the relationship between neuroanatomy and brain dynamics. Neural Netw, 13(8-9), 909-922.

Steels, A. (2008). Grade Data Sheet 303. In A. Steels (Ed.).

Steinberg, E. E., Christoffel, D. J., Deisseroth, K., & Malenka, R. C. (2015). Illuminating circuitry relevant to psychiatric disorders with optogenetics. Curr Opin Neurobiol, 30, 9-16. doi:10.1016/j.conb.2014.08.004

Stimberg, M., Brette, R., & Goodman, D. F. M. (2019). Brian 2, an intuitive and efficient neural simulator. Elife, 8, e47314. doi:10.7554/eLife.47314

Stitt, I., Zhou, Z. C., Radtke-Schuller, S., & Fröhlich, F. (2018). Arousal dependent modulation of thalamo-cortical functional interaction. Nat Commun, 9(1), 2455. doi:10.1038/s41467-018-04785-6

Szczepanski, S. M., Pinsk, M. A., Douglas, M. M., Kastner, S., & Saalmann, Y. B. (2013). Functional and structural architecture of the human dorsal frontoparietal attention network. Proc Natl Acad Sci U S A, 110(39), 15806-15811. doi:10.1073/pnas.1313903110

Taktakishvili, O., Sivan-Loukianova, E., Kultas-Ilinsky, K., & Ilinsky, I. A. (2002). Posterior parietal cortex projections to the ventral lateral and some association thalamic nuclei in Macaca mulatta. Brain Res Bull, 59(2), 135-150.

Tallon-Baudry, C., Bertrand, O., Delpuech, C., & Pernier, J. (1996). Stimulus specificity of phase-locked and non-phase-locked 40 Hz visual responses in human. Journal of Neuroscience, 16(13), 4240-4249.

Terzuolo, C. A., & Bullock, T. H. (1956). Measurement of Imposed Voltage Gradient Adequate to Modulate Neuronal Firing. Proc Natl Acad Sci U S A, 42(9), 687-694.

Thielscher, A., Opitz, A., & Windhoff, M. (2011). Impact of the gyral geometry on the electric field induced by transcranial magnetic stimulation. Neuroimage, 54(1), 234-243. doi:10.1016/j.neuroimage.2010.07.061

Toloza, E. H., Negahbani, E., & Frohlich, F. (2017). Ih Interacts with Somato-Dendritic Structure to Determine Frequency Response to Weak Alternating Electric Field Stimulation. Journal of Neurophysiology, 119.3, 1029-1036.

Toloza, E. H. S., Negahbani, E., & Fröhlich, F. (2018). Ih interacts with somato-dendritic structure to determine frequency response to weak alternating electric field stimulation. J Neurophysiol, 119(3), 1029-1036. doi:10.1152/jn.00541.2017

Tucha, L., Fuermaier, A. B., Koerts, J., Buggenthin, R., Aschenbrenner, S., Weisbrod, M., . . . Tucha, O. (2017). Sustained attention in adult ADHD: Time-on-task effects of various measures of attention. Journal of Neural Transmission, 124(1), 39-53.

Turner, K. M., Peak, J., & Burne, T. H. J. (2015). Measuring Attention in Rodents: Comparison of a Modified Signal Detection Task and the 5-Choice Serial Reaction Time Task. Frontiers in Behavioral Neuroscience, 9, 370. doi:10.3389/fnbeh.2015.00370

Tustison, N. J., Avants, B. B., Cook, P. A., Zheng, Y., Egan, A., Yushkevich, P. A., & Gee, J. C. (2010). N4ITK: improved N3 bias correction. IEEE Transactions on Medical Imaging, 29(6), 1310-1320.

Tye, K. M., & Deisseroth, K. (2012). Optogenetic investigation of neural circuits underlying brain disease in animal models. Nature Reviews Neuroscience, 13(4), 251-266.

Uehara, T., Yamasaki, T., Okamoto, T., Koike, T., Kan, S., Miyauchi, S., . . . Tobimatsu, S. (2014). Efficiency of a "small-world" brain network depends on consciousness level: a resting-state FMRI study. Cereb Cortex, 24(6), 1529-1539. doi:10.1093/cercor/bht004

Uhlhaas, P. J., Haenschel, C., Nikolic, D., & Singer, W. (2008). The role of oscillations and synchrony in cortical networks and their putative relevance for the pathophysiology of schizophrenia. Schizophr Bull, 34(5), 927-943. doi:10.1093/schbul/sbn062

Urban, D. J., & Roth, B. L. (2015). DREADDs (designer receptors exclusively activated by designer drugs): chemogenetic tools with therapeutic utility. Annu Rev Pharmacol Toxicol, 55, 399-417. doi:10.1146/annurev-pharmtox-010814-124803

Vieira, P. G., Krause, M. R., & Pack, C. C. (2019). tACS entrains neural activity while somatosensory input is blocked. BioRxiv, 691022. doi:10.1101/691022

von Stein, A., Chiang, C., & Konig, P. (2000). Top-down processing mediated by interareal synchronization. Proc Natl Acad Sci U S A, 97(26), 14748-14753. doi:10.1073/pnas.97.26.14748

von Stein, A., & Sarnthein, J. (2000). Different frequencies for different scales of cortical integration: from local gamma to long range alpha/theta synchronization. Int J Psychophysiol, 38(3), 301-313.

Vöröslakos, M., Takeuchi, Y., Brinyiczki, K., Zombori, T., Oliva, A., Fernández-Ruiz, A., . . . Berényi, A. (2018). Direct effects of transcranial electric stimulation on brain circuits in rats and humans. Nat Commun, 9(1), 483. doi:10.1038/s41467-018-02928-3

Vossen, A., Gross, J., & Thut, G. (2015). Alpha Power Increase After Transcranial Alternating Current Stimulation at Alpha Frequency (alpha-tACS) Reflects Plastic Changes Rather Than Entrainment. Brain Stimul, 8(3), 499-508. doi:10.1016/j.brs.2014.12.004

Vossen, A., Gross, J., & Thut, G. (2015). Alpha Power Increase After Transcranial Alternating Current Stimulation at Alpha Frequency (α-tACS) Reflects Plastic Changes Rather Than Entrainment. Brain Stimul, 8(3), 499-508. doi:10.1016/j.brs.2014.12.004

Williams, J. H., & Kauer, J. A. (1997). Properties of carbachol-induced oscillatory activity in rat hippocampus. Journal of neurophysiology, 78(5), 2631-2640.

Witkowski, M., Garcia-Cossio, E., Chander, B. S., Braun, C., Birbaumer, N., Robinson, S. E., & Soekadar, S. R. (2016). Mapping entrained brain oscillations during transcranial alternating current stimulation (tACS). Neuroimage, 140, 89-98. doi:10.1016/j.neuroimage.2015.10.024

Wolff, S. B., & Ölveczky, B. P. (2018). The promise and perils of causal circuit manipulations. Curr Opin Neurobiol, 49, 84-94. doi:10.1016/j.conb.2018.01.004

Yu, C., Sellers, K. K., Radtke-Schuller, S., Lu, J., Xing, L., Ghukasyan, V., . . . Fröhlich, F. (2016). Structural and functional connectivity between the lateral posterior–pulvinar complex and primary visual cortex in the ferret. European Journal of Neuroscience, 43(2), 230-244.

Zaehle, T., Rach, S., & Herrmann, C. S. (2010). Transcranial alternating current stimulation enhances individual alpha activity in human EEG. PloS One, 5(11), e13766.

Zar, J. H. (1999). Biostatistical analysis: Pearson Education India.

Zhou, H., Schafer, R. J., & Desimone, R. (2016). Pulvinar-Cortex Interactions in Vision and Attention. Neuron, 89(1), 209-220. doi:10.1016/j.neuron.2015.11.034

Zhou, Y., & Freedman, D. J. (2019). Posterior parietal cortex plays a causal role in perceptual and categorical decisions. Science, 365(6449), 180-185. doi:doi:10.1126/science.aaw8347

Zhou, Z. C., Salzwedel, A. P., Radtke-Schuller, S., Li, Y., Sellers, K. K., Gilmore, J. H., . . . Gao, W. (2016). Resting state network topology of the ferret brain. Neuroimage, 143, 70-81. doi:10.1016/j.neuroimage.2016.09.003

Zhou, Z. C., Yu, C., Sellers, K. K., & Fröhlich, F. (2016). Dorso-lateral frontal cortex of the ferret encodes perceptual difficulty during visual discrimination. Scientific reports, 6, srep23568.

CHAPTER 2: CAUSAL OSCILLATIONS IN THE HIGHER-ORDER THALAMO-CORTICAL NETWORK IN SUSTAINED ATTENTION[1]

INTRODUCTION

Sustained attention is crucial for our survival and cognitive development, from capturing errors in routine work to responding to emergencies while driving (Fortenbaugh, DeGutis, & Esterman, 2017). This process allows the brain to allocate cognitive resources to respond to infrequent, but task-relevant stimuli over an extended period of time (Martin Sarter, Ben Givens, & John P Bruno, 2001). Dysfunction of this process is linked to attention deficit and impulsivity in many psychiatric disorders (Barkley, 1997; Bora, Vahip, & Akdeniz, 2006; Liu et al., 2002; Nuechterlein et al., 2015; Pagliaccio et al., 2017; Tucha et al., 2017). Unlike the bottom-up attention driven by the presentation of a stimulus, sustained attention is a form of attentional control that stresses the maintenance of focus in anticipation of a goal-related stimulus prior to its presentation (Cuthbert & Insel, 2013). This process requires the coordination of the sensory cortices and the higher-order brain regions for top-down control and sensory gating (Clayton, Yeung, & Cohen Kadosh, 2015). This moment-to-moment control can be modeled using network oscillations which represents an important mechanism through which different brain regions communicate and implement cognitive functions (Clayton et al., 2015; Ward, 2003).

A candidate circuit for the top-down control of sustained attention is the higher-order thalamo-cortical visual circuit (Bourgeois, Guedj, Carrera, & Vuilleumier, 2020; Eradath, Pinsk, & Kastner, 2021; Kastner, Fiebelkorn, & Eradath, 2020). Cortical oscillations have been widely implicated in attention, especially serving the role of a top-down control signal generated in the fronto-parietal network (Buschman & Miller, 2007; Scolari, Seidl-Rathkopf, & Kastner, 2015; Sellers et al., 2016). Such cortico-cortical

[1] This chapter is under preparation for submission

synchronization may be driven by subcortical structures such as the higher-order visual thalamus which mediates sensory gating and attentional modulation. Anatomically, the primate pulvinar has highly specialized subdivisions that are reciprocally connected to the visual cortex, superior colliculus, prefrontal cortex, parietal association cortex, and temporal lobe (Kaas & Lyon, 2007). Thus the pulvinar is ideally situated to act as a major hub and potential synchronizer of cortical activity. Functionally, the pulvinar serves an important role as a secondary visual system (Ohye, 2002) and coordinates cortical activity during visual attention behavior (Bourgeois et al., 2020; Eradath et al., 2021; Kastner et al., 2020; McAlonan, Cavanaugh, & Wurtz, 2008; Saalmann, Pinsk, Wang, Li, & Kastner, 2012). In primates, pulvinar activity was found to help predict visual responsiveness and high-frequency synchronous activity in V4 (Zhou, Schafer, & Desimone, 2016) and was reported to synchronize the activity of interconnected V4 and temporo-occipital cortex during the delay period in a visuospatial attention task (Saalmann et al., 2012). Moreover, structural abnormalities in the pulvinar were found to be related to atypical pulvinar-cortical functional connectivity and attention deficits in people with ADHD (Li et al., 2012)**.** Together, these studies suggest a fundamental role of thalamic oscillations in coordinating and modulating cortical activity during attentional tasks. However, it remains unclear to what extent pulvinar activation and interaction with cortical areas represents an epiphenomenon or an actual causal mechanism. Here, we hypothesized that high-order thalamic oscillations modulate thalamo-cortical and cortico-cortical communication in a frequency-specific way to causally facilitate sustained visual attention.

To test this hypothesis, we combined frequency-specific optogenetic targeting of rhythmic activity in the higher-order visual thalamo-cortical network with multisite electrophysiology in ferrets performing a sustained attention task. We found thalamic theta oscillations and functional connectivity with the cortex to be associated with sustained attention. Optogenetic stimulation of the higher-order visual thalamus modulated not only rhythmic thalamic activity but also thalamo-cortical and cortico-cortical functional interactions when compared to sham stimulation. Importantly, optogenetic stimulation in theta but not alpha frequency improved task performance, and this improvement correlated with stimulation-induced

enhancement of theta oscillation in the posterior visual thalamo-cortical network. In summary, rhythmic enhancement of the higher-order visual thalamic activity increased frequency-specific communication in the posterior network and improved sustained attention performance by reducing attentional lapse.

METHODS

Animals

Four adult female ferrets (*Mussel putorius furo,* 16-19 weeks old at the beginning of the experiment, weighing 0.7-1kg, group-housed in a 12hr light/12hr dark cycle, spayed, Marshall BioResources, North Rose, NY) were included in this study. All animal procedures were performed in compliance with the National Institute of Health guide for the care and use of laboratory animals (NIH Publications 8th edition, 2011), and were approved by the Institutional Animal Care and Use Committee of the University of North Carolina at Chapel Hill, and the United States Department of Agriculture (USDA Animal Welfare).

There were 85 sessions of easy level (Animal A = 16, Animal B = 21, Animal C = 21, Animal D = 27) and 42 sessions of hard level (Animal A = 16, Animal C = 12, Animal D = 14, animal B was excluded due to this animal only completed 3 hard level sessions) without optogenetic stimulation. There were another 51 sessions at easy level with optogenetic stimulation (Animal A = 9, Animal B = 11, Animal C = 13, Animal D = 18).

Behavioral Training

A detailed description is in papers (Chunxiu Yu et al., 2016) and (Sellers et al., 2016).

Briefly, each animal was trained individually in a touch-screen-based 5-Choice Serial Reaction Time Task (5-CSRTT) (Bari, Dalley, & Robbins, 2008). There is one difference from the previous paper. To increase the probability of animals facing the screen during the delay period, we installed an IR beam across the chamber in front of the water spout. When the animal is at the spout after initiation, its body would block the IR beam and a new trial would be pending. Only when the animal turned back and unblocked the IR beam, thus correctly facing the screen, the trial and the delay period would start.

There are five main stages of training: 1) Chamber habituation, 2) Touch-reward association, 3) Stimulus-reward association, 4) Task initiation, and 5) 5-CSRTT with delay period. Within each stage, there were substages where the parameters were tuned so that the task difficulty gradually increase. The training stage progressed gradually once the animal met the criteria to move on to the next stage. Animals were trained and tested 1-2 times daily on weekdays during which they were water restricted. Animals were not trained and had free access to water at weekends. During the training and testing, animals received a water reward for correct responses. At the end of each training day, animals also received supplemental water to ensure their total water intake was no less than 60mL/kg/day. Each animal's weight was monitored daily and never dropped below 85%.

Accuracy per session was measured as the main outcome variable (defined as the fraction of trials that the animal touches the correct window over all of the trials completed), together with the reaction time for correct trials.

Virus injection and electrode implantation surgery

The initial induction of anesthesia of each animal was performed by injecting a ketamine/xylazine cocktail (30 mg/kg of ketamine, 1-2 mg/kg of xylazine, intramuscular). After confirming a stable plane of anesthesia by the absence of toe-pinch response, the animal was intubated for subsequent mechanical ventilation with vaporized anesthetic maintenance (0.5–2% isoflurane in 100% oxygen). The animal was administered pain relief medication (meloxicam, 0.2 mg/kg, subcutaneous). The animal was then positioned into a stereotaxic frame, with its head fixed using a mouthpiece and ear bars to ensure the stability of the head throughout the procedure and the precise targeting of studied regions for virus injection and electrode implantation. Coordinates for virus injections and electrode implantations were based on the ferret atlas (Radtke-Schuller, 2018). The vital signs including electroencephalogram, pulse, respiratory rate, partial oxygen concentration, end-tidal CO2, and rectal temperature were continuously monitored and recorded throughout the surgical procedure to maintain the animal in a stable state. Aseptic conditions were maintained during the following surgical procedures. Three craniotomies were performed over the left

hemisphere of dPFC, PPC, and VC. The craniotomy over PPC was enlarged for implant Microelectrode arrays in PPC and optrode in LP/Pul. The dura and pia were removed before virus injection and electrode implantation. Each of the PFC, PPC, VC regions was implanted with a microelectrode array (2 × 8 tungsten electrodes, 35 µm diameter, 5 mm length, 200 µm spacing; a local reference electrode that is 500 µm shorter than recording electrodes Innovative Neurophysiology, Durham, NC) at the depth of around 600 µm. For optogenetic stimulation in LP/Pul, 0.3 µL of viral vector rAAV5-CaMKII-ChR2-mCherry was injected into LP/Pul. Then, an optrode (i.e. a circular electrode array with an optical fiber in the middle) was implanted (electrode tips and optical fibers were implanted 100 and 400 µm above the virus injection site, respectively) (16 channel circular Platinum/Iridium electrode, 125 µm diameter, 10 mm length, 250 µm spacing; fiber optic 9.5 mm length, 200 µm core outer diameter, 0.48 numerical aperture; Microprobes for life science, Gaithersburg, MD). Custom-designed plastic cylinders were implanted around the light fibers to anchor laser cables during behavior and to prevent laser light leakage. Each microelectrode array contained a silver grounding wire that was connected to bone screws on the skull. Additional bone screws were implanted for extra security of the headcap. A headcap was built using dental acrylic (Lang Dental, Wheeling, IL) to secure electrodes and cover the skull and the craniotomy. After hardening of the dental cement, skin and connective tissue were sutured together. Triple antibiotic ointment was applied around the suture to prevent infection. During post-operative care, pain medication (meloxicam, 0.2 mg/kg, subcutaneous) and antibiotics (clavamox, 12.5-13 mg/kg, oral) were given to the animal in addition to regular headcap monitoring and cleaning. The animals recovered with free water access in their home cage for at least a week before retraining and recording.

Animal in vivo recording and optogenetics

After recovery from surgery, animals were retrained on the final level of 5-CSRTT task until they reached stable criteria level (80% accuracy on the easy level) performance again (which took about 1-2 weeks). This time period also allowed for viral expression. At the beginning of a recording session, animals were placed into a custom-designed body fixation tube for stabilization while connecting the implanted

multichannel electrode arrays with a data acquisition system (INTAN technologies). There were two conditions for recording sessions: easy condition (with 2-sec visual stimulus presentation) and hard condition (with 1-sec visual stimulus presentation). The two conditions were randomly assigned to sessions to avoid confounding from the training effect. A same number of sessions of easy and hard conditions were included for a fair comparison.

For sessions with optogenetic stimulation, only the easy condition was implemented. The laser power was tuned to be 30 mW out of the optic fiber cable tip. The optic fiber cable was also connected to the optrode implant interface. A custom-made black light-proof cylindrical sheath was appwlied surrounding the optic cable connection end to prevent light leakage. There were three conditions of trials randomly interleaved during each session: optogenetic stimulation at individual theta frequency band, alpha frequency band, and sham condition where no optogenetic stimulation was delivered. The data acquisition system and the optic fiber cable were connected to a commutator (Tucker-Davis Technologies) positioned on the top of the box to allow freely-moving behavior. From the commutator, another optic patch cable was used to connect to the laser source (Shanghai Laser & Optics Century Co.). The broadband electrophysiological data (1Hz to 5kHz, 20kHz sampling rate) was collected simultaneously with the time-locked event signals (behavioral events and laser pulses) for offline processing. During each session, a high-resolution infrared video was collected throughout and was later synchronized with the other data via frame time matching of the first stimulus onset. The task and behavioral events were executed and recorded by a custom-written Matlab script.

For the optogenetics control session (fig. S4), the optic cable tip was covered by light-proof tape and was attached on top of the optrode implant interface so that the setup was the same as in verum conditions but there was no laser going into the optrode implant.

Histology and verification of electrode locations

After reaching the scientific endpoint, animals were euthanized by injecting an overdose of ketamine/xylazine cocktail (30 mg/kg of ketamine, 1-2 mg/kg of xylazine, intramuscular) and perfused with

4% paraformaldehyde in phosphate-buffered saline. The brain was extracted from the skull and kept in the same solution for post-fixation overnight. Then, the brain was submerged in 30% phosphate-buffered sucrose solution for cryoprotection till it sank. After shock-froze in dry ice, the brain was sliced into 50 µm sections using a cryostat (CM3050S, Leica Microsystems).

Sections were collected into three series: one was stained by Nissl for visualizing cell nuclei, one was for fluorescent imaging, and the last one was stained by cytochrome oxidase for better visualization of the thalamic nuclei. Nissl and CO series were imaged with a bright-field slide scanner at 10x magnification (Aperio VERSA). The fluorescent series was imaged with a widefield fluorescence microscope (Nikon Ti2). Implantation and viral expression locations were verified by overlapping the images with the ferret atlas planes (Radtke-Schuller, 2018). Only electrodes that were verified to be in the targeted location were used for the analysis.

Data analysis

Custom scripts were used to execute all of the offline data analyses in Matlab 2020a (Mathworks).

Data preprocessing:

Raw extracellular potential data were first filtered by a low-band pass filter at 300 Hz to obtain local field potentials (LFPs). LFPs were then downsampled from 30 kHz to 1 kHz sampling rate. Further, data with movement artifacts were interpolated and outlier channels were removed from the dataset using Artifact Subspace Reconstruction (ASR) method (EEGLAB). At last, LFPs were epoched into trials, and trials with high amplitude artifacts were manually removed. On average, 2-3 trials out of 40-60 trials were removed in each session.

Multi-unit spiking activity was exacted from raw extracellular potentials by first applying a band-pass filter between 300 and 5000 Hz and then applying a -3.5 standard deviation threshold below the potential mean. Single-units were extracted using a template-matching algorithm implemented in KiloSort

and KiloSort 2 (Pachitariu, Steinmetz, Kadir, Carandini, & Harris, 2016b) followed by manual curation and template matching via the phy software (Pachitariu, Steinmetz, Kadir, Carandini, & Harris, 2016a).

Spectral analysis:

The spectral decomposition of the LFPs was done with wavelet transformation. We used Morlet wavelets ($w(t, f_0)$) that have Gaussian shape envelop in both time and frequency domain:

$$w(t, f_0) = A \cdot \exp(-t^2/2{\sigma_t}^2) \cdot \exp(-2i\pi f_0 t)$$

where f_0 represents the central frequency of the wavelet, $A = (\sigma_t\sqrt{\pi})^{-1/2}$ is a constant to normalize wavelet energy to 1, and $\sigma_t = 1/2\pi\sigma_f$ is the standard deviation in the time domain as a function of the standard deviation in the frequency domain (σ_f). After convolving with the wavelets, LFPs in the time domain were transformed into complex-valued analytical signals $X(t, f_0)$ at each carrier frequency of f_0. We used a family of 150 wavelets with logarithmically spaced central frequencies between 2 and 128 Hz. The power spectrogram was calculated for each valid channel (by preprocessing and anatomical validation), each studied region, and each animal and then averaged by taking the median across channels and then across sessions and animals.

LFP phase synchronization:

Our main measurement of functional connectivity between regions is phase-locking-value (PLV). We apply PLV to measure phase synchronization between LFPs in different regions (J.-P. Lachaux, E. Rodriguez, J. Martinerie, & F. J. Varela, 1999). We have also calculated coherence, which confounds the consistency of phase difference with amplitude modulation. In general, the two methods yield similar results. Due to the sample-size bias of PLV measurement (with more sample biases PLV to 0, and fewer samples biases PLV to 1), we randomly sampled the same number of trials from each session to be included in the PLV calculation and dropped the sessions that don't have enough trials. The number of subsampled trials N was chosen so that at least 85% of the sessions will be included in each condition (easy vs. hard).

Briefly, the phase angles (e.g. θ^{a} and θ^{b}) of the analytical signal $X(t, f_0)$ were calculated for studied channel pairs (e.g. a and b). The PLV at the carrier frequency of f_0 for N samples was defined as:

$$\mathrm{PLV}(f_0) = \frac{1}{N}\left|\sum_{n=1}^{N} \exp[i(\theta_n^{\mathrm{a}}(f_0) - \theta_n^{\mathrm{b}}(f_0)]\right|$$

PLV for each channel pair was then averaged (median) to produce PLV between a region pair in each session. PLV results were then averaged across sessions for each condition (e.g. easy vs. hard). Because the delay duration of each trial is randomly selected from one of three values, we aligned all of the trials at trial initiation and stimulus onset respectively to obtain time-resolved PLV.

Spike-LFP phase synchronization

To quantify the timing dependence between spikes (apply to both single-unit and multi-unit activity) and the LFP phase, we computed Spike-LFP phase synchronization (J. P. Lachaux, E. Rodriguez, J. Martinerie, & F. J. Varela, 1999) both within and between regions using simultaneously recorded spike and LFP data from all channels. For each region pair, we use LFPs from a representative channel (correlation between channel LFPs within the same region is greater than 0.8), and spikes from all valid channels. LFP phases were computed using wavelet convolution at each frequency of interest. For each spike channel, to calculate the PLV of spike-locked LFP phases across trials, we randomly selected the same number of spikes K per time bin to control for any sample-size bias of the PLV measurement. The spike PLV at a carrier frequency of f_0 for K spikes was defined as:

$$\mathrm{PLV}_{\mathrm{spike}}(f_0) = \frac{1}{K}\exp[i\theta_k^{\mathrm{spike}}(f_0)]$$

where θ^{spike} represents the instantaneous LFP phase at the occurrence of each spike. This random sampling procedure was repeated 200 times to yield a robust average PLV value for each time bin. The channels that do not have enough spikes per time bin were removed from the Spike-LFP analysis. The time-frequency resolved Spike-LFP phase-locking value will be average across channels within the same region, then average across sessions to yield the final result for each animal.

Conditional Granger Causality

Conditional Granger Causality (CGC) is a variant of the Wiener-Granger causality algorithm (J. Geweke, 1982; J. F. Geweke, 1984; Granger, 1969). It measures the influence of one time-series y on another time-series x, conditioned on (i.e. taken into consideration) the information of other time-series z_1 , z_2, etc. The algorithm builds two vector autoregressive (VAR) models to predict the current value of x: a full model that uses the previous values of x, y, and z_i, and a reduced model that uses only the previous values of x and z_i. If the full model results in less residual error than the reduced model, we can infer that time-series y contains critical information that can be used to help predict x, i.e. there is directed information flow from y to x. We applied the MVGC (Multivariate Granger Causality) Matlab toolbox (Barnett & Seth, 2014) to implement the CGC in the frequency domain on the signals from four brain regions we are interested in: PFC, LP/Pul, PPC, and VC. For every studied region-pairs, we calculated CGC for both directions, conditioned on the signals from the other two regions. The LFP time series were downsampled to 200 Hz first and the CGC was calculated for a moving window with 1-second width and 0.1-second step. The MVGC toolbox works by first determining the model order using Akaike or Bayesian information criteria or cross-validation. We used Akaike method for model order estimation with a maximum allowed model order of 20. After the suitable model order is determined, a VAR full model is fitted to the time-series data and the parameters are estimated for both the full model and the reduced model. Finally, the estimators of residuals of covariance matrices are used to calculate the CGC.

Phase-amplitude coupling

Phase-amplitude coupling (PAC) is one of the best-studied forms of cross-frequency coupling (CFC). It measures how the phase of a low frequency oscillation couples (i.e. locked) to the amplitude of a high-frequency oscillation. We use this method to study the mechanism underlying how oscillations at different frequencies modulate each other both within a region and between studied region-pairs. For exploring the whole space of possible phase-amplitude coupling (fig. S2), we first convolved the time series with waveforms at each frequency of interest (from 2 to 128 Hz, logarithmic scale, with 150 frequencies in

total), we then epoched the data by trial. Then for each low-frequency complex signal (within band 2-16 Hz), we calculated the phase at each time point. For each high-frequency complex signal (within band 16-128 Hz), we first convolved the amplitude of the complex signal with low-frequency wavelets and then calculated their phase at each time point. The difference between the low-frequency phase and the phase of the high-frequency amplitude envelope was averaged (i.e. similar concept to calculating the phase-locking value) across a -3 to 0 second time window before stimulus onset for each low-frequency phase and high-frequency amplitude pair. For time-resolved phase-amplitude coupling (fig. S3), we restricted the phase frequency range to the theta frequency band and the amplitude-frequency range to the gamma frequency band, as defined by the significant cluster found in the PAC heatmap (fig. S2).

Optical-tagging test

A detailed description of this method is in (Kvitsiani et al., 2013). Briefly, the optical-tagging test, i.e. Associated spike Latency Test (SALT) is used to identify light-activated neurons. We compared the spike timing of a unit during the optogenetic stimulation period ([-3, 0] s around visual stimulus onset) to that during a sham baseline ([-8, 5] s around visual stimulus onset) and yielded a *p*-value indicating whether there were optogenetically-induced significant changes in spike timing.

Permutation testing

To test for the significant time-frequency differences between conditions of interest (eg. easy vs. hard, theta optogenetic stimulation vs. sham), we applied nonparametric statistical testing across sessions and animals. The permutation testing starts with first computing the cluster size for each condition for each studied region or region pair. Then the conditions were randomly swapped for half of the sessions to establish a baseline where the difference between the conditions should be eliminated. We calculated the difference in contrast between these new condition labels and record the largest negative and positive cluster sizes. We then repeated this randomization process 1000 times to form a null distribution of the largest negative and positive cluster sizes. We used the 25th and 95th percentile values from the null distribution as the critical size values and considered the more extreme values to be statistically significant with an α

level of 0.05. This way, we are able to control for multiple comparisons across time-frequency clusters (BLAIR & KARNISKI, 1993; Maris & Oostenveld, 2007).

Brain-behavior correlation

A correlation was done after excluding outliers defined to be 3 standard deviations from the median of all sessions across 4 animals (although the statistical results did not change much when including outliers). Correlation coefficient r and significance value *p* were calculated using Spearman correlation methods and the results agree with percentage bend correlation, which is a correlation method that is robust to outliers (Pernet, Wilcox, & Rousselet, 2013).

Statistical analysis

Comparison of spectral features between different conditions (eg. easy vs. hard) was done at the session level using a 2-tailed paired t-test. Comparison of the means of behavioral measures between different conditions was done at the session level across animals. To control for the random effect of animal behavioral differences, *P*-values were calculated from linear mixed effect models "Measure = 1 + Condition + (1+Condition|AnimalID)" with significance levels of 0.05. If multiple measures were calculated as a group (i.e. different trial outcomes), then the *P*-values were corrected for multiple comparisons using Holm–Bonferroni method.

Code and data availability

Electrophysiological and behavioral data, as well as custom MATLAB code for the presented analyses, are available from the corresponding author upon request.

RESULTS

Identification of the oscillatory features associated with sustained attention

To probe the network substrate of sustained attention, we employed the five-choice serial reaction time task (5-CSRTT) (Bari et al., 2008) in ferrets (Sellers et al., 2016). In this task, animals sustained

attention during a delay period in anticipation of a brief presentation of a visual stimulus in one of five spatial locations. Successfully touching the correct stimulus window resulted in reward delivery (**Fig. 2.1 A**). To contrast low versus high attentional demand, we introduced long (2 sec) versus short (1 sec) stimulus presentation durations. We recorded electrophysiology signals from three nodes of the posterior thalamo-cortical visual network: the lateral posterior nucleus/pulvinar complex (LP/Pul), posterior parietal cortex (PPC), and visual cortex (VC). The signals were processed to yield local field potentials (LFP) and single-unit activities (**Fig. 2.1 C** example spike waveforms and LFP traces).

We focused on LP/Pul, PPC, and VC in the posterior network due to their anatomical connectivity which provides a foundation for direct interaction. Anatomical connections between these regions were verified in a separate set of animals which showed anatomically reciprocal connections between LP/Pul, PPC, and VC (**Fig. 2.1 B**). The reciprocal connectivity between LP/Pul and VC was previously shown in (Chunxiu Yu et al., 2016). The electrode implantation locations, stimulation fiber sites, and viral expression were histologically verified after the experiment (**Fig. 2.1 C**).

Task-modulated intra- and inter-regional neural activity

Oscillations are a way for neural populations to communicate (Buzsaki, 2006), especially during attentional tasks where rhythmic sampling and gating of the sensory input are essential (Clayton et al., 2015; Kastner et al., 2020). First, we identified the oscillatory features associated with performance during the 5-CSRTT task (N=85 sessions from 4 animals). In our data analysis, trials were aligned to trial initiation and visual stimulus onset respectively (**Fig. 2.2**). The power spectrogram (**Fig. 2.2 A**) showed distinct theta, alpha, and gamma bands. Baseline ([-2, -1] s before trial initiation) normalized spectrogram showed time-frequency clusters that were significantly different from the baseline ($p < 0.05$ via permutation test, see Method: Permutation testing) which expanded from trial initiation throughout the entire delay period (black contours in **Fig. 2.2 B**). In general, after trial initiation, there was an increase in theta band power (for better visualization of the distribution of data: **Fig. 2.2 C**, specifically, LP/Pul: Baseline = -0.29 vs. Delay = 2.71, $P < 0.001$, PPC: Baseline = -0.13 vs. Delay = 1.14, $P < 0.001$, VC: Baseline = 0.16 vs. Delay = -0.39, $P =$

0.331, 1-way ANOVA with Holm–Bonferroni correction for multiple comparison of 3 regions; individual animal data in fig. S1A) as well as a shift in frequency (from ~4 Hz to ~5.5 Hz) in the posterior network (specifically, LP/Pul: from 3-4.5 Hz to 4.5-7.5 Hz, PPC: from 3.5-4.5 Hz to 4.5-6.6 Hz, and VC: from 3-5 Hz to 5-7 Hz). This suggested that theta oscillations were associated with the initiation and sustaining of attention (including during the visual-simulation presentation). In addition, we observed a significant cluster for increased gamma-band power across all 3 regions (black contours in **Fig. 2.2 B**: 45-80 Hz in LP/Pul, 43-128 Hz in PPC, 45-128 Hz in VC) which confirmed that these regions were functionally engaged during the sustained attention period before the visual target was presented. There was also a significant power decrease in the alpha frequency band around 16 Hz in the posterior cortical regions (black contours in **Fig. 2.2 B**: 7-27 Hz in PPC, and 8-30 Hz in VC), which was consistent with the role of alpha oscillation suppressing neural activity during visual-attention tasks (Jensen & Mazaheri, 2010; Klimesch, Sauseng, & Hanslmayr, 2007). The increase in oscillation power that lasted beyond stimulus onset likely reflected visual processing and responding to the stimulus.

This concurrent change in theta oscillations in all three posterior regions motivated us to investigate the synchrony between these regions, which may reflect active communication between these brain regions. Similar to the spectrogram, the PLV was also normalized against the baseline period ([-2, -1] s before trial initiation). Consistent with the enhanced theta oscillation in each posterior region (**Fig. 2.2, A and B**), we found significant enhancement in inter-regional functional connectivity after trial initiation, measured by phase-locking values (PLV) (**Fig. 2.2, D and E,** LP/Pul-PPC: Baseline = 0.71 vs. Delay = 0.78, $P < 0.001$, LP/Pul-VC: Baseline = 0.64 vs. Delay = 0.73, $P < 0.001$, PPC-VC: Baseline = 0.64 vs. Delay = 0.74, $P < 0.001$, 1-way ANOVA with Holm–Bonferroni correction for multiple comparison of 3 regions; individual animal data in Fig. 2.A, B), accompanied by an increase in the frequency of theta (from 3-4.5 Hz to 4.5-7.5 Hz). In addition, there was significant alpha suppression from trial initiation in PPC-VC around 16 Hz (**Fig. 2.2 D**), consistent with the alpha suppression observed in PPC and VC individually (**Fig. 2.2, A and B**).

Attentional demand modulates inter-regional neural synchrony

To further isolate the effect of attention, we tested the effects of varying the 5-CSRTT attentional demand (N = 42 easy and 42 hard randomly interleaved sessions from 3 animals). This was operationalized by adjusting the stimulus duration, where shorter stimulus durations (i.e. hard sessions) required animals to sustain attention more consistently in order to successfully complete a trial. Hard sessions were associated with significantly lower accuracy (mean: Easy = 72% vs. Hard = 59%, $P < 0.001$ after Holm–Bonferroni correction for 4 behavioral outcomes) which mainly resulted from an increased omission rate in hard sessions (mean: Easy = 17% vs. Hard = 25%, $P = 0.002$ after Holm–Bonferroni correction for 4 behavioral outcomes) (**Fig. 2.2 F**). In addition, hard sessions were associated with shorter reaction time for correct trials (median: Easy = 1.14 s vs. Hard= 0.95 s, $P < 0.001$), indicating the successful recruitment of more attentional effort (**Fig. 2.2 G**). In contrast to the previous analyses using PLV in easy sessions, we are further interested in the directionality of the functional interaction in the circuit when there are more attentional resources being recruited (hard vs. easy level). To our surprise, only LP/Pul showed significantly increased drive in hard level compared to the easy level measured by conditional Granger Causality (CGC) (**Fig. 2.2 I**: LP/Pul->VC: median: Easy = 0.064 vs. Hard = 0.169, $P < 0.001$), which computes directed information flow between two regions while controlling for other regions studied (**Fig. 2.2 H** dark inter-regional arrow) (LP/Pul->VC showed significant cluster around 5 Hz, but not in the other direction). Thus the functional interaction in the thalamo-cortical network that was associated with higher attentional demand was mainly contributed by LP/Pul instead of the cortical regions (PPC and VC). This supported a more specific role of thalamic theta oscillations in sustained attention and illustrated the central role of inter-regional neural synchrony.

Phase-amplitude-coupling (PAC) increases with higher attentional demand

We next examined what roles the attention-modulated theta oscillations could play in organizing the overall functional network interactions. Theta oscillations have been implicated in facilitating long-range communication and coordinating higher frequency activity (Lisman & Jensen, 2013; Sweeney-Reed

et al., 2017). One mechanism for long-range organization and integration across populations of neurons is through phase-amplitude cross-frequency coupling (Fries, 2005; Vanhatalo et al., 2004) where the phase of lower frequency (such as theta) oscillations modulates the amplitude of higher frequency (such as gamma) oscillations (Canolty & Knight, 2010). Moreover, theta-gamma amplitude coupling increases during attention control in the frontoparietal network (Szczepanski et al., 2014) and during sustained attention within LP/Pul (Yu et al., 2018). Instead of arbitrarily defining frequency bands of interest, we chose a data-driven approach by examining the cross-frequency coupling between lower and higher frequencies between regions and their relationship to sustained attention.

First, we explored the entire space of low frequency (2-16 Hz) phase coupling to high frequency (16-128 Hz) amplitude (Fig. 2.B) for each region pair. There was a consistent enhancement in coupling between 4-7 Hz (i.e. theta) phase and 40-75 Hz (i.e. gamma) amplitude (as shown by the red blob in the center). This pattern was seen most strongly in LP/Pul and cortical-thalamo region pairs, which indicates that the LP/Pul gamma amplitude (which is an indication of spiking activity) is modulated by the strongly-synchronized theta phase in this posterior visual circuit. Further, there was also a hint of cortico-cortical coupling in the posterior network between PPC and VC albeit insignificant (Fig. 2.B, red blobs for PPC-VC pair).

To investigate the behavioral relevance of this cross-regional PAC, we calculated baseline-normalized time-resolved PAC (Fig. 2.C). The temporal dynamic of PAC tracked the delay period. At trial initiation, there was a sharp increase in cortico-thalamic PAC (i.e. PPC-LP/Pul, VC-LP/Pul) as well as within LP/Pul, which was maintained during the delay period. After stimulus onset, there appeared to be a transient increase in PAC that was probably related to the visual processing of the stimulus, and then the PAC dropped back down to baseline level. This suggests that PAC could be an underlying mechanism through which the thalamus interacts with the posterior network specifically during the delay period when sustained attention is recruited.

Causal engagement of the attention-related oscillatory features by optogenetics

Optogenetic stimulation entrains single-unit firing in a frequency-specific way

Thus far, we demonstrated that higher attentional demand (Fig. 2.2 D) is associated with higher theta drive from LP/Pul to cortical regions. But to test whether the thalamic theta can enhance attention instead of just being a byproduct of the process, we need causal perturbation to target this oscillation. To this end, we implemented optogenetics by expressing rAAV5-CaMKII-ChR2-mCherry in LP/Pul and stimulating LP/Pul using an optrode as well as recording from all three regions during the last 3 seconds of the sustained attention (i.e. delay) period before the presentation of visual stimulation for N = 51 sessions from 4 animals (**Fig. 2.3 A**). In each trial, optogenetic stimulation was given randomly in one of the three conditions: the individualized task-relevant theta or alpha frequency bands found earlier, or a no light sham control. The verification of viral expression and implantation location was shown in Fig. 2.1 C. First, we verified that the single unit (SU) activity was entrained by optogenetic stimulation in LP/Pul and PPC (**Fig. 2.3, B-D,** example SU), which is direct evidence that the optogenetic stimulation successfully activated both the target and its connected region. One example SU waveform per region was shown (**Fig. 2.3 B**). The raster plot (**Fig. 2.3 C**) and trial-averaged peristimulus time histogram (PSTH; **Fig. 2.3 D**) of these example units showed more rhythmic organization of the spiking activity during theta (blue) and alpha (red) optogenetic stimulation conditions than sham (black), especially in LP/Pul (see Method: optical tagging test (Kvitsiani et al., 2013), theta vs. sham: $P < 0.001$, alpha vs. sham: $P < 0.001$) and in PPC (theta vs. sham: $P < 0.001$, alpha vs. sham: $P < 0.001$). This demonstrated that optogenetic stimulation can directly change SU firing activity during the optogenetic time window in LP/Pul and PPC. Further, to investigate the SU entrainment at a population level, we averaged the PSTHs across all single units recorded during all sessions from the four animals (**Fig. 2.3 E**). The group PSTH plots showed clear entrainment of spiking activity corresponding to the frequency of optogenetic stimulation in LP/Pul, as well as an increase in firing rate in PPC and VC (**Fig. 2.3 F**). We did not observe changes in firing rate in VC in response to alpha

optogenetic stimulation. Even though some LP/Pul units were rhythmically entrained by optogenetic stimulation, not all units have increased firing rate, resulting in the overall no change in firing rate.

Optogenetic stimulation entrains oscillations in the posterior network

We next showed this single-unit entrainment related to the LFP network signals by investigating the effect of optogenetic stimulation on the mesoscopic oscillatory features. We contrasted the power spectrogram during theta or alpha (**Fig. 2.3 G**) optogenetic stimulation to the spectrogram during the sham condition (i.e. theta-sham and alpha-sham), and averaged the thete and alpha band power across the 3-second optogenetic stimulation period (**Fig. 2.3 H**). For theta stimulation, there was a significant enhancement of theta oscillation in LP/Pul (**Fig. 2.3 G** first row and **Fig. 2.3 H** first row, 5.3-7 Hz, Theta-Sham = 1.03, $P < 0.001$, 2-tailed t-test with Holm–Bonferroni correction for multiple comparison of 2 frequency bands, 2 optogenetic contrasts, and 3 regions), PPC (5-7 Hz, Theta-Sham = 3.65, $P < 0.001$), and VC (Theta-Sham = 0.39, $P = 0.009$) that was time-locked to the optogenetic stimulation window. The non-targeted alpha frequency band (but very close to the 2nd and 3rd harmonic of theta stimulation frequency) was also significantly enhanced (**Fig. 2.3 H**, second row: alpha frequency band LP/Pul: Theta-Sham = 1.95, $P < 0.001$, PPC: Theta-Sham = 2.16, $P < 0.001$, and VC: Theta-Sham = 0.78, $P = 0.002$). During alpha stimulation, as expected, we saw a distinct enhancement of alpha oscillations in all 3 regions in the posterior network (**Fig. 2.3 G**, second row and **Fig. 2.3 H**, second row: alpha frequency band LP/Pul: Alpha-Sham = 4.5, $P < 0.001$, PPC: Alpha-Sham = 5.28, $P < 0.001$, and VC: Alpha-Sham = 3.21, $P < 0.001$, all centered around 16 Hz) comparing to sham, confirming the frequency-dependent optogenetic enhancement of thalamic and cortical oscillations. It should also be noted that the power increase in VC under alpha stimulation demonstrated that it is possible to enhance power (on LFP level) without changing the firing rate (Fig. 2.3 F right-most bar). Although the entrainment mainly preferred the simulation frequency, there were also power increase in non-targeted bands. This brought us to further investigate which enhanced oscillatory features could engage circuit-level synchrony and if there is frequency-specific effect on functional connectivity.

Optogenetic stimulation induces directed and frequency-specific information flow from LP/Pul to the posterior network

After confirming frequency-specific entrainment on both single-unit as well as LFP levels locally, our next question was how optogenetic-induced intra-regional change in oscillation dynamics affects inter-regional communication. To this end, we computed single-unit phase-locking values (SUPLV) between studied region pairs. During theta stimulation (**Fig. 2.3 I,** above), there was significant phase-locking at the theta frequency band (centered around 5.5 Hz) driven by LP/Pul to PPC, and VC. During alpha stimulation (**Fig. 2.3 I,** below), there was a strong phase-locking at the alpha frequency band driven by LP/Pul to all cortical regions (all centered around 16 Hz). In addition, there was also feedback communication from PPC to LP/Pul and between PPC and VC, indicating that alpha stimulation preferably engages the posterior network. This was consistent with the finding that alpha oscillations dominated in the posterior network before trial initiation (Fig. 2.2 A: alpha oscillations before trial initiation in PPC and VC, which was also shown as an alpha suppression after trial initiation in baseline normalized spectrogram and PLV in Fig. 2.2 B and C). Further quantification of these enhancement during the 3-second optogenetic stimulation period showed frequency-specific enhancement of the thalamo-cortical SUPLV (**Fig. 2.3 J**, LP/Pul->PPC Theta-Sham = 0.086, $P < 0.001$; Alpha-Sham = 0.035, P.= 0.002; LP/Pul->VC, Theta-Sham = 0.011, P.= 0.045; Alpha-Sham = 0.019, P.= 0.050 2-tailed t-ttest with Holm–Bonferroni correction for multiple comparison of 2 frequency bands, 2 optogenetic contrasts, and 6 directed region pairs). In summary, optogenetic stimulation in LP/Pul in theta or alpha frequency bands induced inter-regional thalamo-cortical spike phase locking in theta or alpha frequency bands respectively.

Causal manipulation of sustained attention performance

Theta optogenetic stimulation increases correct response and decreases omission

To determine the effect of optogenetic stimulation on sustained attention and to demonstrate a causal brain-behavior relationship, we quantified how frequency-specific optogenetic stimulation changed behavioral performance during the 5-CSRTT. We determined the change in the percentage of different trial

outcomes (e.g. correct, premature, omission, and incorrect) in each optogenetic stimulation condition compared to the sham condition (**Fig. 2.4 A**). Theta optogenetic stimulation significantly increased the percentage of correct trials (Theta-Sham = 7.1 percentage points, P = 0.0038 after Holm–Bonferroni correction for 4 behavioral outcomes) and reduced the percentage of omission trials (Theta-Sham = -6.3 percentage points, $P < 0.001$ after Holm–Bonferroni correction for 4 behavioral outcomes). Both trends were consistent across all 4 animals (for individual results see shaded bars in Fig. 2.D). However, there was no significant effect of alpha-frequency optogenetic stimulation. In addition, optogenetic stimulation did not affect average velocity during optogenetic stimulation or velocity during reward retrieval (V_{Opto}: Theta-Sham = 0.118, P = 0.798, Alpha-Sham = -0.58, P = 0.210; $V_{Retrieval}$: Theta-Sham = -0.277, P = 0.458, Alpha-Sham = 0.602, P = 0.847) (**Fig. 2.4 B**) or reaction time in correct trials (Theta-Sham = -0.028, P = 0.140, Alpha-Sham = -0.069, P = 0.214) (**Fig. 2.4 C**). This suggested that theta-frequency optogenetic stimulation reduced attentional lapses (i.e. omission) and shifted the system towards a more attentive state with higher accuracy without affecting motor function or arousal or motivation level.

Optogenetically-induced effective connectivity change correlates with behavioral performance change

Sustained attention can be viewed as a gating mechanism for visual information to be transmitted to the higher-order cortices(M. Sarter, B. Givens, & J. P. Bruno, 2001). This is supported by our findings of LP/Pul-VC connectivity being modulated by different levels of attentional demand (Fig. 2.2, H and I). Thus we next tested how the LP/Pul-VC connectivity correlated with behavioral performance (**Fig. 2.4, D and E**). Behavioral performance (y axis) is measured by the different percentage points of accuracy in verum stimulation condition compared to the sham condition. For example, for a session with an accuracy of 90% during theta optogenetic stimulation and 80% during the sham condition, the difference in accuracy for "Theta-Sham" is 10. We focused this analysis on theta and gamma oscillations due to the network-wide task-relevant enhancement of their power, functional connectivity (Fig. 2.2), and cross-frequency coupling (Fig. 2.B., 2.C) during the sustained attention period. The theta stimulation-induced theta spike-PLV change from VC to both LP/Pul (Spearman correlation coefficient r = 0.36, P = 0.02) and PPC (r = 0.27, P = 0.08)

are significantly and positively correlated with stimulation-induced change in accuracy (**Fig. 2.4 D**). However, this correlation was absent during alpha-stimulation (VC->LP/Pul: $r = 0.16$, $P = 0.31$, VC->PPC: $r = -0.02$, $P = 0.92$) (**Fig. 2.4 E**). One hypothesis is that alpha-stimulation suppressed information transmission, which impaired the positive influence of theta spike-PLV on gating sensory input. As a result, the positive correlation between theta spike-PLV and the behavioral performance no longer existed under alpha optogenetic stimulation condition. Interestingly, both theta and alpha stimulation-induced gamma spike-PLV change correlated with accuracy change except for VC to LP/Pul during theta stimulation (theta stimulation: VC->LP/Pul r = 0.35, P = 0.02, VC->PPC r = 0.18, P = 0.26; alpha stimulation: VC->LP/Pul $r = 0.50$, $P < 0.001$, VC->PPC $r = 0.57$, $P < 0.001$). This implies that successful enhancement of communication in specific frequency bands (theta and gamma) from the visual cortex to higher-order visual regions contributed to the performance improvement.

Blocked optogenetic stimulation and delta stimulation do not induce performance change

To control for the effect of laser delivery and potential confounds caused by light leakage, we conducted control sessions with the tip of optogenetic cable blocked but still plugged into the implant (Fig. 2.E, A and B). We did not find any significant change in trial outcomes or reaction time for optogenetic stimulation condition compared to sham (Accuracy: Theta vs. Sham: $P = 0.385$, Alpha vs. Sham: $P = 0.094$; Reaction time: Theta vs. Sham: $P = 0.167$, Alpha vs. Sham: $P = 0.934$). This finding confirms that the optogenetic effects in this study were not due to potential light leakage at the interface of optic cable and implant.

Since both theta and alpha stimulation increased alpha power, we investigated the effect of targeting a different frequency band that is not in proximity to alpha and theta frequencies. Delta optogenetic stimulation (at 2.5 Hz) did not drive a distinct alpha-band power change (Fig. 2.E E), indicating that increased alpha power observed in theta and alpha stimulation conditions was an outcome of frequency-specific optogenetic stimulation and possible cross-frequency coupling. Further, delta stimulation did not

significantly change any behavioral outcome (Delta vs. Sham: Accuracy: P = 0.409, Reaction time: P = 0.595) (Fig. 2.E, C and D).

Task engagement and optogenetic effect are connection-specific

So far, we demonstrated that the cross-regional oscillations in the posterior network were modulated by sustained attention and entrained by optogenetic stimulation in LP/Pul. To investigate whether this result is specific to the posterior network, we chose to study the dorsal prefrontal cortex (dPFC) and its functional connectivity to the posterior network as a control analysis.

We conducted the same recordings and analysis in dPFC (**Fig. 2.5**) mirroring the previous analysis (Fig. 2.1-2.3). Interestingly, even though we saw an enhancement in the low frequency (2-4Hz) and gamma oscillations in dPFC at the beginning of the delay period (**Fig. 2. 5C**), these oscillations were not modulated by attentional demand (**Fig. 2.5 D**). During optogenetic stimulation in LP/Pul, neither theta nor alpha-frequency stimulation-induced any firing rate changes (**Fig. 2.5 E**) or power changes (**Fig. 2.5, F and G**) in dPFC compared to the sham condition. This was expected given the marginal anatomical connection between LP/Pul and dPFC. The only optogenetically-induced changes were found in the single-unit phase-locking value (**Fig. 2.5, H and I**). Interestingly, although not statistically significant, there was a decrease in theta functional connectivity (centered around 5.5 Hz), from dPFC to LP/Pul and PPC, indicating that theta stimulation reduced the endogenous theta drive from dPFC to those regions, which might indicate a competing relationship between the LP/Pul theta and dPFC theta top-down signaling. During the theta and alpha-frequency optogenetic stimulations, LP/Pul spikes phase-locked to theta and alpha oscillations respectively in dPFC, indicating optogenetic stimulations enhanced frequency-specific drive from LP/Pul to dPFC. This could be explained by the strong theta drive in LP/Pul, the scarce direct connections and/or the indirect connections between LP/Pul and dPFC (e.g. theta synchrony via PMC and/or rostral PPC (Sellers et al., 2016)). However, this did not result in enhancement of the cortical communication between dPFC and PPC despite the enhancement of LP/Pul to PPC communication (Fig. 2.3, I and J). This

demonstrated an interesting finding that the enhancement of cortical-thalamo-cortical communication did not necessarily lead to the enhancement of cortico-cortical communication.

DISCUSSION

In this study, we combined electrophysiology and optogenetics in the visual cortico-thalamo-cortical circuits to study the causal role of oscillations and interaction through synchronization in a sustained attention paradigm. The posterior thalamic network (LP/Pul-PPC-VC) demonstrated task modulation during the 5-CSRTT. The theta and gamma power in the network, as well as theta synchrony between region pairs, were increased during the delay period after trial initiation while the animal maintained attention during the period leading up to stimulus presentation, whereas alpha synchrony was suppressed, indicating that enhanced/suppressed communication in specific frequency bands are associated with sustained attention. Interestingly, when contrasting two difficulty levels of the task, only the theta connectivity driven by LP/Pul, but not dPFC, was modulated by attentional demand. This suggested differential roles of thalamo-cortical theta and prefrontal theta in sustained attention. Whereas directed thalamo-cortical theta modulated the level of sustained attention effort exerted in the task, prefrontal theta seemed to be unresponsive to this change. Further, using optogenetics, we successfully engaged this thalamo-cortical theta connectivity without changing the prefronto-parietal theta connectivity and improved task performance. Importantly, enhancing thalamo-cortical alpha or delta connectivity did not improve task performance, suggesting that this effect is connection- and frequency-specific. Lastly, we demonstrated that it is the successful engagement of the feedback circuit (VC->LP/Pul, VC->PPC) during optogenetic stimulation in the theta frequency band that correlates with the task performance, and this correlation was absent during optogenetic stimulation at the alpha frequency band. Together, our findings establish a causal role of theta-frequency synchronization in the posterior visual thalamo-cortical network in sustained attention.

The role of posterior thalamo-cortical network in sustained attention

In primates, pulvinar is well-connected with multiple cortical regions and forms cortical-pulvino-cortical input-output loops, providing the anatomical foundation for a central role in synchronizing thalamo-cortical networks. Pulvino-cortical (temporo-occipital area and V4, respectively) synchrony is modulated by a selective attention task and this synchrony is directed from pulvinar to the cortical regions (Saalmann et al., 2012). Further, deactivating pulvinar with muscimol reduces visual responsiveness as well as high-frequency synchrony within V4 (Zhou et al., 2016). Pulvinar has also been shown to rhythmically engage or disengage fronto-parietal network based on its theta phase during a spatial attention task (Fiebelkorn, Pinsk, & Kastner, 2019). These studies elucidated the important role of pulvinar in modulating cortico-pulvino-cortical interactions, especially during attention-related tasks. However, the causal relationship was either demonstrated using Conditional Granger causality instead of a causal manipulation or via a non-specific silencing of the pulvinar. Further, none of the studies have directly examined the pulvinar-induced cortico-cortical interactions and their relationship with behavioral performance, so until this study it was inconclusive whether the modulation happens via pulvinar interaction with each cortical region individually or via successful synchronization of two cortical regions.

In our study, we were able to explicitly and causally test the role of cortical-pulvino-cortical oscillations by using frequency-specific optogenetics. Ferrets are ideally suited for such an investigation since they exhibit a sufficiently sophisticated thalamo-cortical visual system that generates alpha oscillations (Stitt, Zhou, Radtke-Schuller, & Fröhlich, 2018). In addition, the LP/Pulvinar complex (LP/Pul) in ferrets resembles the primate pulvinar nucleus as it reciprocally connects with VC and the posterior parietal network (C. Yu et al., 2016). This provides an anatomical foundation for the higher-order visual thalamus to modulate cortical communication and visual information integration. We found that LP/Pul drove its reciprocally connected cortical regions PPC and VC during the delay period of the sustained attention task via theta oscillations. This is consistent with the role of theta in facilitating long-range communications between brain regions (Lisman & Jensen, 2013; Sweeney-Reed et al., 2017). In addition,

this directional theta drive was stronger for the hard version of the task with higher attentional demand compared to the easy version, demonstrating the significance of this thalamo-cortical theta drive in maintaining and modulating the magnitude of sustained attention. Further, using frequency-specific optogenetic stimulation, we successfully entrained the posterior network (both pulvino-cortical interaction and cortico-cortical interaction). Importantly, only theta but not alpha frequency stimulation caused significant improvement in the accuracy of the sustained attention task. Further, this causal relationship is mainly explained by a successful engagement of the VC-LP/Pul pathway in the theta stimulation condition which drives up accuracy, and this brain-behavior correlation was absent in the alpha stimulation condition. It should also be noted that there was a trending level significant correlation between VC-PPC spike phase locking at the theta frequency band and accuracy, indicating that cortico-cortical interactions might also play a role in modulating behavioral performance. In summary, our results suggested that LP/Pul theta oscillation is modulated by attentional demand and causally enhances theta synchrony in the pulvino-cortical pathway (i.e. LP/Pul-PPC and LP/Pul-VC) as well as cortico-cortical pathway (i.e. PPC-VC), which in turn improves sustained attention performance.

The lack of engagement between dPFC and the posterior network

The most caudal dPFC is part of the frontoparietal attention network at the intersection of dPFC and PMC in ferrets (Sellers et al., 2016), which might correspond in location and connectivity to the frontal eye field in primates (Radtke-Schuller et al., 2020) -- a key player in the top-down control signaling during attentional tasks (Buschman & Miller, 2007; Scolari et al., 2015; Sellers et al., 2016). In our study, other than the cortex of the dPFC/dPMC junction, we chose dPFC as a control region whose activity was not modulated by different levels of sustained attention demands. The dPFC proper is not structurally connected to PPC nor to the part of VC we were recording from. The connections of LP/Pul to dPFC are marginal (Radtke-Schuller et al., 2020).

There are several possible explanations. In ferrets, there are distinct anatomical connectional differences between dPFC and dPMC. Both dPFC and dPMC are strongly connected with the medial dorsal

thalamus (MD) (Radtke-Schuller et al., 2020). With PPC, dPFC is anatomically connected only with its most caudal part at the dPFC/dPMC junction, whereas dPMC has rich connections with PPC (Radtke-Schuller et al., 2020). In this study, we targeted the dPFC region that is more anterior than the above-mentioned ferret study that targeted dPMC (Sellers et al., 2016). Thus, dPFC connections that are modulated by attentional demand were not captured by the specific connections studied in this paper.

Another possible explanation is that dPFC serves as a switch in selective attention and controlling sensory selection (e.g. between different sensory modalities) but once the state is switched, dPFC is not responsible for tuning the magnitude of sustained attention. This hypothesis is consistent with what other studies have shown. In mice, PFC biases thalamic reticular subnetworks to control thalamic sensory gain (e.g. visual vs. auditory) in order to select certain inputs for further processing (Wimmer et al., 2015). In the above-mentioned sustained attention studies, when one contrasts different behavioral outcomes (correct vs. omission vs. premature) it could be reflecting whether the visual system is engaged or if the animal is distracted by other sensory input or internal impulsivity (de Kloet et al., 2021; Kim, Ährlund-Richter, Wang, Deisseroth, & Carlén, 2016). On the other hand, by contrasting difficulty levels in this study, we aimed to compare two visually attentive states that differ in their magnitude, which might not be the function of dPFC.

Further, due to the almost total lack of connectivity between dPFC and the other studied regions, optogenetic stimulation in LP/Pul did not entrain dPFC nor enhance its functional connectivity with other studied regions. Except for a reduction (albeit not statistically significant) in PFC spikes phase-locking to LP/Pul LFP at the theta frequency band, which could result from being outcompeted by the optogenetic-induced theta in LP/Pul. As a result, the behavioral effects we observed during the optogenetic experiment were most likely caused by the posterior network entrainment rather than the mostly unchanged connectivity between dPFC and the posterior network.

Limitations

Like all scientific research, out study has limitations. First, we did not parameterize the task difficulty based on individual task performance. Different animals learned the task at different rates and some consistently perform better than others. To control for individual ability, one could implement a detailed parameterization of the task so that all animals achieve the same performance. However, such task individualization will introduce more parameters than our sample size could support. To mitigate this issue, our results are mostly focused on contrasts that indicate attentional demand or treatment effect (i.e., the contrast between different difficulty levels or between different optogenetic conditions, respectively) so that the baseline performance is of less importance.

Second, our study did not differentiate layer-specific connections and oscillations. For cortical regions, we primarily targeted the layer IV, V neurons due to the presumable abundance of thalamo-cortical input and cortical-thalamic output from the neocortex. However, it is still under investigation whether this is true for ferrets in the cortices we are interested in and we might underrepresent some cortico-cortical connections. In addition, due to the curvature of the brain, different electrodes may have ended up in different layers, thus we did not have the layer-specificity to study which layer receives input from or sends output to the thalamus and other cortical regions, which are all very interesting questions and could provide more insights to the development of oscillatory interactions during sustained attention and optogenetics.

We recognize that an ideal control for the side-effect of optogenetic stimulation is to use another set of control animals injected with a control viral vector without opsin as in some rodent research. However, given the complexity of the experiment, we decided to use a slightly different approach that allowed for a within-subject design. We used two types of control conditions: within each session, we use a no-light sham condition randomly interleaved with verum stimulation conditions; in addition, we also collected control sessions where the optic cable tip was blocked throughout the session to control for the effect of any potential light leakage.

Lastly, using open-loop optogenetic stimulation, we imposed external oscillations onto the network, which may potentially have interrupted the ongoing oscillations during the task. Although we have demonstrated that 3 seconds of theta optogenetic stimulation was enough to engage thalamo-cortical interactions that enhance sustained attention performance, it is possible that a closed-loop system would be better at achieving this goal. In a closed-loop system, the optogenetic stimulation would be given based on the upcoming phase predicted from the ongoing oscillations and ideally directly enhance the endogenous oscillation without resetting its phase (Grosenick, Marshel, & Deisseroth, 2015).

Implications

Through a logical progression of target identification, engagement, and validation (Kurmann, Gast, Schindler, & Fröhlich, 2018), we demonstrated that the higher-order visual thalamus causally modulates thalamo-cortical and cortico-cortical synchrony to facilitate sustained attention via theta oscillations. Thalamic theta oscillations act as a gating mechanism for visual sustained attention by top-down control of spike-phase alignment as well as phase coupling to the gamma amplitude in the posterior network to prepare the channel for communication and amplify the bottom-up signal from the sensory cortices. The magnitude of communication in the feedback circuit (e.g. VC->PPC, VC->LP/Pul) in turn predicts the sustained attention performance. Since the thalamus is composed of multiple specialized nuclei that are connected to lower and higher sensory cortices, this cortico-thalamo-cortical interaction could be a mechanism underlying thalamic control of cortical synchrony during sensory processing in general.

FIGURES AND TABLES

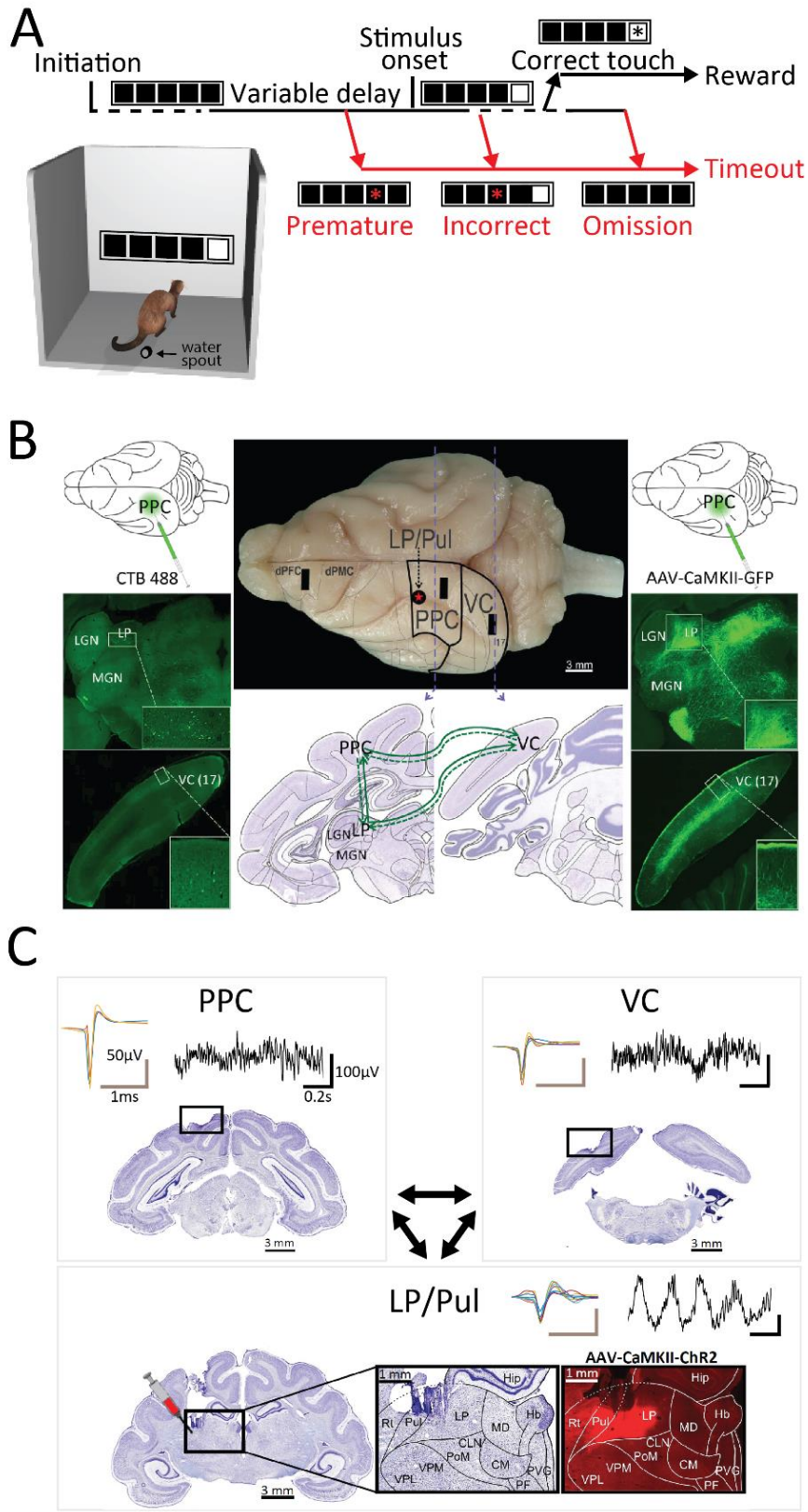

Figure 2.1. Sustained attention task in freely-moving ferrets and histological verification of anatomical connections and recording sites

(**A**) Illustration of the 5-CSRTT timeline and the behavioral box setup. Animals initiate trials at an infrared sensor, then after a variable delay period (4, 5, or 6 sec), a light stimulus is presented randomly in one of the five touchscreen windows. If the animal touches the correct window during stimulus presentation or within a 2 sec hold period, a tone is played and the animal can retrieve a water reward at the lick spout and subsequently start a new trial. Otherwise, a premature touch (before stimulus onset), an incorrect touch (the wrong window was touched), or an omission (no touch was made) all lead to a 5-sec timeout. (**B**) Tracing studies revealed structural connectivity between LP/Pul, PPC, and VC. The middle panel depicts the location of PPC and area 17 (VC) in the atlas brain and summarizes the reciprocal connectivity between the three regions. Left: Injection of retrograde tracer (CTB 488) reveals PPC input from LP/Pul and VC. Right: Anterograde virus AAV-CaMKII-GFP into PPC reveals projections to LP/Pul and VC. (**C**) Example sections with Nissl staining of studied regions show electrode implantation location in LP/Pul, PPC, and VC. Black squares denote the implant locations indicated either by tissue damage or electrode tracks. Example single-unit waveforms as well as raw traces of local field potentials for the delay period in the three studied regions from a recording session without optogenetic stimulation. For LP/Pul, insets showed a zoomed-in view of Nissl staining (left) and rAAV5-CaMKII-ChR2-mCherry expression (right) of LP/Pul.

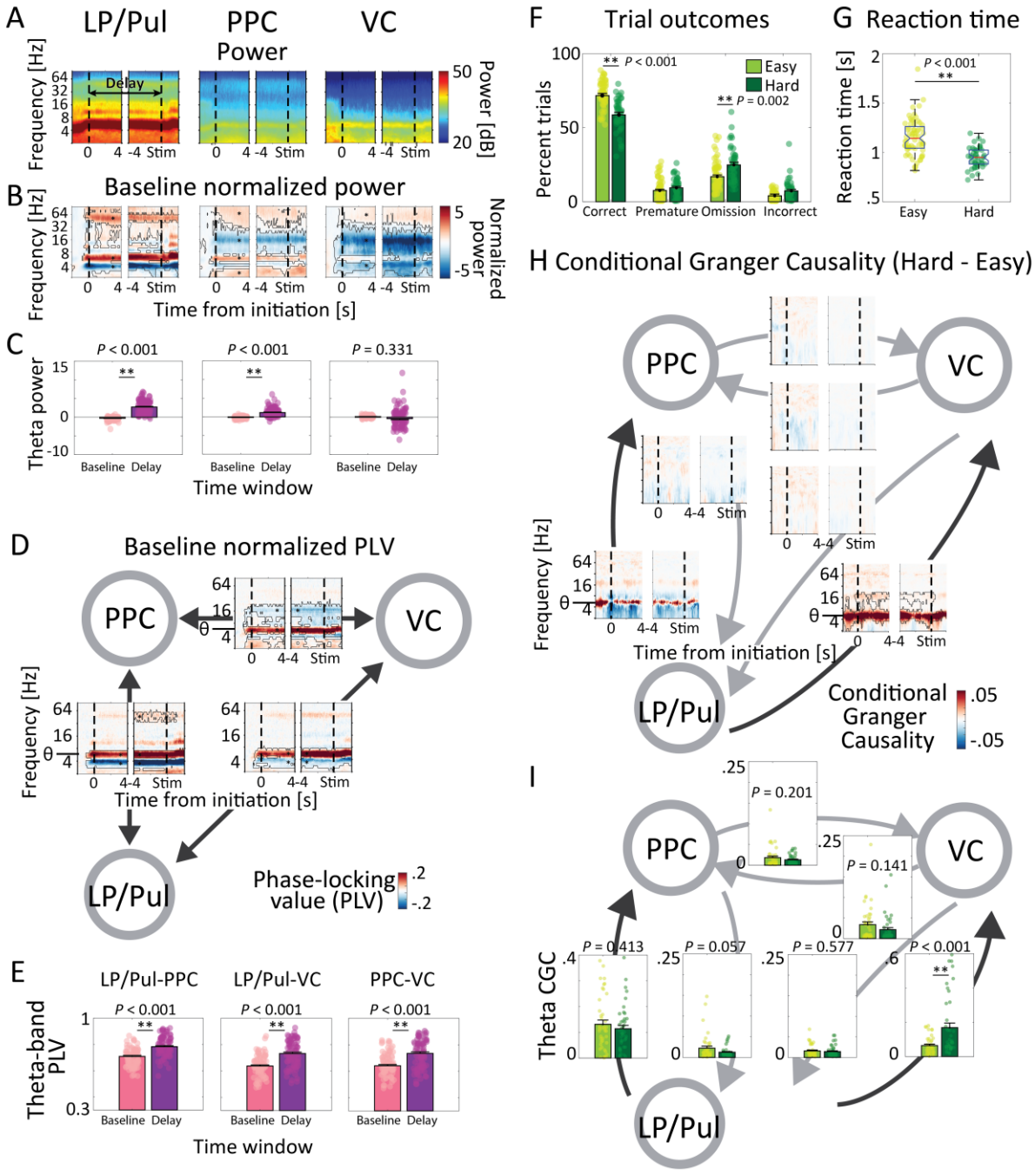

Figure 2.2. Task-modulated power and functional connectivity in the network during 5-CSRTT

(**A**) Power spectrogram during the task, aligned to trial initiation "0" and stimulus onset "Stim", respectively, for studied regions: LP/Pul, PPC, and VC. (**B**) Similar graph for baseline ([-2, -1] s before trial initiation) normalized power spectrogram. (**C**) Comparison of the session means of normalized power in the theta frequency band (4.5-7.5 Hz) during the baseline period and the delay duration (i.e. sustained

attention period) for each studied region. (**D**) Baseline normalized phase-locking value (PLV) between studied region-pairs during the task. (**E**) Comparison of the session means of PLV in the theta frequency band (4.5-7.5 Hz) during the baseline period and the delay duration for each studied region-pair. (**F**) Comparison of trial outcomes (percentage of correct, premature, omission, and incorrect trials) between easy (light green) and hard (dark green) sessions. (**G**) Comparison of reaction time for correct trials between easy (light green) and hard (dark green) sessions. (**H**) Directed functional connectivity determined by conditional granger causality (CGC) between studied region-pairs for hard versus easy conditions, revealing theta drive from LP/Pul to cortical regions modulated by attentional demand. (**I**) Comparison of session means of CGC in the theta frequency band (4.5-7.5 Hz) during the delay duration between easy (light green) and hard (dark green) sessions. For (A-E), N=85 sessions from 4 animals. For (F-I), N=42 easy, 42 hard sessions from 3 animals (i.e. Animals A, C, D). For (B) and (D), black contours delineate statistically significant spectral features compared to baseline activity via permutation testing (number of iterations = 1000). For (H), black contours delineate statistically significant spectral features of easy vs. hard conditions via permutation testing (number of iterations = 1000). For (C), (E), and (I), *P*-values were computed from a 2-tailed paired t-test comparing 2 populations and then corrected for multiple comparisons of regions or region-pairs. For (F) and (G), The *P*-values ware calculated from a linear mixed effect model: PercentTrialOutcome (D) or ReactionTime (E) = 1 + EasyHardContrast + (1+EasyHardContrast|AnimalID) controlling for the random effect of different animals, and then corrected for multiple-comparisons for four trial outcome types using Holm–Bonferroni method. The error bar represents the standard error of the mean. Each dot represents one session. * $P < 0.05$, ** $P < 0.01$.

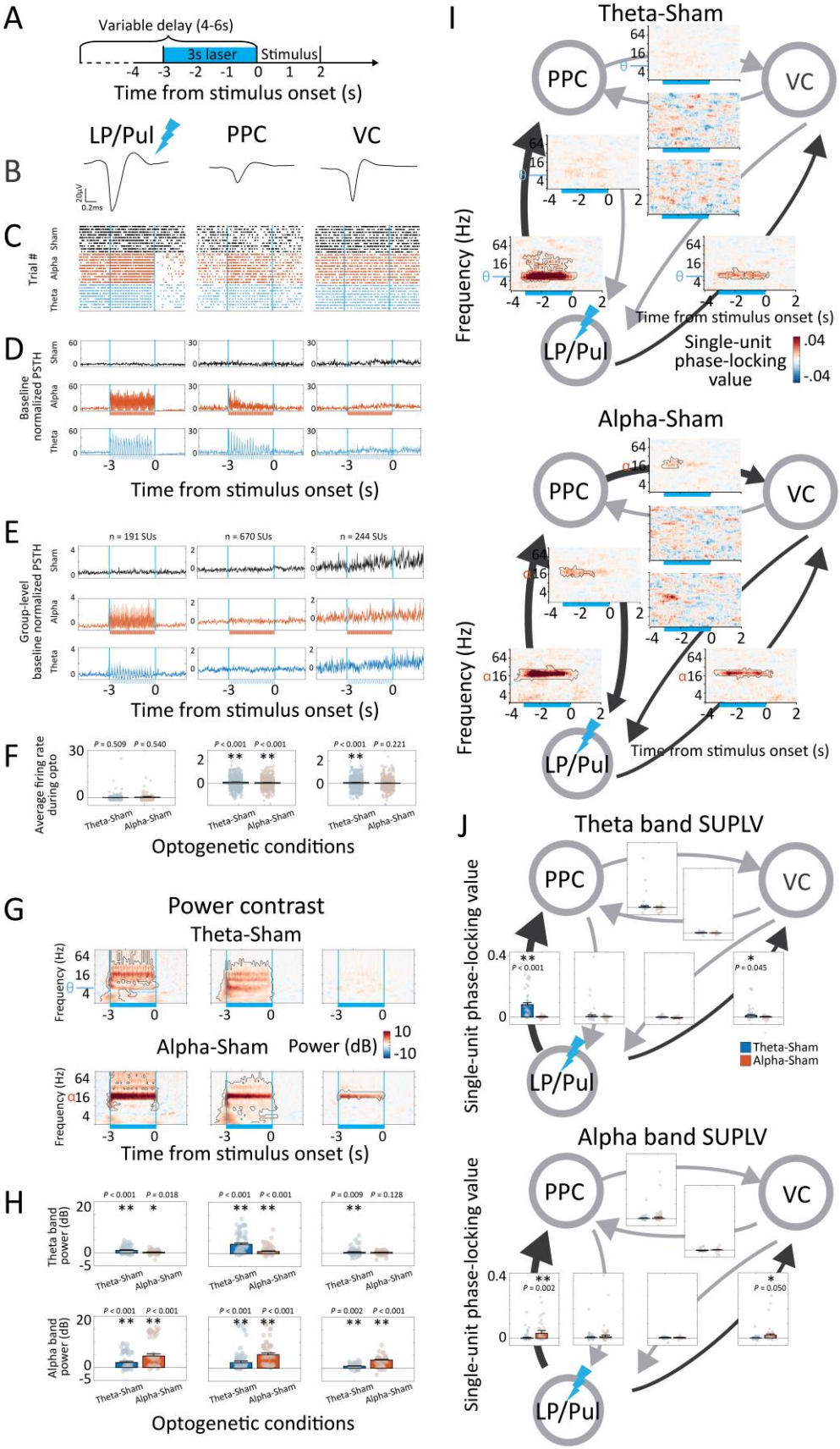
A
Variable delay (4-6s)
3s laser
Stimulus
Time from stimulus onset (s)
B
LP/Pul
PPC
VC
C
Trial #
Sham
Alpha
Theta
D
Baseline normalized PSTH
Time from stimulus onset (s)
E
n = 191 SUs
n = 670 SUs
n = 244 SUs
Group-level baseline normalized PSTH
Time from stimulus onset (s)
F
Average firing rate during opto
Theta-Sham
Alpha-Sham
Optogenetic conditions
G
Power contrast
Theta-Sham
Alpha-Sham
Power (dB)
Frequency (Hz)
Time from stimulus onset (s)
H
Theta band power (dB)
Alpha band power (dB)
Optogenetic conditions
I
Theta-Sham
Alpha-Sham
PPC
VC
LP/Pul
Frequency (Hz)
Time from stimulus onset (s)
Single-unit phase-locking value
J
Theta band SUPLV
Alpha band SUPLV
Single-unit phase-locking value
Theta-Sham
Alpha-Sham

Figure 2.3. Frequency-specific entrainment of single-unit activity, oscillatory features, and cortico-thalamo-cortical functional connectivity by optogenetic stimulation

(A) Experimental timeline with optogenetic stimulation in the blue bar. for easy level only. The (**B**) waveform, (**C**) raster plot, (**D**) baseline normalized firing rate from an example single unit (from 1 session, Animal A) in each region: LP/Pul, PPC, and VC. (**E**) Average baseline normalized firing rate from all single units in each region (mean±sem). (**F**) Average baseline normalized firing rate across the optogenetic stimulation period in theta (blue) and alpha (red) optogenetic stimulation condition compared to sham. Each dot represents one single unit. (**G**) Power spectrogram for each region from -4 to 2 seconds around visual stimulation, contrasting individualized theta-band laser stimulation (first row) or alpha-band laser stimulation (second row) against the sham condition. (**H**) Average of theta (first row) and alpha (second row) frequency band power across the optogenetic stimulation period in theta (blue) and alpha (red) optogenetic stimulation condition compared to sham. Each dot represents one session. (**I**) The single-unit phase-locking value between studied region pairs from -4 to 2 seconds around visual stimulation, contrasting theta frequency laser stimulation or alpha frequency laser stimulation against the sham condition. (**J**) Average of single-unit phase-locking value in the theta and alpha frequency band across the optogenetic stimulation period in theta (blue) and alpha (red) optogenetic stimulation condition compared to sham. Each dot represents one session. N = 51 sessions from 4 animals. Black contours delineate statistically significant differences in spectral features between corresponding optogenetic conditions and sham conditions via permutation testing (number of iterations = 1000). The normalization baseline in D-F was chosen to be -5 to -3.5 seconds before laser stimulation onset to better visualize the optogenetic effect. An identical number of action potentials were used for all connections. Single units with fewer action potentials were excluded. Different signal-to-noise level is the result of fewer single units in VC. * $P < 0.05$, ** $P < 0.01$.

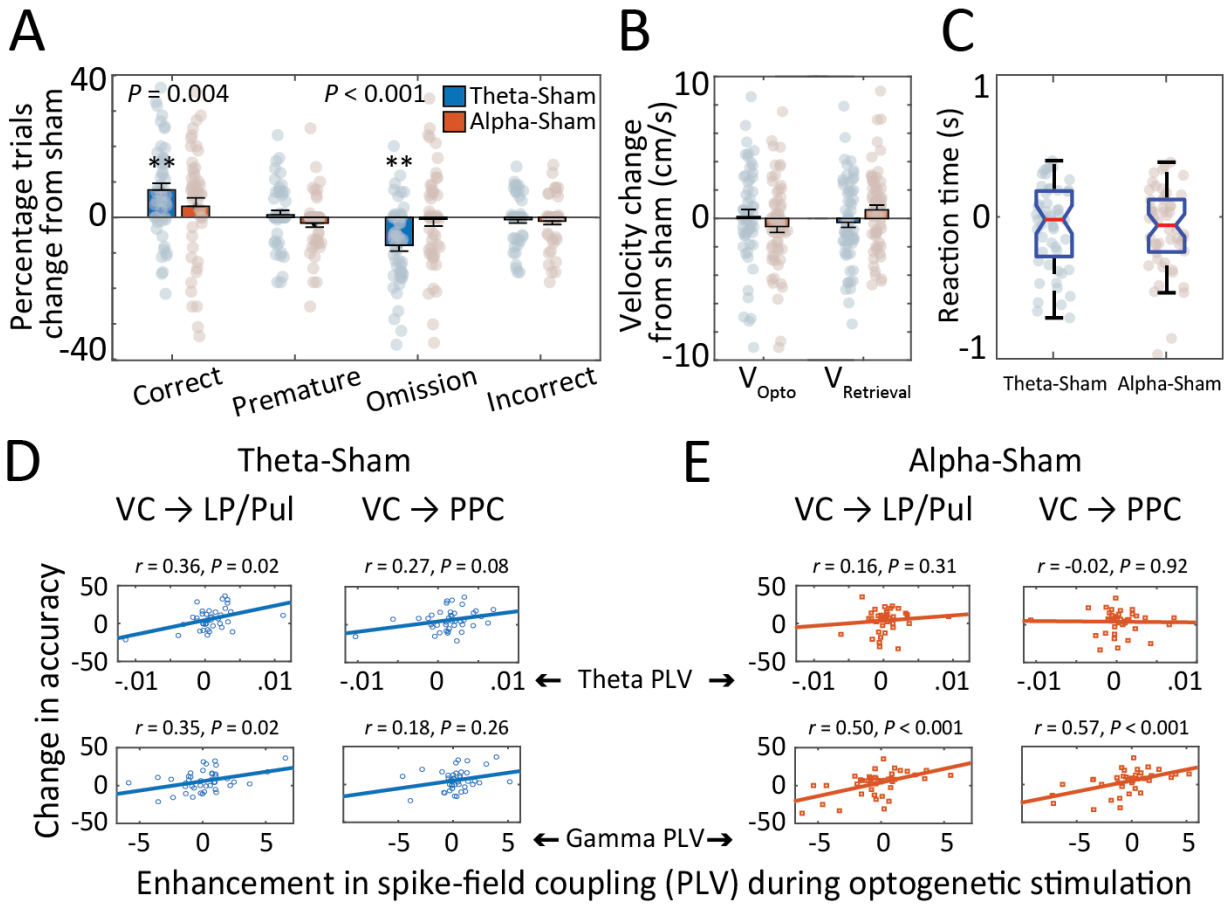

Figure 2.4. Behavioral results of optogenetic stimulation in LP/Pul

(**A**) Optogenetic stimulation-induced change of the percentage of correct / premature / omission / incorrect trials compared to sham conditions. (**B**) No change of average velocity during optogenetic stimulation (V_{Opto}) and reward retrieval ($V_{Retrieval}$) from the sham condition. (**C**) No change of reaction time for correct trials from the sham condition. For A-C, the p-values were calculated from linear mixed effect models: PercentChange (data from **A**) or VelocityChange (**B**) or ReactionTimeChange (**C**) = 1 + OptoContrast + (1+OptoContrast|AnimalID) controlling for the random effect of different animals, and then corrected for multiple comparisons using Holm–Bonferroni method. (**D-E**) Correlation between optogenetics-induced accuracy change (y-axis) and optogenetics-induced average spike-field coupling (PLV) change during the optogenetic stimulation window ([-3,0] second before visual stimulation) (x-axis) for theta-sham (D) and alpha-sham (E), respectively. The first row represents spike-PLV averaged across the theta frequency band (5-7 Hz), and the second row represents spike-PLV averaged across the gamma frequency band (40-75 Hz).

Each dot represents one session. N = 51 sessions from 4 animals. Correlation coefficient r and significance value *P* were calculated using Spearman correlation methods and verified using percentage bend correlation.

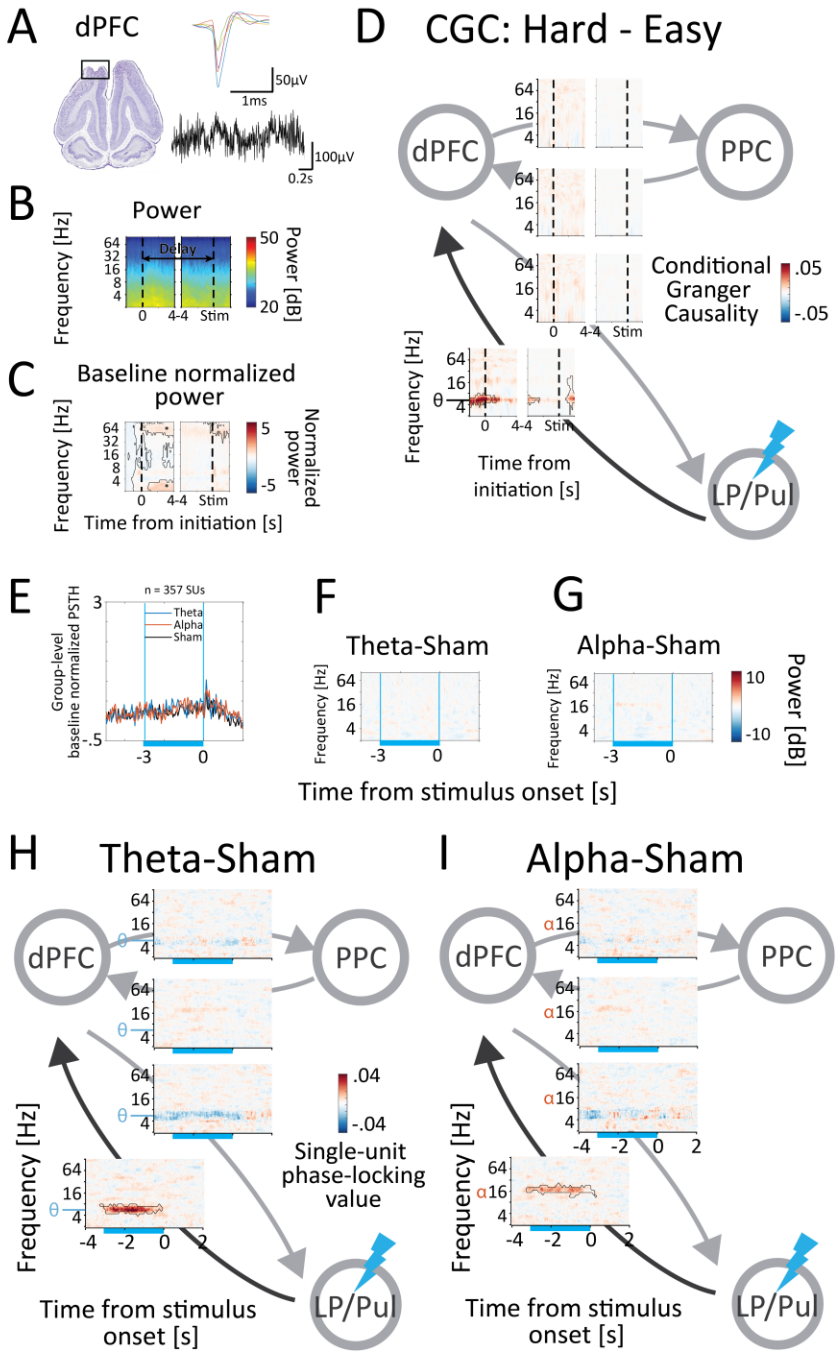

Figure 2.5. Absence of dPFC drive to the posterior network and optogenetic engagement

Same analysis as in Fig. 2.1-2.3 for dPFC and its connections. (**A**) (mirroring Fig. 1C) Nissl stained section with implantation localization in dPFC. Right: Example single-unit waveforms and LFP trace. (**B-D**) (mirroring Fig. 2.2, A, B, and D, respectively) Power spectrogram in dPFC (B), baseline ([-2, -1] s before

trial initiation) normalized power spectrogram in dPFC (C), and Conditional Granger Causality between studied region pairs for hard condition contrast easy condition (D) revealed little engagement of oscillations in dPFC that was modulated by attentional demand. (**E-I**) (mirroring Fig. 2.3, E, G, and I) Average baseline normalized firing rate for all SU in dPFC showed no difference between optogenetic conditions (E). Power spectrogram for dPFC around visual stimulus onset showed no optogenetically-induced oscillation in dPFC by neither theta (F) or alpha (G) optogenetic stimulation. (**H-I**) The single-unit phase-locking value between studied region-pairs from -4 to 2 seconds around visual stimulation, contrasting theta frequency laser stimulation (G) or alpha frequency laser stimulation (H) against the sham condition.

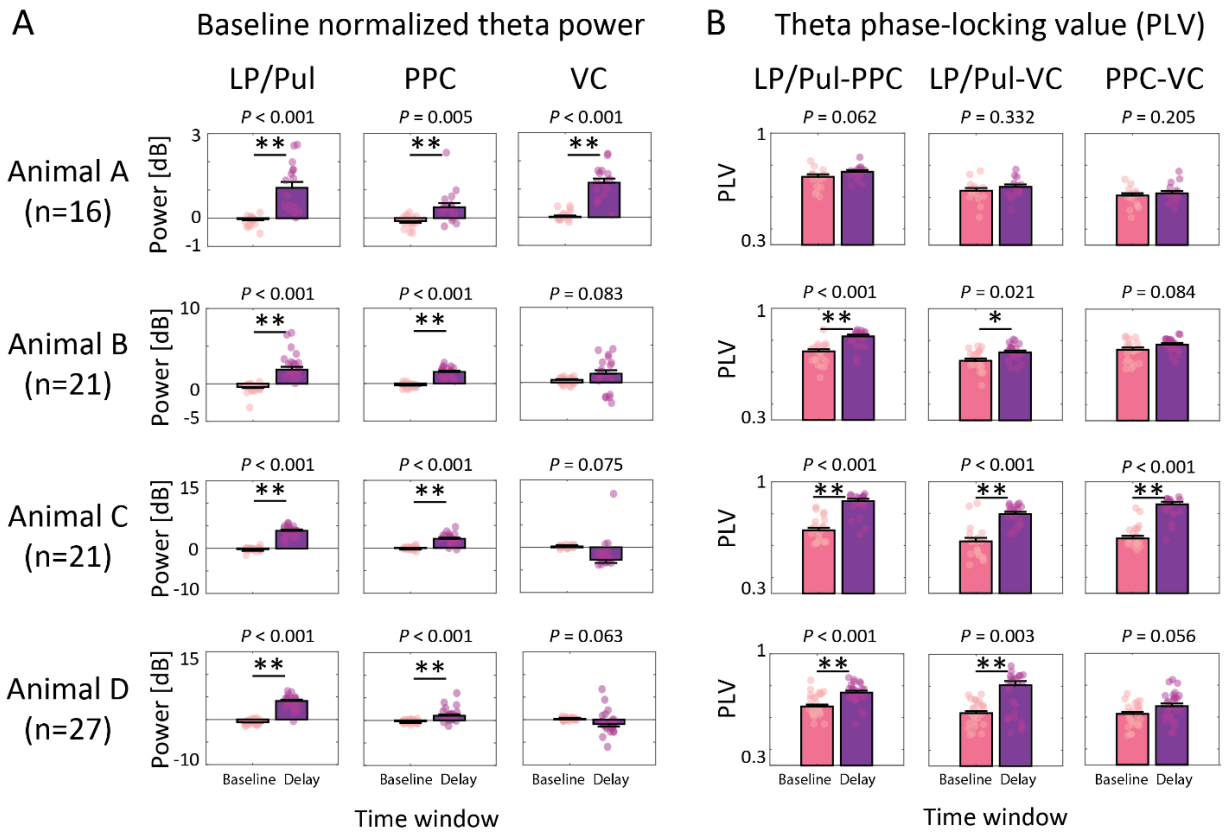

Figure 2.A. Baseline normalized theta power and phase-locking values for individual animals

Baseline ([-2, -1] s before trial initiation) normalized power (**A**) and phase-locking value (**B**) in the theta frequency band (4.5-7.5 Hz) averaged for the baseline period and during the delay duration (i.e. sustained attention period). Each row represents one animal. *P*-values were computed from 2-tailed paired t-test comparing session means during baseline versus delay period and corrected for multiple comparisons of 3 regions. The error bar represents the standard error of the mean. * $P < 0.05$, ** $P < 0.01$. Corresponding to Fig. 2.2, C and E.

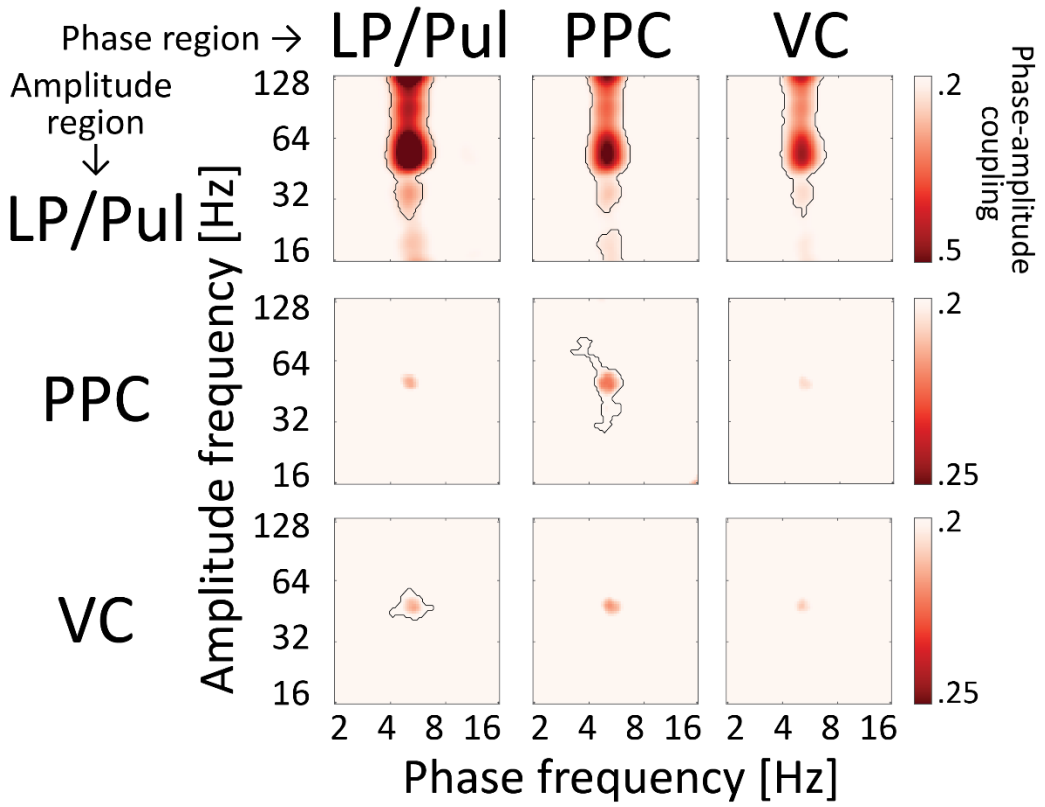

Figure 2.B. Cross-frequency coupling within and across studied regions

Columns represent high-frequency amplitude regions, rows represent low-frequency phase regions (i.e. LP/Pul, PPC, VC). Each plot shows phase-amplitude coupling strength (see Methods) by phase frequency (x-axis) and amplitude frequency (y-axis). Strong coupling is signified by hotter colors. Black contour denotes significant clusters by permutation test ($P < 0.05$). N = 84 sessions from 4 animals.

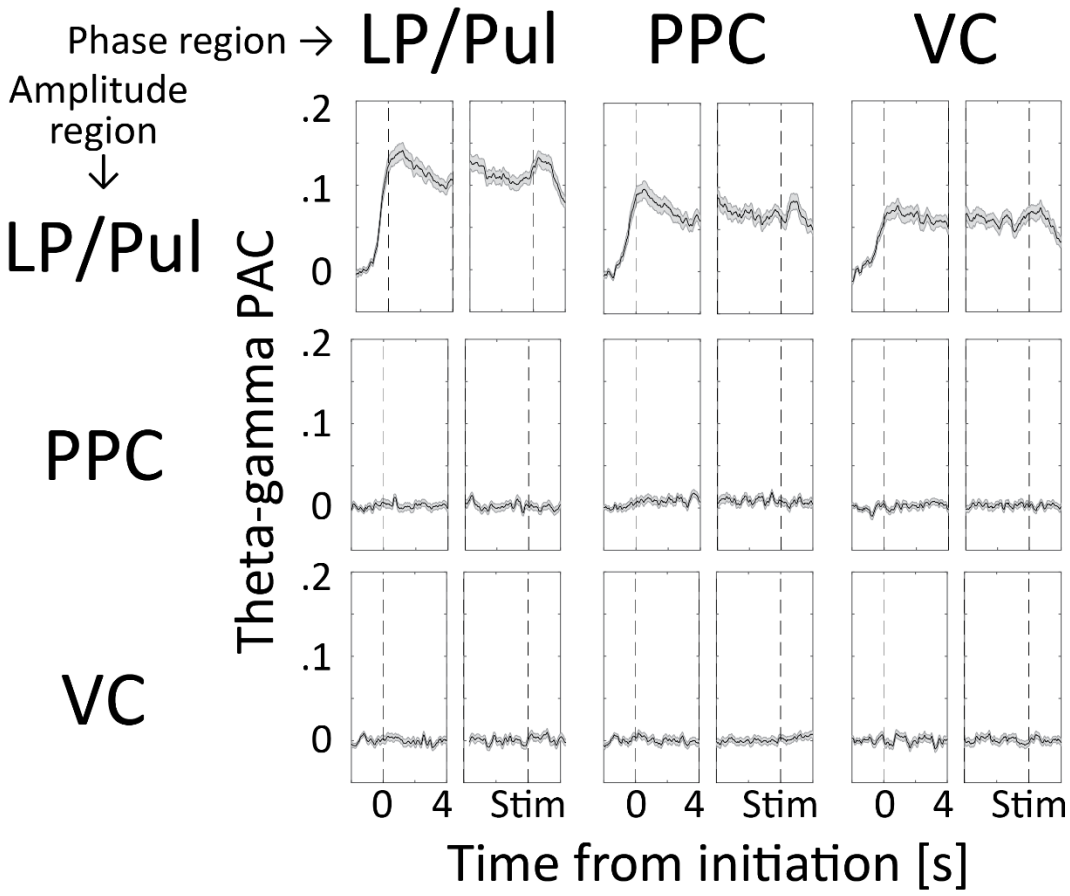

Figure 2.C. Baseline ([-2, -1] sec before initiation) normalized time-resolved theta-gamma phase-amplitude coupling (mean±sem)

Rows represent regions where gamma amplitudes were extracted from, and columns represent regions where theta phases were extracted from. Trials with random delay durations were aligned at trial initiation and stimulus onset separately (N = 84 sessions from 4 animals).

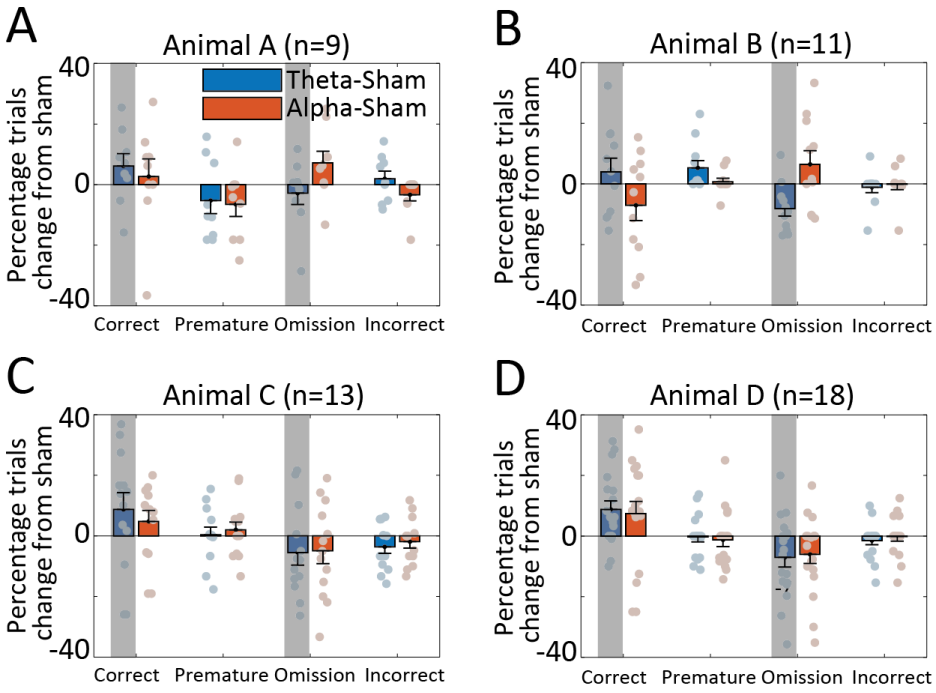

Figure 2.D. Behavioral results of optogenetic stimulation in LP/Pul for individual animals

(**A**) Optogenetic stimulation induced change of percentage points of correct / premature / omission / incorrect trials compared to sham condition for animal A (n = 9 sessions) (**A**), animal B (n = 11 sessions) (**B**), animal C (n = 13 sessions) (**C**), animal D (n = 18 sessions) (**D**). Each dot represents one session. Shaded bars highlighted consistent results across animals. Corresponding to Fig. 2.4 A.

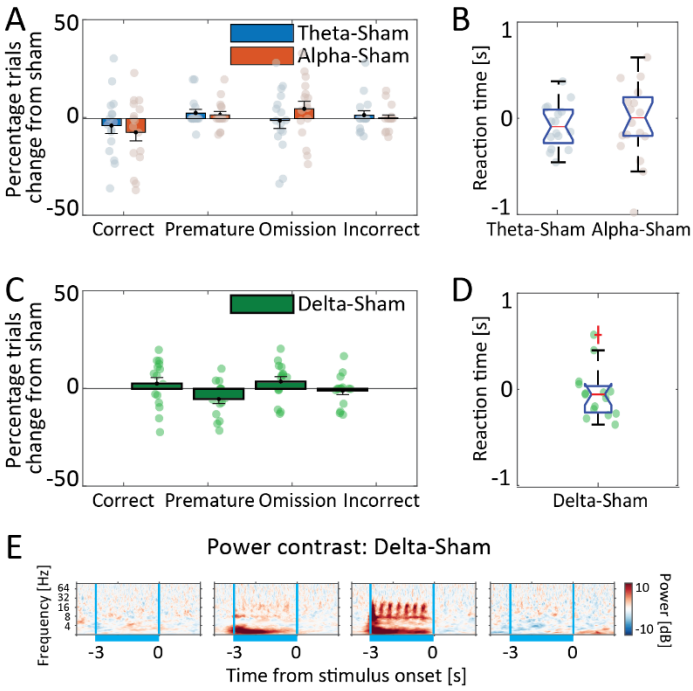

Figure 2.E. Animals' performance during control optogenetic stimulation sessions.

(**A**) Control optogenetic stimulation (with light blocked at the interface between the optic cable and optrode) induced change of percentage of correct / premature / omission / incorrect trials compared to sham condition. (**B**) Reaction time by optogenetic stimulation conditions. No significant changes were found in trial outcome or reaction time due to control optogenetic stimulation. For subplots A and B: N=19 sessions from 3 animals (Animal B, C, and D). (**C**) Control frequency delta stimulation-induced changes of percentage of correct / premature / omission / incorrect trials compared to sham condition. (**D**) Reaction time by optogenetic stimulation conditions. No significant changes were found in trial outcome or reaction time due to control optogenetic stimulation. (**E**) Power spectrum contrast between delta optogenetic stimulation condition and sham condition. For subplot C to E: N=15 sessions from 2 animals (Animal C and D).

REFERENCES

Bari, A., Dalley, J. W., & Robbins, T. W. (2008). The application of the 5-choice serial reaction time task for the assessment of visual attentional processes and impulse control in rats. *Nat Protoc, 3*(5), 759-767. doi:10.1038/nprot.2008.41

Barkley, R. A. (1997). Behavioral inhibition, sustained attention, and executive functions: constructing a unifying theory of ADHD. *Psychological bulletin, 121*(1), 65.

Barnett, L., & Seth, A. K. (2014). The MVGC multivariate Granger causality toolbox: a new approach to Granger-causal inference. *Journal of Neuroscience Methods, 223*, 50-68.

BLAIR, R. C., & KARNISKI, W. (1993). An alternative method for significance testing of waveform difference potentials. *Psychophysiology, 30*(5), 518-524. doi:https://doi.org/10.1111/j.1469-8986.1993.tb02075.x

Bora, E., Vahip, S., & Akdeniz, F. (2006). Sustained attention deficits in manic and euthymic patients with bipolar disorder. *Progress in Neuro-Psychopharmacology and Biological Psychiatry, 30*(6), 1097-1102.

Bourgeois, A., Guedj, C., Carrera, E., & Vuilleumier, P. (2020). Pulvino-cortical interaction: An integrative role in the control of attention. *Neurosci Biobehav Rev, 111*, 104-113. doi:10.1016/j.neubiorev.2020.01.005

Buschman, T. J., & Miller, E. K. (2007). Top-down versus bottom-up control of attention in the prefrontal and posterior parietal cortices. *Science, 315*(5820), 1860-1862.

Buzsaki, G. (2006). *Rhythms of the Brain*: Oxford university press.

Canolty, R. T., & Knight, R. T. (2010). The functional role of cross-frequency coupling. *Trends Cogn Sci, 14*(11), 506-515. doi:10.1016/j.tics.2010.09.001

Clayton, M. S., Yeung, N., & Cohen Kadosh, R. (2015). The roles of cortical oscillations in sustained attention. *Trends in cognitive sciences, 19*(4), 188-195. doi:https://doi.org/10.1016/j.tics.2015.02.004

Cuthbert, B. N., & Insel, T. R. (2013). Toward the future of psychiatric diagnosis: the seven pillars of RDoC. *BMC medicine, 11*(1), 126.

de Kloet, S. F., Bruinsma, B., Terra, H., Heistek, T. S., Passchier, E. M. J., van den Berg, A. R., . . . Mansvelder, H. D. (2021). Bi-directional regulation of cognitive control by distinct prefrontal cortical output neurons to thalamus and striatum. *Nat Commun, 12*(1), 1994. doi:10.1038/s41467-021-22260-7

Eradath, M. K., Pinsk, M. A., & Kastner, S. (2021). A causal role for the pulvinar in coordinating task-independent cortico-cortical interactions. *J Comp Neurol, 529*(17), 3772-3784. doi:10.1002/cne.25193

Fiebelkorn, I. C., Pinsk, M. A., & Kastner, S. (2019). The mediodorsal pulvinar coordinates the macaque fronto-parietal network during rhythmic spatial attention. *Nat Commun, 10*(1), 215. doi:10.1038/s41467-018-08151-4

Fortenbaugh, F. C., DeGutis, J., & Esterman, M. (2017). Recent theoretical, neural, and clinical advances in sustained attention research. *Annals of the New York Academy of Sciences, 1396*(1), 70-91. doi:10.1111/nyas.13318

Fries, P. (2005). A mechanism for cognitive dynamics: neuronal communication through neuronal coherence. *Trends in cognitive sciences, 9*(10), 474-480.

Geweke, J. (1982). Measurement of linear dependence and feedback between multiple time series. *Journal of the American statistical association, 77*(378), 304-313.

Geweke, J. F. (1984). Measures of conditional linear dependence and feedback between time series. *Journal of the American Statistical Association, 79*(388), 907-915.

Granger, C. W. (1969). Investigating causal relations by econometric models and cross-spectral methods. *Econometrica: Journal of the Econometric Society*, 424-438.

Grosenick, L., Marshel, J. H., & Deisseroth, K. (2015). Closed-loop and activity-guided optogenetic control. *Neuron, 86*(1), 106-139. doi:10.1016/j.neuron.2015.03.034

Jensen, O., & Mazaheri, A. (2010). Shaping functional architecture by oscillatory alpha activity: gating by inhibition. *Frontiers in human neuroscience, 4*, 186.

Kaas, J. H., & Lyon, D. C. (2007). Pulvinar contributions to the dorsal and ventral streams of visual processing in primates. *Brain Research Reviews, 55*(2), 285-296.

Kastner, S., Fiebelkorn, I. C., & Eradath, M. K. (2020). Dynamic pulvino-cortical interactions in the primate attention network. *Curr Opin Neurobiol, 65*, 10-19. doi:10.1016/j.conb.2020.08.002

Kim, H., Ährlund-Richter, S., Wang, X., Deisseroth, K., & Carlén, M. (2016). Prefrontal Parvalbumin Neurons in Control of Attention. *Cell, 164*(1-2), 208-218. doi:10.1016/j.cell.2015.11.038

Klimesch, W., Sauseng, P., & Hanslmayr, S. (2007). EEG alpha oscillations: the inhibition–timing hypothesis. *Brain Research Reviews, 53*(1), 63-88.

Kurmann, R., Gast, H., Schindler, K., & Fröhlich, F. (2018). Rational design of transcranial alternating current stimulation: Identification, engagement, and validation of network oscillations as treatment targets. *Clinical and translational neuroscience, 2*(2), 2514183X18793515.

Kvitsiani, D., Ranade, S., Hangya, B., Taniguchi, H., Huang, J. Z., & Kepecs, A. (2013). Distinct behavioural and network correlates of two interneuron types in prefrontal cortex. *Nature, 498*(7454), 363-366. doi:10.1038/nature12176

Lachaux, J.-P., Rodriguez, E., Martinerie, J., & Varela, F. J. (1999). Measuring phase synchrony in brain signals. *Human Brain Mapping, 8*(4), 194-208.

Lachaux, J. P., Rodriguez, E., Martinerie, J., & Varela, F. J. (1999). Measuring phase synchrony in brain signals. *Human Brain Mapping, 8*(4), 194-208.

Li, X., Sroubek, A., Kelly, M. S., Lesser, I., Sussman, E., He, Y., . . . Foxe, J. J. (2012). Atypical pulvinar–cortical pathways during sustained attention performance in children with attention-deficit/hyperactivity disorder. *Journal of the American Academy of Child & Adolescent Psychiatry, 51*(11), 1197-1207. e1194.

Lisman, J. E., & Jensen, O. (2013). The θ-γ neural code. *Neuron, 77*(6), 1002-1016. doi:10.1016/j.neuron.2013.03.007

Liu, S. K., Chiu, C.-H., Chang, C.-J., Hwang, T.-J., Hwu, H.-G., & Chen, W. J. (2002). Deficits in sustained attention in schizophrenia and affective disorders: stable versus state-dependent markers. *American Journal of Psychiatry, 159*(6), 975-982.

Maris, E., & Oostenveld, R. (2007). Nonparametric statistical testing of EEG- and MEG-data. *J Neurosci Methods, 164*(1), 177-190. doi:10.1016/j.jneumeth.2007.03.024

McAlonan, K., Cavanaugh, J., & Wurtz, R. H. (2008). Guarding the gateway to cortex with attention in visual thalamus. *Nature, 456*(7220), 391-394.

Nuechterlein, K. H., Green, M. F., Calkins, M. E., Greenwood, T. A., Gur, R. E., Gur, R. C., . . . Seidman, L. J. (2015). Attention/vigilance in schizophrenia: performance results from a large multi-site

study of the Consortium on the Genetics of Schizophrenia (COGS). *Schizophrenia research, 163*(1), 38-46.

Ohye, C. (2002). Thalamus and Thalamic Damage. In V. S. Ramachandran (Ed.), *Encyclopedia of the Human Brain* (pp. 575-597). New York: Academic Press.

Pachitariu, M., Steinmetz, N. A., Kadir, S. N., Carandini, M., & Harris, K. D. (2016a). Fast and accurate spike sorting of high-channel count probes with KiloSort. *Advances in neural information processing systems, 29*, 4448-4456.

Pachitariu, M., Steinmetz, N. A., Kadir, S. N., Carandini, M., & Harris, K. D. (2016b). *Fast and accurate spike sorting of high-channel count probes with KiloSort.* Paper presented at the Advances in neural information processing systems.

Pagliaccio, D., Wiggins, J. L., Adleman, N. E., Harkins, E., Curhan, A., Towbin, K. E., . . . Leibenluft, E. (2017). Behavioral and neural sustained attention deficits in bipolar disorder and familial risk of bipolar disorder. *Biological psychiatry, 82*(9), 669-678.

Pernet, C., Wilcox, R., & Rousselet, G. (2013). Robust Correlation Analyses: False Positive and Power Validation Using a New Open Source Matlab Toolbox. *Front Psychol, 3*(606). doi:10.3389/fpsyg.2012.00606

Radtke-Schuller, S. (2018). *Cyto-and myeloarchitectural brain atlas of the ferret (Mustela putorius) in MRI aided stereotaxic coordinates*: Springer.

Radtke-Schuller, S., Town, S. M., Yin, P., Elgueda, D., Schuller, G., Bizley, J. K., . . . Fritz, J. B. (2020). Dorsal prefrontal and premotor cortex of the ferret as defined by distinctive patterns of thalamo-cortical projections. *Brain Structure and Function, 225*(5), 1643-1667. doi:10.1007/s00429-020-02086-7

Saalmann, Y. B., Pinsk, M. A., Wang, L., Li, X., & Kastner, S. (2012). The pulvinar regulates information transmission between cortical areas based on attention demands. *Science, 337*(6095), 753-756.

Sarter, M., Givens, B., & Bruno, J. P. (2001). The cognitive neuroscience of sustained attention: where top-down meets bottom-up. *Brain Research Reviews, 35*(2), 146-160.

Sarter, M., Givens, B., & Bruno, J. P. (2001). The cognitive neuroscience of sustained attention: where top-down meets bottom-up. *Brain Res Brain Res Rev, 35*(2), 146-160. doi:10.1016/s0165-0173(01)00044-3

Scolari, M., Seidl-Rathkopf, K. N., & Kastner, S. (2015). Functions of the human frontoparietal attention network: Evidence from neuroimaging. *Current Opinion in Behavioral Sciences, 1*, 32-39. doi:https://doi.org/10.1016/j.cobeha.2014.08.003

Sellers, K. K., Yu, C., Zhou, Z. C., Stitt, I., Li, Y., Radtke-Schuller, S., . . . Fröhlich, F. (2016). Oscillatory dynamics in the frontoparietal attention network during sustained attention in the ferret. *Cell reports, 16*(11), 2864-2874. doi:10.1016/j.celrep.2016.08.055

Stitt, I., Zhou, Z. C., Radtke-Schuller, S., & Fröhlich, F. (2018). Arousal dependent modulation of thalamo-cortical functional interaction. *Nat Commun, 9*(1), 2455. doi:10.1038/s41467-018-04785-6

Sweeney-Reed, C. M., Zaehle, T., Voges, J., Schmitt, F. C., Buentjen, L., Borchardt, V., . . . Knight, R. T. (2017). Anterior Thalamic High Frequency Band Activity Is Coupled with Theta Oscillations at Rest. *Frontiers in human neuroscience, 11*(358). doi:10.3389/fnhum.2017.00358

Szczepanski, S. M., Crone, N. E., Kuperman, R. A., Auguste, K. I., Parvizi, J., & Knight, R. T. (2014). Dynamic changes in phase-amplitude coupling facilitate spatial attention control in fronto-parietal cortex. *PLoS biology, 12*(8), e1001936.

Tucha, L., Fuermaier, A. B., Koerts, J., Buggenthin, R., Aschenbrenner, S., Weisbrod, M., . . . Tucha, O. (2017). Sustained attention in adult ADHD: Time-on-task effects of various measures of attention. *Journal of Neural Transmission, 124*(1), 39-53.

Vanhatalo, S., Palva, J. M., Holmes, M., Miller, J., Voipio, J., & Kaila, K. (2004). Infraslow oscillations modulate excitability and interictal epileptic activity in the human cortex during sleep. *Proceedings of the National Academy of Sciences, 101*(14), 5053-5057.

Ward, L. M. (2003). Synchronous neural oscillations and cognitive processes. *Trends in cognitive sciences, 7*(12), 553-559. doi:https://doi.org/10.1016/j.tics.2003.10.012

Wimmer, R. D., Schmitt, L. I., Davidson, T. J., Nakajima, M., Deisseroth, K., & Halassa, M. M. (2015). Thalamic control of sensory selection in divided attention. *Nature, 526*(7575), 705-709.

Yu, C., Li, Y., Stitt, I. M., Zhou, Z. C., Sellers, K. K., & Frohlich, F. (2018). Theta Oscillations Organize Spiking Activity in Higher-Order Visual Thalamus during Sustained Attention. *Eneuro, 5*(1), ENEURO.0384-0317.2018. doi:10.1523/eneuro.0384-17.2018

Yu, C., Sellers, K. K., Radtke-Schuller, S., Lu, J., Xing, L., Ghukasyan, V., . . . Frohlich, F. (2016). Structural and functional connectivity between the lateral posterior-pulvinar complex and primary visual cortex in the ferret. *Eur J Neurosci, 43*(2), 230-244. doi:10.1111/ejn.13116

Yu, C., Sellers, K. K., Radtke-Schuller, S., Lu, J., Xing, L., Ghukasyan, V., . . . Fröhlich, F. (2016). Structural and functional connectivity between the lateral posterior–pulvinar complex and primary visual cortex in the ferret. *European Journal of Neuroscience, 43*(2), 230-244.

Zhou, H., Schafer, R. J., & Desimone, R. (2016). Pulvinar-cortex interactions in vision and attention. *Neuron, 89*(1), 209-220.

CHAPTER 3: TRANSCRANIAL ALTERNATING CURRENT STIMULATION ENTRAINS ALPHA OSCILLATIONS BY PREFERENTIAL PHASE SYNCHRONIZATION OF FAST-SPIKING CORTICAL NEURONS TO STIMULATION WAVEFORM [2]

INTRODUCTION

Transcranial electric stimulation (tES) is a noninvasive brain stimulation modality that delivers weak electric current of typically up to 2 mA zero-to-peak amplitude to the scalp (Fröhlich, 2014b). Transcranial direct current stimulation (tDCS) and transcranial alternating current stimulation (tACS) are the two most common types of tES, where a constant or sinusoidal current waveform is used for stimulation, respectively. The majority of the stimulation current is shunted by the scalp (Fröhlich, 2016), so a relatively small fraction of the current actually enters the brain and produces electric fields in the range of 0.2–0.5 mV/mm (Datta et al., 2009; Fröhlich, 2016; Pedro Cavaleiro Miranda, Lomarev, & Hallett, 2006; Sadleir, Vannorsdall, Schretlen, & Gordon, 2010). Recently, controversy has engulfed the field due to the heterogeneity of behavioral findings (Brignani, Ruzzoli, Mauri, & Miniussi, 2013; A. Liu et al., 2018; Sahlem et al., 2015) and the claim that weak perturbations are not strong enough to entrain networks (Y. Huang et al., 2017; Lafon et al., 2017; A. Liu et al., 2018; Vöröslakos et al., 2018).

Targeted tACS modulation of cortical oscillations and associated cognitive and behavioral functions have been demonstrated in a number of human studies (Andrea Antal et al., 2008; Boyle &

[2] This chapter previously appeared as an article in Nature Communication; doi: 10.1038/s41467-021-23021-2 (https://www.nature.com/articles/s41467-021-23021-2#citeas). The original citation is as follows: **Huang WA*,** Stitt IM*, Negahbani E, Passey DJ, Ahn S, Davey M, Dannhauer M, Doan TT, Hoover AC, Peterchev AV, Radtke-Schuller S, Fröhlich F. Transcranial alternating current stimulation entrains alpha oscillations by preferential phase synchronization of fast-spiking cortical neurons to stimulation waveform. Nat Commun 12, 3151 (2021).
Huang WA mainly contributed to the animal research. Computational modeling was done by other co-authors.

Frohlich, 2013; Randolph F. Helfrich et al., 2014; Christoph S Herrmann, Murray, Ionta, Hutt, & Lefebvre, 2016b; Florian H Kasten & Christoph S Herrmann, 2017; Neuling, Rach, & Herrmann, 2013; Polanía, Nitsche, Korman, Batsikadze, & Paulus, 2012; Alexandra Vossen, Joachim Gross, & Gregor Thut, 2015; Zaehle, Rach, & Herrmann, 2010). In addition, clinical trials of tACS for the treatment of schizophrenia (Ahn et al., 2019), chronic pain (Ahn, Prim, Alexander, McCulloch, & Fröhlich, 2018) and major depressive disorder (Alexander et al., 2018) have been reported. These clinical trials demonstrated successful target engagement and enhanced alpha oscillations after repeated application of tACS. More is known about these "offline" (i.e., after stimulation) effects since tACS introduces non-trivial artifacts into non-invasive electrophysiology techniques such as EEG (electroencephalography) (Nima Noury, Joerg F. Hipp, & Markus Siegel, 2016). At the level of large-scale neuronal populations, animal studies have provided evidence for "online" (i.e., during stimulation) modulation of neural oscillators by tACS in vitro and in vivo (Ali, Sellers, & Fröhlich, 2013; Jacqueline K Deans, Andrew D Powell, & John GR Jefferys, 2007; Fröhlich & McCormick, 2010; Ozen et al., 2010; Radman, Su, An, Parra, & Bikson, 2007; Davide Reato, Asif Rahman, Marom Bikson, & Lucas C Parra, 2010; Stephen L Schmidt, Iyengar, Foulser, Boyle, & Fröhlich, 2014). At the single neuron level, tACS polarizes neurons with alternating polarity resulting in a subthreshold resonance where the hyperpolarization-activated cation current plays a key role in the neural response (F. Aspart, M. W. Remme, & K. Obermayer, 2018; E. H. Toloza, Negahbani, & Frohlich, 2017). Despite these successful demonstrations that weak periodic electric fields interact with neural oscillators, the mechanism of action remains unclear. Using a computational model of a large-scale cortical network of spiking neurons, we previously studied how tACS entrains ongoing oscillations(Ali et al., 2013). We found a triangular region of high synchrony between the stimulation waveform and endogenous neuronal oscillations where higher stimulation amplitudes yielded a wider range of entrained frequencies. This triangular region of stimulation amplitude and frequency pairs is referred to as an Arnold tongue, which is centered on the frequency of the endogenous oscillation. The Arnold tongue is typically found when studying the dynamical properties of coupled oscillators and when characterizing the regions in parameter space where phase locking occurs between two oscillators (Pikovsky, Rosenblum, & Kurths, 2003). These

model-driven predictions along with the existing entrainment hypothesis, which is supported by in vitro studies and in vivo studies in anesthetized rodents, comprise the current mechanistic understanding of tACS. Despite the successful demonstration of long-lasting tACS effects in human studies, a full mapping of the space of stimulation parameters that demonstrates a pattern of synchronization in the form of the Arnold tongue remains missing. The major roadblocks for this gap are the technical challenges of simultaneous tACS and EEG recording in human studies, even with some recent attempts to avoid or filter the large electrical artefact of tACS (Grossman et al., 2017; Negahbani, Kasten, Herrmann, & Fröhlich, 2018; Nima Noury, Joerg F Hipp, & Markus Siegel, 2016; Noury & Siegel, 2017, 2018; Witkowski et al., 2016).

To address this gap in knowledge, we investigated neural entrainment of alpha oscillations by tACS in awake head-fixed ferrets. We used tACS parameters that induced (computationally estimated) electric field amplitudes of <0.5 mV/mm, which are comparable to the estimated field amplitudes typically reported in human tACS paradigms. We first demonstrated the presence of alpha oscillations (11-17 Hz) in the awake head-fixed ferret with simultaneous recording from the posterior parietal cortex (PPC), the primary visual cortex (VC) and the lateral posterior nucleus/Pulvinar complex of thalamus (LP). In functional agreement with human and non-human primate studies of alpha oscillations, the recordings pointed to top-down control of the network by alpha oscillations (Bollimunta, Mo, Schroeder, & Ding, 2011; S. Palva & Palva, 2011). The alpha amplitude was strongest in PPC which influenced both VC and LP regions in the alpha frequency band as demonstrated by functional and effective connectivity between these areas. Further analysis on putatively classified neuron types showed that the alpha synchrony between the network oscillations and neuronal firing rates was stronger for narrow-spiking neurons compared to broad-spiking neurons. To probe for the presence of an Arnold tongue, the hypothesized mechanism of action of tACS, we systematically varied both stimulation amplitude and frequency. We found evidence supportive of the Arnold tongue for PPC neurons, and narrow-spiking neurons showed stronger phase locking to tACS when compared to broad-spiking neurons. Despite the comparable amplitude of tACS electric field in all three

studied regions, we did not find clear an Arnold tongue for VC or LP neurons. In addition, we addressed and excluded several potential confounds such as entrainment by peripheral stimulation. . We finally examined the effect of tACS in a computational model of the thalamo–cortical network, which confirmed the main features of our experimental findings. Our work provides in-vivo evidences on how weak electric fields (< 0.5 mV/mm) can entrain neuronal activity and supports the model-driven predictions of the Arnold tongue as the mechanism of action of tACS.

METHODS

Animals

Three adult spayed female ferrets (*Mustela putorius furo*, 4 months old at the beginning of the experiment) were used in this study. All animal procedures were performed in compliance with the National Institute of Health guide for the care and use of laboratory animals (NIH publication No. 8023, revised 1987) and the United States Department of Agriculture, and were approved by the Institutional Animal Care and Use Committee of the University of North Carolina at Chapel Hill.

Head-post, bone screws, and electrode implantation surgery

The initial induction of anesthesia was performed with intramuscular injection of ketamine/xylazine (30 mg/kg of ketamine, 1-2 mg/kg of xylazine). After confirming the loss of paw pinch reflex, animals were intubated for isoflurane (0.5-2% in 100% oxygen) delivery via mechanical ventilation. The physiological parameters including electroencephalogram, partial oxygen concentration, end-tidal CO2, and rectal temperature were continuously monitored throughout the surgical procedure to maintain the animal in a stable state of deep anesthesia. All surgical procedures were performed under sterile conditions. The skull was fixed to a stereotactic frame using a mouthpiece and ear bars to enable accurate identification of target regions and electrode implantations. A custom-designed stainless-steel head-post was first secured to the anterior part of the exposed skull via four stainless steel bone screws. A craniotomy was performed over the left hemisphere of PPC to implant Microelectrode arrays in PPC and LP regions. Another craniotomy was performed over the left hemisphere of VC region. The dura and then pia were

removed before lowering the LP microelectrode array (2 × 8 tungsten electrodes, 35 µm diameter, 9 mm length, 250 µm spacing; Microprobes for Life Science, Gaithersburg MD). The second microelectrode array (2 × 8 or 2 × 16 tungsten electrodes, 35 µm diameter, 9 mm length, 200 µm spacing; Innovative Neurophysiology, Durham NC) was lowered to deep cortical layers in the lateral gyrus (PPC). The third microelectrode array (2 × 8 tungsten electrodes, 35 µm diameter, 9 mm length, 200 µm spacing; Innovative Neurophysiology) was implanted in VC area after removal of dura and pia layers. The reference electrode was directly adjacent to the corresponding recording electrodes for all three microelectrode arrays. Each microelectrode array had a silver wire for ground connection. Three bone screws on the other hemisphere were used as ground for each microelectrode array. The EEG bone screws were placed on both sides of the PPC craniotomy. Microelectrode arrays were fixed in place with dental cement. After the dental cement hardened, the muscle and the skin around the incision were sutured together. Animals were administered preventative analgesics and antibiotics for one week after surgery, while recovering in their home cage for at least one week prior to recordings.

For the animals in the bone screw stimulation experiments, two bone screws were screwed half-way into the skull, avoiding direct contact with the cortex. The bone screws were positioned just anterior and posterior to the PPC craniotomy, respectively. The subsequent electrode implantation procedures were the same as described above.

Virus injection and optrode implantation surgery

For the optogenetic stimulation experiment, the preparation and recovery were the same as described above. Before the implantation, 0.4 µL of rAAV5-CaMKII-ChR2-mCherry was injected into PPC. Then, an electrode array that include an optical fiber (optrode) was implanted (electrode tips and optical fibers are secured 100 and 400 µm above the virus injection site, respectively) (16 channel circular Platinum/Iridium electrode, 125 µm diameter, 5 mm length, 250 µm spacing; fiber optic 4.5 mm length, 200 µm core outer diameter; Microprobes for life science, Gaithersburg, MD). Custom-designed plastic cylinders were implanted around the light fibers to anchor the optical fiber from the laser during recordings

and to prevent laser light leakage. Bone screws on the other hemisphere were used as ground for each microelectrode array. Three weeks elapsed before stimulation experiments for sufficient expression of the opsin in the targeted neurons. Resting state recordings were collected 1 week after the surgery to identify the individual endogenous alpha frequency. Sinewave modulated optogenetic stimulation was applied around 3 weeks after the surgery.

Transcranial electric current stimulation procedure

Two circular tACS electrodes (r = 5 mm) were prepared by trimming conventional carbon-silicone tACS electrodes. The electrodes were applied to the ferret head using Ten20 conductive EEG paste over the left frontal area (directly above left eye) and central posterior area (over the neck). The digital tACS waveforms with desired timing and frequency were first generated using a Matlab script, then converted to analogue signal using a National Instruments DAQ device. The analogue outputs were connected to an A395 linear stimulation isolator (World Precision Instruments) to produce the final tACS currents that were delivered to the head via the tACS electrodes. For each stimulation session, the head-fixed animal received 54 stimulation blocks, each 90 sec with 10 sec inter-stimulus intervals. Each stimulation block was randomly selected from a pool of 54 different combination of stimulation amplitudes (5, 10, 15, 20, 40, 80 μA, all zero-to-peak) and frequencies (alpha−4, alpha−3, …, alpha, …, alpha+3, alpha+4 Hz, where alphas stands for the endogenous alpha frequency). This random order was chosen to minimize the theoretical risk of a cumulative effect of stimulation that would bias the results. The stimulation and simultaneous electrophysiological measurements were performed in a room with dim lights while animal was awake and not engaged in any task.

Peripheral nerve electric current stimulation procedure

To control for peripheral nerve activation during tACS, the procedure and parameters of the peripheral nerve electric current stimulation were identical to the tACS stimulation procedure with the only difference being the position of the tACS electrodes. Instead of placing the two circular tACS electrodes

on the head, in this experiment, the tACS electrodes were placed on the shaved back. The distance between the two electrodes were also kept the same as in the tACS stimulation (i.e., around 6 cm).

Long-lasting transcranial electric current stimulation procedure

The same tACS setup was used in this procedure. The stimulation was given once per day for 14 days. In each stimulus session, there was a 5 or 10 minutes of resting state recording before the onset of tACS (i.e., pre), followed by 20 or 40 minutes of continuous tACS, and then followed by another 10 minutes of resting state recording (i.e. post). During the stimulation period, a single frequency (individual endogenous alpha) at 80 μA was applied via the tACS electrodes. The animal was not involved in any other experiment during this long-lasting effect procedure.

Bone screw electric current stimulation procedure

To serve as a control for local stimulation, the procedure and parameters of the electric current stimulation were identical to the tACS stimulation procedure with the only difference being the stimulation electrodes. The distance between the two bone screws was about 11 mm, which is closer than for the tACS setup.

Alternating current modulated optogenetic stimulation procedure

After about three weeks to allow for virus expression, we started simultaneous optogenetics and electrophysiology recording. A blue laser at 475nm (Shanghai Laser & Optics Century Co., Ltd., BL473T3) was used to activate the ChR2 in PPC. Before each session, the laser power was calibrated to ensure consistency across sessions, and black sheets were applied as covers around the optic cable connection to avoid light leakage. Laser intensity was modulated by a custom MATLAB script that was used for tACS, with a minor modification for elevating the baseline voltage to ensure that the light was not modulated only for the positive half of the oscillation cycle. We used 19, 20, 21, 22, 25, 29 mW peak laser power.

Electric potential measurements

To validate the electric field model of tACS in the ferret brain, we collected intracranial measurements of electric potentials from the electrode arrays in PPC, VC, and LP for one animal across three recording sessions. The potentials of the electrodes in all three ROIs were referenced to a single electrode potential in the proximity of a particular ROI that was changed for each recording session (for simplicity all sessions were subsequently re-referenced to the first electrode channel of the LP electrode array). During these in-vivo measurements, sinusoidal electric current was injected through tACS scalp electrodes using a fixed zero-to-peak current amplitude of 60 or 80 μA. Four blocks of measurements were recorded in an alternating pattern (60, 80, 60, 80 μA); other parameters were kept constant: frequency = 14 Hz, measurement trial duration = 3 min, interval between trials = 24 s). Thus, for each tACS current amplitude there were six recording sets (two blocks and three reference schemes). The electrode potentials were recorded with a sampling frequency of 333.33 Hz, and were passed through a digital band-pass filter (order: 263, generalized equiripple filter with passband of 12–16 Hz, stopband cutoff frequencies = 8, 20 Hz; stopband gain = 90 dB; passband gain = 1 dB). To reliably extract the signal amplitude for each electrode, the recorded potentials were fitted to a reference sinewave using the MATLAB function 'fit'. The reference waveform was derived by fitting a sine function to the potential waveforms from the electrode array (LP, PPC or VC) with the largest signal per recording set. The sine frequency and phase estimates for each available array electrode ($r^2 > 0.997$) were averaged to define the reference waveform. The amplitude of the reference sinewave was then fitted to the potential from each electrode in each recording set, and data from noisy electrodes ($r^2 < 0.75$) were discarded. The standard deviation across the recording sets was computed for the remaining fitted amplitudes within each electrode, and the MATLAB 'isoutlier' function (with default settings) was used to exclude electrodes with large standard deviation, and therefore poor reproducibility. The amplitude estimates were averaged within the remaining electrodes to reduce measurement noise in the final values. Out of 9 nominally connected electrodes per array, 8, 6, and 8 electrodes survived these quality checks for the LP, PPC, and VC arrays, respectively.

Computational modeling of electric field distribution in ferret head

We developed a finite element model for a sex- and age-matched ferret head to study the tACS electric field distribution in the brain. The modeling pipeline comprises five steps: image acquisition, image registration, image segmentation and implant model, complete model meshing, and electric field calculation (see Supplementary Fig. 3.E). CT and MRI images of an in vivo ferret head without any surgical alterations were collected and manually co-registered. These images were segmented into six tissue regions with different electrical properties: white matter, gray matter, cerebrospinal fluid, nasal cavity (air), skull, and scalp. The neck was not modeled since it was outside the MRI field of view. We validated this approximation by attaching a cylinder with scalp conductivity where the neck would be in the ferret model, making the model about 25% longer; the electric field distribution in the brain did not change significantly and the peak field strength decreased by only 1.2%, demonstrating low electric field sensitivity to inclusion of the neck. The image segmentation was modified to include craniotomy tissue alterations, such as implanted hardware and insulating materials based on CAD models. The three-dimensional model was meshed into finite tetrahedral elements. Using previously reported values (Y. Huang et al., 2017; Kumar, Rajasekhar, Subhan, Panduranga, & Gupta, 2014; Steels, 2008) a tissue electric conductivity was assigned to each element of the mesh (Supplementary Table S1). Finally, the finite element problem was solved to calculate the electric potentials and electric field.

Image acquisition

In-vivo magnetic resonance imaging (MRI) of an animal without any surgical alterations was acquired in a Bruker 9.4 T scanner (Bruker AVANCE, Billerica, MA). The MR scan was collected using a RARE-sequence, with TR = 2000 ms, TE = 9.610 ms, voxels = isotropic 0.2 mm3, FOV = 42×42×36 mm, 210 sagittal slices. Ex-vivo computed tomography (CT) imaging of the same animal was acquired on an eXplore CT 120 (GE Healthcare) scanner. The CT scan was collected with isotropic 0.0995 mm3 voxels and matrix dimension = 430×363×883. Ex-vivo CT imaging of a different animal with craniotomy was

acquired on an eXplore speCZT (GE Healthcare) scanner. The CT scan was collected with isotropic 0.0995 mm3 voxels and matrix dimension = 430×363×883.

Tissue Segmentation

Ferret head model generation began with manual image co-registration of the MRI and CT scans using 3D Slicer (4.8.0) (Fedorov et al., 2012). To correct for bias field inhomogeneity, N4ITKBiasFieldCorrection (Tustison et al., 2010), a 3D Slicer tool, was applied to the MRI prior to co-registration. This co-registration is able to combine the soft tissues and air seen in the MRI with the hard tissue (skull) seen in the CT. The co-registered images were manually segmented using 3D Slicer into six different regions: white and gray matter, cerebrospinal fluid, nasal cavity (air), skull, and scalp. Further, the three brain ROIs (LP, PPC, and VC) were defined, including both white and gray matter. To avoid problems during meshing of smoothed surfaces derived from the segmentation, we upsampled the segmentation from 430×363×883 isotropic voxels (0.0995 mm^3 each) to 538×454×1104 isotropic voxels (0.0796 mm^3 each). Smoothing and gap filling of the segmentation were performed by utilizing the interactive segmentation software SimpleWare ScanIP (O-2018.12, SIMPLEWARE Ltd., Exeter, UK).

Finite element meshing

All hardware affixations were reconstructed using SolidWorks (2016 X64 Edition) from the registered CT data set, positioned in the model, and converted into segmented regions with the aid of photos taken after surgery, unless specified otherwise. The model represented a post-surgery ferret head with craniotomy, implanted hardware components, and insulating materials used in the experimental setup. Images of the electrodes were used in the reconstruction and positioning of realistically shaped tACS electrodes on the model ferret head. The head post, head post bone screws, dental cement, and acrylic glue were represented in the model. The recording electrode arrays were not modeled as they were too small and had a high electrical impedance. The head post was reconstructed and positioned based on post-surgery CT imaging and photos, replacing skull voxels in that region. The head post bone screws were reconstructed using manufacturer datasheets and positioned into the screw holes of the head post, replacing skull voxels

in that region. The acrylic glue was reconstructed with a rectangular prism shape that was modified to wrap around the head post and the head of the bone screws by subtracting skull, head post, and bone screw voxels from it. The dental cement filling the craniotomy was reconstructed by merging a cylinder and a rectangular prism shape and wrapping the composite around the head post and dental cement. The shape replaced scalp voxels in that region and was subtracted from the skull, head post, and acrylic glue voxels. To prevent overlapping, all tissues and materials were subtracted from each other and combined together from the inside out. The ScanFE module in ScanIP was used to convert the segmented images of both head models to finite element meshes. The resulting mesh consisted of 4.2 million tetrahedrons with 0.74 million nodes.

Electric potential and field computation

The electric potentials, electric field, and current density were computed in COMSOL Multiphysics 5.4 and 5.5 (COMSOL Inc., Burlington, MA, USA). The finite element mesh was imported into COMSOL, and a set of isotropic conductivity values were assigned to the mesh as listed in Supplementary Table S1. The top surface of the occipital stimulation pad was injected with a fixed current of 60 or 80 μA, while the top surface of the frontal stimulation pad was assigned as ground. To calculate the electric potential and field distribution, the quasi-static Laplace equation

$$\nabla.(\sigma\nabla V) = 0 \quad (1)$$

was solved with appropriate boundary conditions using the preconditioned conjugate solver and a relative tolerance of 10−6, where V and σ represent the electric potential and electric conductivity, respectively. Using the quasi-static approximation makes it possible to scale the stimulation current linearly to achieve the desired electric potential or electric field. The electric potentials were extracted from specific coordinate points in the model corresponding to the ideal ROI electrode locations, as the ROI electrodes were assumed to be small point-like electrodes.

Figure 4 a-c and 4 f-j were plotted in MATLAB R2019a. Figure 4 d,e and Supplementary Figure S7 were plotted in COMSOL Multiphysics 5.4/5.5. Supplementary Figure S6 was created using MATLAB

R2019a and visualized in SCIRun 4.7 (R45839) after exporting the finite element mesh and the current density at the center of each tetrahedral element from COMSOL and converting it to electric field strength using respective tissue conductivities. To extract the surface-normal electric field component, first outward-pointing normal vectors of unit length were computed for each brain-surface triangle as averages of surrounding triangles. SCIRun was used to linearly interpolate the electric field in the gray matter onto the surface-nodes, and the dot product of the field and the nodal surface normal was taken to compute the surface-normal electric field component.

Verifying electrode positions with histology

The animals were euthanized with an overdose of ketamine/xylazine after reaching the scientific endpoint and perfused immediately with 4% phosphate buffered paraformaldehyde. After removing the brain from the skull, it was post-fixed overnight in the same solution, cryoprotected in 30% phosphate buffered sucrose solution, shock frozen in dry ice and cut into 50 µm thick sections with a with a cryostat (CM3050S, Leica Microsystems). Sections were separated into two series and stained for cells (Nissl) or cytochrome oxidase. Imaging was conducted with an Aperio VERSA bright-field slide scanner at 10x magnification. The electrode arrays were located in the sections by electrode tracks, tissue damage or loss and atlas based reconstructed by comparing and documenting the sections to ferret atlas plates (Radtke-Schuller, 2018).

Electrophysiological data analysis

Spectral domain analysis: We used wavelet transform for spectral decomposition. The wavelets ($w(t, f_0)$ have Gaussian shape both in time and frequency:

$$w(t, f_0) = A \cdot exp(-t^2/2{\sigma_t}^2) \cdot exp(-2i\pi f_0 t) \quad (2)$$

where f_0 is the central frequency, $A = \left(\sigma_t\sqrt{\pi}\right)^{-1/2}$ is a normalization factor to make the wavelet energy equal to 1, and σ_t is the time domain standard deviation that relates to frequency domain standard deviation (σ_f) as

$$\sigma_t = \frac{1}{2\pi\sigma_f} \quad (3)$$

The frequency domain standard deviation is defined as a constant depending on central frequency of the wavelet as $\sigma_f = f_0/7$ (Tallon-Baudry, Bertrand, Delpuech, & Pernier, 1996). The local field potential or EEG signal was then convolved with Morlet's wavelets to produce the complex-value analytical signal $X(t, f_0)$ at each frequency of interest. We used a family of 100 Morlet wavelets with central frequencies logarithmically spaced between 2 and 100 Hz. Then, the power spectrum of the signal was computed by squaring the absolute value of analytical signal. For a given region of interest, session and animal, the power spectrum traces corresponding to all channels were plotted collectively to visually identify and exclude noisy channels. For each animal and for each region of interest we computed the average power spectrum as the mean spectrum across channels and then across sessions.

Spike extraction, sorting and clustering: LFP signals were first high-pass filtered (300 Hz, 4th order Butterworth filter). We determined the filter order by comparing the spectral contents of filtered signal using different filter orders to fully suppress the stimulation. The spiking threshold was set to negative four times standard deviation of the high-passed filtered signal, to extract spike times and spike waveforms. The extracted spikes were automatically sorted based on a template matching method implemented in Kilosort (Pachitariu, Steinmetz, Kadir, Carandini, & Harris, 2016), followed by an automatic post-hoc merging, and finally a manual curation by merging the automatically assigned spike groups. Next we used spike half-width to perform k-means clustering of neurons to two putative subgroups of narrow- and broad-spiking neurons (Peter Barthó et al., 2004). Increasing the number of clusters did not improve the clustering performance as measured by within cluster sums of point to centroid distances. Other spike shape features (trough-to-peak time, peak value of normalized spikes, upward slope, spike energy, absolute peak-to-trough ratio, repolarization area, spike minimum amplitude, spike maximum amplitude) did not have multi-modal distributions and were not used in spike clustering.

Phase locking value (PLV): The consistency of phase differences between two signals is indicative of an existing phase synchrony and can be measured by PLV (J.-P. Lachaux, E. Rodriguez, J. Martinerie, & F. J. Varela, 1999). We computed the PLV to quantify the phase synchrony between two LFP signals or the phase synchrony between individual spikes and tACS waveform. According to the instantaneous phase of tACS waveform at a specific carrier frequency (f_c), we assigned a phase to every spike of a single unit, and built a phase distribution for each unit. Then we computed PLV of each unit with N spikes at a carrier frequency of $f_c$defined by the following formula:

$$PLV(f_c) = \frac{1}{N}\left|\sum_{n=1}^{N} e^{i(\theta_n(f_c))}\right| \quad (4)$$

where $\theta_n(f_c)$ is the instantaneous phase at frequency f_c assigned to a spike. We used a fixed number of $N = 200$ randomly selected spikes per unit, computed PLV, and repeated for each unit 200 times, with the mean PLV across all permutations as the final result. We assessed the significance of modulation of spike phases by tACS using Rayleigh's test of uniformity, controlled for number of spikes (Zar, 1999). The PLV between spikes and LFP was computed in a similar way with the exception that spike phase was determined using LFP phases, and a fixed number of 1000 spikes were used to extract the PLV. The PLV between two LFP signals was computed in a similar way as used for computation PLV for spike-tACS, with the exception that in this case $\theta_n(f_c)$ was the difference between instantaneous phases of two LFP signals.

Directed functional connectivity: The Wiener-Granger causality algorithm (J. Geweke, 1982; J. F. Geweke, 1984; Granger, 1969) infers the influence of a process y on a process x by building two autoregressive models: a full model where previous values of both x and y processes are used to estimate the current value of x, and a reduced model where the prediction of current x value is made solely based on previous x values. The algorithm then compares corresponding residuals from two models and infers the directionality from y to x if the full model results in less residual error. We used the MVGC toolbox (Barnett & Seth, 2014) to apply conditional form of Wiener-Granger causality analysis in frequency domain to study

the directionality of different oscillatory frequencies in a network of three nodes at PPC, VC and LP. The MVGC toolbox models the observed data using a vector autoregressive (VAR) approach without assuming a linear scheme for observed real data. The process starts with estimating the model order in MVGC toolbox using Akaike or Bayesian information criteria or cross validation. The next step is to estimate the parameters of VAR model for both full model (considering the effects of both time series) and reduced model (considering only one time-series). Finally, the Granger causality measure was estimated based on the estimators of residuals of covariance matrices. We performed directionality analysis on LFP time series down sampled to 200 Hz, then windowed into segments of 10 seconds length (with %75 overlap). LFP time series were collected from 10 randomly selected channels from each region, the directionality analysis was performed on all possible pairs, then averaged across to produce final results for PPC-VC, PPC-LP, and VC-LP pairs. We used Akaike method for model order estimation with maximum allowed model order of 20.

Spike triggered population firing rate and spike-triggered EEG: We computed the population firing rate function for each region of interest using spike times collected from that region via multiple channels of implanted microelectrode array. For each region, the spike times from all channels were pooled together, then sorted, then a binary time-series were constructed based on sorted collective spike times with assigned value of one at time of spikes occurrence, and zero otherwise. We next convolved the binary time-series with a Gaussian kernel with standard deviation of $c = 4.6$ ms and kernel width of 30 ms. We constructed the spike-triggered population firing rate and spike-triggered EEG by extracting a 1-sec window of population firing rate or EEG around each spike, then averaging across spikes.

Computational modeling of thalamo-cortical network

We adopted our previously developed computational models of cortex (Negahbani et al., 2018) and thalamus (Guoshi Li, Craig S Henriquez, & Flavio Fröhlich, 2017a) and connected them in a biologically plausible way (Izhikevich & Edelman, 2008) to form the unified thalamo-cortical (TC) model. In short, cortical part includes 80 pyramidal (PY) and 20 fast spiking inhibitory (FS) neurons, spatially arranged on

a line. Connections within PY neurons is global with connection probability of 0.5. Each FS was connected to 10 adjacent FS neurons with probability of 0.8. The reciprocal PY-FS connection was local where every FS was randomly connected to 0.8 of 32 surrounding PY. A biophysical synaptic model based on α-amino-3hydroxy-5-isoxazolepropionic acid (AMPA) or γ-aminobutyric acid type A (GABAA) mediated synaptic currents was used to connect cell populations. Individual PY and FS cells were modelled using Izhikevich formalism for point neurons (Izhikevich, 2007) with same parameter values reported previously (Negahbani et al., 2018). The thalamic network included 144 relay-model thalamic cells (RTC), 100 reticular inhibitory neurons (RE), 49 high-threshold bursting thalamic cells (HTC) and 64 local interneurons (IN), all placed in a two-dimensional grid. All chemical synaptic connections were global in thalamic model with connection probability of 0.3 for HTC→IN, IN→RTC, and 0.2 for HTC→RE, RTC→RE, RE→HTC, RE→RTC and RE→RE. All gap junction connections were local, with connection probability of 0.3. All thalamic neurons were modelled using Hodgkin-Huxley formalism of point neurons, connected with glutamatergic (mediated by both AMPA and NMDA receptors) and GABAergic (mediated by GABAA receptors) synaptic currents (with implemented short-term synaptic depression), or via gap junctions, with parameter values described previously (G. Li et al., 2017a). The synthetic local field potential (LFP) for cortex was modelled as the average sum of the absolute values of excitatory and inhibitory currents entering PY neurons (Mazzoni et al., 2015). The thalamic LFP was obtained from average membrane potential of neurons. The tACS was modelled as a current injection into PY neurons. The stimulation amplitude was systemically varied up to 10 pA, which caused a 2mV change in membrane voltage in an isolated model neuron. Given that an electric field of 2V/m has been found to cause an approximately 0.5mV polarization of the membrane voltage(Fröhlich & McCormick, 2010), the lower amplitude values in our simulations span the range of human tACS studies, whereas the upper values are of relevance for a more complete picture of the response dynamics and for future studies employing higher stimulation amplitudes. The computational modeling of thalamo-cortical network was implemented using Brian2 simulator in Python (Stimberg, Brette, & Goodman, 2019).

Our model was implemented by connecting a thalamic model, constructed exactly as previously outlined(Guoshi Li, Craig S. Henriquez, & Flavio Fröhlich, 2017b), to a cortical model, constructed as previously described in detail (Negahbani et al., 2018) with some minor changes in parameter values. Changes to the parameter values are noted in the following brief description of the model equations. Full parameter definitions and values have been reported both for the thalamic (G. Li et al., 2017b)parameters and the cortical model (Negahbani et al., 2018).

Thalamic Model

Current Balance

$$C_m \frac{dV}{dt} = -g_L(V - E_L) - g_{KL}(V - E_{KL}) - \sum I^{\int} \quad - \sum I^{syn} + I_{app} \quad (5)$$

Ion currents

$$I_i = g_i m^p h^q (V - E_i) \quad (6)$$

* I_{CAN} current uses modified equation. See [Li et. al. 2018][62] for details.

Maximal Conductance Densities g_i (mS/cm^2) of Ionic Currents

	I_{Na}	I_{DR}	I_H	$I_{Ca/L}$	$I_{Ca/T}$	$I_{Ca/HT}$	I_{AHP}	I_{CAN}
HTC	90	10	0.01	0.5	2.1	3.0	0.3	0.5
RTC	90	10	0.01	0.3	2.1	0.6	0.1	0.6
IN	90	10	0.05	–	–	2.5	0.2	0.1
RE	90	10	–	–	1.3	–	0.2	0.2

Gating Variable (m or h) Kinetic Equations

$$\frac{dx}{dt} = \varphi_x \frac{x_\infty(V,[Ca]_i) - x}{\tau_x(V,[Ca]_i)} \quad (7)$$

(Or in an equivalent form below)

$$\frac{dx}{dt} = \phi_x(\alpha_x(V,[Ca]_i)(1-x) - \beta_x(V,[Ca]_i)x) \quad (8)$$

Kinetic Parameters of All Gating Variables

Current Type	Gating Variable	ϕ_x	αx or x_∞	βx or τx (ms)
*I*Na	*p=3*	1	$\alpha_m = \frac{0.32(V - V_{SH} - 13)}{1 - \exp(-(V - V_{SH} - 13)/4)}$ V_{SH} = -30 for HTC and IN V_{SH} = -40 for RTC and RE	$\beta_m = \frac{-0.28(V - V_{SH} - 40)}{1 - \exp((V - V_{SH} - 40)/5)}$
*I*Na	*q=1*	1	$\alpha_h = 0.128\exp(-(V - V_{SH} - 17)/18)$	$\beta_h = \frac{4}{1 + \exp(-(V - V_{SH} - 40)/5)}$

*I*DR	*p=4*	0.25 (RE: 1)	$\alpha_m = \frac{0.032(V - V_{SH} - 15)}{1 - \exp(-(V - V_{SH} - 15)/5)}$	$\beta_m = 0.5\exp(-(V - V - 10)/40)$
*I*H	*p=1*	1	$m_\infty = \frac{1}{1 + \exp((V + 75)/5.5)}$	$\tau_m = \frac{1}{\exp(-0.086V - 14.59) + \exp(0.0701V - 1.87)}$
*I*Ca/L	*p=2*	4.6	$m_\infty = \frac{1}{1 + \exp(-(V + 10)/4)}$	$\tau_m = 0.4 + \frac{0.7}{\exp(-(V + 5)/15) + \exp((V + 5)/15))}$
*I*Ca/L	*q=1*	3.7	$h_\infty = \frac{1}{1 + \exp((V + 25)/2)}$	$\tau_h = 300 + \frac{100}{\exp(-(V + 40)/9.5) + \exp((V + 40)/9.5))}$
*I*Ca/T	*p=2*	4.6	$m_\infty = \frac{1}{1 + \exp(-(V + 62)/6.2)}$	$\tau_m = 0.612 + \frac{1}{\exp(-(V + 135)/16.7) + \exp((V + 19.8)/18.2)}$
*I*Ca/T	*q=1*	3.7	$h_\infty = \frac{1}{1 + \exp((V + 86)/4)}$	When V < -83 mV, $\tau_h = \exp((V + 470)/66.6)$ When V ≥ -83 mV, $\tau_h = \exp(-(V + 25)/10.5) + 28$
*I*Ca/HT	*p=2*	4.6	$m_\infty = \frac{1}{1 + \exp(-(V + 34)/6.2)}$	$\tau_m = 0.612 + \frac{1}{\exp(-(V + 107)/16.7) + \exp((V - 8.2)/18.2))}$

*I*Ca/HT	*q=1*	3.7	$h_\infty = \frac{1}{1+\exp((V+58)/4)}$	When V < -55 mV, $\tau_h = \exp((V+442)/66.6)$ When V ≥ -55 mV, $\tau_h = \exp(-(V-3)/10.5)+28$
*I*Ca/T (RE)	*p=2*	6.9	$m_\infty = \frac{1}{1+\exp(-(V+55)/7.4)}$	$\tau_m = 3+\frac{1}{\exp((V+30)/10)+\exp(-(V+105)/15))}$
*I*Ca/T (RE)	*q=1*	3.7	$h_\infty = \frac{1}{1+\exp((V+83)/5)}$	$\tau_m = 85+\frac{1}{\exp((V+51)/4)+\exp(-(V+410)/50))}$
*I*CAN	*p=1*	1	$m_\infty = \frac{1}{1+\exp(-(V+43)/5.2)}$	$\tau_m = 1.6+\frac{2.7}{\exp(-(V+55)/15)+\exp((V+55)/15))}$
*I*AHP	*p=1*	1	$m_\infty = \frac{48\cdot[Ca]^2{}_i}{48\cdot[Ca]^2{}_i+0.09}$	$\tau_m = \frac{1}{48\cdot[Ca]^2{}_i+0.09}$

Calcium Dynamics

$$d$$

Gap Junction

$$I_{gap} = \frac{V_{post}-V_{pre}}{R_g} \quad (10)$$

Synaptic Current

$$I_{syn} = sDg_{syn}B(V)\big(V - E_{syn}\big) \quad (11)$$

Gating Variable

$$\frac{ds}{dt} = \alpha[T](1 - s) - \beta s \quad (12)$$

Magnesium Block for NMDA Synapses

$$B(V) = 1\Big/\left(1 + exp\left(\frac{-(V + 25)}{12.5}\right)\right)^{*} \quad (13)$$

** For $GABA_A$ and AMPA, $B(V) = 1$.

Short-Term Synaptic Depression

$$D = 1 - \big(1 - D_i(1 - U)\big)exp\left(\frac{-t - t_i}{\tau}\right) \quad (14)$$

See [Li et. al. 2018][62] for full details.

<u>*Cortical Model*</u>

Current Balance (PY)

$$100\frac{dv}{dt} = 0.7(v + 60)(v + 40) - u + I \quad (15)$$

$$\frac{du}{dt} = 0.03[-2(v + 60) - u] \quad (16)$$

$$I = I_{dc} + I_{syn} + I_{stim} + I_{noise} \quad (17)$$

$resetrule: if v \geq +35, then v \leftarrow -50, u \leftarrow u + 100.$

Current Balance (FS)

$$20\frac{dv}{dt} = (v+55)(v+40) - u + I \quad (18)$$

$$\frac{du}{dt} = 0.2\{U(v) - u\}, U(v) = \begin{cases} 0 when v \leq v_b \\ 0.025(v+55)^3 otherwise \end{cases} \quad (19)$$

$$I = I_{dc} + I_{syn} + I_{stim} + I_{noise} \quad (20)$$

$$resetrule: if\, v \geq +25, then v \leftarrow -45$$

Synapses

$$I_{syn} = g(t)B(V_m)(V_m - E_{rev}) \quad (21)$$

$$g(t) = g_{t_{spike}} exp(-t/\tau) \quad (22)$$

Upon presynaptic action potential: $g_{t_{spike}} \leftarrow g + g_{max}$ (23)

Magnesium Block for NMDA Synapses

$$B(V_m) = \frac{\left(\frac{V_m+80}{60}\right)^2}{1+\left(\frac{V_m+80}{60}\right)^2} \quad (24)^*$$

** For $GABA_A$ and AMPA, $B(V_m) = 1$.

Cortical LFP Measured from PY Neurons

$$LFP = \sum_{i=1}^{N} \frac{|I_{AMPA,i}| + |I_{NMDA,i}| + |I_{GABA_A,i}|}{N}, N: number of PY neurons \quad (25)$$

Addition of NMDA synapses to the cortical model.

For experiments with NMDA synapses in the cortical model (Supplementary Fig. 3.N), NMDA synapses were added to existing PY→PY glutamatergic connections. NMDA synapse parameters were set to $g_{max} = 0.015$ nS,$\tau = 150$mS, and $E_{rev} = 0$ mV [Izhikevich et. al. 2008][80]. The conductance increase g_{max} for RTC -> PY AMPA synapses was reduced from 0.3nS to 0.1nS and direct current stimulation to PY and FS cells was adjusted to $I_{dc} = 75$ pA for PY cells, and $I_{dc} = 58$pA for FS cells.

Statistical analysis

The comparison of means for two populations were performed using independent t-test with significance levels at 0.05 or 0.01. The significance of phase-locking values was assessed by Rayleigh test for non-uniformity of circular distribution of phases.

RESULTS

Endogenous alpha-band oscillations in awake head-fixed ferrets.

We hypothesized that the effect of tACS on network dynamics was a result of the synergistic interaction of endogenous network activity and the exogenous electric field delivered by tACS. Thus, understanding the endogenous network dynamics was a necessary step to identify the stimulation targets before examining their engagement by tACS. We first characterized the endogenous oscillations to validate the existence of previously reported alpha oscillations in the thalamo-cortical system of awake head-fixed ferrets (Stitt et al., 2018). The extracellular broadband signals were recorded from implanted microelectrode arrays in PPC, VC, and LP regions (Fig. 3.1 a). The post-mortem histological investigation verified the correct implant locations (Fig. 3.1 a.i-iii).

The local field potential (LFP) signals were acquired by low-pass filtering (<300 Hz) the extracellular broadband recordings (Fig. 3.1 b). Spectral analysis of cranial screw EEG and LFP signals in PPC, VC, and LP showed an alpha peak (12–16 Hz) in PPC, VC, and LP and EEG recordings for all three animals (Fig. 3.1 c). An alpha oscillation was defined as an increase in power (a “bump”) beyond the 1/f

power distribution that permeates the background of electrophysiological recordings. The alpha peaks were strongest in PPC and VC, with slight differences in individual alpha peak frequencies between animals: 14.42, 12.32, 14.42 Hz for animals 1, 2, and 3 respectively. Prominent theta oscillations (3-5 Hz) were evident in LP for all animals. To analyze the endogenous oscillations at the neuronal level, we extracted the extracellular spikes (n=1539, 701, 391 units in PPC, VC and LP respectively), and clustered the unit waveforms based on spike duration (spkD) defined as trough-to-peak time. We identified two populations of neurons in PPC (narrow spiking, n=689: spkD=0.361±0.005 ms, broad spiking, n=850: spkD=0.810±0.005 ms) and VC (narrow spiking, n=416: spkD=0.283±0.005 ms, broad spiking, n=285: spkD=0.651±0.009 ms), but only broad spiking neurons in LP (n=391, spkD=0.642±0.008) (Fig. 3.1 b, c). We next examined how different neurons from each region interacted with each other and with the meso- and macroscale neuronal signals (LFP and EEG, respectively).

Population coupling was stronger for narrow-spiking neurons and oscillates at alpha frequency.

We recorded broad-band extracellular activity from cortical and thalamic regions and the EEG signal to measure endogenous oscillations. This recording enabled us to examine the interaction between neural activity at the level of single-units and network activity at the level of the LFP or EEG to better understand the underlying mechanisms of the endogenous oscillations. We first asked if there was a relationship between single unit activity and the local dynamics in each region by measuring population coupling (Okun et al., 2015). We constructed the population firing rate function for each region of interest (ROI) based on its spiking activity. Spike-triggered average population firing rates were extracted at the occurrence of individual spikes for all unit types by region and given as a percentage of the baseline value in the 500 ms before spike generation. The within-region average of this value provided a measure of how strongly each unit was coupled to local oscillations (Fig. 3.2 a-c) (Okun et al., 2015). We observed that the coupling of single units to the population rate in all regions oscillated in alpha frequency range, confirmed by spectral analysis. We found a prominent peak in the alpha (11-17 Hz) frequency band for all three regions (Fig. 3.2 d-f). A weaker theta-band (3-8 Hz) oscillation was also evident in all regions [defined as an

increase beyond the electrical background noise]. Comparing the narrow- and broad-spiking neurons, we found that narrow-spiking neurons had stronger population coupling than broad-spiking neurons (Fig. 3.2 d-f, amplitudes at time lag zero), and the fluctuation of the coupling had more oscillatory power over a wide frequency range including alpha band in both PPC and VC (Fig. 3.2 d-f).

Alpha synchronization between EEG and spikes, and prominent engagement of narrow-spiking neurons.

Next, we examined alpha synchrony at the network scale by quantifying the synchronization between single units in all three ROIs and EEG oscillations. The average spike-triggered EEG showed an oscillatory pattern at alpha frequency band (Fig. 3.2 g-i). Further analysis showed a non-uniform phase histogram for each region (Fig. 3.2 j-l). Narrow-spiking PPC units preferred to spike at 174.67°, confidence interval (CI) = [172.71°, 176.63°] phase of EEG alpha oscillations. The preferred phase for broad-spiking neurons was 173.14°, CI = [170.95°, 175.32°]. For VC neurons, the preferred phase was slightly different between narrow (94.06°, CI = [89.50°, 98.62°]) and broad spiking (109.63°, CI = [105.48°, 113.77°]) neurons. The preferred synchronization phase for LP units was 142.63°, CI = [138.44°, 146.82°]. We extracted the phase locking value (PLV) to examine the strength of spike-to-EEG phase locking as a function of frequency. While the PPC units were phase locked to EEG at a wide frequency range of ~3-32 Hz (Fig. 3.2 m), the peak in PLV was limited to a narrower band of ~10-32 Hz for VC (Fig. 3.2 n) and LP units (Fig. 3.2 o). Synchronization in the alpha frequency band (12-17 Hz) was evident for single units of all three ROIs. We found that the phase-locking between EEG and single units was stronger for narrow-spiking neurons when compared with broad-spiking ones. This pattern was evident in both PPC and VC (Fig. 3.2 m, n).

We further analyzed the relationship between population coupling of single neurons (as shown in Fig. 3.2 a-f) and spike phase-locking to more global EEG alpha oscillations (see Fig. 3.2 g-o). We found a strong correlation between population coupling and spike phase locking to EEG signal in alpha frequency band in PPC, no correlation in VC and weak correlation in LP (Fig. 3.2 p-r). In summary, these results

indicate that the more a PPC unit was coupled to the population dynamics, the more it was coupled to the macroscopic alpha oscillation measured by EEG. Conversely, the less a PPC unit was coupled to local dynamics, the less it was coupled to the alpha oscillations measured by EEG.

Synchronization directed functional connectivity in thalamo–cortical network.

To better understand the dynamics of endogenous network oscillations, we examined the synchronization between all three region pairs using spiking and LFP activity. We first looked at the synchronization of spiking activity between recording regions. The population-averaged spike cross-correlations demonstrated synchronous oscillatory structure occurring within the alpha frequency band between all three region pairs (Fig. 3.3 a-c). The mean power spectrum (±SEM) of cross-correlations indicated a prominent peak in the alpha band (centered on ~15.23 Hz, Fig. 3.3 d-f). These results showed that spiking activity in PPC, VC, and LP were synchronized in the alpha frequency. We next examined the phase-locking between spikes and the LFP for each region pair to understand the between-region synchronization. The spikes from all three ROIs were significantly phase-locked to the alpha oscillation in the LFP from PPC (Fig. 3.3 g), VC (Fig. 3.3 h) and LP (Fig. 3.3 i). We computed population average phase locking between LFPs obtained from three regions to understand their interactions (see Supplementary Figure 3.A for individual animals). We found strong phase locking in the alpha range (peak frequency at 15.23 Hz) and weak synchronization in theta range (peak value at 3.75 Hz) between the two cortical regions (Fig. 3.3 j). When considering the synchronization between one of the two cortical regions and LP, we found strong phase-locking at both theta and alpha frequencies (Fig. 3.3 k, l). The theta and alpha synchronization between PPC and LP was larger when compared to the corresponding values between VC and LP. These results indicate that the two cortical regions synchronize in the alpha range, while the synchronization between the cortical regions and LP occurred in both alpha and theta frequency ranges as previously reported (Stitt et al., 2018). Further analysis by population average conditional Granger causality measure (cGC) showed that alpha synchronization between cortical regions was more directed from PPC to VC than the opposing direction (Fig. 3.3 m, see Supplementary Fig. 3.A for cGC measures for individual

animals). The results of directed functional connectivity analysis also suggested that LP influenced both cortical regions in the theta range, and to a smaller extent that the PPC drove the LP in alpha range (Fig. 3.3 n, o). Our results did not indicate a preference in directionality of alpha oscillations between VC and LP (Fig. 3.3 o). Taken together, these results showed that alpha oscillations originated primarily in PPC and propagated to both VC and LP, whereas theta oscillations originated primarily in LP and propagated to the other two regions.

Measurements and modeling of tACS electric field in the ferret brain.

We identified the endogenous alpha oscillations that originated in PPC as a potential target for transcranial stimulation. To examine the effect of tACS on neurons, we approximately matched the electrode current density of human tACS. The tACS current density is ~ 1 μA/mm^2 per electrode for a typical dual-site human tACS protocol in which the peak current is 2 mA zero-to-peak.(Ahn et al., 2019) We trimmed carbon-silicone tACS electrodes used in human studies to make smaller circular electrodes with radius of $r = 5mm$ to apply to the ferret head. To achieve a current density comparable to values used in human settings, we used current amplitudes up to 80 μA zero-to-peak in our experiments.

We examined what electric field strengths were generated inside the ferret brain when applying tACS currents with amplitudes ≤ 80 μA. To estimate the electric field magnitude in the ROIs and the entire ferret brain, we developed a computational model of the current flow in the ferret head (Supplementary Fig. 3.E). The model included detailed anatomical structures, head-post, bone screws, dental cement, and surgical craniotomies based on MRI and CT scan data and tissue conductivities from the literature (Supplementary Table 3.A). We validated the model adequacy by comparing its predictions to experimentally measured electric potentials for stimulation currents of 80 μA and 60 μA. The electric potentials were measured with the same implanted electrode arrays used for the electrophysiology recordings. The model prediction for the electric potentials was highly correlated with the experimental data (Fig. 3.4 a, b respectively, correlation coefficient r = 0.99, p < 0.0001 for both validations). The error bars of each measurement in the plots stem from variation across the six sets of recordings corresponding to two recording blocks and three

different reference electrode schemes, after re-referencing the data and excluding electrodes with poor signal quality (see Methods / Electric Potential Measurements for details). The simulated distribution of the electric field magnitude in the three ROIs is summarized in Fig. 3.4 c. The estimated electric field magnitude was slightly higher for the VC region compared to PPC and LP, but most of the magnitudes across all ROIs fell into a relatively narrow range of 0.22–0.30 mV/mm. Fig. 3.4 d, e show the surface-normal component of the electric field on the brain surface (see also Supplementary Fig. 3.F for more details), corresponding to peaks and troughs of the tACS current cycle. The areas underneath the stimulation electrodes (indicated by large open circles on the left frontal and medial occipital regions, see also Supplementary Fig. 3.H) showed maximum field strength with directions flipped according to the stimulation wave polarity. Fig. 3.4 f-i visualize the electric field strength and direction in deeper cortical and sub-cortical regions (for current density see also Supplementary Fig. 3.G) across coronal and sagittal sections including the implanted recording sites. As expected, the direction of the electric field was predominantly along the posterior–anterior axis as shown by red arrows in the coronal and sagittal sections.

These results indicated that neither the surface-normal nor the total magnitude of the tACS electric field exceeded 0.53 mV/mm in the brain. The modeling results also indicated that the arrangement of the tACS electrodes in our experiments did not necessarily result in maximum electric field in the PPC, VC, and LP regions where all cortical recordings were obtained. The electric field strength was in the range of values reported for humans and non-human primates in models and experiments (Y. Huang et al., 2017; Opitz et al., 2016). These results supported our decision to use 80 μA as stimulation intensity to produce comparable electric fields at the site of the implanted electrodes as in human tACS experiments.

Transcranial alternating current stimulation engages cortical alpha oscillations at the single neuron level.

We found that synchronization between spikes and both local (Fig. 3.2 a-f) and network-scale oscillations (Fig. 3.2 g-o) was highest for alpha-band oscillations across all three animals. In addition, we identified the PPC as the source of alpha oscillations that drives VC and LP (Fig. 3.3). These results

suggested that alpha oscillations were the ideal candidate target for tACS. Furthermore, we identified that tACS with an amplitude of 80 μA resulted in a weak electric field of < 0.5 mV/mm across the entire ferret brain that was comparable to tACS in humans. Thus, we performed a comprehensive series of experiments in which we applied tACS with different frequencies and amplitudes and simultaneously measured the spiking activity in PPC, VC and LP regions. Nine stimulation frequencies centered on each animal's endogenous alpha frequency (EAF) ($f_{stim} = [-4,-3,-2,-1,0,1,2,3,4] + EAF$) and 6 amplitudes ($I_{stim} = [5,10,15,20,40,80]\mu A, peakvalues$) were applied over multiple sessions per animal (n=16, 21, 14 sessions for animals 1 to 3 respectively). We hypothesized that if entrainment was the underlying mechanism of how tACS effects neural activity, then the synchronization between endogenous oscillations and external tACS waveform should increase as the tACS frequency approaches the endogenous alpha frequency. This increased synchrony between an external periodic perturbation and an oscillator is a well-known phenomenon in dynamical systems; as the amplitude of the stimulation is increased, the range of frequencies for which entrainment occurs is also increased. This relationship results in a triangular Arnold tongue region with increased coupling on a two-dimensional heat-map that plots the amplitude (y-axis) and frequency (x-axis) of stimulation (Pikovsky, Rosenblum, et al., 2003).

First, we analyzed the phase locking of all spikes to the tACS waveform regardless of spike shape in a pooled dataset for all three animals (see Supplementary Figures S2–S4 for individual animals). A triangular region centered on the endogenous alpha frequency was found for PPC units (Fig. 3.5 a top, synchronization maps, darker shades of blue indicate higher PLV). We evaluated the modulation of spike phases by tACS using Rayleigh's test for non-uniformity of circular data and found that the z-statistics also displays a triangular shape for PPC neurons (Fig. 3.5 a, second row). The percentage of PPC units with a significant phase modulation was low (< 2%, Fig. 3.5 a, third row). Furthermore, the firing rates of PPC neurons displayed a random modulation as a function of stimulation waveform and did not display the triangular, Arnold tongue, shape. These analyses confirmed that the applied tACS amplitude was subthreshold and did not modify the firing rate of the units (Fig. 3.5 a bottom). To differentiate the cell-

type-specific effect of tACS, we extracted the synchronization maps (i.e. spike PLV to tACS as a function of tACS frequency and amplitude) for narrow- and broad-spiking neurons separately. We performed the same analysis on clustered units in PPC based on spike shapes: the narrow-spiking neurons (n=685) displayed darker triangular region when compared to their broad-spiking counterparts (n=864) (Fig. 3.5 b, c, top). The synchronization map between VC units and tACS (for collective or clustered spikes) did not show a triangular Arnold tongue shape (Fig. 3.5 d-f top) as observed for PPC units. Instead, a weak modulation was observed for frequencies close to the endogenous alpha frequency, and became more evident for stimulation amplitudes above 20 μA and was skewed toward frequencies higher than endogenous alpha as indicated by dark region on top right corner in Fig. 3.5 d, e. We did not find synchrony regions for LP neurons (Fig. 3.5 g, top). As for PPC, the Rayleigh's z-statistics in VC and LP (Fig. 3.5 d-g, second row) showed similar pattern to corresponding PLV maps (Fig. 3.5 d-g, top), and the percentage of units showing significant phase modulation was low (<2%, Fig. 3.5 d-g, third row). Similar to PPC, tACS did not modulated the firing rate of individual units in VC or LP (Fig. 3.5 d-g, bottom row). Taken together these results show the synchronization map between single units and tACS that induced electric field of < 0.5 mV/mm across the ferret brain. The synchronization region follows a triangular Arnold tongue shape, with phase locking values that are just slightly higher than their neighbor regions. The PPC units exhibited an Arnold tongue pattern indicative of their weak entrainment by tACS. The VC units demonstrated a partial Arnold tongue, and no regular pattern of synchrony was observed for LP neurons. Among narrow- and broad-spiking neurons, the former ones showed more defined Arnold tongue regions.

Peripheral-nerve alternating current stimulation failed to entrain PPC neurons in a frequency- and amplitude dependent way.

Since tACS was applied to the scalp, it was important to consider whether the entrainment of neurons was a direct effect from the electric field delivered to the brain or an indirect effect from the activation of peripheral nerves. To control for peripheral nerve activation, we applied the identical tACS paradigm to the shaved lower back of two ferrets (Supplementary Fig. 3.H a). If the Arnold tongue patterns

in Fig. 3.8 were a result of peripheral nerve activation, we would expect to see a similar Arnold tongue pattern in this experiment where the skin, but not the brain, was stimulated. We used the identical analysis pipeline and again extracted two types of neurons based on the waveform of the action potentials (Supplementary Fig. 3.H b) similar to the findings in the main experiment (Fig. 3.1 e PPC). However, in stark contrast, we did not find a triangular region centered on the endogenous alpha frequency indicative of the Arnold tongue for PPC units. Instead, we observed a more random pattern of PLV (Supplementary Fig. 3.H c-e, top row), Raleigh's z distance (Supplementary Fig. 3.H c-e, second row), percent of significant units (Supplementary Fig. 3.H c-e, third row), and firing rate (c-e, bottom row), in both unit types (d,e). This suggests that peripheral nerve stimulation is not the underlying mechanism of action of tACS.

Repeated tACS sessions do not produce long-lasting effect on neuronal synchrony

Due to the long session duration, we would like to investigate whether there is any long-lasting effect on neural synchrony after repeated tACS sessions. To study this, we conducted a separate experiment of 14 repeated tACS sessions (n=1 ferret). Both spiking and LFP data was recording from PPC, and VC, and LP using multi-electrode arrays. The tACS electrode locations (Supplementary Fig. 3.I a) were identical to the main tACS experiment that showed the Arnold tongue. To rigorously test the potential confound of cumulative changes to the spiking behavior due to repeated stimulation for determining the Arnold tongue, we stimulated at a single frequency (endogenous peak alpha frequency, 14.5 Hz) and at the highest amplitude investigated in this study (80 μA), which presumably would maximize the long-lasting effect if there were any. We recorded resting-state data before the onset of tACS, followed by 20 or 40 minutes of continuous tACS, and then recorded post-stimulation resting-state. Of note, the 20 or 40 min of stimulation was much longer than the 90 second per condition in the tACS paradigm that showed the Arnold tongue. Thus, if no long-lasting effect were found for this paradigm, then it could be assumed that carry-over effects did not significantly affect the emergence of the Arnold tongue. Phase-locking values (PLV) between spiking in single units and instantaneous alpha-frequency phase in LFP were calculated for the resting-state periods before and after stimulation. We did not see a significant increase in PLV compared to baseline,

which indicated that there was no long-lasting effect of the stimulation session in terms of promoting neuronal synchrony (Supplementary Fig. 3.I b). Therefore, the Arnold tongue that we found was not the result of a cumulative effect of stimulation, but rather a reflection of the instantaneous effects of stimulation. The cause for persistent effects of tACS on neural activity that are reported in the human literature thus remains an open question.

Local rhythmic stimulation in PPC engaged cortical alpha oscillations at the level of individual neurons.

Due to the potential lack of spatial specificity of tACS, we cannot rule out the possibility that entrainment of neural activity in PPC was an indirect effect due to modulation of activity in another region. To further clarify the potential direct and indirect effect of tACS on neural activity and whether broad network-level stimulation was required to drive neural synchrony, we conducted two control experiments to localize the stimulation in PPC, in contrast to the spatially distributed electric field induced by scalp tACS. In the first experiment, we applied ACS through bones screws (instead of tACS to the scalp) that flanked the PPC in the anterior-posterior direction (Supplementary Fig. 3.J a) to maximize stimulation of PPC while sparing VC (n = 3 animals). In the second experiment, we applied AC-modulated optogenetic stimulation of PPC (Supplementary Fig. 3.K a, n = 2 animals). Given the high spatial specificity of optogenetic stimulation by virtue of the localized viral injection, this experiment provided additional insights on the role of local stimulation.

In the bone screw stimulation experiment, the stimulation site, i.e., PPC, showed increased spike-field PLV as stimulation amplitude increased. It should be noted that the PLV values for PPC were much higher when compared to tACS as a result of the more localized stimulation and the higher current density due to the small surface area of the bone screws compared to the tACS electrodes. In contrast to the scalp tACS experiments, this more localized stimulation caused broad synchronization of neural activity to the stimulation waveform across different frequencies, which may be an indication of a ceiling effect. Such an observation is predicted by the Arnold tongue, where higher stimulation amplitudes do not show a

dependence of the synchronization on the stimulation frequency (i.e., top of an Arnold tongue, where the synchronization is strong across all stimulation frequency, Supplementary Fig. 3.J d).

Importantly, the investigation of neural activity in VC provides additional insights since VC received stimulation in the tACS but not the bone screw experiments. In particular, this additional experiment provides a unique opportunity to dissociate the direct tACS effect from a more indirect effect through network interactions. The neural synchronization in VC showed a preference for high amplitude and high frequency bone-screw stimulation that was higher than the endogenous alpha frequency (Supplementary Fig. 3.J c). This pattern resembled the result of tACS in VC under high amplitude and frequency above the endogenous peak (Fig. 3.5 d top two rows). This suggests that this preference might be due to a network related phenomenon induced by PPC-VC connectivity. On the other hand, since only the tACS (but not bone screw) stimulation induced stronger spike-field synchrony around the endogenous alpha frequency in VC, it implies that this effect does require direct stimulation. In another word, the Arnold tongue like pattern was not evoked by network stimulation (through the PPC-VC connection).

In the optogenetic stimulation experiment, we modulated the amplitude of the laser input in a sinusoidal waveform of different amplitudes and frequencies (Supplementary Fig. 3.K a) to mimic the setup of the tACS experiment. We implemented the same stimulation paradigm as in the tACS experiment (randomly interleaved frequency and amplitude combinations). We found that PPC units exhibited a triangular Arnold tongue pattern in both the synchronization map and spike-phase modulation map (Supplementary Fig. 3.K b). This pattern was similar to the scalp tACS experiment (Fig. 3.5 a), indicating a common underlying principle for entrainment by the AC-modulated optogenetic stimulation and tACS. The PLV value here (from 0.128 to 0.14, Supplementary Fig. 3.K b top) was higher than the tACS weak entrainment (from 0.063 to 0.066, Fig. 3.5 top row), which is not surprising given that the biophysical mechanisms for optogenetic (directly opens ion channels) and electric stimulation (polarizes neuron by electric field) are different. However, despite these inherent differences, we have replicated the general Arnold tongue shape of the synchronization map. Taken together, these results show that tACS was able to

entrain single units in an Arnold tongue pattern that was similar to the one induced by sinewave modulated optogenetic stimulation. Therefore, we propose that the Arnold tongue is indeed a general principle of how oscillating brain networks respond to weak periodic perturbations.

Endogenous alpha oscillations in a biophysical model of thalamo-cortical network and dynamics of synchronization by tACS.

We adapted and connected two previously developed computational models of a cortical (Negahbani et al., 2018) and thalamic (G. Li et al., 2017a) network for a complementary investigation of the mechanism of action of tACS. The cortical model was composed of fast spiking inhibitory neurons (FS) and regular spiking excitatory pyramidal neurons (PY). The thalamic model included excitatory relay-mode thalamo-cortical cells (RTC), excitatory high-threshold bursting thalamic cells (HTC), inhibitory thalamic reticular cells (RE) and inhibitory thalamic interneurons (IN). Synaptic and gap junction connection patterns between neuronal populations followed previous modeling work (Fig. 3.6 a). Without stimulation, the network reproduced the major oscillatory patterns observed in our experimental LFP recordings from cortex (PPC) and thalamus (LP) (Fig. 3.6 b). In the model, the simulated LFP displayed dominant alpha (~ 13.5 Hz) and weak theta-band (~ 3.6 Hz) oscillations in cortex and dominant theta (~ 3.6 Hz) and weak alpha (7.3 Hz) in thalamus (Fig. 3.6 b, right, spectral plots). We next stimulated PY neurons according to the same protocol we used in experimental investigation of entrainment by tACS. We first demonstrate how simulated tACS with a frequency matching the endogenous alpha oscillation (13.5 Hz) entrains individual neurons and the entire network. The network response to 13.5 Hz and 8 pA stimulation is shown in Fig. 3.6 c, demonstrating the collective entrainment of different neuronal types to stimulation in terms of increased amplitude of cortical LFP compared to its amplitude without stimulation. The membrane potential of a randomly selected neuron from each neuron type in the network shows how individual FS and PY neurons adjust their spike times to tACS. We next applied a comprehensive set of tACS waveforms to cortical PY neurons with frequencies between 3 and 30 Hz and amplitudes between 1 and 10 pA and computed the phase-locking of spikes to tACS for all neuron types (Fig. 3.6 d). We found Arnold tongue patterns

(indicated by dark blue shades) centered on the endogenous alpha frequency only for cortical neurons. Compared to cortical neurons, only very weak entrainment was overall observed for thalamic neurons. We observed weak entrainment in the theta frequency, which represents the dominant frequency peak in absence of stimulation. These findings are in agreement with our experimental findings where tACS entrained cortical neurons in PPC, but not thalamic neurons in LP. Interestingly, we found that tACS entrained FS more than PY as indicated by wider and darker Arnold tongue pattern for FS. This behavior agrees with our experimental observations where narrow-spiking neurons of PPC showed greater phase-locking to tACS when compared to broad-spiking neurons. To clarify the neuronal response to tACS at different parts of the PLV heat-map, we further examined a PY neuron's response to two tACS waveforms with equal amplitudes, but different frequencies: (i) A point on Arnold tongue (13.5 Hz, 8 pA), where PY neuron fires regularly after the peak of tACS, with a phase preference between 90 and 180 degrees as shown in phase histogram (Fig. 3.6 d top right), indicating high synchronization by tACS. (ii) A point outside of Arnold tongue (18.5 Hz, 8 pA), where PY neuron fires at random phases of tACS, without a phase preference (Fig. 3.6 d bottom right), indicating a lack of synchronization by tACS. Finally, we used the biophysical model of thalamo-cortical network to test if the frequency mismatch between dominant thalamic oscillations and alpha tACS was the reason for absence of Arnold tongues in thalamic records in our experiments. To answer this question, we altered thalamic endogenous oscillations from being theta-dominated to alpha by increasing the DC drive current of HTC neurons from 0 pA to 50 pA and decreasing the drive current of RTC neurons from 100 pA to 75 pA. Then we stimulated the pyramidal neurons using the same tACS parameters as we used previously and extracted the phase-locking maps. Indeed, we found that both cortical and thalamic neurons were entrained by tACS and displayed Arnold tongues (Supplementary Fig. 3.L). We next explored the effect of tACS delivered to both PY and FS cells. We again found that the Arnold tongue governed the interaction between the endogenous oscillation and the applied stimulation waveform. In contrast to the simulation in which only PYs received input, there was a more pronounced Arnold tongue at the first harmonic of the endogenous frequency (Fig. 3.7). The same pattern was maintained when both PY and FS cells were stimulated (Supplementary Fig. 3.L). Finally, adding

NMDA receptors to the cortical network did not qualitatively change the presence of the Arnold tongue in response to tACS (Supplementary Fig. 3.N). Together these modeling results provided support for our experimental data that showed stronger phase-locking in narrow spiking neurons when compared to broad-spiking ones in response to tACS.

DISCUSSION

tACS entrains spiking activity during endogenous alpha oscillations in awake head-fixed ferrets

We demonstrated the acute effect of tACS on neuronal firing coupled to the endogenous alpha oscillations and thereby provide experimental evidence for the previous predictions derived from computational modeling studies about the mechanism of action of entrainment of ongoing oscillations. We found that tACS entrained the spiking of individual cortical neurons but did not alter the neuronal firing rate. We developed a finite element model of the ferret head, validated the model predictions with experimental measurements of tACS electric potentials in the ferret brain, and tuned the tACS amplitude to produce electric fields comparable to those reported in humans and nonhuman primates. We found that the phase-locking of spikes by tACS depended on stimulation frequency: matching the frequency of stimulation with endogenous alpha resulted in phase synchronization of spikes regardless of stimulation intensity. For tACS frequencies adjacent to endogenous alpha, higher stimulation intensities were required to achieve similar phase-locking between spikes and tACS. This behavior resulted in a triangular-shaped synchrony region when quantifying the spike-tACS phase-locking as a function of stimulation frequency and amplitude. The triangular region was centered on the endogenous alpha frequency and is known as the Arnold tongue, as previously reported in computational modeling studies of tACS (Ali et al., 2013; Christoph S Herrmann, Murray, Ionta, Hutt, & Lefebvre, 2016a; Lefebvre, Hutt, & Frohlich, 2017; G. Li et al., 2017a; Negahbani et al., 2018). Despite being statistically significant in only a small fraction of neurons, the Arnold tongue was evident in PPC. The Arnold tongue was less developed and less clear in VC, and was absent in thalamus (LP). Furthermore, we identified that the effect of tACS was cell-type specific. The phase-locking between tACS and spikes was stronger for narrow-spiking neurons compared

to their broad-spiking counterparts. This cell-type specificity was further supported by a computational model of thalamo-cortical network with ongoing alpha oscillations (Fig. 3.6). In the model, the fast-spiking cortical neurons demonstrated higher phase-locking to tACS than broad-spiking neurons.

Weak electric fields (< 0.5 mV/mm) comparable to tACS field strength in humans and nonhuman primates can entrain neural spiking

To examine the underlying mechanisms of how tACS modulates oscillatory interactions in the thalamo-cortical network, we first delineated the functional interactions in the PPC-LP-VC network. We identified endogenous alpha oscillations in three regions based on three quantitative measures: LFP spectrum, phase-locking of spikes to population firing rate, and spike-EEG synchrony. Further analysis supported PPC as the source (or driver) of alpha oscillations in the three-node network in resting awake ferrets. These findings of prominent resting-state alpha oscillations in the ferret posterior cortex closely correspond to what has been known for a long time about the dominance of the alpha oscillation in the resting-state EEG in humans(Florian H. Kasten & Christoph S. Herrmann, 2017) (ADRIAN & MATTHEWS, 1934). Despite this presence of alpha oscillations in all three recording regions and the existing evidence for enhanced phase synchrony by weak electric fields when stimulation and endogenous frequencies are close (Alagapan et al., 2016; Neuling et al., 2013; Stephen L Schmidt et al., 2014), we only found a clear Arnold tongue pattern for PPC neurons. Compared to PPC, VC neurons showed less-defined triangular region when looking at PLV as a function of stimulation parameters. In addition, the LP neurons did not demonstrate systematic phase locking to tACS. The magnitude of the tACS electric field (model-driven value) was comparable in all three regions. Thus, differential field strength is unlikely to be the explanation. Rather, by being the source of alpha oscillations, PPC may respond more strongly to tACS in the alpha frequency. In contradiction to recent reports of failure of electric fields less than 1mV/mm (resulting from commonly applied tACS intensities) in modulating the dynamics of neuronal circuits (Y. Huang et al., 2017; Lafon et al., 2017; Vöröslakos et al., 2018), the identified PPC Arnold tongue in our work demonstrates how weak electric fields (<0.5 mV/mm) can engage individual neurons provided that

the directionality of information flow and the source of target oscillations are considered when designing the stimulation protocol. Our results demonstrate in vivo how an electric field comparable to (or slightly lower than) the fields predicted and measured in human and nonhuman primate tACS studies (Opitz et al., 2016) can result in Arnold tongue regions in synchronization maps.

The head-fixed awake ferret model to study underlying mechanisms of alpha tACS effects

Modulation of spiking activity by externally applied subthreshold electric fields has been previously demonstrated in animal studies. Application of a subthreshold (< 10 mV/mm) 20 or 50 Hz oscillating electric field modulated the power and frequency of pharmacologically induced gamma oscillations in CA3 pyramidal cells in rat brain slices (J. K. Deans, A. D. Powell, & J. G. R. Jefferys, 2007; D. Reato, A. Rahman, M. Bikson, & L. C. Parra, 2010b). Fröhlich and McCormick showed how subthreshold oscillating electric field can enhance slow oscillations recorded from ferret visual cortex slices with effects demonstrated at field amplitudes as low as 0.25 mV/mm (Fröhlich & McCormick, 2010). Ozen et al. performed in vivo recordings from anesthetized and behaving rats while applying low intensity slow electric fields (<1.7 Hz) via electrodes placed on skull or dura, and reported reliable entrainment of neurons (Ozen et al., 2010). A direct comparison with this study is difficult since it employed voltage and not current stimulation. Ali et al. reported tACS-induced enhancement of slow endogenous oscillations in an anesthetized ferret with stimulation electrodes placed on skull (Ali et al., 2013). Despite the fact that these experimental reports present evidence for cellular-level effects of tACS, these studies share three common limitations. First, they have taken advantage of slow wave oscillations (~1 Hz, under anesthesia or in vitro) or fast gamma band oscillations (~ 30 Hz, pharmacologically induced, in vitro). Neither of these ongoing oscillations are the best model for the dominant alpha oscillations in the awake brain. Second, using in vitro preparations or animal models with lissencephalic brains imposes limitations on the translation to human tACS. In addition, the way tACS electrodes were configured (bath application in vitro, and direct placement on dura or skull in vivo) does not match with standard practices for tACS electrode placement on the scalp in humans. Third, none of the above-mentioned animal studies have explored the parameters of stimulation

in a systematic way to present a comprehensive entrainment map as a function of stimulation frequency and amplitude. Our study overcomes these limitations by taking the advantage of using an awake head-fixed ferret animal model. Ferrets are gyrencephalic and display alpha oscillations in the awake state (Stitt et al., 2018). This current paper provides acomprehensive demonstration of how the alpha oscillation in the ferret originates in PPC and drives both thalamus and primary visual cortex, in conceptual agreement with previous findings from studies of non-human primates (Bollimunta et al., 2011). Thus, the ferret represents a promising additional model system to investigate tACS and other brain stimulation strategies that target alpha oscillations. In addition, the placement of tACS rubber electrodes on the scalp with conductive gel also made our setting more comparable with commonly used strategies used in human tACS studies.

Cell-specific effects of tACS

We identified two types of neurons based on their spike waveform shape in PPC and VC: narrow-spiking and broad-spiking neurons. With tACS, the phase of firing was modulated for both cell types, but the effects were more prominent for narrow-spiking neurons in PPC. In VC, despite the lack of a clear Arnold tongue structure, the narrow-spiking neurons also displayed stronger phase-locking to the stimulation waveform. The stronger coupling of narrow-spiking neurons to tACS was consistent with their behavior in absence of tACS (Fig. 3.2). The narrow-spiking neurons showed stronger coupling to local (population firing rate) and large-scale (EEG) alpha oscillations when compared to broad-spiking neurons. The population ratio of narrow to broad-spiking neurons were 0.81 and 1.46 in PPC and VC, respectively. These ratios differ from the reported excitatory to inhibitory population ration of 0.25 in cortical regions of mammalian brain (Braitenberg & Schüz, 2013). We are unable to make a definite statement about the reason for this mismatch. It could be that more fast-spiking cells are engaged in the alpha oscillation. Or, an alternative explanation could be that axonal spikes get misclassified as fast-spiking units as previously reported for thalamus (Péter Barthó et al., 2014). However, we did not find a bimodal distribution of spike duration for thalamus, which makes this explanation less likely. Nevertheless, although layer V pyramidal neurons have been suggested to be the direct targets of tACS due to their elongated somato–dendritic axis,

our findings suggested that tACS might also modulate the activity of other neuron types including fast-spiking interneurons as previously reported (B. Krause, Márquez-Ruiz, & Cohen Kadosh, 2013; Molaee-Ardekani et al., 2013; Moliadze, Antal, & Paulus, 2010; Thomas Radman, Raddy L Ramos, Joshua C Brumberg, & Marom Bikson, 2009; Davide Reato, Rahman, Bikson, & Parra, 2013). Given that the change in somatic membrane voltage is the largest for pyramidal cell and minimal in spherically symmetrical interneurons, the effects on interneurons are likely the result of their functional role in the targeted network activity and not their morphology[51]. Indeed, in our computational model of thalamo–cortical network that reproduced the key spectral features of our in vivo recordings in ferret PPC and LP, we applied tACS to only pyramidal neurons, and found that both pyramidal and fast-spiking neurons displayed phase-locking to tACS, with fast-spiking neurons showing more phase-locking to tACS (Fig. 3.6). This supports the notion that the response to tACS can be mediated via direct engagement or indirect network effects that is shaped by the endogenous activity of the cells and their role in the generation of the network activity patterns.

Limitations

Like all scientific studies, our study has several limitations. First, in the tACS experiments, the phase locking values for the regions inside the Arnold tongues were small and only slightly higher than the corresponding values for adjacent regions. In addition, only a small number of units (~ 2%) showed significant phase locking as tested by Rayleigh's test. We propose that higher synchronization values might be measured if the electrophysiological recordings were acquired from the regions with higher tACS electric field strength as predicted by the computational model of the field distribution in the ferret head. Second, we did not investigate stimulation frequencies in other frequency bands to examine the presence of additional Arnold tongues at the (sub)harmonics (Pikovsky, Rosenblum, et al., 2003). This was an experimental design choice based on time constraints for keeping ferrets comfortably head-fixed. We prioritized the collection of many trials for the stimulation parameters that we examined. In agreement with previous modeling work of tACS (Ali et al., 2013; G. Li, Henriquez, & Fröhlich, 2018; Negahbani et al., 2018), we did observe an Arnold tongue at the harmonic of the endogenous alpha frequency in our

computational model of the thalamo–cortical network. Third, we found comparable electric field magnitudes in cortex and thalamus for our stimulation montage. Given this lack of focal delivery of electric stimulation by tACS, we cannot exclude that tACS modulated the neural oscillations in other brain areas that we were not able to record from. For example, stimulation may have altered oscillations in other brain areas that in turn modulated the alpha oscillation in PPC. In this study, we have simultaneously recorded activity from three anatomically and functionally interconnected brain areas and found differential effects of the stimulation. Our functional connectivity analysis showed that PPC drives both VC and LP in the alpha frequency band, and it is thus unlikely that primary stimulation effects in VC and LP are the cause of the modulation by tACS in PPC. To further investigate whether the effect on PPC was due to the electric field induced by tACS directly or an indirect effect from other brain regions, we conducted electric stimulation via bone screws and optogenetics in PPC. Both experiment results support that focal stimulations in PPC modulate the neural oscillations directly. In addition, the amount of space on the scalp to attach the stimulation electrodes was limited to an anterior–posterior setup similar to what has been typically used in human studies(Florian H. Kasten & Christoph S. Herrmann, 2017). Since the electric field strength was not maximal in these three areas, we are probably underestimating the effect of tACS in our experiments. Furthermore, our results demonstrate that the field strength on its own is not the main determinant of the effect on neuronal networks but rather that endogenous activity patterns and other factors shape the presence and magnitude of neuronal entrainment by tACS. Fourth, our electric field modeling results indicate that the electric field in cortical regions is largely in the posterior-anterior direction, which is perpendicular to the somato-dendritic axis of many pyramidal neurons. Ideally the stimulation electrodes should be placed to maximize the component of the electric field that is normal to ROI cortical surface to increase the field-induced polarization in pyramidal neurons in order to impose stronger phase-locking in target pyramidal neurons. The hardware-imposed constrains of implanted electrodes prevented us from placing tACS electrodes directly above the ROIs, which would have increased the electric field magnitude and component normal to the cortical surface. Future studies should consider the specific geometry of the delivered electric field with respect to the geometry of the targeted neurons and brain areas. Fifth, our

simulations of the electric potentials resulting from stimulation closely match up with our experimental measurements. However, we were unable to reliably estimate the local electric field strength within the electrode arrays. This is because, in principle, only two of the three electric field vector components can be estimated with the planar arrangement of the contacts in an electrode array. Further, these estimates are highly sensitive to the specific orientation of the array plane with respect to the local current flow, which cannot be reconstructed accurately. Finally, the electric field components are computed by subtracting the potentials of neighboring contacts and dividing by the distance between the contacts. The small inter-contact distance (0.20 or 0.25 mm) results in large fluctuations of the estimates due to various perturbations in the individual potential recordings, such as from microscopic conductivity conditions at the electrode–tissue interface and small differences in the amplifier gains. Overall, however, our results align with what has been reported in human studies, where more uniform sampling with larger electrode contact spacing (10 mm instead of 100 μm) allowed further validation of electric field amplitude.(Y. Huang et al., 2017) Sixth, one important question is if tACS elicited phosphenes by direct stimulation of the eye. It is unlikely that the animal experienced phosphenes, but in humans, phosphenes of retinal origin are commonly induced by tACS, especially with frontal electrodes.(Haberbosch et al., 2019; Laakso & Hirata, 2013; Raco, Bauer, Olenik, Brkic, & Gharabaghi, 2014) The maximal current density in the eye orbit in our ferret FEM model was 0.103 A/m^2 with a median of 0.0369 A/m^2 for the eye closest to the frontal electrode pad in the 80 μA stimulation current condition. Both of these values exceed the estimated threshold for inducing retinal phosphenes of 0.008–0.030 A/m^2 (0.011–0.043 mV/mm).(Laakso & Hirata, 2013) Thus, direct retinal stimulation is possible. However, if the reported effects were the results of spurious activation of the visual system by stimulation of the retina or optic nerve, we would expect to see the strongest entrainment effect in VC and not in PPC. Future studies could address this point by training animals to report phosphenes or developing an implant/electrode configuration that minimizes the electric field reaching the orbits. Seventh, tACS can activate nerves in the scalp.(Raco et al., 2014) This is a possibility in our ferret model as well since we matched the electrode current density to that of human tACS. The threshold for peripheral nerve stimulation with low frequency waveforms has been estimated to be 3.8–5.8 mV/mm. (So, Stuchly, &

Nyenhuis, 2004) In our FEM model, the electric field in the scalp for 80 μA current injection reached a maximum of 10.7 mV/mm and exceeded the range of 3.8 mV/mm in a scalp volume of 12.8 mm^3 in the vicinity of the tACS electrode edges. Thus, stimulation of scalp nerves is a possibility. To address this, in a control experiment we demonstrated that only stimulating a peripheral nerve on the animal's back did not produce the Arnold tongue pattern. This is consistent with Asamoah and colleagues' work where they showed entrainment in the anesthetized animal for comparable field amplitudes when electrical stimulation was directly applied to the skull(Asamoah, Khatoun, & Mc Laughlin, 2019), thus demonstrating entrainment by tACS via exclusively cortical stimulation. Eighth, our experimental design was based on the assumption of a fixed endogenous alpha frequency. This was motivated by our observation that individual ferrets display a constant peak frequency that is stable across recording sessions but different between animals. However, fluctuations around this mean peak frequency could have contributed to an underestimation of entrainment since for some stimulation segments the stimulation matched in frequency could have been actually mismatched. We indeed found that the entrainment effect was reduced for stimulation epochs preceding a period where the endogenous alpha frequency did not match the average peak frequency. This numerical effect was present for narrow-spiking cells ($r = -0.21$, $p = 0.17$) but not for the broad-spiking cells ($r = 0.06$, $p = 0.68$), in further agreement with our discovery of a differential role of the two cell types in terms of their response to stimulation. Ninth, our computational biophysical model of the thalamo-cortical network was designed to include the required biophysical complexity to generate alpha oscillations but was not designed to capture all features of the experimental recordings, and was also not tuned to exhibit specific behavior to avoid artificial alignment of computational and biological results due to overfitting. Specifically, our model includes only a single cortical region, in contrast to our experimental recordings from two cortical area. Our cortical model network consists of only two major cell types and does not capture the richness of different interneuron subtypes. It is also worth pointing out that the entrainment in our computational model is more pronounced than in our experimental data. The main reason for that is that a computational model of this size is too tightly coupled (i.e., too densely connected with too strong synapses) when compared to a real brain. Future work could leverage large-scale simulations that

exhibit more plausible levels of endogenous synchronization and thus likely also lower entrainment by tACS.

In conclusion, we found that weak electric fields (< 0.5 mV/mm) can entrain neuronal activity. Of note, the field strength resulting from the stimulation used in our study is comparable to the field strength measured in tACS experiments in humans and nonhuman primates. In addition, our findings provide in vivo evidence to support the model-driven predictions about how tACS entrains ongoing neuronal oscillations as demonstrated by the Arnold tongue pattern. Our findings underline the importance of considering the endogenous activity patterns, their directionality, and spatial sources for successful entrainment. Our findings re-emphasize the importance of animal models in tACS studies by providing evidence for effectiveness of weak electric fields in modulating the network oscillations via entraining the activity of neuronal populations.

FIGURES AND TABLES

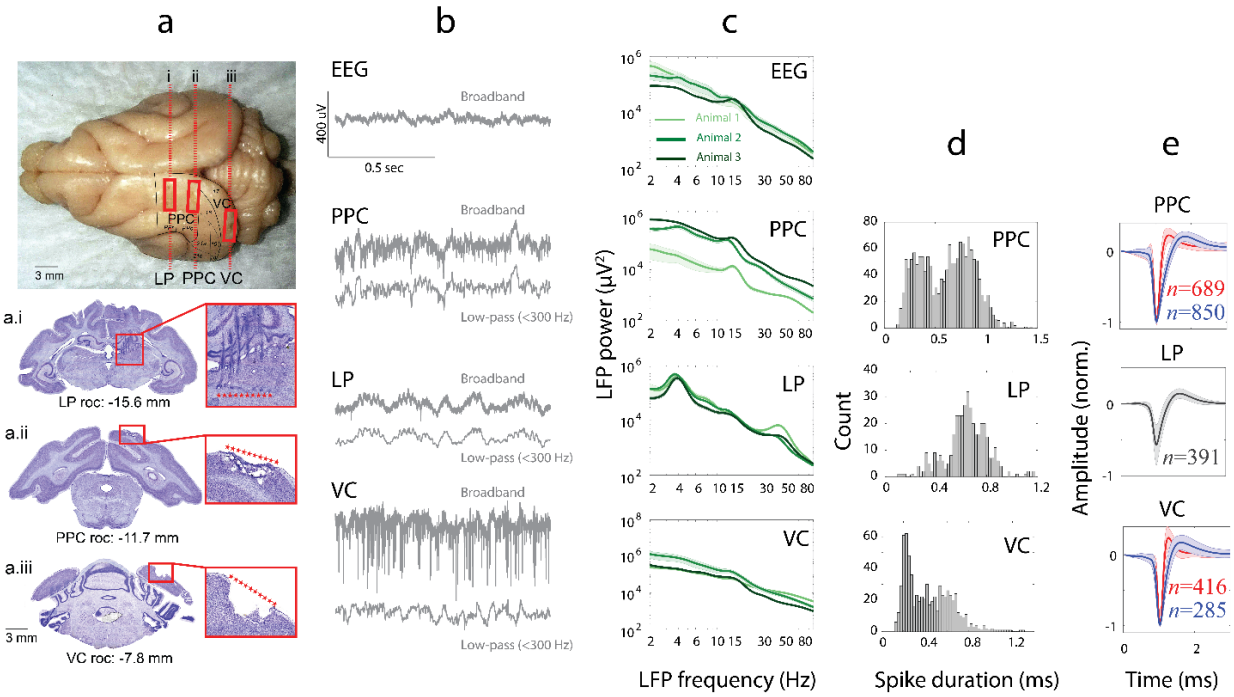

Figure 3.1. Histology and endogenous alpha-band oscillations in awake head-fixed ferrets.

Histology verification of implant locations. (a) Ferret brain with marks (highlighted by rectangles) left by microelectrode array implants in LP, PPC, and VC regions. Outlines of cortical fields are based on a published ferret neuroanatomical atlas (Radtke-Schuller, 2018). Dashed lines indicate the location of cell-stained coronal cross-sections through the center of the multi-electrode array implanted sites shown below (i-iii). Corresponding anterior-posterior atlas coordinates are indicated below each section in mm, relative to occipital crest. (a.i) Coronal cross-section through the LP implant region shows implant electrode tracks and endpoints (dark spots of cell agglomerations above red stars). (a.ii) Coronal cross-section through the PPC implant region demonstrates the tissue damage at the site of the electrode array caused by the removal of the implant during brain extraction (below red stars). (a.iii) Coronal cross-section through the VC implant region marked by tissue loss (below red stars) caused by the removal of the implant during brain extraction after completion of the experiment. "roc" indicates “reference to occipital crest”. (b) Sample 1–sec length EEG, broad-band extracellular recordings and local field potential signals (LFPs) from posterior parietal cortex (PPC), visual cortex (VC) and lateral posterior nucleus/Pulvinar complex (LP) from a head-fixed

awake ferret (resting state, no task performed by animal). (c) Spectral analysis of EEG and LFPs showing the spectrum (mean±SEM) with error-bars in light background from three animals (each animal in a different shade of green). The scalp EEG signal demonstrated weak alpha band peak for all animals. PPC showed clear alpha band activity (12-16 Hz) for all animals. LP showed prominent theta, gamma (35-50 Hz) and a weak alpha activity for all animals. A weak alpha-band activity is also evident for visual cortex (VC) for all three animals. A closer look at PPC spectra indicates slight differences in the individual alpha frequency between animals (14.42, 12.32, 14.42 Hz for animals 1, 2, and 3 respectively). (d) Histogram of spike duration was defined as the time from trough to peak in PPC, LP, and VC. Color coded spike waveforms (mean±SEM) were calculated for two identified clusters of narrow-spiking (red, n=689 in PPC, n=416 in VC) and broad-spiking (blue, n=850 in PPC, n=285 in VC) neurons in PPC and VC. LP neurons comprised only one cluster (n=391).

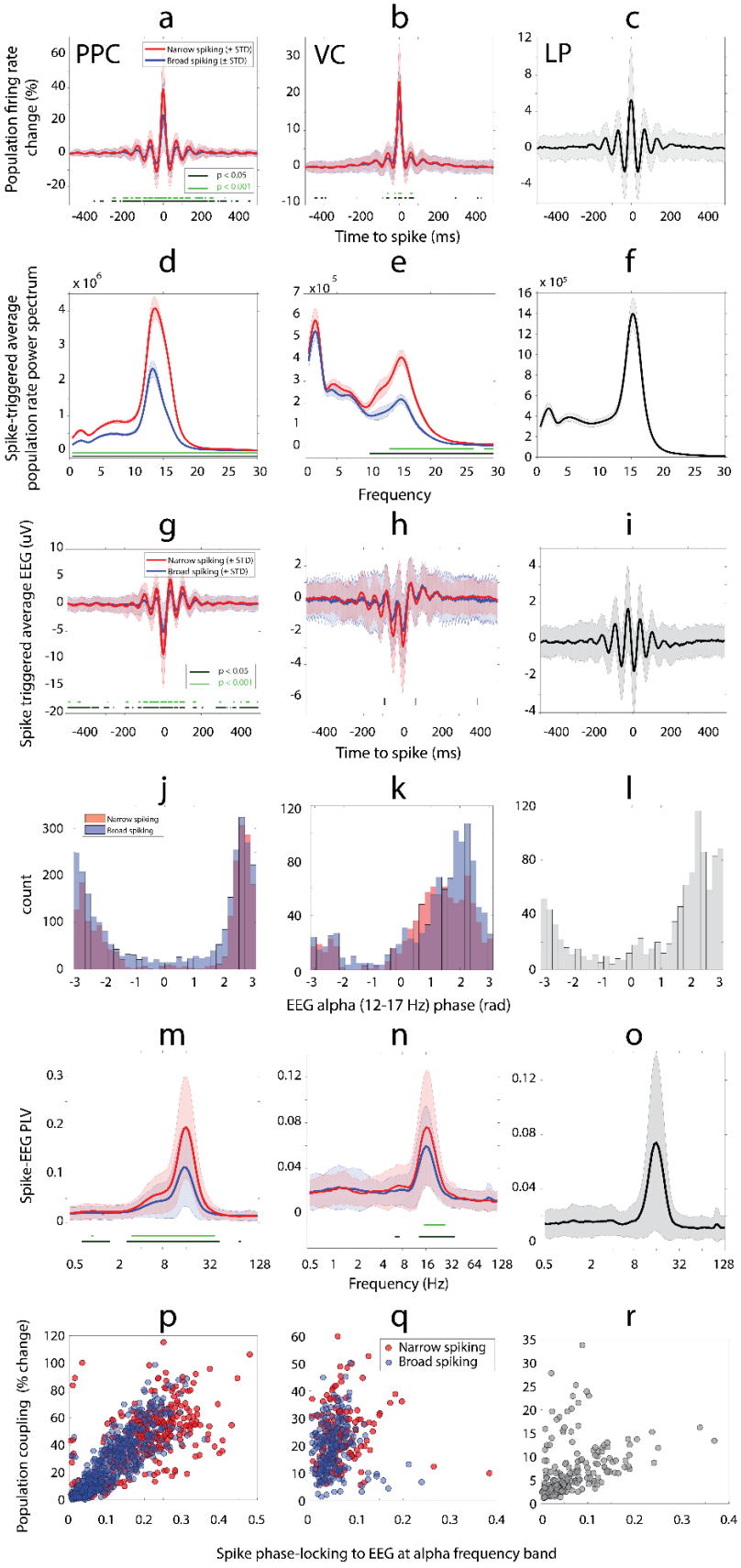
a
b
c
PPC
VC
LP
Narrow spiking (+ STD)
Broad spiking (+ STD)
p < 0.05
p < 0.001
Population firing rate change (%)
Time to spike (ms)
d
e
f
Spike-triggered average population rate power spectrum
Frequency
g
h
i
Spike triggered average EEG (uV)
Time to spike (ms)
j
k
l
count
EEG alpha (12-17 Hz) phase (rad)
m
n
o
Spike-EEG PLV
Frequency (Hz)
p
q
r
Narrow spiking
Broad spiking
Population coupling (% change)
Spike phase-locking to EEG at alpha frequency band

Figure 3.2. Population coupling and spike-EEG coupling is stronger for narrow-spiking neurons and oscillates in alpha frequency band.

a, b, c) Percentage change of spike triggered population firing rate (mean ± STD) as a function of time-to-spike. The percentage change is computed relative to the corresponding baseline value at t=-500 ms in PPC, VC and LP. The spike-triggered population firing rate functions have larger amplitude at spike instant (time lag zero) for narrow-spiking units (red) compared to broad-spiking cells (blue) in both cortical regions (two-sample t-test between broad and narrow-spiking units at each time point at two significant levels indicated by horizontal green lines).

d, e, f) The power spectrum (mean ± SEM) of the spike-triggered population firing rate in PPC, VC and LP. A prominent peak in the alpha [11–17 Hz] frequency band is evident for all three regions. The alpha power is higher for narrow-spiking units (red) when compared to broad-spiking units (blue) in both cortical regions (two-sample t-test at each frequency point at two significant levels indicated by horizontal green lines).

g-o) Alpha synchronization between EEG and spikes, and prominent engagement of narrow-spiking neurons.

g, h, i) Spike-triggered EEG (mean ± STD) as a function of the time-to-spike in PPC, VC, and LP. Spike-triggered average EEG shows an oscillatory pattern for all three regions and shows larger amplitudes at peaks and troughs for narrow-spiking (red) when compared to broad-spiking (blue) neurons (two-sample t-test at each time point at two significant levels indicated by horizontal green lines).

j, k, l) The histogram of phase preference of spiking units in PPC, VC and LP as a function of the instantaneous phase of the alpha-band (12-17 Hz) EEG oscillation. Color denotes the counts for narrow- and broad-spiking neurons. Two classes of neurons show similar phase preference in PPC (Broad-spiking neurons: 3.02±0.02 rad, Narrow-spiking neurons: 3.05±0.02 rad), and slightly different phase preference in VC (Broad-spiking neurons: 1.91±0.03 rad, Narrow-spiking neurons: 1.64±0.04 rad).

m, n, o) Phase locking between single units and EEG measured by PLV (mean ± SEM) as a function of EEG frequency. Synchronization was increased across a broad range from 3-32 Hz range with a prominent

peak in the alpha (12-17 Hz) frequency range for recorded cortical and thalamic sites. The narrow-spiking cells (red) show significantly higher PLV compared to broad-spiking units (blue) (two-sample t-test at each frequency point with p-values <0.05 indicated by horizontal line).

p, q, r) Population coupling of single neurons and their engagement with globally measured alpha correlate strongly in PPC but not in VC and LP. Significant correlations were tested by 2-sided Pearson correlation test. No multiple comparisons adjustment for p-value was performed.

p) Population coupling of single units versus their engagement by alpha-band EEG is plotted for PPC. There is a strong correlation between population coupling and large-scale alpha synchronization for narrow-spiking (red, n = 403, Pearson correlation test, r = 0.71, 2-sided p = $1.3*e^{-61}$, 95% CI [0.66, 0.75]) and broad-spiking (blue, n = 582, Pearson correlation test, r = 0.86, 2-sided p = $3.46*e^{-168}$, 95% CI [0.84, 0.88]) in PPC. Color denotes the neuron type.

q) Population coupling of single units versus their engagement by alpha-band EEG is plotted for VC. Population correlation and large-scale alpha synchrony do not correlate in VC (narrow-spiking: red, n = 173, Pearson correlation test, r = 0.06, 2-sided p = 0.46, 95% CI [-0.09, 0.21], and broad-spiking: blue, n = 221, Pearson correlation test, r = 0.01, p = 0.88, 95% CI [-0.12, 0.14])

r) Population coupling of single units versus their engagement by alpha-band EEG is plotted for LP. This analysis revealed that population coupling and long-range synchrony are weakly correlated in LP (n = 251, Pearson correlation test, r = 0.35, 2-sided p = $3.5*e^{-7}$, 95% CI [0.22, 0.46]). The values on the vertical axis for all figures are the percentage-change in spike-triggered population firing rate at time of spike generation relative to the corresponding baseline value at t=-500 ms.

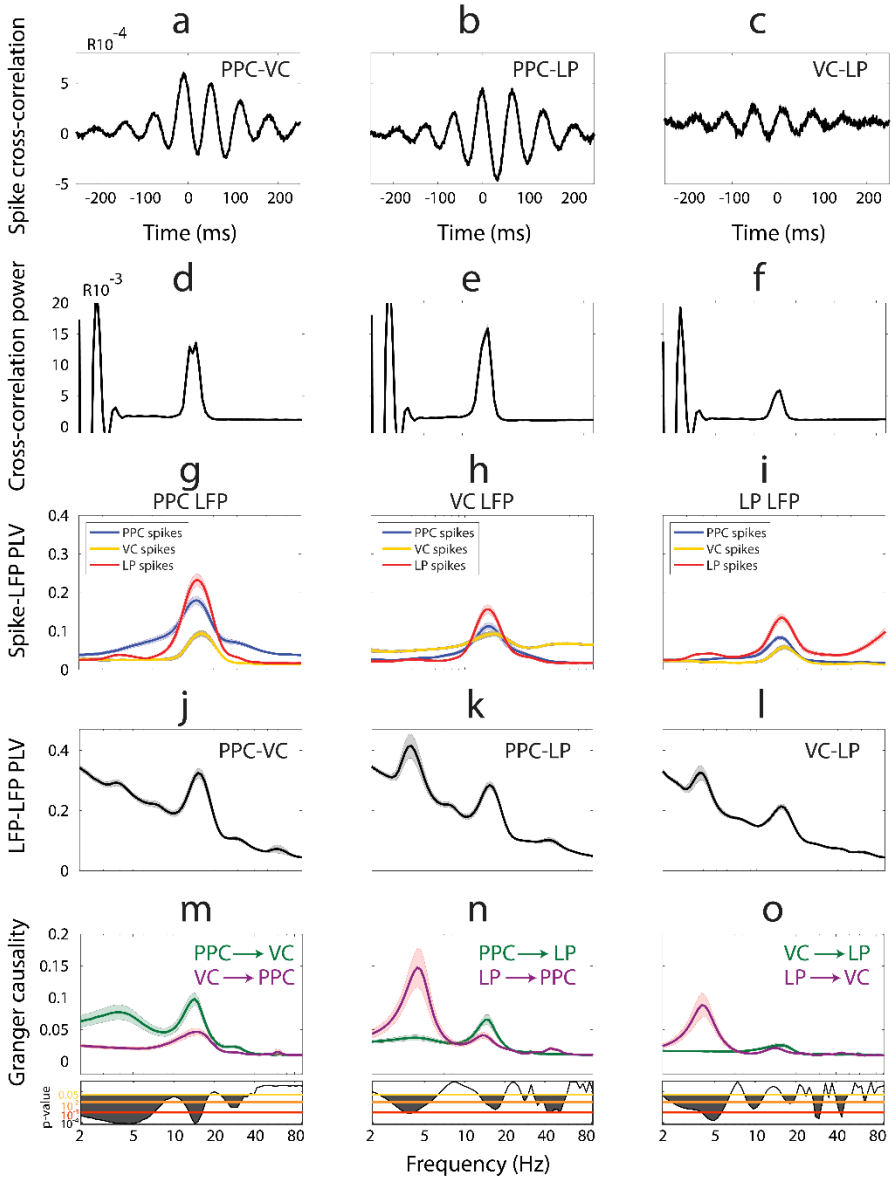

Figure 3.3. Synchronization between brain regions and directed functional connectivity in thalamo-cortical network.

Population averaged spike cross-correlation measured between (a) PPC and VC, (b) PPC and LP, and (c) VC and LP. The mean power spectrum of spike-correlations displayed a prominent peak in the alpha band (centered on ~15.23 Hz) for PPC-VC (d), PPC-LP (e), and VC-LP (f) spike cross-correlations.

g) Phase locking between spikes from PPC, VC, and LP and the LFP from PPC region.

h) Phase locking between spikes from PPC, VC, and LP and the LFP from VC.

i) Phase locking between spikes from PPC, VC, and LP and the LFP from LP.

j) Phase-locking value (PLV) between the LFP recorded from PPC and VC regions as a function of frequency indicates synchronization in the alpha frequency band.

k) PPC and LP are synchronized in both the theta and alpha band.

l) Theta and alpha-band synchronization is evident between VC and LP regions.

m) Spectrally resolved Granger causality shows that the influence of PPC on VC (green) is larger than influence of VC on PPC (violet) in all examined frequencies including alpha band (2-sided t-test, indicated by the exact p-values below the p=0.05 line (yellow)).

n) LP has a causal influence on PPC at theta frequency range (violet). In return, PPC has a causal influence on LP at alpha frequency band (green).

o) LP drives VC at theta frequency range (violet). VC and LP drive each other comparably (2-sided t-test, indicated by the exact p-value around the p=0.05 line (yellow)) at alpha frequency range.

g-o) Each recording session was treated as an independent sample unit. All measures are shown as mean (thick line) ± SEM (light background).

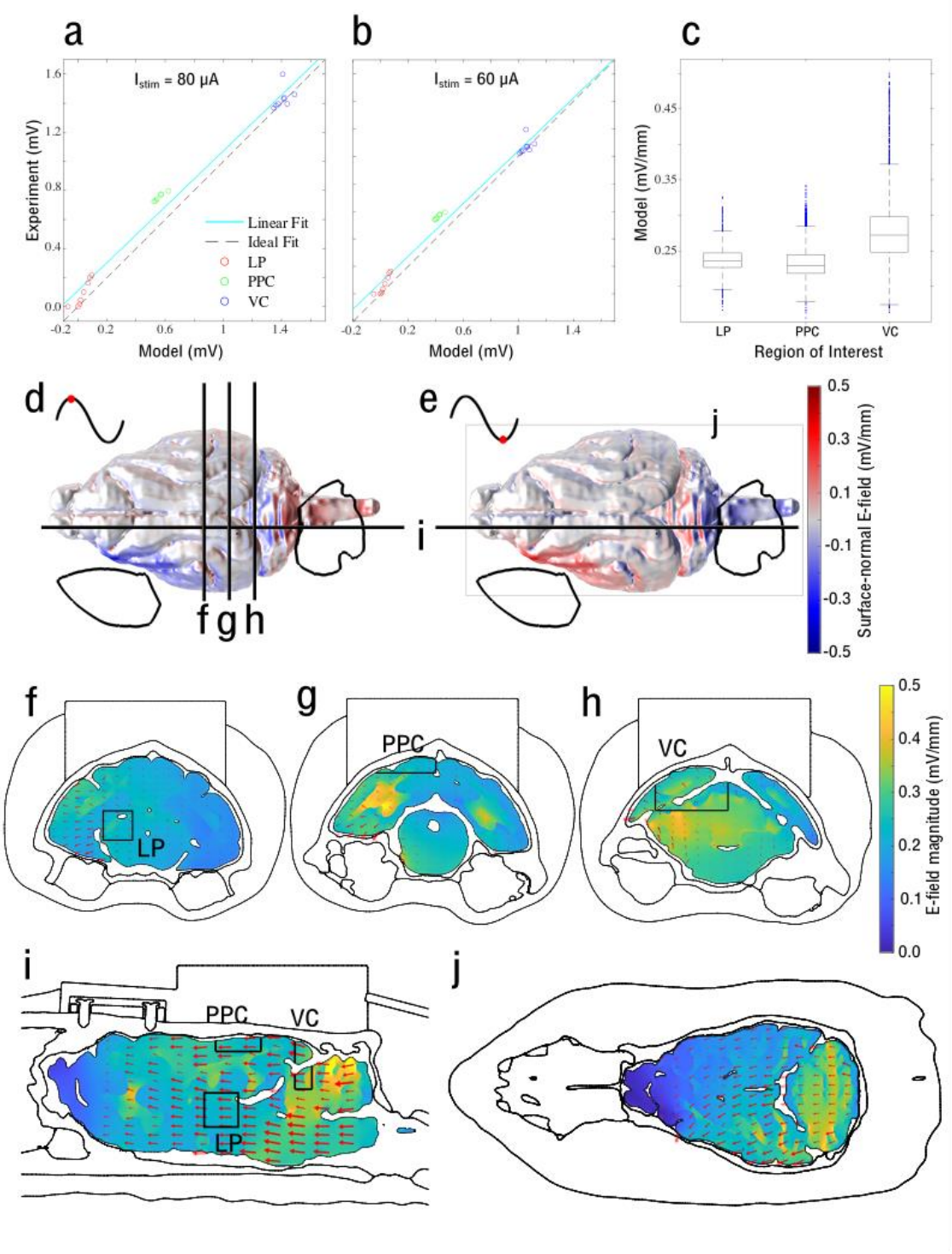

Figure 3.4. Measurement and modeling of the tACS electric field in the ferret brain.

a, b) Comparison between recorded and simulated electric potentials using stimulation current intensity of 80 µA and 60 µA in three recording sites: LP, PPC, and VC with 8, 6, and 8 grid electrodes, respectively.

The y axis represents the experimental values averaged over n = 6 measurements (2 blocks and 3 electrode refence schemes), while the x axis shows the corresponding potential value from the model. Solid cyan line represents the linear regression of the data, which ideally should match the dashed black unity line.

c) Distribution of the electric field magnitude in the three ROIs, predicted by the model. The central mark in each box indicates the median, and the bottom and top edges indicate the 25th and 75th percentiles, respectively. The whiskers extend to the most extreme data points not considered outliers (99.3% of the data), and the outliers are plotted as blue dots. The number of samples in each ROI correspond to the number of finite elements: n = 2327, 8782, and 7944 for LP, PPC, and VC, respectively. These data demonstrate a relatively weak electric field of ~ 0.25 mV/mm in the ROIs. Source data are provided as a Source Data file.

d, e) Spatial distribution of the magnitude of the electric field surface-normal component (min: −0.497 mV/mm, max: 0.507 mV/mm) on the brain surface at, respectively, 90□ and 270□ phase of the tACS wave (red dots on a cycle of sine wave). The electric field magnitude is greatest in areas proximal to stimulation electrodes (open black circles in left frontal and midline occipital regions). The direction of the surface normal electric field flips according to the tACS phase.

f-j) The electric field distribution along three coronal sections (including ROIs), one sagittal section (dashed lines in d and e) and a transversal section is displayed in f-j. The model prediction shows that the electric field magnitude is less than 0.5 mV/mm in all sections. The maximum electric field (bright yellow) occurs outside the ROIs. Arrows representing the direction of the electric field components are scaled in length by the electric field strength in the plane of the sections in f-j and demonstrate dominant posterior–anterior electric field direction.

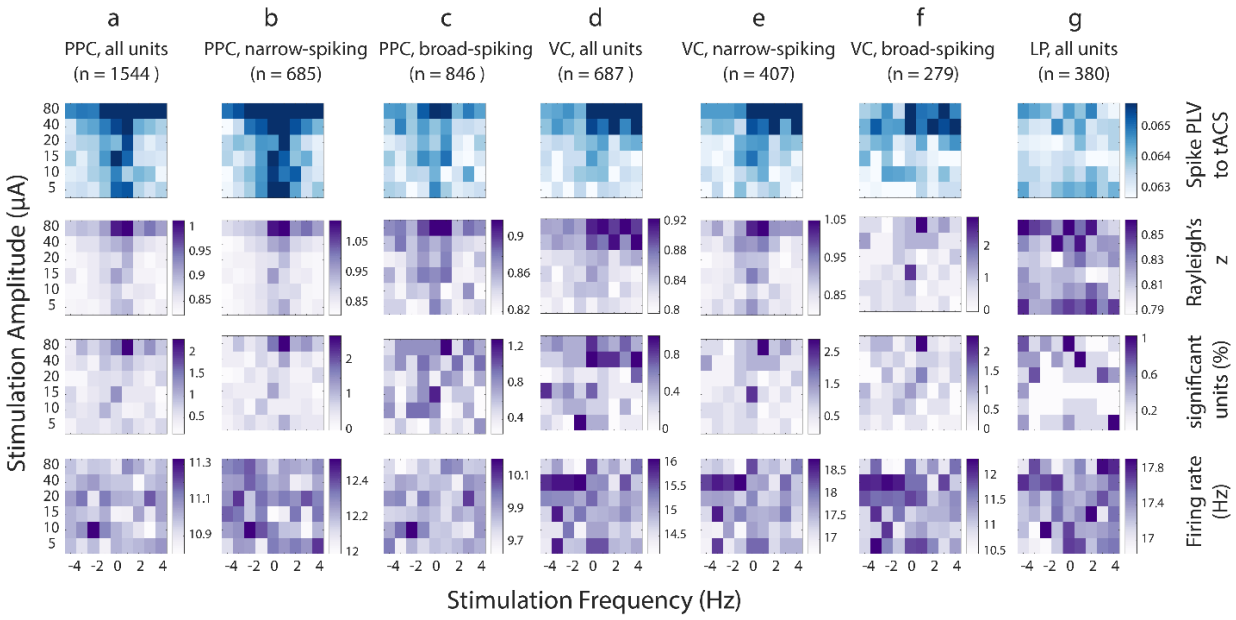

Figure 3.5. Transcranial alternating current stimulation engages cortical alpha oscillations at the level of individual neurons.

Synchronization maps (blue) and corresponding Rayleigh's z-score (purple, second row), percentage of units with significant phase-locking value (purple, third row) and firing rate maps (purple, bottom row) as a function of stimulation parameters for PPC (a-c), VC (d-f), and LP (g). The synchronization maps show phase locking between individual spikes and tACS wave as measured by phase-locking value (PLV) averaged across units. The horizontal axis indicates the distance (in Hz) from individual alpha frequency, and the vertical axis shows the stimulation amplitude.

(a, top two rows) tACS entrains PPC units as indicated by the Arnold tongue centered at the individual endogenous alpha frequency.

(b, c, top two rows) Narrow-spiking units in PPC show stronger phase locking to tACS when compared to their broad-spiking counterparts.

(d-f, top two rows) VC units are phase locked to tACS, but the area of entrainment is asymmetric and favors stimulation at frequencies above the endogenous peak frequency.

(g, top two rows) The map for LP units does not show prominent synchronization.

(a-g, third row) Only a small percent of units (<2%) show significant modulation of spike phases as measured by Rayleigh's test.

(a-g, bottom row) The random pattern of firing rate maps for all regions/unit types indicates that tACS did not modulate the firing rate of target neurons.

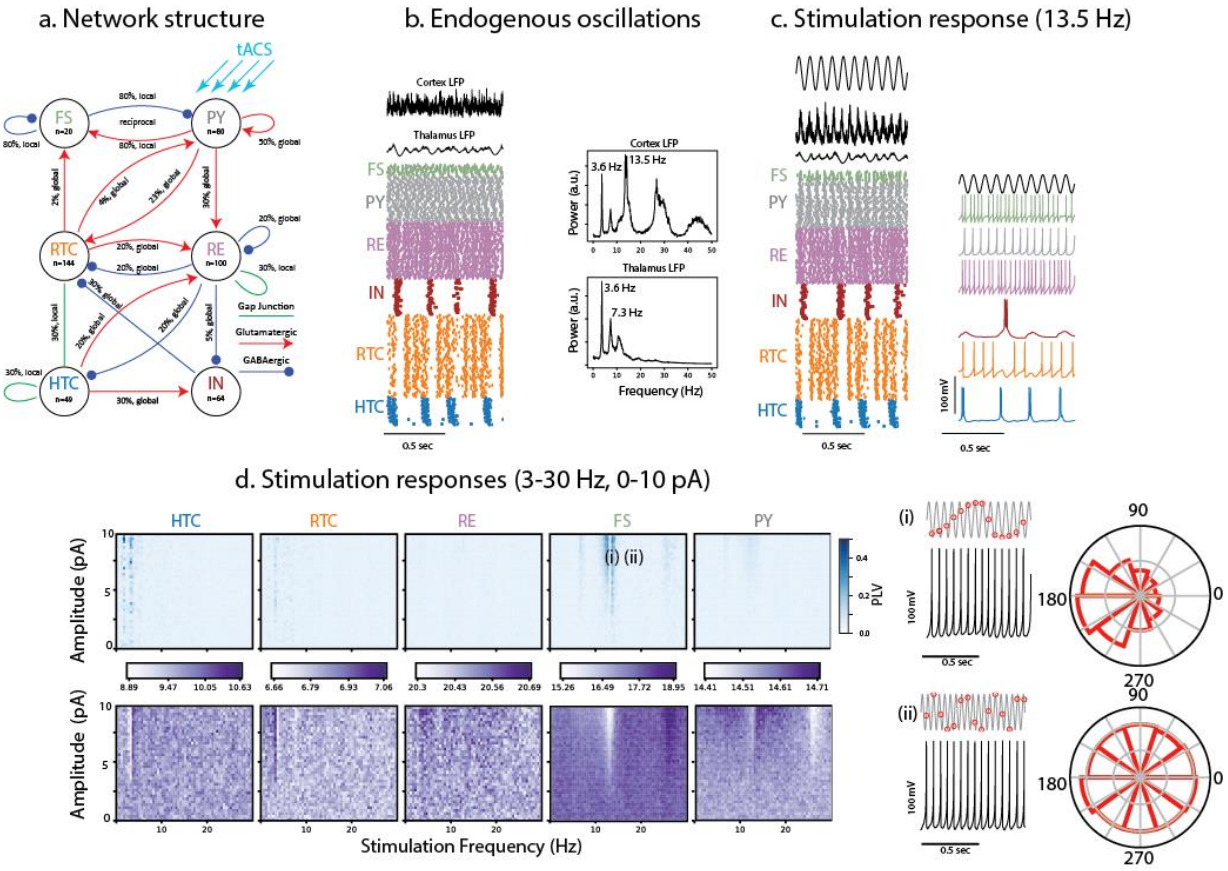

Figure 3.6. Endogenous alpha oscillations in a thalamo-cortical model and synchronization by tACS.

a) The structure of the thalamocortical network with excitatory, inhibitory and gap-junction connections between neuronal populations. The cortical network includes fast-spiking inhibitory (FS) and regular-spiking pyramidal (PY) neurons. The thalamic network includes relay thalamo-cortical (RTC), reticular (RE), high-threshold bursting (HTC), and thalamic local inhibitory (IN) neurons. The tACS is applied only to pyramidal neurons (blue arrows).

b) Endogenous oscillations shown by (top) 1-sec cortical and thalamic local field potential (LFP) traces, and (bottom left) the raster plot with each dot representing the firing instant of a neuron. (Bottom right) The cortical LFP has a dominant spectral peak at alpha range (13.5 Hz), and a smaller peak at theta range (3.6 Hz). The thalamic LFP has a dominant theta peak (3.6 Hz), its harmonic (7.3 Hz), and a weak alpha peak (13.5 Hz).

c) Network response to a 13.5 Hz, 8 pA tACS. The cortical and thalamic LFP traces, and the raster plot showing firing of all neurons (left), and the membrane voltage traces of sample neuron from each cell type (right).

d) Network response to a group of stimuli with frequencies between 3 and 30 Hz, and amplitudes between 0 to 10 pA. Top left heat-maps: The color-coded phase locking value (PLV) as a function of stimulation frequency (horizontal axis), and stimulation amplitude (vertical axis) for each neuron type. Darker colors indicate higher synchronization between individual neurons and tACS with corresponding frequency and amplitude. The FS and PY neurons show triangular-shape high PLV regions centered on the alpha peak frequency (13.5 Hz). Bottom left heat-maps: The firing rate (FR) maps for each neuron type. The color at each point indicates the average firing rate (in Hz) across neurons in response to tACS with corresponding frequency (horizontal axis) and amplitude (vertical axis). Two points on PLV and FR maps are selected for further analysis: (i) A point with high PLV on Arnold tongue region with tACS parameters of 13.5 Hz and 8 pA. The tACS waveform and membrane potential of a sample PY neuron (top right) shows that the PY neuron fires regularly after the peak of the tACS wave (red circles). The phase distribution of tACS wave at firing instances of PY neuron shows a phase preference between 90 and 180 degrees. (ii) A point with low PLV outside of the Arnold tongue region with tACS parameters of 18.5 Hz and 8 pA. The tACS waveform and membrane potential of a sample PY neuron (bottom right) shows that the PY neuron fires at random phases of tACS wave (red circles). The phase distribution of the tACS waveform when PY neurons fired shows a uniform phase distribution.

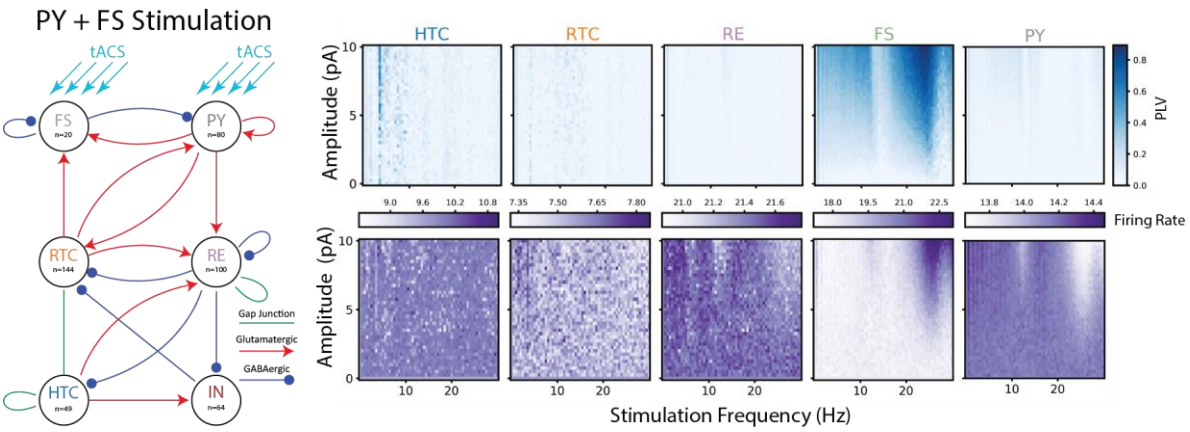

Figure 3.7. Modeling tACS Stimulation to Both PY and FS Cells.

Phase locking (top) and firing rate (bottom) response to tACS applied to both the PY and FS cells. Each pixel in the histogram represents five seconds of simulation with the appropriate amplitude tACS stimulation. In the plot, tACS amplitude and frequency range from 0–10 pA and 0–30 Hz respectively. Black arrows indicate the center of Arnold tongues. The FS neurons exhibit two Arnold tongues, the first centered around the endogenous frequency for the PY neurons, 13.5 Hz, and the second centered at the first harmonic. For PY neurons, an Arnold tongue is also present at the endogenous frequency. Phase locking for the FS neurons is high compared to the model where FS neurons were not stimulated, especially at the first harmonic. In this plot, the high phase locking in the FS neurons overshadows the Arnold tongue in the PY neurons, but it is still present.

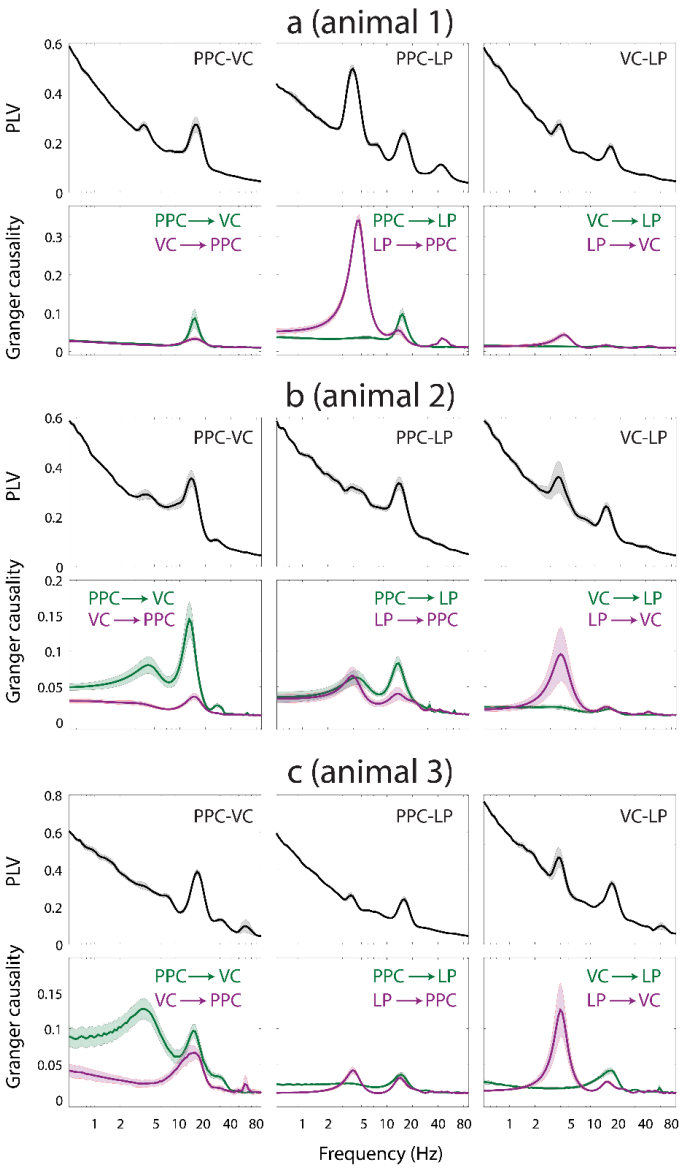

Figure 3.A. Synchronization between regions and directionality analysis for individual animals. For each animal, the top row shows the frequency dependent phase-locking values (PLV), and the bottom row displays the spectrally resolved conditional Granger causality results. The scales for PLV and GC were chosen to facilitate comparisons between regions within each animal. Different animals might have different ranges of values due to individual differences, and the goal here was not to compare between animals. Related to Figure 3. All measures are shown as mean (thick line) ± SEM (light background). N=12, 13, 12 sessions for animal 1, 2, 3 respectively.

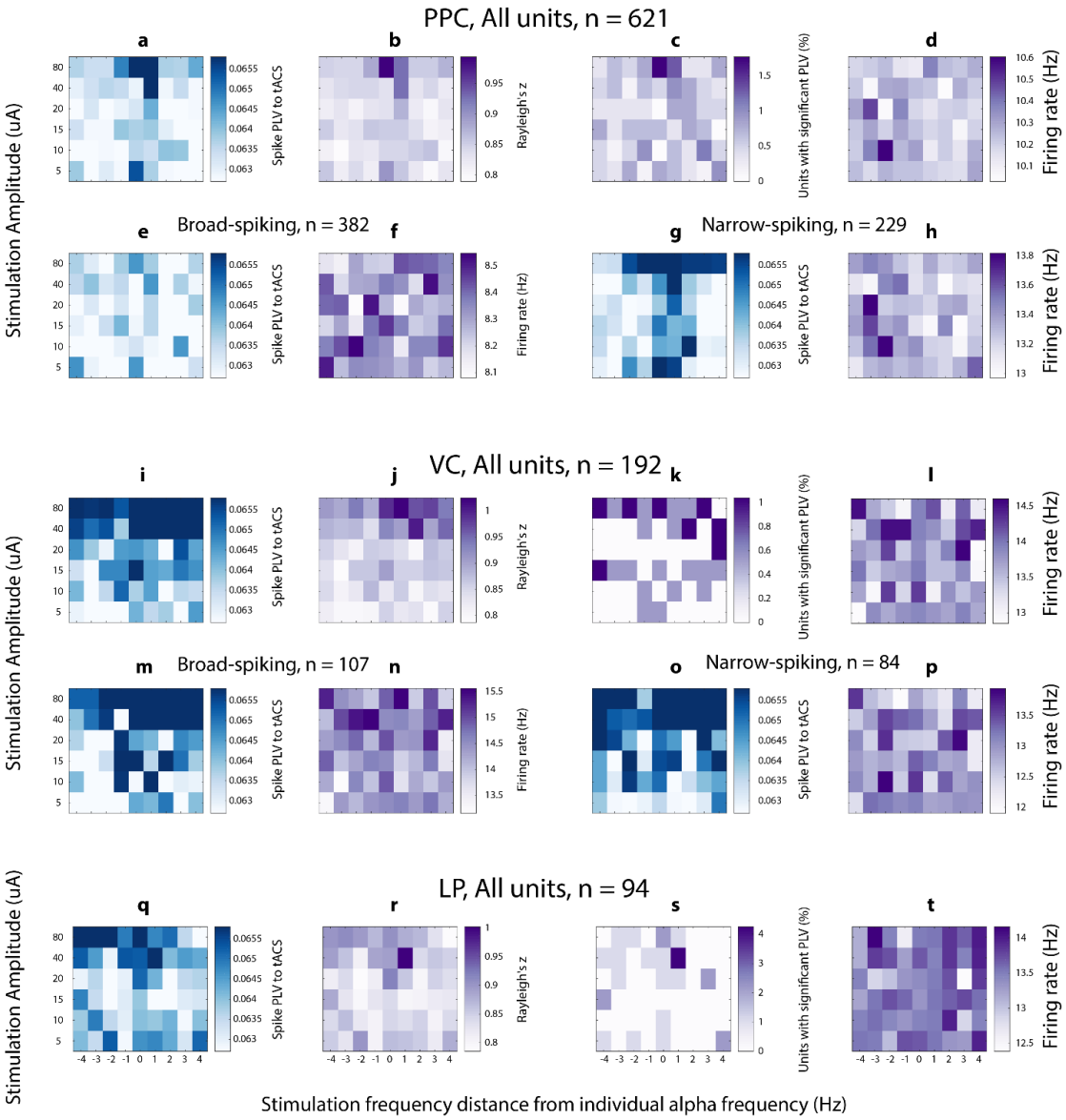

Figure 3.B. Synchronization and firing rate maps for animal 1.

a) Average phase locking of PPC spikes (averaged across 621 units) to tACS phase as measured by phase-locking value (PLV) as a function of stimulation frequency (horizontal axis) and stimulation amplitude (vertical axis).

b) Average Rayleigh's z-score (across all PPC units) as a function of stimulation parameters.

c) Percentage of PPC units with significant PLV as indicated by Rayleigh's test.

d) Average firing rate of all PPC units.

e) Average PLV of broad-spiking PPC units (n=382).

f) Average firing rate of broad-spiking PPC units.

g) Average PLV of narrow-spiking PPC units (n=229).

h) Average firing rate of narrow-spiking PPC units.

i-p) Corresponding measures of (a-h) for VC.

q-t) Corresponding measures of (a-d) for LP. The horizontal axis shows the distance from endogenous alpha frequency in Hz. Related to Figure 3.5.

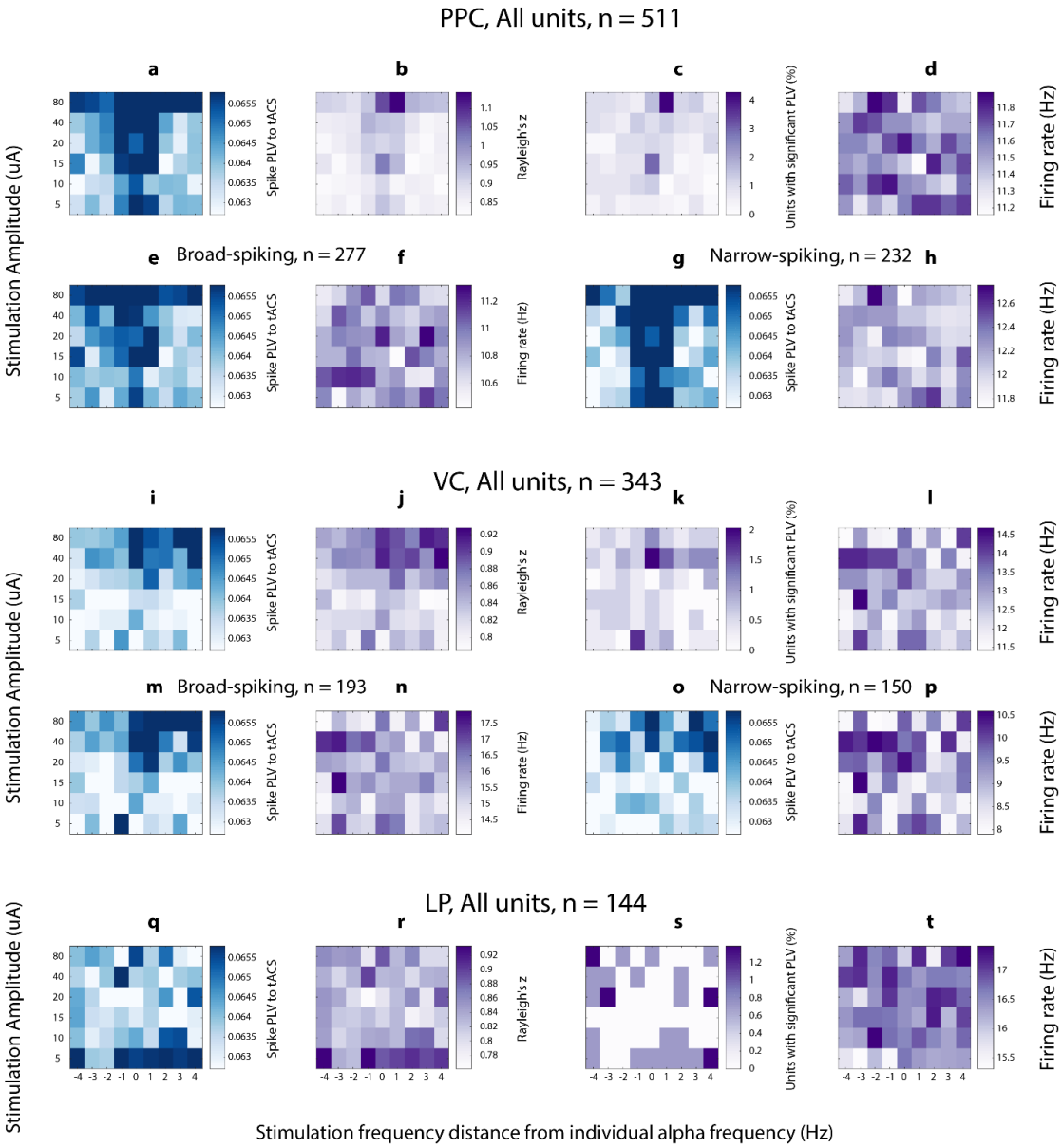

Figure 3.C. Synchronization and firing rate maps for animal 2.

a) Average phase locking of PPC spikes (averaged across 621 units) to tACS phase as measured by phase-locking value (PLV) as a function of stimulation frequency (horizontal axis) and stimulation amplitude (vertical axis).

b) Average Rayleigh's z-score (across all PPC units) as a function of stimulation parameters.

c) Percentage of PPC units with significant PLV as indicated by Rayleigh's test.

d) Average firing rate of all PPC units.

e) Average PLV of broad-spiking PPC units (n=382).

f) Average firing rate of broad-spiking PPC units.

g) Average PLV of narrow-spiking PPC units (n=229).

h) Average firing rate of narrow-spiking PPC units.

i-p) Corresponding measures of (a-h) for VC.

q-t) Corresponding measures of (a-d) for LP. The horizontal axis shows the distance from endogenous alpha frequency in Hz. Related to Figure 3.5.

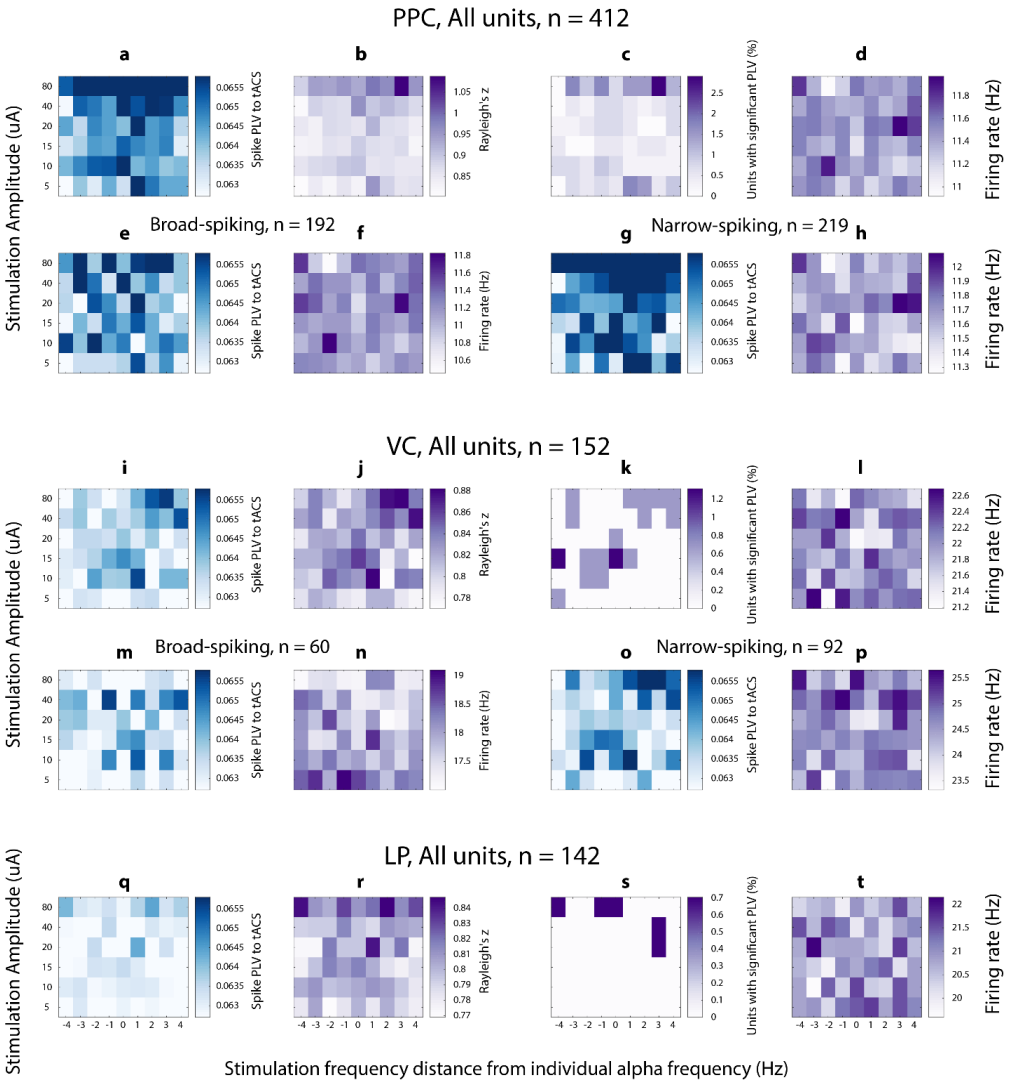

Figure 3.D. Synchronization and firing rate maps for animal 3.

a) Average phase locking of PPC spikes (averaged across 621 units) to tACS phase as measured by phase-locking value (PLV) as a function of stimulation frequency (horizontal axis) and stimulation amplitude (vertical axis).

b) Average Rayleigh's z-score (across all PPC units) as a function of stimulation parameters.

c) Percentage of PPC units with significant PLV as indicated by Rayleigh's test.

d) Average firing rate of all PPC units.

e) Average PLV of broad-spiking PPC units (n=382).

f) Average firing rate of broad-spiking PPC units.

g) Average PLV of narrow-spiking PPC units (n=229).

h) Average firing rate of narrow-spiking PPC units.

i-p) Corresponding measures of (a-h) for VC.

q-t) Corresponding measures of (a-d) for LP. The horizontal axis shows the distance from endogenous alpha frequency in Hz. Related to Figure 3.5.

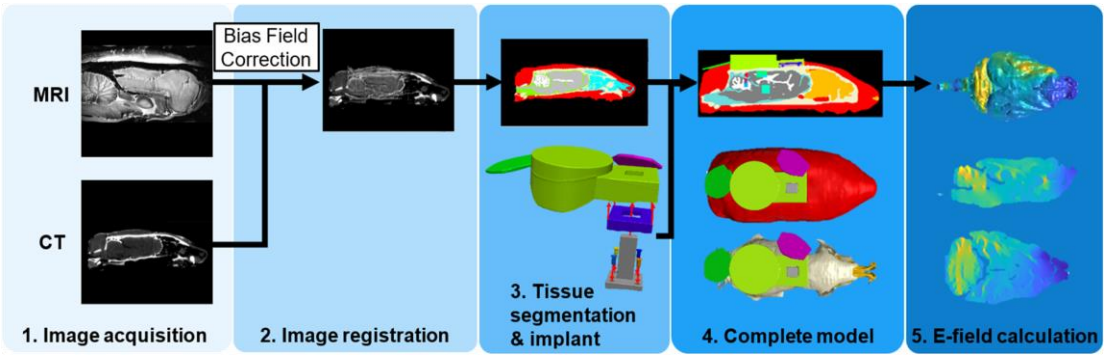

Figure 3.E. Pipeline for computational modeling for tACS electric field in ferret head.

The CT and MRI imaging data were co-registered to allow segmentation of hard and soft tissues (1-3). Implanted hardware and surface tACS electrodes were added to this segmentation (3) and meshed (4) with finite elements to create a three-dimensional representation of the experimental setup. Tissue and hardware conductivities were assigned based on the literature (see Supplementary Table S3.A) and COMSOL was used to solve the quasi-static Poisson equation for nodal electric potentials, from which the electric field was calculated (5). Related to Figure 3.4.

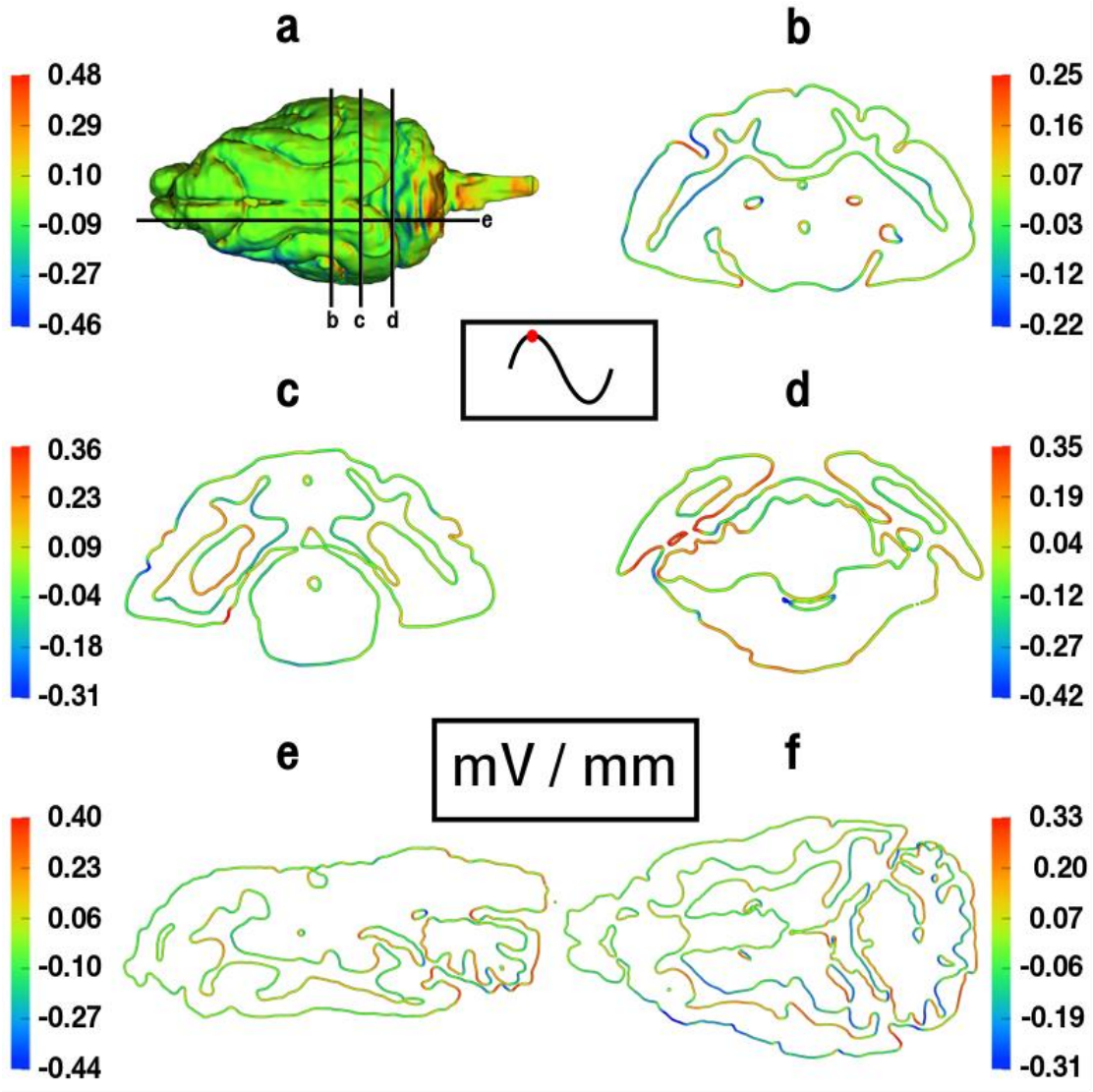

Figure 3.F. Surface-normal component of electric field (nE) at 80 µA stimulation current depicted on:

(a) ferret brain surface as well as through brain volume where nE is shown at gray matter interface only;

(b-d) coronal slices, (e) sagittal and (f) axial brain slice. Related to Figure 3.4.

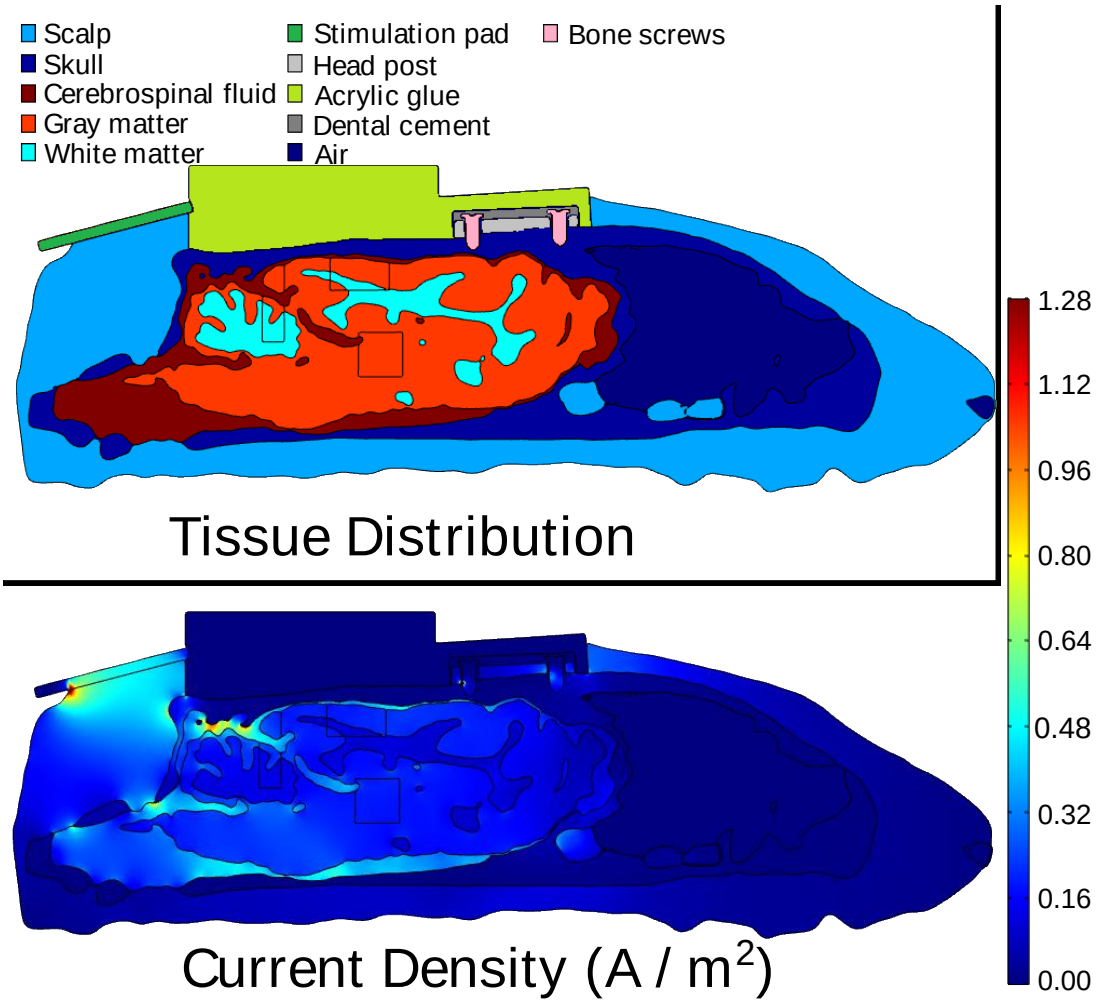

Figure 3.G. Current density (80 µA) in sagittal cross-sectional view. Plane cuts through posterior tACS electrode and head post screws.

Top: color-coded map of tissues and materials. Bottom: simulated current density shown here between 0–1.28 A/m^2 (volumetric maximum: 5.12 A/m^2 under electrode). The head screws perturb the current density only in their immediate vicinity near the skull–CSF interface. An advantageous feature of the experimental setup is the lack of significant current channeling through the screws, which is due to them being coated with insulating dental cement and acrylic glue on top. Related to Figure 3.4.

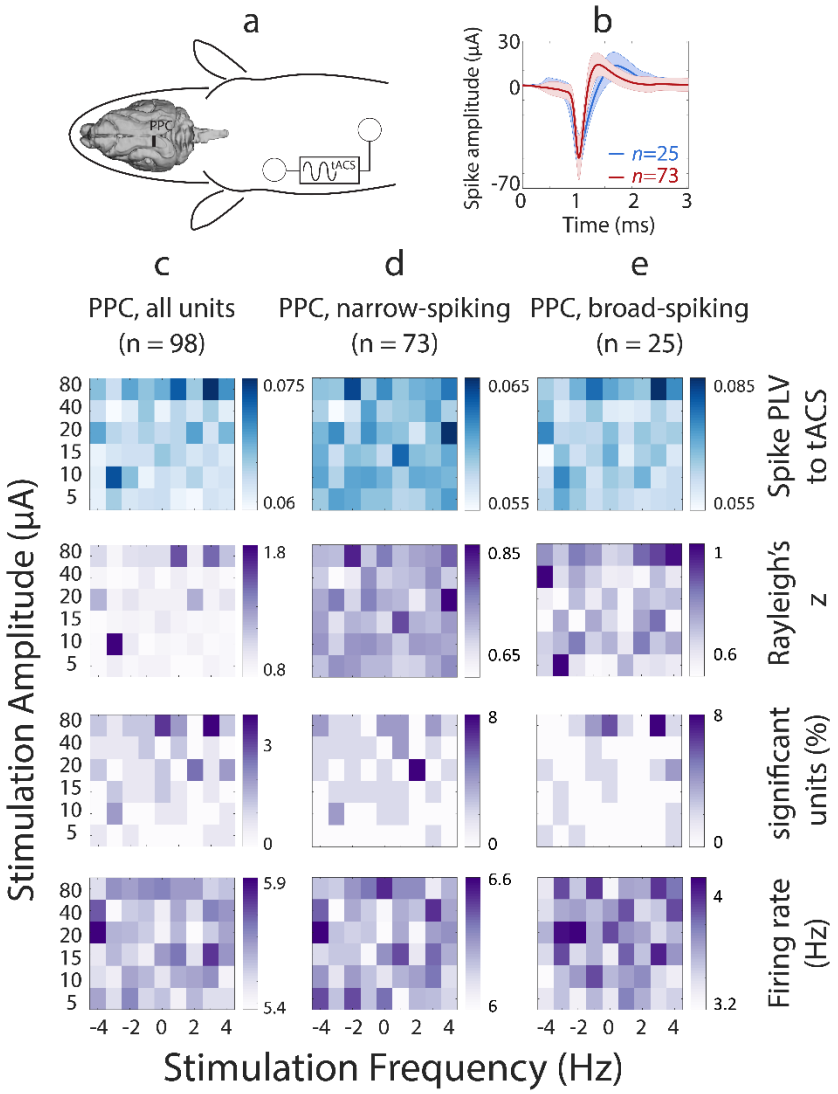

Figure 3.H. Peripheral nerve stimulation failed to produce an Arnold tongue pattern in PPC at the level of individual neurons.

Synchronization maps (blue, top row) and corresponding Rayleigh's z-score (purple, second row), percentage of units with significant phase-locking value (purple, third row) and firing rate maps (purple, bottom row) as a function of stimulation parameters for PPC. The synchronization maps show phase locking between individual spikes and the alternating current stimulation waveform as measured by phase-locking value (PLV) averaged across units. The horizontal axis indicates the distance (in Hz) from individual alpha frequency, and the vertical axis shows the stimulation amplitude.

a) Illustration of peripheral nerve stimulation by placement of the stimulation electrodes on the lower back of the ferret. The relative distance between the stimulation pads as well as stimulation parameters were all identical to those in the main tACS experiment in Figure 3.5.

b) Color coded spike waveforms (mean±SEM) for two identified clusters of narrow-spiking (red, n=73) and broad-spiking (blue, n=25) neurons in PPC.

(c-e, top two rows) There is no clear pattern of entrainment of PPC neurons centered at the individual endogenous alpha frequency.

(c-e, third row) A small percent of units (<8%) show significant modulation of spike phases as measured by Rayleigh's test for both types of neurons, however, due to the small sample size, the testing is highly unreliable.

(c-e, bottom row) The random pattern of firing rate maps for all unit types indicates that stimulation of peripheral nerves did not modulate the firing rate of the target neurons.

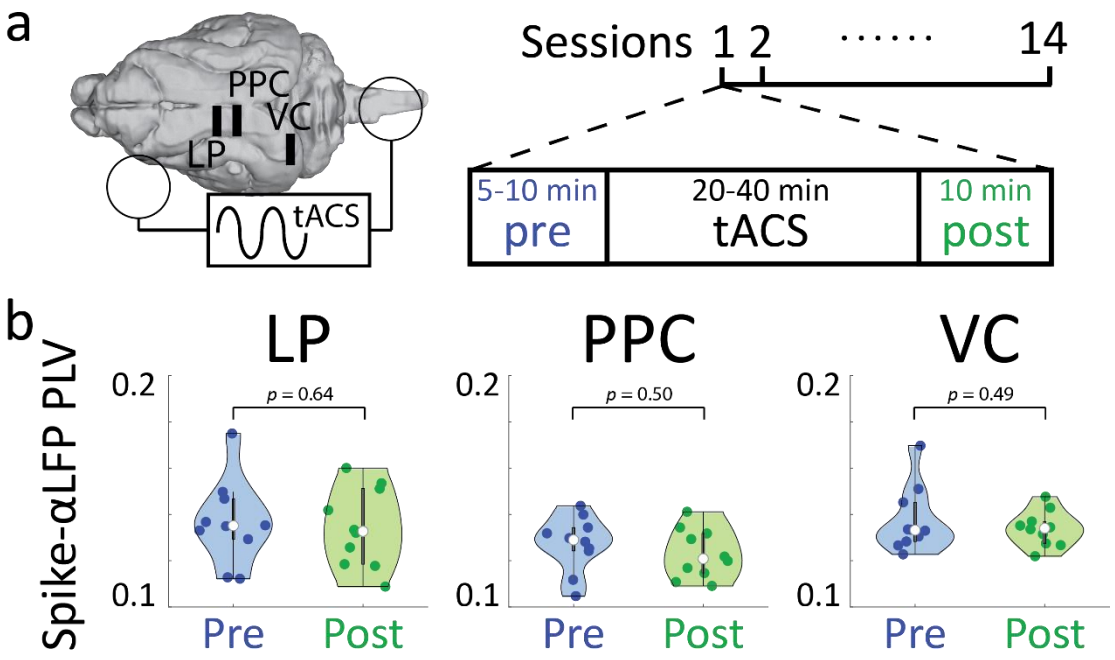

Figure 3.I. Repeated tACS sessions do not produce long-lasting effect on neuronal synchrony.

a) Illustration of the experimental setup. The tACS pads were placed at the same location as the tACS experiment for determination of the Arnold tongue.

b) Scatter plots showing phase-locking value between single units and the endogenous alpha oscillation for pre (blue) and post (green) each tACS session. The violin plots showed the kernel density of PLV for each condition. The white middle point represented the median of data, the thick line flanking the middle point is the interquartile range. Each dot represents one PLV value between one single unit and alpha frequency component of the average LFP. The differences in phase-locking values between pre and post are not significant in all three regions (paired two-sided t-test, n=10 single units, LP: p=0.64, PPC: p=0.50, VC: p=0.49, without multiple comparisons adjustment), indicating the absence of a long-lasting effect after prolonged tACS sessions (20-40 minutes). Source data are provided as a Source Data file.

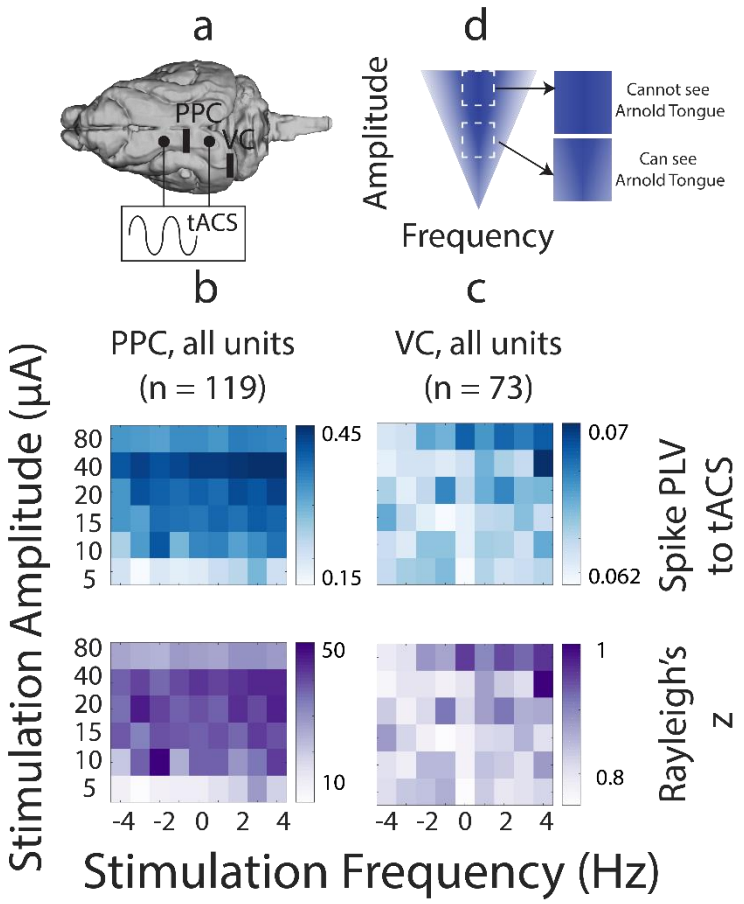

Figure 3.J. Local bone screw stimulation engages cortical alpha oscillations at the level of individual neurons.

Synchronization maps (blue) and corresponding Rayleigh's z-score (purple, second row) as a function of stimulation parameters for PPC and VC. The synchronization maps show phase locking between individual spikes and the stimulation waveform as measured by phase-locking value (PLV) averaged across units. The horizontal axis indicates the distance (in Hz) from individual alpha frequency, and the vertical axis shows the stimulation amplitude.

a) Illustration of bone screw stimulation near PPC in the anterior-posterior axis.

b) There is a gradual increase in PPC neuron entrainment as the amplitude increases from 10 to 40 μA. There is no clear pattern of entrainment of PPC neuron centered at the individual endogenous alpha frequency.

c) The synchronization in VC shows a preference to higher amplitude and higher frequency (relative to the endogenous frequency), but no clear preference to the individual endogenous alpha frequency for lower stimulation amplitudes.

d) A cartoon illustration of the Arnold Tongue shows the expected synchronization behavior for different parameter subspaces. When the amplitude is higher, such as in our bone screw stimulation experiment, the synchronization map is saturated and it is hard to see an Arnold Tongue pattern (top). When the amplitude is in the lower range, such as in our tACS experiment, the synchronization map shows a clearer Arnold Tongue pattern (bottom).

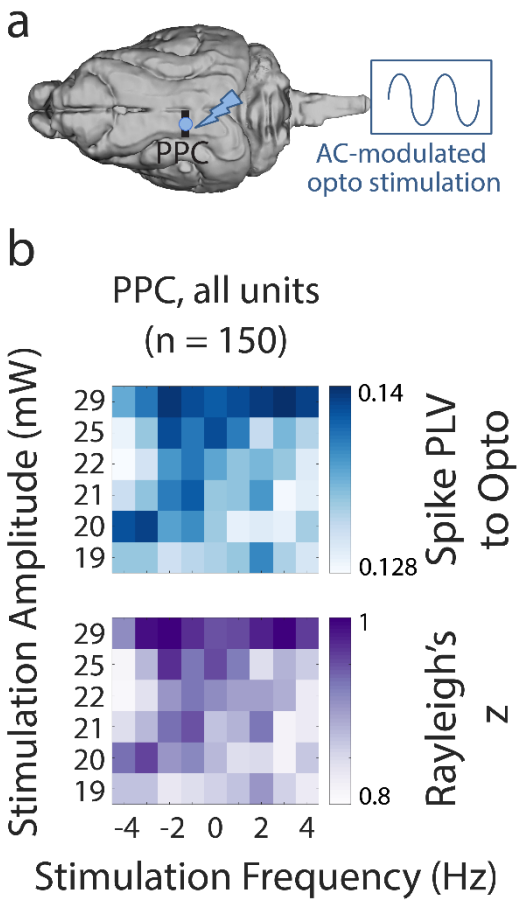

Figure 3.K. Optogenetic stimulation in PPC engages cortical alpha oscillations at the level of individual neurons.

Synchronization maps (blue) and corresponding Rayleigh's z-score (purple, second row) as a function of stimulation parameters for PPC and VC. The synchronization maps show phase locking between individual spikes and the stimulation waveform as measured by phase-locking value (PLV) averaged across units. The horizontal axis indicates the distance (in Hz) from the individual alpha frequency, and the vertical axis shows the stimulation amplitude.

a) Illustration of optogenetics stimulation in PPC with simultaneous electrophysiology recording. Laser power was modulated by a sinusoidal wave to mimic ACS.

b) Top: Synchronization plot between PPC units and the laser amplitude modulation displayed an Arnold tongue shape. The highest amplitude (29 mW) entrained neuron at all frequencies tested, and the lowest amplitude (19 mW) also did not show preference for a specific frequency. However, in between the two

extremes, we observed amplitude- and frequency-dependent synchronization around the endogenous frequency, albeit a little left shifted. Bottom: The z-statistics from Rayleigh's test for non-uniformity of circular data also displays a similar triangular shape for PPC neurons, confirming the amplitude- and frequency-dependent spike-phase modulation.

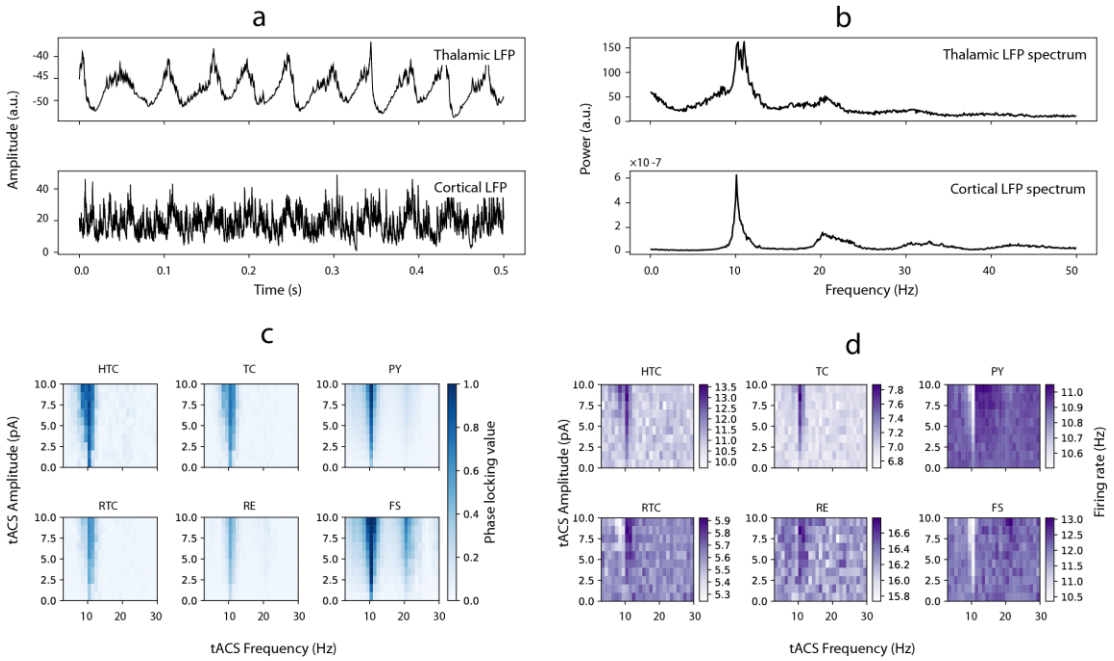

Figure 3.L. Synchronization by tACS in modified thalamo-cortical network. In this modified network, both thalamus and cortex exhibit a spectral peak in the alpha frequency peak.

In contrast to the main model (and the experimental data), thalamus does not exhibit a theta spectral peak anymore. As a result, tACS in the alpha frequency entrains both the cortical and thalamic neuronal populations in this modified model. HTC: excitatory high-threshold bursting thalamic cells, TC: thalamo-cortical cells, PY: excitatory pyramidal neurons, RTC: thalamo-cortical relay cells, RE: inhibitory thalamic reticular cells, FS: fast-spiking inhibitory neurons

a) Both cortical and thalamic LFPs show alpha endogenous oscillations. Raw traces of simulated LFPs.

b) Spectra for LPF traces shown in a).

c) Color-coded phase locking value (PLV) of spiking activity of different neuron types to tACS as a function of tACS frequency (horizontal axis) and tACS amplitude (vertical axis). Triangular-shape high-synchrony Arnold tongue regions centered on alpha frequency are evident for all neuron types.

d) Color-coded firing rate maps corresponding to PLV maps for all neuron types.

Related to Figure 3.6.

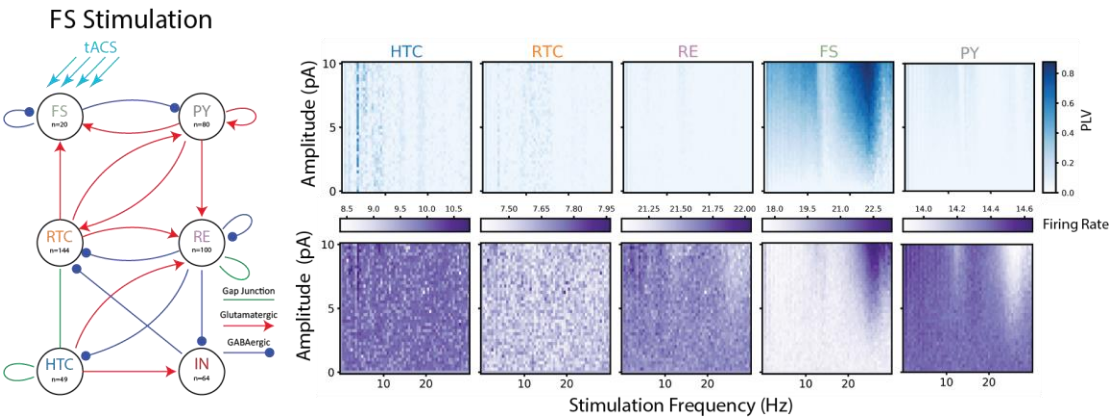

Figure 3.M. Modeling tACS Stimulation to FS Neurons Only.

Thalamocortical model response to different amplitudes and frequencies of tACS s applied only to FS neurons. Each pixel in the histogram represents five seconds of simulation with the appropriate amplitude and frequency tACS wave. tACS amplitude ranges from 0–10 pA and tACS frequency ranges from 0–30 Hz. Arnold tongues appear at the same frequencies as they do when both PY and FS cells receive tACS stimulation (Figure 7). Phase locking in the FS neurons is higher at the first harmonic compared to simulations where FS neurons do not receive stimulation.

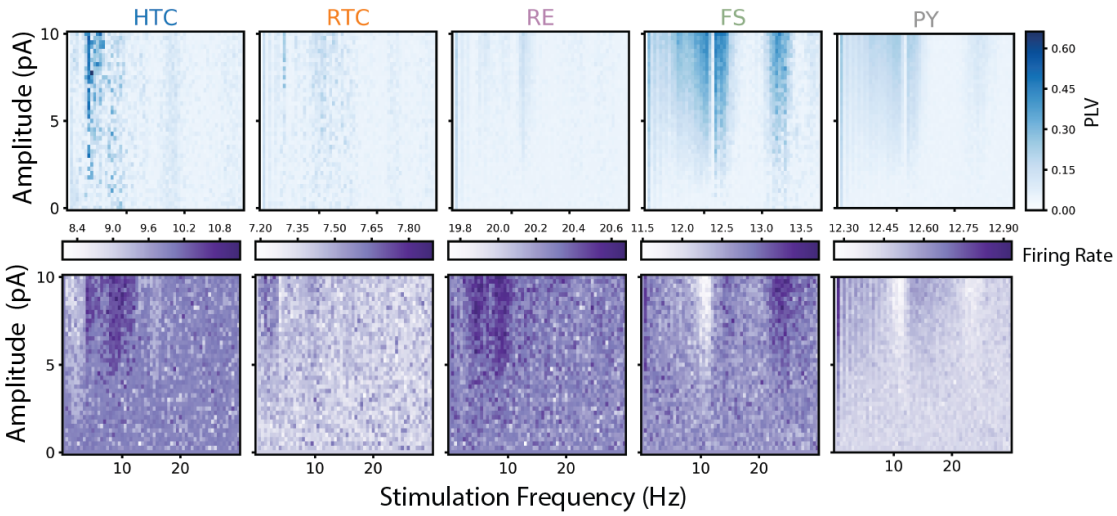

Figure 3.N. Modeling tACS Stimulation in Model with NMDA receptors in Cortical Network.

When NMDA synapses are added to the cortical portion of the model and biases are adjusted to achieve similar firing rates, the model exhibits similar phase locking and firing rate behavior to the model without cortical NMDA synapses.

Table 3.A. Tissue/Material electrical conductivities. Related to Figure 3.4.

Tissue/Material	Electrical Conductivity [S/m]
Scalp	0.29
Skull	0.03
Cerebrospinal fluid	1.65
Grey matter	0.82
White matter	0.38
Stimulation pad	5.9×10^{7}
Head post, bone screws	1.39×10^{6}
Acrylic glue	3.6×10^{-5}
Dental cement	2.5×10^{-14}
Air	2.5×10^{-14}

REFERENCES

ADRIAN, E. D., & MATTHEWS, B. H. C. (1934). THE BERGER RHYTHM: POTENTIAL CHANGES FROM THE OCCIPITAL LOBES IN MAN. *Brain, 57*(4), 355-385. doi:10.1093/brain/57.4.355

Ahn, S., Mellin, J. M., Alagapan, S., Alexander, M. L., Gilmore, J. H., Jarskog, L. F., & Fröhlich, F. (2019). Targeting reduced neural oscillations in patients with schizophrenia by transcranial alternating current stimulation. *Neuroimage, 186*, 126-136.

Ahn, S., Prim, J. H., Alexander, M. L., McCulloch, K. L., & Fröhlich, F. (2018). Identifying and Engaging Neuronal Oscillations by Transcranial Alternating Current Stimulation in Patients with Chronic Low Back Pain: A Randomized, Crossover, Double-Blind, Sham-Controlled Pilot Study. *The Journal of Pain*.

Alagapan, S., Schmidt, S. L., Lefebvre, J., Hadar, E., Shin, H. W., & Fröhlich, F. (2016). Modulation of cortical oscillations by low-frequency direct cortical stimulation is state-dependent. *PLoS Biology, 14*(3), e1002424.

Alexander, M., Alagapan, S., Lugo, C., Mellin, J., Lustenberger, C., Rubinow, D., & Frohlich, F. (2018). S102. Pilot Double-Blind, Placebo-Controlled Clinical Trial of Transcranial Alternating Current Stimulation (tACS) for the Treatment of Major Depressive Disorder. *Biological Psychiatry, 83*(9), S386-S387.

Ali, M. M., Sellers, K. K., & Fröhlich, F. (2013). Transcranial alternating current stimulation modulates large-scale cortical network activity by network resonance. *The Journal of neuroscience, 33*(27), 11262-11275.

Antal, A., Boros, K., Poreisz, C., Chaieb, L., Terney, D., & Paulus, W. (2008). Comparatively weak after-effects of transcranial alternating current stimulation (tACS) on cortical excitability in humans. *Brain stimulation, 1*(2), 97-105.

Asamoah, B., Khatoun, A., & Mc Laughlin, M. (2019). tACS motor system effects can be caused by transcutaneous stimulation of peripheral nerves. *Nat Commun, 10*(1), 266. doi:10.1038/s41467-018-08183-w

Aspart, F., Remme, M. W., & Obermayer, K. (2018). Differential polarization of cortical pyramidal neuron dendrites through weak extracellular fields. *PLoS Computational Biology, 14*(5), e1006124.

Barnett, L., & Seth, A. K. (2014). The MVGC multivariate Granger causality toolbox: a new approach to Granger-causal inference. *Journal of Neuroscience Methods, 223*, 50-68.

Barthó, P., Hirase, H., Monconduit, L., Zugaro, M., Harris, K. D., & Buzsaki, G. (2004). Characterization of neocortical principal cells and interneurons by network interactions and extracellular features. *Journal of Neurophysiology, 92*(1), 600-608.

Barthó, P., Slézia, A., Mátyás, F., Faradzs-Zade, L., Ulbert, I., Harris, K. D., & Acsády, L. (2014). Ongoing network state controls the length of sleep spindles via inhibitory activity. *Neuron, 82*(6), 1367-1379.

Bollimunta, A., Mo, J., Schroeder, C. E., & Ding, M. (2011). Neuronal Mechanisms and Attentional Modulation of Corticothalamic Alpha Oscillations. *31*(13), 4935-4943. doi:10.1523/JNEUROSCI.5580-10.2011 %J The Journal of Neuroscience

Boyle, M. R., & Frohlich, F. (2013). *EEG feedback-controlled transcranial alternating current stimulation.* Paper presented at the Neural Engineering (NER), 2013 6th International IEEE/EMBS Conference on.

Braitenberg, V., & Schüz, A. (2013). *Anatomy of the cortex: statistics and geometry* (Vol. 18): Springer Science & Business Media.

Brignani, D., Ruzzoli, M., Mauri, P., & Miniussi, C. (2013). Is transcranial alternating current stimulation effective in modulating brain oscillations? *PloS One, 8*(2), e56589.

Datta, A., Bansal, V., Diaz, J., Patel, J., Reato, D., & Bikson, M. (2009). Gyri-precise head model of transcranial direct current stimulation: improved spatial focality using a ring electrode versus conventional rectangular pad. *Brain stimulation, 2*(4), 201-207. e201.

Deans, J. K., Powell, A. D., & Jefferys, J. G. (2007). Sensitivity of coherent oscillations in rat hippocampus to AC electric fields. *The Journal of Physiology, 583*(2), 555-565.

Deans, J. K., Powell, A. D., & Jefferys, J. G. R. (2007). Sensitivity of coherent oscillations in rat hippocampus to AC electric fields. *The Journal of Physiology, 583*(Pt 2), 555-565. doi:10.1113/jphysiol.2007.137711

Fedorov, A., Beichel, R., Kalpathy-Cramer, J., Finet, J., Fillion-Robin, J.-C., Pujol, S., . . . Sonka, M. (2012). 3D Slicer as an image computing platform for the Quantitative Imaging Network. *Magnetic Resonance Imaging, 30*(9), 1323-1341.

Fröhlich, F. (2014). Endogenous and exogenous electric fields as modifiers of brain activity: rational design of noninvasive brain stimulation with transcranial alternating current stimulation. *Dialogues in Clinical Neuroscience, 16*(1), 93-102.

Fröhlich, F. (2016). *Network neuroscience*: Academic Press.

Fröhlich, F., & McCormick, D. A. (2010). Endogenous electric fields may guide neocortical network activity. *Neuron, 67*(1), 129-143.

Geweke, J. (1982). Measurement of linear dependence and feedback between multiple time series. *Journal of the American statistical association, 77*(378), 304-313.

Geweke, J. F. (1984). Measures of conditional linear dependence and feedback between time series. *Journal of the American Statistical Association, 79*(388), 907-915.

Granger, C. W. (1969). Investigating causal relations by econometric models and cross-spectral methods. *Econometrica: Journal of the Econometric Society*, 424-438.

Grossman, N., Bono, D., Dedic, N., Kodandaramaiah, S. B., Rudenko, A., Suk, H.-J., . . . Tsai, L.-H. (2017). Noninvasive Deep Brain Stimulation via Temporally Interfering Electric Fields. *Cell, 169*(6), 1029-1041. e1016.

Haberbosch, L., Datta, A., Thomas, C., Jooß, A., Köhn, A., Rönnefarth, M., . . . Schmidt, S. (2019). Safety Aspects, Tolerability and Modeling of Retinofugal Alternating Current Stimulation. *Frontiers in Neuroscience, 13*(783). doi:10.3389/fnins.2019.00783

Helfrich, Randolph F., Schneider, Till R., Rach, S., Trautmann-Lengsfeld, Sina A., Engel, Andreas K., & Herrmann, Christoph S. (2014). Entrainment of Brain Oscillations by Transcranial Alternating Current Stimulation. *Current Biology, 24*(3), 333-339. doi:10.1016/j.cub.2013.12.041

Herrmann, C. S., Murray, M. M., Ionta, S., Hutt, A., & Lefebvre, J. (2016a). Shaping intrinsic neural oscillations with periodic stimulation. *Journal of Neuroscience, 36*(19), 5328-5337.

Herrmann, C. S., Murray, M. M., Ionta, S., Hutt, A., & Lefebvre, J. (2016b). Shaping intrinsic neural oscillations with periodic stimulation. *The Journal of neuroscience, 36*(19), 5328-5337.

Huang, Y., Liu, A. A., Lafon, B., Friedman, D., Dayan, M., Wang, X., . . . Parra, L. C. (2017). Measurements and models of electric fields in the in vivo human brain during transcranial electric stimulation. *Elife, 6*, e18834.

Izhikevich, E. M. (2007). *Dynamical systems in neuroscience*: MIT press.

Izhikevich, E. M., & Edelman, G. M. (2008). Large-scale model of mammalian thalamocortical systems. *Proceedings of the national academy of sciences, 105*(9), 3593-3598.

Kasten, F. H., & Herrmann, C. S. (2017). Transcranial alternating current stimulation (tACS) enhances mental rotation performance during and after stimulation. *Frontiers in Human Neuroscience, 11*.

Kasten, F. H., & Herrmann, C. S. (2017). Transcranial Alternating Current Stimulation (tACS) Enhances Mental Rotation Performance during and after Stimulation. *Frontiers in human neuroscience, 11*, 2-2. doi:10.3389/fnhum.2017.00002

Krause, B., Márquez-Ruiz, J., & Cohen Kadosh, R. (2013). The effect of transcranial direct current stimulation: a role for cortical excitation/inhibition balance? *Frontiers in Human Neuroscience, 7*, 602.

Kumar, R. J., Rajasekhar, E., Subhan, C., Panduranga, P., & Gupta, N. (2014). Dielectric Studies of Acrylic Resin, Alginate, Dental Plaster, Dental Stone, Glass Ionomer and Silver Amalgam. *Indian Journal of Advances in Chemical Science, 2*(2), 98-103.

Laakso, I., & Hirata, A. (2013). Computational analysis shows why transcranial alternating current stimulation induces retinal phosphenes. *J Neural Eng, 10*(4), 046009. doi:10.1088/1741-2560/10/4/046009

Lachaux, J.-P., Rodriguez, E., Martinerie, J., & Varela, F. J. (1999). Measuring phase synchrony in brain signals. *Human Brain Mapping, 8*(4), 194-208.

Lafon, B., Henin, S., Huang, Y., Friedman, D., Melloni, L., Thesen, T., . . . Parra, L. C. (2017). Low frequency transcranial electrical stimulation does not entrain sleep rhythms measured by human intracranial recordings. *Nature Communications, 8*(1), 1199.

Lefebvre, J., Hutt, A., & Frohlich, F. (2017). Stochastic resonance mediates the state-dependent effect of periodic stimulation on cortical alpha oscillations. *eLife, 6*, e32054.

Li, G., Henriquez, C. S., & Fröhlich, F. (2017a). Unified thalamic model generates multiple distinct oscillations with state-dependent entrainment by stimulation. *PLoS Comput. Biol., 13*(10), e1005797. doi:10.1371/journal.pcbi.1005797

Li, G., Henriquez, C. S., & Fröhlich, F. (2017b). Unified thalamic model generates multiple distinct oscillations with state-dependent entrainment by stimulation. *PLoS Computational Biology, 13*(10), e1005797.

Li, G., Henriquez, C. S., & Fröhlich, F. (2018). Rhythmic Modulation of Thalamic Oscillations Depends on Intrinsic Cellular Dynamics. *Journal of Neural Engineering*.

Liu, A., Vöröslakos, M., Kronberg, G., Henin, S., Krause, M. R., Huang, Y., . . . Krekelberg, B. (2018). Immediate neurophysiological effects of transcranial electrical stimulation. *Nature Communications, 9*(1), 5092.

Mazzoni, A., Lindén, H., Cuntz, H., Lansner, A., Panzeri, S., & Einevoll, G. T. (2015). Computing the Local Field Potential (LFP) from Integrate-and-Fire Network Models. *PLoS computational biology, 11*(12), e1004584. doi:10.1371/journal.pcbi.1004584

Miranda, P. C., Lomarev, M., & Hallett, M. (2006). Modeling the current distribution during transcranial direct current stimulation. *Clinical Neurophysiology, 117*(7), 1623-1629.

Molaee-Ardekani, B., Márquez-Ruiz, J., Merlet, I., Leal-Campanario, R., Gruart, A., Sánchez-Campusano, R., . . . Wendling, F. (2013). Effects of transcranial Direct Current Stimulation (tDCS) on cortical activity: a computational modeling study. *Brain stimulation, 6*(1), 25-39.

Moliadze, V., Antal, A., & Paulus, W. (2010). Boosting brain excitability by transcranial high frequency stimulation in the ripple range. *The Journal of Physiology, 588*(24), 4891-4904.

Negahbani, E., Kasten, F. H., Herrmann, C. S., & Fröhlich, F. (2018). Targeting alpha-band oscillations in a cortical model with amplitude-modulated high-frequency transcranial electric stimulation. *Neuroimage, 173*, 3-12.

Neuling, T., Rach, S., & Herrmann, C. S. (2013). Orchestrating neuronal networks: sustained after-effects of transcranial alternating current stimulation depend upon brain states. *Frontiers in Human Neuroscience, 7*, 161.

Noury, N., Hipp, J. F., & Siegel, M. (2016). Physiological processes non-linearly affect electrophysiological recordings during transcranial electric stimulation. *Neuroimage, 140*, 99-109.

Noury, N., Hipp, J. F., & Siegel, M. (2016). Physiological processes non-linearly affect electrophysiological recordings during transcranial electric stimulation. *Neuroimage, 140*(Supplement C), 99-109. doi:https://doi.org/10.1016/j.neuroimage.2016.03.065

Noury, N., & Siegel, M. (2017). Phase properties of transcranial electrical stimulation artifacts in electrophysiological recordings. *Neuroimage, 158*, 406-416.

Noury, N., & Siegel, M. (2018). Analyzing EEG and MEG signals recorded during tES, a reply. *Neuroimage, 167*, 53-61.

Okun, M., Steinmetz, N. A., Cossell, L., Iacaruso, M. F., Ko, H., Barthó, P., . . . Carandini, M. (2015). Diverse coupling of neurons to populations in sensory cortex. *Nature, 521*(7553), 511.

Opitz, A., Falchier, A., Yan, C.-G., Yeagle, E. M., Linn, G. S., Megevand, P., . . . Schroeder, C. E. (2016). Spatiotemporal structure of intracranial electric fields induced by transcranial electric stimulation in humans and nonhuman primates. *Scientific Reports, 6*, 31236.

Ozen, S., Sirota, A., Belluscio, M. A., Anastassiou, C. A., Stark, E., Koch, C., & Buzsaki, G. (2010). Transcranial electric stimulation entrains cortical neuronal populations in rats. *The Journal of neuroscience, 30*(34), 11476-11485. doi:10.1523/JNEUROSCI.5252-09.2010

Pachitariu, M., Steinmetz, N. A., Kadir, S. N., Carandini, M., & Harris, K. D. (2016). *Fast and accurate spike sorting of high-channel count probes with KiloSort.* Paper presented at the Advances in neural information processing systems.

Palva, S., & Palva, J. M. (2011). Functional Roles of Alpha-Band Phase Synchronization in Local and Large-Scale Cortical Networks. *Frontiers in Psychology, 2*(204). doi:10.3389/fpsyg.2011.00204

Pikovsky, A., Rosenblum, M., & Kurths, J. (2003). *Synchronization: a universal concept in nonlinear sciences* (Vol. 12): Cambridge university press.

Polanía, R., Nitsche, M. A., Korman, C., Batsikadze, G., & Paulus, W. (2012). The importance of timing in segregated theta phase-coupling for cognitive performance. *Current Biology, 22*(14), 1314-1318.

Raco, V., Bauer, R., Olenik, M., Brkic, D., & Gharabaghi, A. (2014). Neurosensory effects of transcranial alternating current stimulation. *Brain Stimul, 7*(6), 823-831. doi:10.1016/j.brs.2014.08.005

Radman, T., Ramos, R. L., Brumberg, J. C., & Bikson, M. (2009). Role of cortical cell type and morphology in subthreshold and suprathreshold uniform electric field stimulation in vitro. *Brain stimulation, 2*(4), 215-228. e213.

Radman, T., Su, Y., An, J. H., Parra, L. C., & Bikson, M. (2007). Spike timing amplifies the effect of electric fields on neurons: implications for endogenous field effects. *The Journal of neuroscience, 27*(11), 3030-3036.

Radtke-Schuller, S. (2018). *Cyto- and Myeloarchitectural Brain Atlas of the Ferret (Mustela putorius) in MRI Aided Stereotaxic Coordinates* (1 ed.): Springer International Publishing.

Reato, D., Rahman, A., Bikson, M., & Parra, L. C. (2010). Low-intensity electrical stimulation affects network dynamics by modulating population rate and spike timing. *J Neurosci, 30*(45), 15067-15079. doi:30/45/15067 [pii]

10.1523/JNEUROSCI.2059-10.2010

Reato, D., Rahman, A., Bikson, M., & Parra, L. C. (2010). Low-intensity electrical stimulation affects network dynamics by modulating population rate and spike timing. *Journal of Neuroscience, 30*(45), 15067-15079.

Reato, D., Rahman, A., Bikson, M., & Parra, L. C. (2013). Effects of weak transcranial alternating current stimulation on brain activity—a review of known mechanisms from animal studies. *Frontiers in Human Neuroscience, 7*, 687.

Sadleir, R. J., Vannorsdall, T. D., Schretlen, D. J., & Gordon, B. (2010). Transcranial direct current stimulation (tDCS) in a realistic head model. *Neuroimage, 51*(4), 1310-1318.

Sahlem, G. L., Badran, B. W., Halford, J. J., Williams, N. R., Korte, J. E., Leslie, K., . . . Bachman, D. L. (2015). Oscillating square wave transcranial direct current stimulation (tDCS) delivered during slow wave sleep does not improve declarative memory more than sham: a randomized sham controlled crossover study. *Brain stimulation, 8*(3), 528-534.

Schmidt, S. L., Iyengar, A. K., Foulser, A. A., Boyle, M. R., & Fröhlich, F. (2014). Endogenous cortical oscillations constrain neuromodulation by weak electric fields. *Brain stimulation, 7*(6), 878-889.

So, P. P. M., Stuchly, M. A., & Nyenhuis, J. A. (2004). Peripheral nerve stimulation by gradient switching fields in magnetic resonance imaging. *IEEE Transactions on Biomedical Engineering, 51*(11), 1907-1914. doi:10.1109/TBME.2004.834251

Steels, A. (2008). Grade Data Sheet 303. In A. Steels (Ed.).

Stimberg, M., Brette, R., & Goodman, D. F. M. (2019). Brian 2, an intuitive and efficient neural simulator. *Elife, 8*, e47314. doi:10.7554/eLife.47314

Stitt, I., Zhou, Z. C., Radtke-Schuller, S., & Fröhlich, F. (2018). Arousal dependent modulation of thalamo-cortical functional interaction. *Nat Commun, 9*(1), 2455. doi:10.1038/s41467-018-04785-6

Tallon-Baudry, C., Bertrand, O., Delpuech, C., & Pernier, J. (1996). Stimulus specificity of phase-locked and non-phase-locked 40 Hz visual responses in human. *Journal of Neuroscience, 16*(13), 4240-4249.

Toloza, E. H., Negahbani, E., & Frohlich, F. (2017). Ih Interacts with Somato-Dendritic Structure to Determine Frequency Response to Weak Alternating Electric Field Stimulation. *Journal of Neurophysiology, 119.3*, 1029-1036.

Tustison, N. J., Avants, B. B., Cook, P. A., Zheng, Y., Egan, A., Yushkevich, P. A., & Gee, J. C. (2010). N4ITK: improved N3 bias correction. *IEEE Transactions on Medical Imaging, 29*(6), 1310-1320.

Vöröslakos, M., Takeuchi, Y., Brinyiczki, K., Zombori, T., Oliva, A., Fernández-Ruiz, A., . . . Berényi, A. (2018). Direct effects of transcranial electric stimulation on brain circuits in rats and humans. *Nat Commun, 9*(1), 483. doi:10.1038/s41467-018-02928-3

Vossen, A., Gross, J., & Thut, G. (2015). Alpha Power Increase After Transcranial Alternating Current Stimulation at Alpha Frequency (α-tACS) Reflects Plastic Changes Rather Than Entrainment. *Brain Stimul, 8*(3), 499-508. doi:10.1016/j.brs.2014.12.004

Witkowski, M., Garcia-Cossio, E., Chander, B. S., Braun, C., Birbaumer, N., Robinson, S. E., & Soekadar, S. R. (2016). Mapping entrained brain oscillations during transcranial alternating current stimulation (tACS). *Neuroimage, 140*, 89-98. doi:10.1016/j.neuroimage.2015.10.024

Zaehle, T., Rach, S., & Herrmann, C. S. (2010). Transcranial alternating current stimulation enhances individual alpha activity in human EEG. PloS One, 5(11), e13766.

Zar, J. H. (1999). Biostatistical analysis: Pearson Education India.

CHAPTER 4: TARGET ENGAGEMENT WITH TRANSCRANIAL CURRENT STIMULATION[3]

INTRODUCTION

Transcranial electric stimulation (tES) applies a weak electric current to the scalp which causes an electric field in the brain that can modulate neuronal activity and behavior. Despite the rapidly growing number of studies that report successful modulation of behavior by tES, comparably little is known about how tES modulates brain activity. In this chapter, we discuss what we know and what we do not know about the targeting of brain networks with tES. We provide an in-depth review of studies that use computational models, *in vitro* and *in vivo* animal models, and human participants to elucidate the mechanism of action of tES. The main emerging themes are that (1) the stimulation interacts with endogenous network dynamics resulting in state-dependent target engagement, (2) spatial and temporal targeting of specific neuronal network oscillations can be used to modulate and restore cognitive function, (3) low-frequency cortical oscillations during sleep represent a promising network target to elucidate the mechanisms of tES, and (4) that transcranial alternating current stimulation (tACS) has shown promise as

[3] This chapter previously appeared as part of a book chapter in "Target Engagement with Transcranial Current Stimulation. In: Brunoni A.R., Nitsche M.A., Loo C.K. (eds) Transcranial Direct Current Stimulation in Neuropsychiatric Disorders: Clinical Principles and Management." (https://doi.org/10.1007/978-3-030-76136-3_11)
The original citation is as follows: Frohlich F*, Force R*, **Huang WA***, Lustenberger C*, McPherson T*, Riddle J*, Walker C* (2020). Target Engagement with Transcranial Current Stimulation. In: Brunoni A.R., Nitsche M.A., Loo C.K. (eds) Transcranial Direct Current Stimulation in Neuropsychiatric Disorders: Clinical Principles and Management. New York (NY): Springer. p. 197-122.
The authors thank the contributors to the previous version of this book chapter for laying the groundwork for this version (in alphabetical order): Sankaraleengam Alagapan, Michael R. Boyle1, Franz Hamilton, Guoshi Li, and Stephen L. Schmidt.
Huang WA mainly contributed to the section "Mechanistic Insights from Animal Studies" which is presented here. The rest of the sections are not included in this dissertation.

a safe and potentially efficacious strategy to modulate impaired neuronal network oscillations and associated symptoms in psychiatry.

It has been known for a long time that electricity interacts with both the central and peripheral nervous system. Today, electric brain stimulation is used both as a research tool for the study of brain function and as a clinical tool for the treatment of neurological and psychiatric disorders. In this chapter, we will focus on one form of non-invasive brain stimulation, transcranial electric stimulation (tES, also referred to as transcranial current stimulation, tCS), which has recently attracted broad attention due to a large number of promising study results.

TES applies a weak electric current to the scalp. There are two main types of tES: transcranial direct current stimulation (tDCS) applies a constant current and transcranial alternating current stimulation (tACS) uses a sine-wave stimulation waveform. The aim of tES is to modulate brain function; the *target* of tES is the electrical activity in brain circuits. Most tES studies, however, only use behavioral outcomes and do not measure the changes in brain activity caused by stimulation. Therefore, the questions of how and by what mechanism tES engages network-level targets in the brain have remained mostly unanswered.

Here, we will review the research that is aimed at uncovering the mechanisms by which tES modulates neuronal network dynamics and behavior. As we will see, the mechanisms of action by which weak electric fields modulate neuronal activity have been studied with a range of different methods. *In vitro* studies using live brain slices have contributed to a mechanistic understanding of the effect of weak electric fields on neuronal activity at the cellular and microcircuit levels. *In vivo* animal studies have enabled the characterization of the effects of tES on intact brains with invasive recording methods with microscale spatial resolution. Non-invasive electrophysiology and imaging studies in humans have contributed insights into how stimulation interacts with endogenous network activity. In addition to these experimental approaches, computational modeling studies have provided important insights into targeting of specific networks and their endogenous network dynamics. The combination of these methods has proven to be very useful to understand how a weak electric field can change brain function by vertical integration.

In this chapter, we will provide an overview of the potential mechanisms of tES that have been uncovered using these diverse methodological approaches. First, we will review *in vitro* and *in vivo* studies. (This is followed by a discussion of computational modeling studies, which provide mechanistic insights on the effects of tES at a cellular and network level. Next, we focus on human studies that measured changes in brain activity by tES. Then, we turn our attention to the future and delineate what we believe are the rising new areas of tES research that deserve particular attention by the field. First, we discuss recent innovative strategies to target brain network oscillations in time and space for restoring and enhancing cognitive function. Second, we look at one promising network target where the different methodological approaches discussed here have come together in a synergistic way: low frequency oscillations during sleep. Third, we provide a brief outlook towards mechanism-based clinical trials. Together, this chapter aims to equip the reader with a comprehensive understanding of how tES engages network targets.)[4]

MECHANISTIC INSIGHTS FROM ANIMAL STUDIES

Although tES is a non-invasive stimulation modality with an outstanding safety track record for the use in humans, studies in animal models are of high importance. They play a crucial role in understanding the mechanisms by which tES modulates brain activity. First, animal experiments allow for the use of invasive electrophysiology such as the insertion of recording microelectrodes into the brain. This enables the investigation of how neuronal spiking is modulated by external electric fields. Second, reduced *in vitro* preparations such as the slice preparation offer the opportunity to study the effects of weak electric fields under controlled experimental conditions, which bypass the questions about delivery of the electric field through the scalp and the skull in the intact animal.

Effect of Electric Fields on Individual Neurons

One of the first observations of the effect of electric fields on neurons goes back many decades when Terzuolo and Bullock (Terzuolo & Bullock, 1956) applied a 1 mV/mm field to spontaneously active

[4] Content in parenthesis is not part of this dissertation work thus its corresponding sections were not included.

cardiac ganglion neurons of a lobster. The spontaneous firing rate of the cells was increased by the electric field. Similar modulation of neuronal firing rates by constant electric fields was also reported for other species (Creutzfeldt, Fromm, & Kapp, 1962; Purpura & McMurtry, 1965). In 1988, Chan and colleagues (Chan, Hounsgaard, & Nicholson, 1988) demonstrated that an applied electric field depolarizes the membrane voltage even when action potentials were blocked with the sodium-channel blocker tetrodotoxin. This demonstrated that the membrane depolarization caused by electric fields was a passive event, i.e. no opening or closing of ion channels was required. The underlying mechanism of fields altering the membrane voltage is that the ions within neurons change position in the presence of an external electric field. As the charge carriers redistribute within the cell to compensate for the applied field, the intracellular potential changes. As a result, the membrane voltage that is defined as the difference between the intracellular and extracellular potentials changes. The two distal poles of the structure aligned with electric field exhibit a depolarization and a hyperpolarization, respectively. This process is called *polarization* and depends on the overall length of the neuron as measured along the direction of the applied electric field. Specifically, there is a concomitant change in the membrane voltage in the apical dendrites of cortical pyramidal cells of opposite polarity to the effect in the soma (F. Aspart, M. W. H. Remme, & K. Obermayer, 2018; E. H. S. Toloza, Negahbani, & Fröhlich, 2018). Therefore, the orientation, morphology, and size of the cell play a role in the response to the application of electric fields.

In addition, the change in the membrane voltage also depends on both the amplitude and frequency of the applied field. To demonstrate that the change in membrane voltage is dependent on the strength of the electric field, fields ranging from -40 to +60 mV/mm were applied along the somato-dendritic axis of CA1 cells and the change in membrane voltage at somata recorded in acute hippocampal slices (Bikson et al., 2004). The resulting polarization linearly depended on the strength of the applied electric field. This work was then extended to sine-wave (AC) electric fields in CA3 pyramidal cells (J. K. Deans, A. D. Powell, & J. G. Jefferys, 2007). The change in membrane potentials resulting from AC electric fields were less than those of DC fields of the same strength. The relationship between the field strength and the membrane depolarization was still linear but the slope, which quantifies the change in membrane voltage

for every V/m of electric field, was decreased with increased frequency. Frequencies ranging from 5 to 100 Hz were applied and the change in the slope exponentially decays with the frequency of the applied electric field. This frequency dependence is caused by the low-pass filtering property of the passive cell membrane. Further, computational models demonstrate that AC induced frequency-dependent resonance in neurons (especially apical dendrites) is shaped by the dynamic interaction of the somato-dendritic morphology and the high-pass filtering property of the hyperpolarization-activated depolarizing cation current (I_h) (F. Aspart et al., 2018; E. H. S. Toloza et al., 2018).

tES effect on neuronal firing rate and spike timing

To understand the neuronal mechanism of tES, *in vivo* animal research with invasive recordings of the neuronal spiking activity is of essence. The modulation of both neuronal firing rate and spike timing are two candidate mechanisms through which tES may shape neuronal network dynamics. Using intracellular and extracellular recordings in rats, Vöröslakos et al. showed that at least 1 mV/mm EF is necessary to affect the neuronal spiking rate (Vöröslakos et al., 2018). Another mechanism through which tACS affects neuronal activity is through entrainment (spike timing modulation such that spikes lock to a preferred phase of the sine-wave electric field), especially when tACS is too weak to induce firing rate changes. Krause et al. applied tACS (4mA peak to peak, similar to human studies) through two scalp electrodes in two rhesus macaques and measured the effect on single-unit neural entrainment in the hippocampus and basal ganglia via depth electrodes. They found that tACS consistently influences the timing, but not the rate, of spiking activity (M. R. Krause, Vieira, Csorba, Pilly, & Pack, 2019). TACS applied on awake ferrets also showed entrainment of cortical neurons but no change in firing rate (Negahbani et al., 2019).

An alternative hypothesis is that the tES effect may be mediated by the stimulation of peripheral nerves in the scalp. Single neuron activity recordings in the rat motor cortex have shown that transcranial and transcutaneous electrical stimulation can entrain neuronal oscillations (~1Hz), and that anesthetizing the scalp significantly decreases the effect of tACS on tremor in humans (Asamoah et al., 2019). This particular study caused quite some discussion but was ultimately recognized as limited in implications due to lack of construct validity (human tremor as a marker of cortical oscillations) and statistical conclusion

validity (lack of statistical significance due to low sample size). Follow-up work that employed appropriate neurophysiological strategies showed that, when somatosensory input was blocked (by topical anesthesia), tACS (2mA) entrained hippocampal and visual cortex neurons, suggesting that peripheral input is not required for tACS to entrain neurons (Vieira, Krause, & Pack, 2019). Nevertheless, it cannot be excluded at this point that the two mechanisms have a combined effect on neuronal entrainment and behavioral performance, and more research is needed.

Interactions of Network Oscillations and Electric Fields

The change in membrane voltage of a single neuron by tES electric fields is too small to evoke action potentials in a cell at its resting potential in absence of synaptic input. Therefore, the effects of tDCS and tACS depend on the interaction of the applied stimulation and the endogenous network dynamics. In particular, slice experiments have provided important insights on the interactions between the ongoing network activity and the applied electric fields. Few slice preparations exhibit spontaneous network oscillations, presumably because of (1) the relative lack of synaptic inputs due to the deafferentation inherent to this preparation and (2) impaired neuromodulatory tone in tissue slices in comparison to the intact brain. However, oscillations may occur spontaneously in the slice preparation in more *in vivo*-like ionic conditions (Sanchez-Vives & McCormick, 2000) and in response to pharmacological activation (Williams & Kauer, 1997). More recently, optogenetic stimulation has uncovered in vivo-like activity patterns in the slice preparation (Beltramo et al., 2013). Therefore, these experimental strategies can be combined with the application of external electric fields for the study of the mechanisms of tES. For example, pharmacological activation of hippocampal slices caused the emergence of gamma oscillations that were susceptible to weak DC electric fields (D. Reato, A. Rahman, M. Bikson, & L. C. Parra, 2010a). Interestingly, the effect of the DC field was asymmetric with regards to the polarity. Hyperpolarizing fields were more effective at suppressing this network oscillation than depolarizing fields were at enhancing the same activity pattern. This asymmetry is supportive of the framework where ongoing activity shapes the response to stimulation. In the case of AC fields, for sufficiently low stimulation frequency, the amplitude of the gamma oscillation was periodically modulated, reminiscent of the theta-nested gamma oscillation

(Canolty et al., 2006). The most complex effect occurred if the stimulation frequency was similar to the frequency of the endogenous oscillation. In this case, three simultaneous frequencies were observed. The endogenous oscillation was reduced (but still present) while oscillations half a harmonic above and below the endogenous frequency appeared. However, *in vivo*, tACS entrains neural oscillations in a triangular Arnold tongue pattern – with only a small amplitude needed to entrain at the endogenous frequency and higher amplitudes needed for frequencies further away from the endogenous frequency (W. A. Huang et al., 2021). The Arnold tongues refers to the parameter space where phase-locking appears in a coupled oscillators system (Pikovsky, Kurths, Rosenblum, & Kurths, 2003). This model-driven prediction supports the mechanistic understanding of AC stimulation effects.

The interaction of electric field stimulation and endogenous oscillations appear to not only depend on the frequencies of both but on their relative amplitudes as well. In a study of low frequency (1 Hz) oscillations evoked by optogenetic stimulation, it was observed that electric fields of a mismatched frequency would enhance the power of the endogenous oscillation often without increasing power at the frequency of the electric field (S. L. Schmidt, Iyengar, Foulser, Boyle, & Frohlich, 2014). This occurred when the optogenetic drive, and therefore the "endogenous" oscillations, were strong and the electric field was relatively weak. However, the power of the oscillations at the stimulation frequency was enhanced when the magnitude of the endogenous oscillation was reduced (lower light intensity for optogenetic stimulation) or the strength of the electric field was increased. Taken together, the response of neural networks depends both on the frequency and the power (relative to the endogenous oscillation) of the electric field used for stimulation. Furthermore, these results suggest that the response of cortical networks to tES may be non-linear in nature.

So far, we have focused on the response to stationary stimulation waveforms; however, endogenous neural activity is not stationary. To this end endogenous activity may be better manipulated with feedback control algorithms than with static pre-programmed stimulation waveforms. One such example is the modulation of seizure-like, epileptiform electric events in slices. The application of DC fields can suppress

epileptiform activity in hippocampal slices which exhibit spontaneous seizure-like activity; however, the network quickly adapted to the stimulation and epileptiform activity returned (Gluckman et al., 1996). In a follow-up study, non-stationary electric stimulation was applied to suppress seizure-like activity (Gluckman, Nguyen, Weinstein, & Schiff, 2001). The authors were able to suppress seizure activity for 16 minutes using a negative feedback stimulation paradigm in a hippocampal slice which exhibited electrographic seizure events every 40 seconds. Critically, spontaneous activity still occurred while epileptiform activity was suppressed. Thus, in the case of suppression of epileptiform activity with tES, these studies show that adaptive feedback stimulation may have greater effect on network dynamics than constant stimulation. Indeed, there is also evidence that feedback stimulation has uses outside of suppression of aberrant activity. In spontaneously oscillating slices of ferret visual cortex, positive feedback stimulation with electric field was shown to decrease the length of time between cortical up states and increase the strength of the endogenous oscillation (Frohlich & McCormick, 2010). Conversely, the application of negative feedback stimulation to the slices reduced strength of the endogenous oscillation. Interestingly, this effect was accomplished with stimulation amplitudes similar to the amplitude of endogenous electric fields recorded *in vivo* (1 mV/mm). These results are at the core of our current understanding of how weak endogenous electric fields act as an amplifier of endogenous rhythmic activity (Fröhlich, 2014a).

Outlasting Effects of Electric Fields

One of the most exciting aspects of tES is that the effects of stimulation can outlast the stimulation as demonstrated by sustained modulation of motor-evoked potentials after completion of stimulation (Nitsche & Paulus, 2000). This "outlasting effect" of tDCS has been studied in animal models and slice preparations. In contrast, most *in vitro* studies have reported no outlasting effects of weak electric fields. however the stimulation duration in these studies was typically short. With a longer stimulation duration, outlasting effects were observed more than 10 minutes after the end of 10 minute DC stimulation with higher field amplitudes (i.e. 10 V/m and higher) than what can be expected to occur with tES in humans (D. Reato, Bikson, & Parra, 2015). *In vivo*, tDCS over somatosensory cortex applied to rabbits modulated

eye blink conditioning; however, an outlasting effect of tDCS only occurred for cathodal stimulation (Marquez-Ruiz et al., 2012). The underlying mechanism was probed by paired pulse experiments which revealed that spike-time dependent long-term depression (LTD) was activated by tDCS. Moreover, the resulting LTD was suppressed by pharmacological blockade of adenosine receptors by a local injection. Similarly, evoked potentials were enhanced by application of electric fields *in vivo* in anesthetized rats with effects that outlasted the stimulation for hours (Bindman, Lippold, & Redfearn, 1964). Both long-term potentiation (LTP) and paired-pulse facilitation (PPF) were increased after DC field application in hippocampal slices (Rohan, Carhuatanta, McInturf, Miklasevich, & Jankord, 2015). Intriguingly, LTP (but not PPF) was also enhanced in hippocampal slices of rats which had received anodal tDCS 24 hours earlier. Application of an NMDA antagonist prevented LTP induction but not paired pulse facilitation. In slices of mouse motor cortex, the application of DC field enhanced synaptic strength when paired with a low-frequency electric stimulation of afferent pathways (Fritsch et al., 2010). Importantly, this observed form of LTP depended on NMDA receptors and brain-derived neurotrophic factor (BDNF). Todays limited evidence therefore suggests that tDCS activates multiple, diverse plasticity mechanisms, both pre- and postsynaptic, depending on the brain region, polarity (anodal vs cathodal) of stimulation, and other poorly understood factors. In addition, enhancement of oscillation following tACS have also been attributed to plasticity (A. Vossen, J. Gross, & G. Thut, 2015); however, direct experimental evidence for such a mechanism is lacking. More recently, it was reported that the enhancement of alpha oscillations with tACS depended on BDNF genotype (Riddle et al.), which suggests a role for synaptic plasticity in enabling "outlasting effects".

Interaction of Cellular and Network Mechanisms

The main targets of tES are cortical networks due to their positions closest to the stimulation electrodes. The circuits in neocortex are composed of different cell types that exhibit distinct morphology and electrophysiological properties. Importantly, not all cell types respond equally to weak electric fields. This was demonstrated by the combination of patch recordings of the somatic membrane voltage with careful reconstruction of cell morphology (T. Radman, R. L. Ramos, J. C. Brumberg, & M. Bikson, 2009).

Layer 5 (L5) pyramidal cells had largest change in membrane voltage in response to externally applied electric fields due to their morphology and orientation within cortex. These cells exhibit an elongated somato-dendritic axis that spans from L5 to L1. In addition, the somato-dendritic axis is approximately perpendicular to the surface of the brain meaning that the cells are properly aligned to receive energy from an external electric field orthogonal to the skull. Note that the folding of cortex may introduce additional complexity. Since L5 pyramidal neurons are the likely primary targets of tES, we can expect that their response to stimulation play a critical role in the modulation of cortical network dynamics. Therefore, considering the intrinsic dynamics of this cell type will provide clues with regards to the network-level effects of stimulation. The response of L5 pyramidal cells to subthreshold changes in membrane voltages, particularly in the prefrontal cortex, has been well studied by current-clamp whole-cell patch clamp experiments; these cells respond best to subthreshold perturbations in the theta frequency (4-8 Hz) band (Hu, Vervaeke, & Storm, 2002; Hutcheon & Yarom, 2000). This suggests that electric fields of a given strength will cause the largest subthreshold oscillations in the theta band and that AC field stimulation preferentially modulates low frequency oscillation in cortex. However, *in vivo* study has shown that tACS more strongly entrains narrow-spiking neurons (presumed fast-spiking inhibitory interneurons) than broad-spiking neurons (presumed pyramidal cells), which can be explained by the tighter phase-locking of the former to the endogenous rhythmic network activity (W. A. Huang et al., 2021). More direct experimental evidence confirming this link between single cell excitability, cell morphology, and network level effects is needed. In addition, non-neuronal cells have also been shown to be activated by tES. For example, both anodal and cathodal tDCS applied to the awake mouse brain induce microglia activation and neurogenesis from the subventricular zone (Pikhovych et al., 2016).

As exemplified by the daydreaming student drifting in and out of focus during class, the brain exhibits the ability to rapidly transition between states of varying engagement with the external world. Rather than resulting from changes in anatomical connections between neurons, such moment-to-moment variability in internal brain state arises through changes in network-level activity patterns that are constrained by the brains structural framework(Deco, Jirsa, & McIntosh, 2011). In this scheme, cognition

and behavior emerge from the dynamic interaction of widely distributed, but functionally specialized cortical and subcortical brain regions(Koch, Massimini, Boly, & Tononi, 2016; Siegel et al., 2012).

REFERENCES

Adrian, E.D.M., B. H. C. The Berger rhythm; potential changes from the occipital lobes in man. *Brain* **57**, 355-385 (1934).

Aston-Jones, G. & Cohen, J.D. An integrative theory of locus coeruleus-norepinephrine function: adaptive gain and optimal performance. *Annual review of neuroscience* **28**, 403-450 (2005).

Bollimunta, A., Mo, J., Schroeder, C.E. & Ding, M. Neuronal mechanisms and attentional modulation of corticothalamic alpha oscillations. *The Journal of neuroscience : the official journal of the Society for Neuroscience* **31**, 4935-4943 (2011).

Bonnet, M.H. & Arand, D.L. Impact of activity and arousal upon spectral EEG parameters. *Physiology & behavior* **74**, 291-298 (2001).

Bosman, C.A., *et al.* Attentional stimulus selection through selective synchronization between monkey visual areas. *Neuron* **75**, 875-888 (2012).

Bosman, C.A., Womelsdorf, T., Desimone, R. & Fries, P. A microsaccadic rhythm modulates gamma-band synchronization and behavior. *The Journal of neuroscience : the official journal of the Society for Neuroscience* **29**, 9471-9480 (2009).

Chandler, D.J., Gao, W.J. & Waterhouse, B.D. Heterogeneous organization of the locus coeruleus projections to prefrontal and motor cortices. *Proceedings of the National Academy of Sciences of the United States of America* **111**, 6816-6821 (2014).

da Silva, F.H., van Lierop, T.H., Schrijer, C.F. & van Leeuwen, W.S. Organization of thalamic and cortical alpha rhythms: spectra and coherences. *Electroencephalography and clinical neurophysiology* **35**, 627-639 (1973).

Deco, G., Jirsa, V.K. & McIntosh, A.R. Emerging concepts for the dynamical organization of resting-state activity in the brain. *Nature reviews. Neuroscience* **12**, 43-56 (2011).

Fink, A. & Benedek, M. EEG alpha power and creative ideation. *Neuroscience and biobehavioral reviews* **44**, 111-123 (2014).

Foote, S.L. & Morrison, J.H. Extrathalamic modulation of cortical function. *Annual review of neuroscience* **10**, 67-95 (1987).

Fries, P. Rhythms for Cognition: Communication through Coherence. *Neuron* **88**, 220-235 (2015).

Garcia-Junco-Clemente, P., *et al.* An inhibitory pull-push circuit in frontal cortex. *Nature neuroscience* (2017).

Heeger, D.J. Theory of cortical function. *Proceedings of the National Academy of Sciences of the United States of America* (2017).

Hughes, S.W., *et al.* Synchronized oscillations at alpha and theta frequencies in the lateral geniculate nucleus. *Neuron* **42**, 253-268 (2004).

Jones, E.G. The thalamic matrix and thalamocortical synchrony. *Trends in neurosciences* **24**, 595-601 (2001).

Joshi, S., Li, Y., Kalwani, R.M. & Gold, J.I. Relationships between Pupil Diameter and Neuronal Activity in the Locus Coeruleus, Colliculi, and Cingulate Cortex. *Neuron* **89**, 221-234 (2016).

Kirst, C., Timme, M. & Battaglia, D. Dynamic information routing in complex networks. *Nature communications* **7**, 11061 (2016).

Klimesch, W. alpha-band oscillations, attention, and controlled access to stored information. *Trends in cognitive sciences* **16**, 606-617 (2012).

Koch, C., Massimini, M., Boly, M. & Tononi, G. Neural correlates of consciousness: progress and problems. *Nature reviews. Neuroscience* **17**, 307-321 (2016).

Laeng, B., Sirois, S. & Gredeback, G. Pupillometry: A Window to the Preconscious? *Perspectives on psychological science : a journal of the Association for Psychological Science* **7**, 18-27 (2012).

Liversedge, S.P. & Findlay, J.M. Saccadic eye movements and cognition. *Trends in cognitive sciences* **4**, 6-14 (2000).

Lorincz, M.L., Crunelli, V. & Hughes, S.W. Cellular dynamics of cholinergically induced alpha (8-13 Hz) rhythms in sensory thalamic nuclei in vitro. *The Journal of neuroscience : the official journal of the Society for Neuroscience* **28**, 660-671 (2008).

Manger, P.R., Masiello, I. & Innocenti, G.M. Areal organization of the posterior parietal cortex of the ferret (Mustela putorius). *Cerebral cortex (New York, N.Y. : 1991)* **12**, 1280-1297 (2002).

McCormick, D.A. Cholinergic and noradrenergic modulation of thalamocortical processing. *Trends in neurosciences* **12**, 215-221 (1989).

McCormick, D.A., Wang, Z. & Huguenard, J. Neurotransmitter control of neocortical neuronal activity and excitability. *Cerebral cortex (New York, N.Y. : 1991)* **3**, 387-398 (1993).

McGinley, M.J., David, S.V. & McCormick, D.A. Cortical Membrane Potential Signature of Optimal States for Sensory Signal Detection. *Neuron* **87**, 179-192 (2015).

McGinley, M.J., *et al*. Waking State: Rapid Variations Modulate Neural and Behavioral Responses. *Neuron* **87**, 1143-1161 (2015).

Nieuwenhuis, S., De Geus, E.J. & Aston-Jones, G. The anatomical and functional relationship between the P3 and autonomic components of the orienting response. *Psychophysiology* **48**, 162-175 (2011).

Otero-Millan, J., Troncoso, X.G., Macknik, S.L., Serrano-Pedraza, I. & Martinez-Conde, S. Saccades and microsaccades during visual fixation, exploration, and search: foundations for a common saccadic generator. *Journal of vision* **8**, 21.21-18 (2008).

Pape, H.C. & McCormick, D.A. Noradrenaline and serotonin selectively modulate thalamic burst firing by enhancing a hyperpolarization-activated cation current. *Nature* **340**, 715-718 (1989).

Polack, P.O., Friedman, J. & Golshani, P. Cellular mechanisms of brain state-dependent gain modulation in visual cortex. *Nature neuroscience* **16**, 1331-1339 (2013).

Purushothaman, G., Marion, R., Li, K. & Casagrande, V.A. Gating and control of primary visual cortex by pulvinar. *Nature neuroscience* **15**, 905-912 (2012).

Reimer, J., *et al*. Pupil fluctuations track rapid changes in adrenergic and cholinergic activity in cortex. *Nature communications* **7**, 13289 (2016).

Rogawski, M.A. & Aghajanian, G.K. Modulation of lateral geniculate neurone excitability by noradrenaline microiontophoresis or locus coeruleus stimulation. *Nature* **287**, 731-734 (1980).

Roth, M.M., *et al*. Thalamic nuclei convey diverse contextual information to layer 1 of visual cortex. *Nature neuroscience* **19**, 299-307 (2016).

Roux, F. & Uhlhaas, P.J. Working memory and neural oscillations: alpha-gamma versus theta-gamma codes for distinct WM information? *Trends in cognitive sciences* **18**, 16-25 (2014).

Saalmann, Y.B. & Kastner, S. Cognitive and perceptual functions of the visual thalamus. *Neuron* **71**, 209-223 (2011).

Saalmann, Y.B. Intralaminar and medial thalamic influence on cortical synchrony, information transmission and cognition. *Frontiers in systems neuroscience* **8**, 83 (2014).

Saalmann, Y.B., Pinsk, M.A., Wang, L., Li, X. & Kastner, S. The pulvinar regulates information transmission between cortical areas based on attention demands. *Science (New York, N.Y.)* **337**, 753-756 (2012).

Salgado, H., Trevino, M. & Atzori, M. Layer- and area-specific actions of norepinephrine on cortical synaptic transmission. *Brain research* **1641**, 163-176 (2016).

Siegel, M., Donner, T.H. & Engel, A.K. Spectral fingerprints of large-scale neuronal interactions. *Nature reviews. Neuroscience* **13**, 121-134 (2012).

Stitt, I., *et al.* Intrinsic coupling modes reveal the functional architecture of cortico-tectal networks. *Science advances* **1**, e1500229 (2015).

Totah, N.K., Neves, R.M., Panzeri, S., Logothetis, N.K. & Eschenko, O. Monitoring large populations of locus coeruleus neurons reveals the non-global nature of the norepinephrine neuromodulatory system. *bioRxiv* (2017).

Uhlhaas, P.J. & Singer, W. Neuronal dynamics and neuropsychiatric disorders: toward a translational paradigm for dysfunctional large-scale networks. *Neuron* **75**, 963-980 (2012).

van den Brink, R.L., *et al.* Catecholaminergic Neuromodulation Shapes Intrinsic MRI Functional Connectivity in the Human Brain. *The Journal of neuroscience : the official journal of the Society for Neuroscience* **36**, 7865-7876 (2016).

Vinck, M., Batista-Brito, R., Knoblich, U. & Cardin, J.A. Arousal and locomotion make distinct contributions to cortical activity patterns and visual encoding. *Neuron* **86**, 740-754 (2015).

Wang, C.A. & Munoz, D.P. A circuit for pupil orienting responses: implications for cognitive modulation of pupil size. *Current opinion in neurobiology* **33**, 134-140 (2015).

Yu, C., *et al.* Structural and functional connectivity between the lateral posterior-pulvinar complex and primary visual cortex in the ferret. *The European journal of neuroscience* **43**, 230-244 (2016).

Zagha, E. & McCormick, D.A. Neural control of brain state. *Current opinion in neurobiology* **29**, 178-186 (2014).

CHAPTER 5: GENERAL DISCUSSION

The studies presented in this dissertation provided causal evidence for how different brain stimulation techniques alter thalamo-cortical oscillatory features that are important for visual attention with the dissection of circuit dynamics at the level of LFP and single units.

In Chapter 2, we investigated the role of oscillatory features of the higher-order visual thalamo-cortical circuit during sustained attention and demonstrated their causal influence on attentional behavior. Through optogenetic stimulation at theta and alpha frequencies in the LP/Pul, we successfully entrained the posterior visual network (LP/Pul–PPC–VC) in a frequency-specific way. By enhancing power and thalamo-cortical functional connectivity at the theta frequency band, we were able to improve sustained attention performance by reducing omission. The performance improvement is further correlated with the stimulation-induced enhancement of theta oscillation in the posterior visual cortico-cortical network. In summary, we demonstrated that thalamic theta oscillations causally modulated thalamo-cortical connectivity which in turn enhanced attentional performance. This finding signifies the potential of the posterior visual circuit oscillations as a therapeutic target for the treatment of attention-related disorders.

Since targeting a subcortical region using optogenetics would not be feasible in most human subjects, we next aim to use non-invasive brain stimulation to engage the same network to enhance the translational value of the work. To lay the foundations for future works, it is essential to first understand how neuronal firing was modulated by tACS. In Chapter 3, we demonstrated the neuronal mechanism underlying tACS entrainment of alpha oscillation in the higher-order visual thalamo-cortical circuit. The use of an animal model was advantageous because we can directly record neuronal spiking activities using invasive methods that are not suitable for human subjects. We first showed that endogenous alpha oscillations in PPC drive the V1 and the higher-order visual thalamus. Spike-field coherence was largest

for the alpha frequency band, and presumed fast-spiking inhibitory interneurons exhibited the strongest coupling to this oscillation. We then applied alpha-tACS that resulted in a field strength comparable to what is commonly used in humans (< 0.5 mV/mm). Both in these ferret experiments and a detailed computational model of the thalamo-cortical system, tACS entrained alpha oscillations by following the theoretically predicted Arnold tongue. Intriguingly, the fast-spiking inhibitory interneurons exhibited a stronger entrainment response to tACS in both the ferret experiments and the computational model, likely due to their stronger endogenous coupling to the alpha oscillation. Our findings provided in vivo demonstration of the mechanism of action for the modulation of the alpha oscillation by tACS.

In Chapter 4, I provided an overview of current research on tES in animal models. The effect of electric fields on individual neurons depends on the amplitude and frequency of the applied field. Even though the majority of the current is shunted by the skull and skin, the weak current could still modulate the timing (i.e. phase) of spikes (Krause, Vieira, Csorba, Pilly, & Pack, 2019). When applied at high amplitude, it could also increase the neuronal firing rate (although not normally the intention) (Vöröslakos et al., 2018). Different endogenous dynamics (frequency and amplitude) also shape how the neurons respond to the change in the electric field. One example is the Arnold tongue pattern studied in Chapter 3, where phase-locking is strongest when the external stimulation matches the endogenous frequency. In slice, it was shown that adaptive (i.e. feedback) non-stationary tES could improve the efficacy of electric stimulation in suppressing seizure-like activity (Gluckman, Nguyen, Weinstein, & Schiff, 2001). In addition to the online effect, there is also evidence for NMDA and BDNF-dependent synaptic plasticity at play underlying the long-lasting effect of tES. This chapter provided a summary of our current understanding of how a weak electric field could have a non-trivial effect on the network dynamics.

The two studies are complementary to each other in that they investigated the same circuit using different stimulation methods and targeted different nodes in two different internal states. The first study used a data-driven approach to first identify the circuitry target that is modulated by attentional demand – the thalamic theta oscillations and then use rhythmic optogenetic stimulation to target it. It is believed that the higher-order thalamus shares a general top-down control mechanism with the higher-order cortices

where they gate or facilitate sensory processing by modulating the gains of information from lower-order cortices (Fiebelkorn, Pinsk, & Kastner, 2019; Purushothaman, Marion, Li, & Casagrande, 2012; M. M. Roth et al., 2016; Y. B. Saalmann, M. A. Pinsk, L. Wang, X. Li, & S. Kastner, 2012; H. Zhou, R. J. Schafer, & R. Desimone, 2016). As a result, our findings on the thalamic control such as the spike-phase-locking mechanism as well as the theta-gamma coupling mechanism could inform human cortical stimulation studies.

The Arnold tongue pattern discovered in Chapter 3 can be seen as a general mechanism to entrain the network, which can be applied to optogenetics and other types of rhythmic stimulation. In fact, in Chapter 3, we attempted to generalize this finding by applying optogenetic stimulation with sinusoid-modulated power to mimic the effects of alternating current stimulation in PPC. Indeed, we found a similar Arnold tongue pattern of neuronal entrainment of PPC, which implies that similar entrainment mechanisms are at play despite the drastic difference between the biophysical mechanism of optogenetics and tACS. This further signifies the importance of individualized stimulation that targets the endogenous frequency of each subject, which was performed in Chapter 2. In addition, the endogenous oscillation could also shift in frequency based on the task such as in Chapter 2. The theta oscillations shifted up about 0.5 Hz after trial initiation, which implies frequency-specific coordination of the circuit during a sustained attention period. As a result, we targeted the task-relevant theta (i.e. the up-shifted theta) to enhance sustained attention. Taken together, our studies imply that both individualized and state-dependent stimulation could be crucial for successful engagement of the task-relevant circuit and modulation of task performance.

The limitations of the work presented in this dissertation are also opportunities for exciting follow-up experiments that dig deeper into the mechanisms underlying sustained attention and the function of the posterior visual network. One interesting pattern that we saw in the sustained attention paradigm is the theta-alpha antagonism (Chapter 2). During the sustained attention period, there is an enhancement of theta power and functional connectivity as well as a suppression of alpha power, especially in cortical regions (PPC and VC). In our studies, we targeted the regions where the two oscillations are the strongest (i.e. theta in thalamus in Chapter 2 with alpha as control, and alpha in PPC in Chapter 3). A logical next step is to

apply theta and alpha optogenetic stimulation in PPC during the sustained attention period to gain a complete picture of the interplay of the two higher-order sensory nodes (i.e. LP/Pul and PPC). Since we did not see a behavioral effect under alpha optogenetic stimulation in LP/Pul, one hypothesis is that the alpha frequency is not driven by LP/Pul thus changing alpha in LP/Pul does not modulate sustained attention. In contrast, PPC shows a strong alpha in baseline before the delay period (Chapter 2) as well as when the animal is not actively engaged in a task (Chapter 3). The theta-alpha interaction and their direction in the thalamo-cortical circuit have been linked to arousal, with lower arousal associated with stronger alpha from PPC to LP/Pul and higher arousal associated with stronger theta from LP/Pul to PPC (Stitt et al., 2018). Our study and the follow-up experiments could add to the rising theory that rhythmic interaction between brain regions at different frequencies can serve as separate channels of communication under different states (Engel, Fries, & Singer, 2001; P. Fries, 2005; Singer, 1999).

To expand on the optogenetics results, a future direction would be to apply projection-specific stimulation. One strategy is to inject retrograde virus with ChR2 into PPC and V1 and stimulate the PPC and V1 projecting LP/Pul neurons. Another strategy is to inject the virus with ChR2 into LP/Pul and then laser stimulate labeled axons in PPC and V1. This strategy has a successful track record in mice (S.-Y. Kim et al., 2013; Spellman et al., 2015) but might have limited effects due to labeling efficiency. Both strategies will allow us to specifically activate LP/Pul->PPC and LP/Pul->VC pathway instead of all of the excitatory LP/Pul cells. This could further narrow down the task-relevant projections.

Even though we successfully engaged theta functional connectivity using open-loop optogenetics, the techniques and effect could be improved by more precise timing of stimulation. Closed-loop stimulation has been at the center of recent brain stimulation research due to its potential for more precise temporal targeting and its ability to vary according to ongoing neural activity and related state changes. In the case of epilepsy, a closed-loop solution that detects specific activity signatures has received FDA approval for the control of seizures (Heck et al., 2014; Morrell, 2011). I expect that closed-loop optogenetic activation of the LP/Pul in-phase of the cortical theta oscillation during the delay period will further enhance cortical functional connectivity and attentional performance.

To expand vertically, one could use a depth electrode in the cortex to gain a better understanding of the layer-specificity of the circuit connections. Layer-specific projections in the thalamo-cortical circuit are important for conveying diverse sensory information in V1 (Morgane M Roth et al., 2016) and for anatomically delineating sub-regions within PPC (Manger, Masiello, & Innocenti, 2002).

Another direction is to expand horizontally to study the interplay between the fronto-pariatal (PMC-PPC) network and the thalamo-cortical network. Fronto-parietal network plays important role in coordinating cortical activity during visual processing (Buschman & Miller, 2007; Scolari et al., 2015; Sellers et al., 2016). In primates, theta phases in both frontal eye fields (FEF) and the lateral intraparietal area (LIP, part of PPC) shape spatial attention performance (R. F. Helfrich et al., 2018). In mice, different subgroups of the medial prefrontal cortex (mPFC) bidirectionally regulate inhibitory control (premature trials) in sustained attention tasks (de Kloet et al., 2021). In addition, inhibitory parvalbumin neurons in mPFC causally modulate sustained attention performance via gamma oscillation (H. Kim, Ährlund-Richter, Wang, Deisseroth, & Carlén, 2016). Since previous work has found that in ferrets, theta synchronization between anatomically connected regions dorsal premotor cortex (dPMC) and the posterior parietal cortex (PPC) is modulated by sustained attention tasks (Sellers et al., 2016). It should be noted that in our study in Chapter 2, the PFC we targeted is located more anterior than the PMC that is connected to PPC. The lack of anatomical connections between PFC and PPC as well as between PFC and LP/Pul might explain the lack of functional engagement of those connections during the task and the lack of entrainment of PFC by the optogenetic stimulation in LP/Pul. The fact that the PFC oscillations are not modulated by task demand also suggests that the PFC is not the region that is sensitive to the level of sustained attention. It would be interesting to see whether PMC-PPC connection is modulated by attentional demand.

The work in this dissertation supports the overarching perspective that the oscillatory dynamics in and between specialized brain regions are fundamental to healthy cognitive functions and behavior (Bassett & Gazzaniga, 2011; Bassett & Sporns, 2017; Foster et al., 2016; Fröhlich, 2016), and the external perturbation of these dynamics needs to be done in an individualized and state-dependent manner (Figee & Mayberg, 2021; Grover, Nguyen, Viswanathan, & Reinhart, 2021; Saturnino et al., 2019; Scangos, Makhoul, Sugrue, Chang, &

Krystal, 2021). The findings also touched upon several themes in neuroscience: 1) a convergent mechanism of different rhythmic perturbation methods to modulate circuit dynamics; 2) the causal relationship between functional connectivity, sensory-processing, and behavior in higher-order brain regions; 3) the individualized and state/task-dependent targeting of oscillatory dynamics. Overall, these studies provided a foundation for translational work between animal and human research to provide neuronal and circuit-level understanding of how brain stimulation works to change cognitive function and behavior. Hopefully, our findings in this dissertation will provide insights to further basic science as well as the development of circuit-based therapies for psychiatric disorders.

REFERENCES

Barthó, P., Hirase, H., Monconduit, L., Zugaro, M., Harris, K. D., & Buzsaki, G. (2004). Characterization of neocortical principal cells and interneurons by network interactions and extracellular features. Journal of Neurophysiology, 92(1), 600-608.

Barthó, P., Slézia, A., Mátyás, F., Faradzs-Zade, L., Ulbert, I., Harris, K. D., & Acsády, L. (2014). Ongoing network state controls the length of sleep spindles via inhibitory activity. Neuron, 82(6), 1367-1379.

Bassett, D. S., & Gazzaniga, M. S. (2011). Understanding complexity in the human brain. Trends Cogn Sci, 15(5), 200-209. doi:10.1016/j.tics.2011.03.006

Bassett, D. S., & Sporns, O. (2017). Network neuroscience. Nat Neurosci, 20(3), 353-364. doi:10.1038/nn.4502

Beltramo, R., D'Urso, G., Dal Maschio, M., Farisello, P., Bovetti, S., Clovis, Y., . . . Fellin, T. (2013). Layer-specific excitatory circuits differentially control recurrent network dynamics in the neocortex. Nature neuroscience, 16(2), 227-234. doi:10.1038/nn.3306

Berger, H. (1929). Über das Elektrenkephalogramm des Menschen. Archiv für Psychiatrie und Nervenkrankheiten, 87(1), 527-570.

Bikson, M., Inoue, M., Akiyama, H., Deans, J. K., Fox, J. E., Miyakawa, H., & Jefferys, J. G. (2004). Effects of uniform extracellular DC electric fields on excitability in rat hippocampal slices in vitro. The Journal of physiology, 557(Pt 1), 175-190. doi:10.1113/jphysiol.2003.055772

Bindman, L. J., Lippold, O. C., & Redfearn, J. W. (1964). The Action of Brief Polarizing Currents on the Cerebral Cortex of the Rat (1) during Current Flow and (2) in the Production of Long-Lasting after-Effects. J Physiol, 172, 369-382.

Bollimunta, A., Mo, J., Schroeder, C. E., & Ding, M. (2011). Neuronal Mechanisms and Attentional Modulation of Corticothalamic Alpha Oscillations. 31(13), 4935-4943. doi:10.1523/JNEUROSCI.5580-10.2011 %J The Journal of Neuroscience

Bora, E., Vahip, S., & Akdeniz, F. (2006). Sustained attention deficits in manic and euthymic patients with bipolar disorder. Progress in Neuro-Psychopharmacology and Biological Psychiatry, 30(6), 1097-1102.

Boyce, R., Glasgow, S. D., Williams, S., & Adamantidis, A. (2016). Causal evidence for the role of REM sleep theta rhythm in contextual memory consolidation. Science, 352(6287), 812-816. doi:10.1126/science.aad5252

Boyle, M. R., & Frohlich, F. (2013). EEG feedback-controlled transcranial alternating current stimulation. Paper presented at the Neural Engineering (NER), 2013 6th International IEEE/EMBS Conference on.

Braitenberg, V., & Schüz, A. (2013). Anatomy of the cortex: statistics and geometry (Vol. 18): Springer Science & Business Media.

Brignani, D., Ruzzoli, M., Mauri, P., & Miniussi, C. (2013). Is transcranial alternating current stimulation effective in modulating brain oscillations? PloS One, 8(2), e56589.

Bullmore, E., & Sporns, O. (2012). The economy of brain network organization. Nat Rev Neurosci, 13(5), 336-349. doi:10.1038/nrn3214

Buschman, T. J., & Miller, E. K. (2007). Top-down versus bottom-up control of attention in the prefrontal and posterior parietal cortices. Science, 315(5820), 1860-1862.

Buzsaki, G. (2006). Rhythms of the Brain: Oxford university press.

Buzsaki, G., & Draguhn, A. (2004). Neuronal oscillations in cortical networks. Science, 304(5679), 1926-1929. doi:10.1126/science.1099745

Canolty, R. T., Edwards, E., Dalal, S. S., Soltani, M., Nagarajan, S. S., Kirsch, H. E., . . . Knight, R. T. (2006). High gamma power is phase-locked to theta oscillations in human neocortex. Science, 313(5793), 1626-1628. doi:10.1126/science.1128115

Canolty, R. T., & Knight, R. T. (2010). The functional role of cross-frequency coupling. Trends Cogn Sci, 14(11), 506-515. doi:10.1016/j.tics.2010.09.001

Cardin, J. A., Carlen, M., Meletis, K., Knoblich, U., Zhang, F., Deisseroth, K., . . . Moore, C. I. (2009). Driving fast-spiking cells induces gamma rhythm and controls sensory responses. Nature, 459(7247), 663-667. doi:10.1038/nature08002

Chan, C. Y., Hounsgaard, J., & Nicholson, C. (1988). Effects of electric fields on transmembrane potential and excitability of turtle cerebellar Purkinje cells in vitro. J Physiol, 402, 751-771.

Corbetta, M., & Shulman, G. L. (2002). Control of goal-directed and stimulus-driven attention in the brain. Nat Rev Neurosci, 3(3), 201-215. doi:10.1038/nrn755

Corsi-Cabrera, M., Pérez-Garci, E., Río-Portilla, Y. D., Ugalde, E., & Guevara, M. A. (2001). EEG bands during wakefulness, slow-wave, and paradoxical sleep as a result of principal component analysis in the rat. Sleep, 24(4), 374-380.

Creutzfeldt, O. D., Fromm, G. H., & Kapp, H. (1962). Influence of transcortical d-c currents on cortical neuronal activity. Exp Neurol, 5, 436-452.

Datta, A., Bansal, V., Diaz, J., Patel, J., Reato, D., & Bikson, M. (2009). Gyri-precise head model of transcranial direct current stimulation: improved spatial focality using a ring electrode versus conventional rectangular pad. Brain stimulation, 2(4), 201-207. e201.

de Kloet, S. F., Bruinsma, B., Terra, H., Heistek, T. S., Passchier, E. M. J., van den Berg, A. R., . . . Mansvelder, H. D. (2021). Bi-directional regulation of cognitive control by distinct prefrontal cortical output neurons to thalamus and striatum. Nat Commun, 12(1), 1994. doi:10.1038/s41467-021-22260-7

Deans, J. K., Powell, A. D., & Jefferys, J. G. (2007). Sensitivity of coherent oscillations in rat hippocampus to AC electric fields. The Journal of physiology, 583(Pt 2), 555-565. doi:10.1113/jphysiol.2007.137711

Deans, J. K., Powell, A. D., & Jefferys, J. G. (2007). Sensitivity of coherent oscillations in rat hippocampus to AC electric fields. The Journal of Physiology, 583(2), 555-565.

Deans, J. K., Powell, A. D., & Jefferys, J. G. R. (2007). Sensitivity of coherent oscillations in rat hippocampus to AC electric fields. The Journal of Physiology, 583(Pt 2), 555-565. doi:10.1113/jphysiol.2007.137711

Deco, G., Jirsa, V. K., & McIntosh, A. R. (2011). Emerging concepts for the dynamical organization of resting-state activity in the brain. Nature Reviews: Neuroscience, 12(1), 43-56. doi:10.1038/nrn2961

Deisseroth, K. (2014). Circuit dynamics of adaptive and maladaptive behaviour. Nature, 505(7483), 309-317. doi:10.1038/nature12982

Engel, A. K., Fries, P., & Singer, W. (2001). Dynamic predictions: oscillations and synchrony in top-down processing. Nat Rev Neurosci, 2(10), 704-716. doi:10.1038/35094565

Featherstone, R. E., Rizos, Z., Nobrega, J. N., Kapur, S., & Fletcher, P. J. (2007). Gestational methylazoxymethanol acetate treatment impairs select cognitive functions: parallels to schizophrenia. Neuropsychopharmacology, 32(2), 483-492. doi:10.1038/sj.npp.1301223

Fedorov, A., Beichel, R., Kalpathy-Cramer, J., Finet, J., Fillion-Robin, J.-C., Pujol, S., . . . Sonka, M. (2012). 3D Slicer as an image computing platform for the Quantitative Imaging Network. Magnetic Resonance Imaging, 30(9), 1323-1341.

Fernández, V., Llinares-Benadero, C., & Borrell, V. (2016). Cerebral cortex expansion and folding: what have we learned? The EMBO journal, 35(10), 1021-1044.

Fiebelkorn, I. C., Pinsk, M. A., & Kastner, S. (2019). The mediodorsal pulvinar coordinates the macaque fronto-parietal network during rhythmic spatial attention. Nat Commun, 10(1), 215. doi:10.1038/s41467-018-08151-4

Figee, M., & Mayberg, H. (2021). The future of personalized brain stimulation. Nature Medicine, 27(2), 196-197. doi:10.1038/s41591-021-01243-7

Fortenbaugh, F. C., DeGutis, J., & Esterman, M. (2017). Recent theoretical, neural, and clinical advances in sustained attention research. Annals of the New York Academy of Sciences.

Foster, B. L., He, B. J., Honey, C. J., Jerbi, K., Maier, A., & Saalmann, Y. B. (2016). Spontaneous Neural Dynamics and Multi-scale Network Organization. Front Syst Neurosci, 10, 7. doi:10.3389/fnsys.2016.00007

Fries, P. (2005). A mechanism for cognitive dynamics: neuronal communication through neuronal coherence. Trends Cogn Sci, 9(10), 474-480. doi:10.1016/j.tics.2005.08.011

Fries, P. (2005). A mechanism for cognitive dynamics: neuronal communication through neuronal coherence. Trends in cognitive sciences, 9(10), 474-480.

Fries, P. (2015). Rhythms for Cognition: Communication through Coherence. Neuron, 88(1), 220-235. doi:10.1016/j.neuron.2015.09.034

Fritsch, B., Reis, J., Martinowich, K., Schambra, H. M., Ji, Y., Cohen, L. G., & Lu, B. (2010). Direct current stimulation promotes BDNF-dependent synaptic plasticity: potential implications for motor learning. Neuron, 66(2), 198-204. doi:10.1016/j.neuron.2010.03.035

Fröhlich, F. (2014a). Endogenous and exogenous electric fields as modifiers of brain activity: rational design of noninvasive brain stimulation with transcranial alternating current stimulation. Dialogues Clin. Neurosci., 16(1), 93-102.

Fröhlich, F. (2014b). Endogenous and exogenous electric fields as modifiers of brain activity: rational design of noninvasive brain stimulation with transcranial alternating current stimulation. Dialogues in Clinical Neuroscience, 16(1), 93-102.

Fröhlich, F. (2016). Network neuroscience: Academic Press.

Fröhlich, F. (2016). Network neuroscience. Amsterdam ; Boston: Academic Press.

Fröhlich, F., Force, R., Huang, W. A., Lustenberger, C., McPherson, T., Riddle, J., & Walker, C. (2021). Target Engagement with Transcranial Current Stimulation Transcranial Direct Current Stimulation in Neuropsychiatric Disorders (pp. 211-242): Springer.

Frohlich, F., & McCormick, D. A. (2010). Endogenous electric fields may guide neocortical network activity. Neuron, 67(1), 129-143. doi:10.1016/j.neuron.2010.06.005

Fröhlich, F., & McCormick, D. A. (2010). Endogenous electric fields may guide neocortical network activity. Neuron, 67(1), 129-143.

Geweke, J. (1982). Measurement of linear dependence and feedback between multiple time series. Journal of the American statistical association, 77(378), 304-313.

Geweke, J. F. (1984). Measures of conditional linear dependence and feedback between time series. Journal of the American Statistical Association, 79(388), 907-915.

Gharbawie, O. A., Stepniewska, I., Burish, M. J., & Kaas, J. H. (2010). Thalamocortical connections of functional zones in posterior parietal cortex and frontal cortex motor regions in New World monkeys. Cereb Cortex, 20(10), 2391-2410. doi:10.1093/cercor/bhp308

Gilardi, C., & Kalebic, N. (2021). The Ferret as a Model System for Neocortex Development and Evolution. Frontiers in Cell and Developmental Biology, 9. doi:10.3389/fcell.2021.661759

Gluckman, B. J., Neel, E. J., Netoff, T. I., Ditto, W. L., Spano, M. L., & Schiff, S. J. (1996). Electric field suppression of epileptiform activity in hippocampal slices. Journal of neurophysiology, 76(6), 4202-4205.

Gluckman, B. J., Nguyen, H., Weinstein, S. L., & Schiff, S. J. (2001). Adaptive electric field control of epileptic seizures. The Journal of neuroscience : the official journal of the Society for Neuroscience, 21(2), 590-600.

Granger, C. W. (1969). Investigating causal relations by econometric models and cross-spectral methods. Econometrica: Journal of the Econometric Society, 424-438.

Grea, H., Pisella, L., Rossetti, Y., Desmurget, M., Tilikete, C., Grafton, S., . . . Vighetto, A. (2002). A lesion of the posterior parietal cortex disrupts on-line adjustments during aiming movements. Neuropsychologia, 40(13), 2471-2480.

Grossman, N., Bono, D., Dedic, N., Kodandaramaiah, S. B., Rudenko, A., Suk, H.-J., . . . Tsai, L.-H. (2017). Noninvasive Deep Brain Stimulation via Temporally Interfering Electric Fields. Cell, 169(6), 1029-1041. e1016.

Grover, S., Nguyen, J. A., Viswanathan, V., & Reinhart, R. M. G. (2021). High-frequency neuromodulation improves obsessive–compulsive behavior. Nature Medicine, 27(2), 232-238. doi:10.1038/s41591-020-01173-w

Haberbosch, L., Datta, A., Thomas, C., Jooß, A., Köhn, A., Rönnefarth, M., . . . Schmidt, S. (2019). Safety Aspects, Tolerability and Modeling of Retinofugal Alternating Current Stimulation. Frontiers in Neuroscience, 13(783). doi:10.3389/fnins.2019.00783

Hasse, J. M., & Briggs, F. (2017). Corticogeniculate feedback sharpens the temporal precision and spatial resolution of visual signals in the ferret. Proceedings of the National Academy of Sciences, 114(30), E6222-E6230. doi:10.1073/pnas.1704524114

Heck, C. N., King-Stephens, D., Massey, A. D., Nair, D. R., Jobst, B. C., Barkley, G. L., . . . Gwinn, R. P. (2014). Two-year seizure reduction in adults with medically intractable partial onset epilepsy treated with responsive neurostimulation: Final results of the RNS System Pivotal trial. Epilepsia, 55(3), 432-441.

Helfrich, R. F., Fiebelkorn, I. C., Szczepanski, S. M., Lin, J. J., Parvizi, J., Knight, R. T., & Kastner, S. (2018). Neural Mechanisms of Sustained Attention Are Rhythmic. Neuron, 99(4), 854-865 e855. doi:10.1016/j.neuron.2018.07.032

Helfrich, Randolph F., Schneider, Till R., Rach, S., Trautmann-Lengsfeld, Sina A., Engel, Andreas K., & Herrmann, Christoph S. (2014). Entrainment of Brain Oscillations by Transcranial Alternating Current Stimulation. Current Biology, 24(3), 333-339. doi:10.1016/j.cub.2013.12.041

Herrmann, C. S., Murray, M. M., Ionta, S., Hutt, A., & Lefebvre, J. (2016a). Shaping intrinsic neural oscillations with periodic stimulation. The Journal of neuroscience, 36(19), 5328-5337.

Herrmann, C. S., Murray, M. M., Ionta, S., Hutt, A., & Lefebvre, J. (2016b). Shaping intrinsic neural oscillations with periodic stimulation. Journal of Neuroscience, 36(19), 5328-5337.

Herrmann, C. S., Struber, D., Helfrich, R. F., & Engel, A. K. (2016). EEG oscillations: From correlation to causality. Int J Psychophysiol, 103, 12-21. doi:10.1016/j.ijpsycho.2015.02.003

Hu, H., Vervaeke, K., & Storm, J. F. (2002). Two forms of electrical resonance at theta frequencies, generated by M-current, h-current and persistent Na+ current in rat hippocampal pyramidal cells. The Journal of physiology, 545(Pt 3), 783-805.

Huang, W. A., Stitt, I. M., Negahbani, E., Passey, D. J., Ahn, S., Davey, M., . . . Fröhlich, F. (2021). Transcranial alternating current stimulation entrains alpha oscillations by preferential phase synchronization of fast-spiking cortical neurons to stimulation waveform. Nat Commun, 12(1), 3151. doi:10.1038/s41467-021-23021-2

Huang, Y., Liu, A. A., Lafon, B., Friedman, D., Dayan, M., Wang, X., . . . Parra, L. C. (2017). Measurements and models of electric fields in the in vivo human brain during transcranial electric stimulation. Elife, 6, e18834.

Hutcheon, B., & Yarom, Y. (2000). Resonance, oscillation and the intrinsic frequency preferences of neurons. Trends in neurosciences, 23(5), 216-222.

Izhikevich, E. M. (2007). Dynamical systems in neuroscience: MIT press.

Izhikevich, E. M., & Edelman, G. M. (2008). Large-scale model of mammalian thalamocortical systems. Proceedings of the national academy of sciences, 105(9), 3593-3598.

Juczewski, K., Koussa, J. A., Kesner, A. J., Lee, J. O., & Lovinger, D. M. (2020). Stress and behavioral correlates in the head-fixed method: stress measurements, habituation dynamics, locomotion, and motor-skill learning in mice. Scientific reports, 10(1), 12245. doi:10.1038/s41598-020-69132-6

Kasten, F. H., & Herrmann, C. S. (2017). Transcranial Alternating Current Stimulation (tACS) Enhances Mental Rotation Performance during and after Stimulation. Frontiers in human neuroscience, 11, 2-2. doi:10.3389/fnhum.2017.00002

Kasten, F. H., & Herrmann, C. S. (2017). Transcranial alternating current stimulation (tACS) enhances mental rotation performance during and after stimulation. Frontiers in Human Neuroscience, 11.

Khoshkhoo, S., Vogt, D., & Sohal, V. S. (2017). Dynamic, Cell-Type-Specific Roles for GABAergic Interneurons in a Mouse Model of Optogenetically Inducible Seizures. Neuron, 93(2), 291-298. doi:10.1016/j.neuron.2016.11.043

Kim, H., Ährlund-Richter, S., Wang, X., Deisseroth, K., & Carlén, M. (2016). Prefrontal Parvalbumin Neurons in Control of Attention. Cell, 164(1-2), 208-218. doi:10.1016/j.cell.2015.11.038

Kim, S.-Y., Adhikari, A., Lee, S. Y., Marshel, J. H., Kim, C. K., Mallory, C. S., . . . Lim, B. K. (2013). Diverging neural pathways assemble a behavioural state from separable features in anxiety. Nature, 496(7444), 219-223.

Koch, C., Massimini, M., Boly, M., & Tononi, G. (2016). Neural correlates of consciousness: progress and problems. Nature Reviews: Neuroscience, 17(5), 307-321. doi:10.1038/nrn.2016.22

Kopell, N., Ermentrout, G. B., Whittington, M. A., & Traub, R. D. (2000). Gamma rhythms and beta rhythms have different synchronization properties. Proc Natl Acad Sci U S A, 97(4), 1867-1872.

Krause, B., Márquez-Ruiz, J., & Cohen Kadosh, R. (2013). The effect of transcranial direct current stimulation: a role for cortical excitation/inhibition balance? Frontiers in Human Neuroscience, 7, 602.

Krause, M. R., Vieira, P. G., Csorba, B. A., Pilly, P. K., & Pack, C. C. (2019). Transcranial alternating current stimulation entrains single-neuron activity in the primate brain. Proceedings of the National Academy of Sciences, 116(12), 5747-5755. doi:10.1073/pnas.1815958116

Kumar, R. J., Rajasekhar, E., Subhan, C., Panduranga, P., & Gupta, N. (2014). Dielectric Studies of Acrylic Resin, Alginate, Dental Plaster, Dental Stone, Glass Ionomer and Silver Amalgam. Indian Journal of Advances in Chemical Science, 2(2), 98-103.

Laakso, I., & Hirata, A. (2013). Computational analysis shows why transcranial alternating current stimulation induces retinal phosphenes. J Neural Eng, 10(4), 046009. doi:10.1088/1741-2560/10/4/046009

Lachaux, J.-P., Rodriguez, E., Martinerie, J., & Varela, F. J. (1999). Measuring phase synchrony in brain signals. Human Brain Mapping, 8(4), 194-208.

Lachaux, J. P., Rodriguez, E., Martinerie, J., & Varela, F. J. (1999). Measuring phase synchrony in brain signals. Hum Brain Mapp, 8(4), 194-208.

Lafon, B., Henin, S., Huang, Y., Friedman, D., Melloni, L., Thesen, T., . . . Parra, L. C. (2017). Low frequency transcranial electrical stimulation does not entrain sleep rhythms measured by human intracranial recordings. Nature Communications, 8(1), 1199.

Langner, R., & Eickhoff, S. B. (2013). Sustaining attention to simple tasks: a meta-analytic review of the neural mechanisms of vigilant attention. Psychol Bull, 139(4), 870-900. doi:10.1037/a0030694

Lee, J., & Park, S. (2006). The role of stimulus salience in CPT-AX performance of schizophrenia patients. Schizophrenia Research, 81(2), 191-197.

Lefebvre, J., Hutt, A., & Frohlich, F. (2017). Stochastic resonance mediates the state-dependent effect of periodic stimulation on cortical alpha oscillations. eLife, 6, e32054.

Levinoff, E. J., Saumier, D., & Chertkow, H. (2005). Focused attention deficits in patients with Alzheimer's disease and mild cognitive impairment. Brain and cognition, 57(2), 127-130.

Lewin, J. S., Friedman, L., Wu, D., Miller, D. A., Thompson, L. A., Klein, S. K., . . . Duerk, J. L. (1996). Cortical Localization of Human Sustained Attention: Detection with Functional MR Using a Visual Vigilance Paradigm. Journal of Computer Assisted Tomography, 20(5), 695-701.

Li, G., Henriquez, C. S., & Fröhlich, F. (2017a). Unified thalamic model generates multiple distinct oscillations with state-dependent entrainment by stimulation. PLoS Computational Biology, 13(10), e1005797.

Li, G., Henriquez, C. S., & Fröhlich, F. (2017b). Unified thalamic model generates multiple distinct oscillations with state-dependent entrainment by stimulation. PLoS Comput. Biol., 13(10), e1005797. doi:10.1371/journal.pcbi.1005797

Li, G., Henriquez, C. S., & Fröhlich, F. (2018). Rhythmic Modulation of Thalamic Oscillations Depends on Intrinsic Cellular Dynamics. Journal of Neural Engineering.

Li, X., Sroubek, A., Kelly, M. S., Lesser, I., Sussman, E., He, Y., . . . Foxe, J. J. (2012). Atypical pulvinar–cortical pathways during sustained attention performance in children with attention-deficit/hyperactivity disorder. Journal of the American Academy of Child & Adolescent Psychiatry, 51(11), 1197-1207. e1194.

Liebe, S., Hoerzer, G. M., Logothetis, N. K., & Rainer, G. (2012). Theta coupling between V4 and prefrontal cortex predicts visual short-term memory performance. Nat Neurosci, 15(3), 456-462, S451-452. doi:10.1038/nn.3038

Lisman, J. (2005). The theta/gamma discrete phase code occuring during the hippocampal phase precession may be a more general brain coding scheme. Hippocampus, 15(7), 913-922. doi:10.1002/hipo.20121

Lisman, J. E., & Jensen, O. (2013). The theta-gamma neural code. Neuron, 77(6), 1002-1016. doi:10.1016/j.neuron.2013.03.007

Liu, A., Vöröslakos, M., Kronberg, G., Henin, S., Krause, M. R., Huang, Y., . . . Krekelberg, B. (2018). Immediate neurophysiological effects of transcranial electrical stimulation. Nature Communications, 9(1), 5092.

Liu, S. K., Chiu, C.-H., Chang, C.-J., Hwang, T.-J., Hwu, H.-G., & Chen, W. J. (2002). Deficits in sustained attention in schizophrenia and affective disorders: stable versus state-dependent markers. American Journal of Psychiatry, 159(6), 975-982.

Lustenberger, C., Boyle, M. R., Alagapan, S., Mellin, J. M., Vaughn, B. V., & Frohlich, F. (2016). Feedback-Controlled Transcranial Alternating Current Stimulation Reveals a Functional Role of Sleep Spindles in Motor Memory Consolidation. Curr Biol, 26(16), 2127-2136. doi:10.1016/j.cub.2016.06.044

Manger, P. R., Masiello, I., & Innocenti, G. M. (2002). Areal Organization of the Posterior Parietal Cortex of the Ferret (Mustela putorius). Cerebral Cortex, 12(12), 1280-1297. doi:10.1093/cercor/12.12.1280

Marquez-Ruiz, J., Leal-Campanario, R., Sanchez-Campusano, R., Molaee-Ardekani, B., Wendling, F., Miranda, P. C., . . . Delgado-Garcia, J. M. (2012). Transcranial direct-current stimulation modulates synaptic mechanisms involved in associative learning in behaving rabbits. Proc Natl Acad Sci U S A, 109(17), 6710-6715. doi:10.1073/pnas.1121147109

Mazzoni, A., Lindén, H., Cuntz, H., Lansner, A., Panzeri, S., & Einevoll, G. T. (2015). Computing the Local Field Potential (LFP) from Integrate-and-Fire Network Models. PLoS computational biology, 11(12), e1004584. doi:10.1371/journal.pcbi.1004584

McAlonan, K., Cavanaugh, J., & Wurtz, R. H. (2008). Guarding the gateway to cortex with attention in visual thalamus. Nature, 456(7220), 391-394.

Miranda, P. C., Lomarev, M., & Hallett, M. (2006). Modeling the current distribution during transcranial direct current stimulation. Clinical Neurophysiology, 117(7), 1623-1629.

Miranda, P. C., Mekonnen, A., Salvador, R., & Ruffini, G. (2013). The electric field in the cortex during transcranial current stimulation. Neuroimage, 70, 48-58. doi:10.1016/j.neuroimage.2012.12.034

Molaee-Ardekani, B., Márquez-Ruiz, J., Merlet, I., Leal-Campanario, R., Gruart, A., Sánchez-Campusano, R., . . . Wendling, F. (2013). Effects of transcranial Direct Current Stimulation (tDCS) on cortical activity: a computational modeling study. Brain stimulation, 6(1), 25-39.

Moliadze, V., Antal, A., & Paulus, W. (2010). Boosting brain excitability by transcranial high frequency stimulation in the ripple range. The Journal of Physiology, 588(24), 4891-4904.

Moret, B., Donato, R., Nucci, M., Cona, G., & Campana, G. (2019). Transcranial random noise stimulation (tRNS): a wide range of frequencies is needed for increasing cortical excitability. Scientific reports, 9(1), 15150. doi:10.1038/s41598-019-51553-7

Morrell, M. J. (2011). Responsive cortical stimulation for the treatment of medically intractable partial epilepsy. Neurology, 77(13), 1295-1304.

Negahbani, E., Kasten, F. H., Herrmann, C. S., & Fröhlich, F. (2018). Targeting alpha-band oscillations in a cortical model with amplitude-modulated high-frequency transcranial electric stimulation. Neuroimage, 173, 3-12.

Negahbani, E., Stitt, I. M., Davey, M., Doan, T. T., Dannhauer, M., Hoover, A. C., . . . Fröhlich, F. (2019). Transcranial Alternating Current Stimulation (tACS) Entrains Alpha Oscillations by Preferential Phase Synchronization of Fast-Spiking Cortical Neurons to Stimulation Waveform. BioRxiv, 563163. doi:10.1101/563163

Neuling, T., Rach, S., & Herrmann, C. S. (2013). Orchestrating neuronal networks: sustained after-effects of transcranial alternating current stimulation depend upon brain states. Frontiers in Human Neuroscience, 7, 161.

Nitsche, M. A., & Paulus, W. (2000). Excitability changes induced in the human motor cortex by weak transcranial direct current stimulation. The Journal of physiology, 527 Pt 3, 633-639.

Noury, N., Hipp, J. F., & Siegel, M. (2016). Physiological processes non-linearly affect electrophysiological recordings during transcranial electric stimulation. Neuroimage, 140(Supplement C), 99-109. doi:https://doi.org/10.1016/j.neuroimage.2016.03.065

Noury, N., Hipp, J. F., & Siegel, M. (2016). Physiological processes non-linearly affect electrophysiological recordings during transcranial electric stimulation. Neuroimage, 140, 99-109.

Noury, N., & Siegel, M. (2017). Phase properties of transcranial electrical stimulation artifacts in electrophysiological recordings. Neuroimage, 158, 406-416.

Noury, N., & Siegel, M. (2018). Analyzing EEG and MEG signals recorded during tES, a reply. Neuroimage, 167, 53-61.

Nuechterlein, K. H., Green, M. F., Calkins, M. E., Greenwood, T. A., Gur, R. E., Gur, R. C., . . . Seidman, L. J. (2015). Attention/vigilance in schizophrenia: performance results from a large multi-site study of the Consortium on the Genetics of Schizophrenia (COGS). Schizophrenia research, 163(1), 38-46.

Okun, M., Steinmetz, N. A., Cossell, L., Iacaruso, M. F., Ko, H., Barthó, P., . . . Carandini, M. (2015). Diverse coupling of neurons to populations in sensory cortex. Nature, 521(7553), 511.

Olson, C. R., & Musil, S. Y. (1992). Topographic organization of cortical and subcortical projections to posterior cingulate cortex in the cat: evidence for somatic, ocular, and complex subregions. J Comp Neurol, 324(2), 237-260. doi:10.1002/cne.903240207

Opitz, A., Falchier, A., Yan, C.-G., Yeagle, E. M., Linn, G. S., Megevand, P., . . . Schroeder, C. E. (2016). Spatiotemporal structure of intracranial electric fields induced by transcranial electric stimulation in humans and nonhuman primates. Scientific Reports, 6, 31236.

Ozen, S., Sirota, A., Belluscio, M. A., Anastassiou, C. A., Stark, E., Koch, C., & Buzsaki, G. (2010). Transcranial electric stimulation entrains cortical neuronal populations in rats. The Journal of neuroscience, 30(34), 11476-11485. doi:10.1523/JNEUROSCI.5252-09.2010

Pachitariu, M., Steinmetz, N. A., Kadir, S. N., Carandini, M., & Harris, K. D. (2016). Fast and accurate spike sorting of high-channel count probes with KiloSort. Paper presented at the Advances in neural information processing systems.

Pagliaccio, D., Wiggins, J. L., Adleman, N. E., Harkins, E., Curhan, A., Towbin, K. E., . . . Leibenluft, E. (2017). Behavioral and neural sustained attention deficits in bipolar disorder and familial risk of bipolar disorder. Biological psychiatry, 82(9), 669-678.

Palva, J. M., Palva, S., & Kaila, K. (2005). Phase Synchrony among Neuronal Oscillations in the Human Cortex. The Journal of Neuroscience, 25(15), 3962-3972. doi:10.1523/jneurosci.4250-04.2005

Palva, S., & Palva, J. M. (2011). Functional Roles of Alpha-Band Phase Synchronization in Local and Large-Scale Cortical Networks. Frontiers in Psychology, 2(204). doi:10.3389/fpsyg.2011.00204

Petersen, S. E., & Posner, M. I. (2012). The attention system of the human brain: 20 years after. Annual review of neuroscience, 35, 73-89.

Pikhovych, A., Stolberg, N. P., Jessica Flitsch, L., Walter, H. L., Graf, R., Fink, G. R., . . . Rueger, M. A. (2016). Transcranial Direct Current Stimulation Modulates Neurogenesis and Microglia Activation in the Mouse Brain. Stem Cells Int, 2016, 2715196. doi:10.1155/2016/2715196

Pikovsky, A., Kurths, J., Rosenblum, M., & Kurths, J. (2003). Synchronization: a universal concept in nonlinear sciences (Vol. 12): Cambridge university press.

Pikovsky, A., Rosenblum, M., & Kurths, J. (2003). Synchronization: a universal concept in nonlinear sciences (Vol. 12): Cambridge university press.

Polanía, R., Nitsche, M. A., Korman, C., Batsikadze, G., & Paulus, W. (2012). The importance of timing in segregated theta phase-coupling for cognitive performance. Current Biology, 22(14), 1314-1318.

Purpura, D. P., & McMurtry, J. G. (1965). Intracellular Activities and Evoked Potential Changes during Polarization of Motor Cortex. Journal of neurophysiology, 28, 166-185.

Purushothaman, G., Marion, R., Li, K., & Casagrande, V. A. (2012). Gating and control of primary visual cortex by pulvinar. Nat Neurosci, 15(6), 905-912. doi:10.1038/nn.3106

Raco, V., Bauer, R., Olenik, M., Brkic, D., & Gharabaghi, A. (2014). Neurosensory effects of transcranial alternating current stimulation. Brain Stimul, 7(6), 823-831. doi:10.1016/j.brs.2014.08.005

Raczkowski, D., & Rosenquist, A. C. (1983). Connections of the multiple visual cortical areas with the lateral posterior-pulvinar complex and adjacent thalamic nuclei in the cat. J Neurosci, 3(10), 1912-1942.

Radman, T., Ramos, R. L., Brumberg, J. C., & Bikson, M. (2009). Role of cortical cell type and morphology in subthreshold and suprathreshold uniform electric field stimulation in vitro. Brain stimulation, 2(4), 215-228. e213.

Radman, T., Ramos, R. L., Brumberg, J. C., & Bikson, M. (2009). Role of cortical cell type and morphology in subthreshold and suprathreshold uniform electric field stimulation in vitro. Brain Stimul, 2(4), 215-228, 228 e211-213. doi:10.1016/j.brs.2009.03.007

Radman, T., Su, Y., An, J. H., Parra, L. C., & Bikson, M. (2007). Spike timing amplifies the effect of electric fields on neurons: implications for endogenous field effects. The Journal of neuroscience, 27(11), 3030-3036.

Radtke-Schuller, S. (2018). Cyto- and Myeloarchitectural Brain Atlas of the Ferret (Mustela putorius) in MRI Aided Stereotaxic Coordinates (1 ed.): Springer International Publishing.

Rakic, P., & Lombroso, P. J. (1998). Development of the cerebral cortex: I. Forming the cortical structure. Journal of the American Academy of Child & Adolescent Psychiatry, 37(1), 116-117.

Rana, K. D., & Vaina, L. M. (2014). Functional roles of 10 Hz alpha-band power modulating engagement and disengagement of cortical networks in a complex visual motion task. PLoS One, 9(10), e107715-e107715. doi:10.1371/journal.pone.0107715

Reato, D., Bikson, M., & Parra, L. C. (2015). Lasting modulation of in vitro oscillatory activity with weak direct current stimulation. Journal of neurophysiology, 113(5), 1334-1341. doi:10.1152/jn.00208.2014

Reato, D., Rahman, A., Bikson, M., & Parra, L. C. (2010). Low-intensity electrical stimulation affects network dynamics by modulating population rate and spike timing. Journal of Neuroscience, 30(45), 15067-15079.

Reato, D., Rahman, A., Bikson, M., & Parra, L. C. (2010a). Low-intensity electrical stimulation affects network dynamics by modulating population rate and spike timing. The Journal of neuroscience :

the official journal of the Society for Neuroscience, 30(45), 15067-15079. doi:10.1523/JNEUROSCI.2059-10.2010

Reato, D., Rahman, A., Bikson, M., & Parra, L. C. (2010b). Low-intensity electrical stimulation affects network dynamics by modulating population rate and spike timing. J Neurosci, 30(45), 15067-15079. doi:30/45/15067 [pii]10.1523/JNEUROSCI.2059-10.2010

Reato, D., Rahman, A., Bikson, M., & Parra, L. C. (2013). Effects of weak transcranial alternating current stimulation on brain activity—a review of known mechanisms from animal studies. Frontiers in Human Neuroscience, 7, 687.

Riccio, C. A., Reynolds, C. R., Lowe, P., & Moore, J. J. (2002). The continuous performance test: a window on the neural substrates for attention? Archives of Clinical Neuropsychology, 17(3), 235-272. doi:http://dx.doi.org/10.1016/S0887-6177(01)00111-1

Riddle, J., McPherson, T., Atkins, A. K., Walker, C., Ahn, S., & Frohlich, F. Brain-derived neurotrophic factor (BDNF) polymorphism may influence the efficacy of tACS to modulate neural oscillations. Brain Stimulation: Basic, Translational, and Clinical Research in Neuromodulation. doi:10.1016/j.brs.2020.04.012

Robbins, T. (2002). The 5-choice serial reaction time task: behavioural pharmacology and functional neurochemistry. Psychopharmacology, 163(3-4), 362-380.

Rohan, J. G., Carhuatanta, K. A., McInturf, S. M., Miklasevich, M. K., & Jankord, R. (2015). Modulating Hippocampal Plasticity with In Vivo Brain Stimulation. The Journal of neuroscience : the official journal of the Society for Neuroscience, 35(37), 12824-12832. doi:10.1523/JNEUROSCI.2376-15.2015

Roth, M. M., Dahmen, J. C., Muir, D. R., Imhof, F., Martini, F. J., & Hofer, S. B. (2016). Thalamic nuclei convey diverse contextual information to layer 1 of visual cortex. Nat Neurosci, 19(2), 299-307. doi:10.1038/nn.4197

Roth, M. M., Dahmen, J. C., Muir, D. R., Imhof, F., Martini, F. J., & Hofer, S. B. (2016). Thalamic nuclei convey diverse contextual information to layer 1 of visual cortex. Nat Neurosci, 19(2), 299.

Saalmann, Y. B., Pinsk, M. A., Wang, L., Li, X., & Kastner, S. (2012). The pulvinar regulates information transmission between cortical areas based on attention demands. Science, 337(6095), 753-756. doi:10.1126/science.1223082

Saalmann, Y. B., Pinsk, M. A., Wang, L., Li, X., & Kastner, S. (2012). The pulvinar regulates information transmission between cortical areas based on attention demands. Science, 337(6095), 753-756.

Sadleir, R. J., Vannorsdall, T. D., Schretlen, D. J., & Gordon, B. (2010). Transcranial direct current stimulation (tDCS) in a realistic head model. Neuroimage, 51(4), 1310-1318.

Sahlem, G. L., Badran, B. W., Halford, J. J., Williams, N. R., Korte, J. E., Leslie, K., . . . Bachman, D. L. (2015). Oscillating square wave transcranial direct current stimulation (tDCS) delivered during slow wave sleep does not improve declarative memory more than sham: a randomized sham controlled crossover study. Brain stimulation, 8(3), 528-534.

Sanchez-Vives, M. V., & McCormick, D. A. (2000). Cellular and network mechanisms of rhythmic recurrent activity in neocortex. Nature neuroscience, 3(10), 1027-1034. doi:10.1038/79848

Sandran, N., Hillier, S., & Hordacre, B. (2019). Strategies to implement and monitor in-home transcranial electrical stimulation in neurological and psychiatric patient populations: a systematic review. Journal of NeuroEngineering and Rehabilitation, 16(1), 58. doi:10.1186/s12984-019-0529-5

Sarter, M., Givens, B., & Bruno, J. P. (2001). The cognitive neuroscience of sustained attention: where top-down meets bottom-up. Brain Research Reviews, 35(2), 146-160.

Saturnino, G. B., Puonti, O., Nielsen, J. D., Antonenko, D., Madsen, K. H., & Thielscher, A. (2019). SimNIBS 2.1: a comprehensive pipeline for individualized electric field modelling for transcranial brain stimulation. Brain and human body modeling, 3-25.

Scangos, K. W., Makhoul, G. S., Sugrue, L. P., Chang, E. F., & Krystal, A. D. (2021). State-dependent responses to intracranial brain stimulation in a patient with depression. Nature Medicine, 27(2), 229-231. doi:10.1038/s41591-020-01175-8

Schmidt, S. L., Iyengar, A. K., Foulser, A. A., Boyle, M. R., & Frohlich, F. (2014). Endogenous cortical oscillations constrain neuromodulation by weak electric fields. Brain Stimul, 7(6), 878-889. doi:10.1016/j.brs.2014.07.033

Schmidt, S. L., Iyengar, A. K., Foulser, A. A., Boyle, M. R., & Fröhlich, F. (2014). Endogenous cortical oscillations constrain neuromodulation by weak electric fields. Brain stimulation, 7(6), 878-889.

Scolari, M., Seidl-Rathkopf, K. N., & Kastner, S. (2015). Functions of the human frontoparietal attention network: Evidence from neuroimaging. Current Opinion in Behavioral Sciences, 1, 32-39. doi:https://doi.org/10.1016/j.cobeha.2014.08.003

Sellers, K. K., Yu, C., Zhou, Z. C., Stitt, I., Li, Y., Radtke-Schuller, S., . . . Fröhlich, F. (2016). Oscillatory dynamics in the frontoparietal attention network during sustained attention in the ferret. Cell reports, 16(11), 2864-2874. doi:10.1016/j.celrep.2016.08.055

Siegel, M., Donner, T. H., & Engel, A. K. (2012). Spectral fingerprints of large-scale neuronal interactions. Nature Reviews: Neuroscience, 13(2), 121-134. doi:10.1038/nrn3137

Singer, W. (1999). Neuronal synchrony: a versatile code for the definition of relations? Neuron, 24(1), 49-65, 111-125.

So, P. P. M., Stuchly, M. A., & Nyenhuis, J. A. (2004). Peripheral nerve stimulation by gradient switching fields in magnetic resonance imaging. IEEE Transactions on Biomedical Engineering, 51(11), 1907-1914. doi:10.1109/TBME.2004.834251

Sousa, A. M., Meyer, K. A., Santpere, G., Gulden, F. O., & Sestan, N. (2017). Evolution of the human nervous system function, structure, and development. Cell, 170(2), 226-247.

Spellman, T., Rigotti, M., Ahmari, S. E., Fusi, S., Gogos, J. A., & Gordon, J. A. (2015). Hippocampal-prefrontal input supports spatial encoding in working memory. Nature, 522(7556), 309-314.

Sporns, O., Tononi, G., & Edelman, G. M. (2000). Connectivity and complexity: the relationship between neuroanatomy and brain dynamics. Neural Netw, 13(8-9), 909-922.

Steels, A. (2008). Grade Data Sheet 303. In A. Steels (Ed.).

Steinberg, E. E., Christoffel, D. J., Deisseroth, K., & Malenka, R. C. (2015). Illuminating circuitry relevant to psychiatric disorders with optogenetics. Curr Opin Neurobiol, 30, 9-16. doi:10.1016/j.conb.2014.08.004

Stimberg, M., Brette, R., & Goodman, D. F. M. (2019). Brian 2, an intuitive and efficient neural simulator. Elife, 8, e47314. doi:10.7554/eLife.47314

Stitt, I., Zhou, Z. C., Radtke-Schuller, S., & Fröhlich, F. (2018). Arousal dependent modulation of thalamo-cortical functional interaction. Nat Commun, 9(1), 2455. doi:10.1038/s41467-018-04785-6

Szczepanski, S. M., Pinsk, M. A., Douglas, M. M., Kastner, S., & Saalmann, Y. B. (2013). Functional and structural architecture of the human dorsal frontoparietal attention network. Proc Natl Acad Sci U S A, 110(39), 15806-15811. doi:10.1073/pnas.1313903110

Taktakishvili, O., Sivan-Loukianova, E., Kultas-Ilinsky, K., & Ilinsky, I. A. (2002). Posterior parietal cortex projections to the ventral lateral and some association thalamic nuclei in Macaca mulatta. Brain Res Bull, 59(2), 135-150.

Tallon-Baudry, C., Bertrand, O., Delpuech, C., & Pernier, J. (1996). Stimulus specificity of phase-locked and non-phase-locked 40 Hz visual responses in human. Journal of Neuroscience, 16(13), 4240-4249.

Terzuolo, C. A., & Bullock, T. H. (1956). Measurement of Imposed Voltage Gradient Adequate to Modulate Neuronal Firing. Proc Natl Acad Sci U S A, 42(9), 687-694.

Thielscher, A., Opitz, A., & Windhoff, M. (2011). Impact of the gyral geometry on the electric field induced by transcranial magnetic stimulation. Neuroimage, 54(1), 234-243. doi:10.1016/j.neuroimage.2010.07.061

Toloza, E. H., Negahbani, E., & Frohlich, F. (2017). Ih Interacts with Somato-Dendritic Structure to Determine Frequency Response to Weak Alternating Electric Field Stimulation. Journal of Neurophysiology, 119.3, 1029-1036.

Toloza, E. H. S., Negahbani, E., & Fröhlich, F. (2018). Ih interacts with somato-dendritic structure to determine frequency response to weak alternating electric field stimulation. J Neurophysiol, 119(3), 1029-1036. doi:10.1152/jn.00541.2017

Tucha, L., Fuermaier, A. B., Koerts, J., Buggenthin, R., Aschenbrenner, S., Weisbrod, M., . . . Tucha, O. (2017). Sustained attention in adult ADHD: Time-on-task effects of various measures of attention. Journal of Neural Transmission, 124(1), 39-53.

Turner, K. M., Peak, J., & Burne, T. H. J. (2015). Measuring Attention in Rodents: Comparison of a Modified Signal Detection Task and the 5-Choice Serial Reaction Time Task. Frontiers in Behavioral Neuroscience, 9, 370. doi:10.3389/fnbeh.2015.00370

Tustison, N. J., Avants, B. B., Cook, P. A., Zheng, Y., Egan, A., Yushkevich, P. A., & Gee, J. C. (2010). N4ITK: improved N3 bias correction. IEEE Transactions on Medical Imaging, 29(6), 1310-1320.

Tye, K. M., & Deisseroth, K. (2012). Optogenetic investigation of neural circuits underlying brain disease in animal models. Nature Reviews Neuroscience, 13(4), 251-266.

Uehara, T., Yamasaki, T., Okamoto, T., Koike, T., Kan, S., Miyauchi, S., . . . Tobimatsu, S. (2014). Efficiency of a "small-world" brain network depends on consciousness level: a resting-state FMRI study. Cereb Cortex, 24(6), 1529-1539. doi:10.1093/cercor/bht004

Uhlhaas, P. J., Haenschel, C., Nikolic, D., & Singer, W. (2008). The role of oscillations and synchrony in cortical networks and their putative relevance for the pathophysiology of schizophrenia. Schizophr Bull, 34(5), 927-943. doi:10.1093/schbul/sbn062

Urban, D. J., & Roth, B. L. (2015). DREADDs (designer receptors exclusively activated by designer drugs): chemogenetic tools with therapeutic utility. Annu Rev Pharmacol Toxicol, 55, 399-417. doi:10.1146/annurev-pharmtox-010814-124803

Vieira, P. G., Krause, M. R., & Pack, C. C. (2019). tACS entrains neural activity while somatosensory input is blocked. BioRxiv, 691022. doi:10.1101/691022

von Stein, A., Chiang, C., & Konig, P. (2000). Top-down processing mediated by interareal synchronization. Proc Natl Acad Sci U S A, 97(26), 14748-14753. doi:10.1073/pnas.97.26.14748

von Stein, A., & Sarnthein, J. (2000). Different frequencies for different scales of cortical integration: from local gamma to long range alpha/theta synchronization. Int J Psychophysiol, 38(3), 301-313.

Vöröslakos, M., Takeuchi, Y., Brinyiczki, K., Zombori, T., Oliva, A., Fernández-Ruiz, A., . . . Berényi, A. (2018). Direct effects of transcranial electric stimulation on brain circuits in rats and humans. Nat Commun, 9(1), 483. doi:10.1038/s41467-018-02928-3

Vossen, A., Gross, J., & Thut, G. (2015). Alpha Power Increase After Transcranial Alternating Current Stimulation at Alpha Frequency (alpha-tACS) Reflects Plastic Changes Rather Than Entrainment. Brain Stimul, 8(3), 499-508. doi:10.1016/j.brs.2014.12.004

Vossen, A., Gross, J., & Thut, G. (2015). Alpha Power Increase After Transcranial Alternating Current Stimulation at Alpha Frequency (α-tACS) Reflects Plastic Changes Rather Than Entrainment. Brain Stimul, 8(3), 499-508. doi:10.1016/j.brs.2014.12.004

Williams, J. H., & Kauer, J. A. (1997). Properties of carbachol-induced oscillatory activity in rat hippocampus. Journal of neurophysiology, 78(5), 2631-2640.

Witkowski, M., Garcia-Cossio, E., Chander, B. S., Braun, C., Birbaumer, N., Robinson, S. E., & Soekadar, S. R. (2016). Mapping entrained brain oscillations during transcranial alternating current stimulation (tACS). Neuroimage, 140, 89-98. doi:10.1016/j.neuroimage.2015.10.024

Wolff, S. B., & Ölveczky, B. P. (2018). The promise and perils of causal circuit manipulations. Curr Opin Neurobiol, 49, 84-94. doi:10.1016/j.conb.2018.01.004

Yu, C., Sellers, K. K., Radtke-Schuller, S., Lu, J., Xing, L., Ghukasyan, V., . . . Fröhlich, F. (2016). Structural and functional connectivity between the lateral posterior–pulvinar complex and primary visual cortex in the ferret. European Journal of Neuroscience, 43(2), 230-244.

Zaehle, T., Rach, S., & Herrmann, C. S. (2010). Transcranial alternating current stimulation enhances individual alpha activity in human EEG. PloS One, 5(11), e13766.

Zar, J. H. (1999). Biostatistical analysis: Pearson Education India.

Zhou, H., Schafer, R. J., & Desimone, R. (2016). Pulvinar-Cortex Interactions in Vision and Attention. Neuron, 89(1), 209-220. doi:10.1016/j.neuron.2015.11.034

Zhou, Y., & Freedman, D. J. (2019). Posterior parietal cortex plays a causal role in perceptual and categorical decisions. Science, 365(6449), 180-185. doi:doi:10.1126/science.aaw8347

Zhou, Z. C., Salzwedel, A. P., Radtke-Schuller, S., Li, Y., Sellers, K. K., Gilmore, J. H., . . . Gao, W. (2016). Resting state network topology of the ferret brain. Neuroimage, 143, 70-81. doi:10.1016/j.neuroimage.2016.09.003

Zhou, Z. C., Yu, C., Sellers, K. K., & Fröhlich, F. (2016). Dorso-lateral frontal cortex of the ferret encodes perceptual difficulty during visual discrimination. Scientific reports, 6, srep23568.